The University Of Sheffield.

QUANTITATIVE COMPUTATIONAL EVALUATION OF CARDIAC AND CORONARY PHYSIOLOGY

Martina Ignazia Sciola

Faculty of Medicine, Dentistry and Health
Department of Infection and Immunity and Cardiovascular Disease
Mathematical Modelling and Medicine Group

Submitted for the degree of PhD

Date of submission
December 2017

ABSTRACT

Background

Coronary artery disease (CAD) is a clinical condition characterised by an obstruction of the blood flow to the myocardium. Coronary angiography is the gold standard clinical procedure to assess the coronary stenosis based on the vessel anatomy. Fractional flow reserve (FFR) describes the physiological severity of the stenosis during maximum coronary flow, induced by adenosine infusion.

Hypothesis

Mathematical models can be used to represent the cardiovascular system and be employed as investigative and predictive tools to assess CAD in individual patients.

Aims

To support the computational estimation of coronary FFR (vFFR) by characterising and predicting the response to the administration of adenosine in terms of the myocardial resistance and by investigating correlations between patient parameters and myocardial resistance.

Methods & Results

1) A zero-dimensional (0D) cardiovascular model has been developed starting from published models to simulate adenosine-induced hyperaemia as a function and is shown to reproduce qualitatively the effects described in the literature using generic parameters. A sensitivity analysis was performed to introduce and test assumptions, including the decoupling of the systemic model from the local coronary compartment, which later facilitates the process of tuning model parameters to individual patient data.

2) Clinical data from patients with CAD have been used to personalise the systemic cardiovascular system and subsequently, at a coronary level, to represent the individual-specific response to adenosine. The 0D coronary model included representation of a vessel stenosis, characterised by a computational fluid dynamics analysis, and the myocardial impedance. The nature of the response of individual patients to the administration of adenosine was quantitatively characterised in terms of the underlying parameters described by the model. The myocardium adenosine concentration profile and resistance were used to identify correlation with patient parameters. No statistically significant associations were found between the type of response and observations in the clinical records.

3) Considering the lack of consensus on the definition of FFR under hyperaemia, an algorithm has been developed to objectively identify stable and minimum FFR.

Conclusions

It is possible to use a 0D model to support the individual characterisation of the response to adenosine, and thus to provide insight into the nature of the physiological response to this drug. However, this approach does not support the reliable prediction of this response in individuals with CAD from baseline measurements that are made in the routine clinical pathway. Arising from this work, a robust algorithm has been developed to identify the stable and minimum FFR, which can be used to improve clinical decision making.

STATEMENT OF CONTRIBUTIONS

This thesis investigates the combination of zero-dimensional modelling with sparse clinical data to predict individual patient response to the administration of adenosine. The main contributions of this thesis are:

1) A 0-D model to represent adenosine response in a generic individual, simulating some of the physiological effects produced by adenosine, based on literature information;
2) A sensitivity analysis of the relative influence of model parameters on the simulated adenosine response;
3) An algorithm to identify the minimum and stable FFR during adenosine response, which can support the objectivity of the definition of the FFR on which the clinical decision is made;
4) An optimisation method to personalise the parameters of the model to represent the patient-specific coronary and systemic circulations
5) A method to quantify the myocardial resistance during hyperaemic response to find correlations with patients‘ characteristics for predictive purposes;
6) A method to define the myocardial blood volume during adenosine administration based on an optimisation process on the myocardial resistance and the coronary tree-structure model.

PUBLICATIONS AND CONFERENCES PROCEEDINGS LIST

[1] **M.I. Sciola**, P.D. Morris, R. Gosling, P.V. Lawford, D.R. Hose, J.P. Gunn, *The impact of objective mathematical analysis during Fractional Flow Reserve measurement*, Eurointervention, Feb.2018, DOI: 10.4244/EIJ-D-17-00826.

[2] **M.I. Sciola**, P.D. Morris, P.V. Lawford, D.R. Hose, J.P. Gunn, *Quantitative computational evaluation of cardiac and coronary physiology: preliminary results*, Proceedings of VPH conference 2016, Amsterdam.

[3] **M.I. Sciola**, P.D. Morris, P.V. Lawford, D.R. Hose, J.P. Gunn, *A novel mathematical signal processing application which automates and improves the accuracy of FFR assessment*, Proceedings of ESC Congress 2017, Barcelona.

ACKNOWLEDGEMENTS

First of all, I would like to express my sincere gratitude to my supervisors Prof. Rod Hose, Prof. Patricia Lawford and Prof. Julian Gunn for their academic, educational and psychological support during all my PhD. This work would not be completed without your supervision.
I would like to thank Prof. Hose for his patience and his help in solving trivial problems, for the long discussions we had in all these years and his invaluable guidance.
My appreciation goes also to Prof. Lawford and Prof. Gunn, for their encouragement and support and their genuine attention since I started my adventure.

I would like to thank also Dr. Paul Morris for his clinical guidance and his help in the interpretation of the data, for his enthusiasm on computational modelling.
My acknowledgments are extended to the Mathematical Modelling in Medicine Group old and new staff members and students, who have been like a second family for me. To Steve for his technical support. To Chiara and Becky for their last-minute consultancy in statistics.

I would like to thank all my friends, who have been very supportive and encouraging even from distance and even if they did not understand what my PhD was about. In particular Federica with whom I shared the same PhD anxiety, although she has always been way more anxious than me.
Above ground, my thoughts go to my family: my father, my mother and my sisters, who have always believed in me. It is also their credit if I have reached this important achievement in my life.
Last, but not least, I would like to thank Marco for his patience, support and care during the most difficult moments, for his encouragement day-by-day. I am looking forward to return the favour soon.

CONTENTS

LIST OF TABLES

LIST OF FIGURES

LIST OF ABBREVIATIONS

AF: Atrial Fibrillation

CAD: Coronary artery Disease

CO: cardiac output

COPD: Chronic Obstructive Pulmonary Disease

DX: Diagonal Artery

EF: ejection fraction

FFR: Fractional Flow Reserve index

FFR_{CL}: FFR measured in Cathlab

FFR_{min}: FFR at peak hyperaemia

FFR_{stable}: FFR at stable hyperaemia

HR: heart rate

HTN: Hypertension

ICA: Invasive Coronary Angiography

LA: Left Atrium

LAD: Left Descendent Artery

LC: Left Coronary

LCX: Left Circumflex Artery

LMS: Left Main Stem Artery

LV: Left Ventricle

ESV: end-diastolic volume in the left ventricle

EDV: end-systolic volume in the left ventricle

MAP: mean arterial pressure

MI: Myocardial Infarction

P_a: proximal pressure

P_d: distal pressure

P_{DIA}: diastolic pressure

P_{SYS}: systolic pressure

PAS: Pulmonary Artery Sinus

PAR Pulmonary Arterioles

PAR Pulmonary Arterioles

PAT: Pulmonary Arteries

PCI: Percutaneous Coronary Intervention

PCP: Pulmonary Capillaries

PVD: Peripheral Vascular Disease

PVN: Pulmonary Veins

QCA: Quantitiative Coronary Angiography

RA: Right Atrium

RC: Right Coronary

RCA: Right Coronary Artery

R_{myo}: myocardial distal resistance

$R_{myo\ HY}$: myocardial resistance at hyperaemia

$R_{myo\ BL}$: myocardial resistance at baseline

ΔR_{myo}: absolute change in R_{myo}

$\%\Delta R_{myo}$: percentage change in R_{myo}

RV: Right Ventricle

SAR: Systemic Arterioles:

SAS: Systemic Aortic Sinus

SAT: Systemic Arteries

SCP: Systemic Capillaries

SV: stroke volume

SVN: Systemic Veins

V_{BL}: myocardial volume at baseline

Z_1: stenosis Poiseuille coefficient

Z_2: stenosis Bernoulli coefficient

CHAPTER 1
INTRODUCTION & BACKGROUND

BACKGROUND

This section presents an introduction to terms and concepts together with background review of the three essential components of this thesis.

- The anatomy and physiology of the cardiovascular system is reviewed, including the regulatory control maintaining adequate blood pressure and flow in all the organs.
- The use of mathematical models to study the cardiovascular system is widespread and the literature provides access to an enormous number of *in silico* studies on the cardiovascular system. Models, from 0 dimensional to 3 dimensional, are used separately or in combination, to represent a specific cardiovascular compartment or the overall cardiovascular system. In the current project, the 0-D model (lumped-parameter) model has been chosen to represent system physiology, using the electric-hydraulic analogy.
- At the end of this chapter, the focus will move onto the clinical context of coronary artery disease. Diagnostic and therapeutic processes are discussed, including angiography and the use of the Fractional Flow Reserve index.

OVERVIEW

The cardiovascular system plays an essential role in transporting the blood and carrying metabolites, to and from all the tissues in a body. The coronary arteries are responsible for supplying blood to the heart muscle (the myocardium), enabling its pumping function [1, 2]. In common with many other arteries, coronary arteries can be affected by arterial disease with plaque deposition resulting in stenosis which may lead to a reduction of the blood flowing to the myocardium. Vessel narrowing can result in an inadequate blood supply (myocardial ischemia) and limit the quantity of metabolites which can be transported to and from the myocardial cells. In severe cases, this can lead to death [3, 4].

Quantification of the reduction in blood flow to the myocardium has been demonstrated to be a valuable diagnostic and prognostic tool in the evaluation of the impact of coronary disease. Moreover, the reduction in flow is linked to the physiological state of the patient (for example the reduction might be greater in an exercise state). A computational model can be a powerful aid in this context since it has the potential to be employed to quantify the effect of the stenosis under different physiological states.

A major challenge in the development of a computational model for diagnostic purposes in an individual patient is the personalisation of the model, which consists of a selection of the parameters values to represent the individual cardiovascular model. The success of the process, and the degree to which a model can be personalised, is critically dependent on the availability, and quality, of measured data. Typically, a wealth of clinical information is accessible, including patient demographics, comorbidities, laboratory test results, and images. However, physiological information (such as pressure and flow data) that can be used directly to tune the model is often insufficient and, indeed, as will be demonstrated in this thesis, may often be contradictory.

It is evident that the chances of a computational work flow being adopted into the clinical process will be greater if the information already collected as part of the routine clinical protocol can be exploited to provide the inputs rather than requiring new measurements which will inevitably increase costs. Of course, this point of view may change as confidence in the process increases and as savings associated with better diagnosis and management are quantified but, for now at least, this remains the pragmatic starting point.

The clinical community is increasingly aware of the importance of physiological assessment of the severity of the stenosis [5, 6] and technology provides an important aid to achieve this [7, 8]. Angiography has become the gold standard clinical procedure to visualise the lumen of the diseased coronary artery. This process requires catheterisation of the patient to provide access to inject a radio-opaque agent directly into the coronary artery of interest [http://www.nhs.uk/]. Images of the diseased artery are then evaluated by clinicians to determine the severity of the stenosis and hence the best treatment. This evaluation might be subjective, but more often it is based on a quantitative measurement derived from the image data (Quantitative Coronary Angiography, QCA). However, the assessment of the severity of the stenosis based on anatomy alone is a major limitation. For this reason, the concept of Fractional Flow Reserve index (FFR) has been introduced to support assessment of the physiological severity of the stenosis during angiography [5, 9, 10]. The FFR represents the stenosis severity as the ratio between the hyperaemic coronary flow in presence of the lesion and the hyperaemic coronary flow that would be expected in the absence of disease. In order to measure this, it is necessary to stimulate hyperaemia, under the assumption that when the coronary flow is maximum the impact of the lesion is more evident.

Although the clinical merit of FFR is recognised across the world, it is still conducted in only a small percentage of patients primarily due to the necessity of skills and the increase of procedure's costs and time [11]. Furthermore, the lack of a standardised protocol leads to inter-

operator variability [12]. These concerns have motivated the development of the concept of a virtual FFR (vFFR) [13], which could be introduced as an addition to the angiography and bring more objectivity in the lesion severity assessment.

The clinical process of FFR measurement produces exactly the type of physiological information that can be used to personalise (tune) a computational model. The pressure data is collected over the transition from resting to hyperaemic state resulting from the administration of a hyperaemic drug (adenosine). An immediate benefit of the personalisation of a mathematical model of coronary flow to reproduce the patient measurements is that it might be possible to derive relationships between the model parameters and the broader patient characteristics. These relationships could then be used predictively in a vFFR model for those cases when FFR has not been measured clinically, making assessment less invasive.

AIMS AND OBJECTIVES

The challenges of vFFR computation are described by Morris *et al.* [13]. The local pressure/flow characteristics of the lesion itself can be computed from its anatomy, using Computational Fluid Dynamics, but it remains a major challenge to estimate the patient- and vessel-specific distal resistance associated with the smaller vessels in the myocardium.

The primary aims of the project described in this thesis are:

1. to characterise the time-course response of coronary pressure and flow under a change of physiological state, and specifically during the administration of adenosine in the clinical protocol for induction of coronary hyperaemia;
2. to investigate correlations between patient parameters and myocardial resistance, and with changes of myocardial resistance in the transition from a baseline to a hyperaemic state.

To support the characterisation of response, and the understanding and interpretation of these characteristics, the secondary aims of the project are:

i. to develop a model to represent the clinical process, including significant compartments and regulatory mechanisms;
ii. to personalise the parameters in the model to describe the response of individual patients in which coronary pressure is measured and coronary flow is evaluated with CFD.

1.1 THE CARDIOVASCULAR SYSTEM

The cardiovascular system distributes blood to tissue and organs throughout the body, supplying them with nutrients, such as oxygen, amino-acids, hormones, electrolytes, and removing waste products, such as carbon dioxide. The cardiovascular system plays an important role in the maintenance of homeostasis, e.g. stabilising the body temperature and pH, and it takes part in the immune response. This section presents a description of the anatomy and physiology of the cardiovascular system, with particular focus on the haemodynamic properties necessary to be represented in a model that is targeted at the description of pressure and flow distributions in the system and their changes under a change of physiological state.

1.1.1 Anatomy

1.1.1.1 Heart and systemic circulation

The cardiovascular system consists of the heart and a closed system of vessels (Figure 1.1). The heart is a four-chambered muscular organ, which pumps blood through the vessels distributing blood to all the tissues. The heart can be divided into left and right sides, each of which comprises an *atrium* and a *ventricle* separated by a valve; the *tricuspid valve* on the right side and the *mitral valve* on the left side. The ventricles are separated from the vascular tree by another valve, the *pulmonary valve* on the right side and the *aortic valve* on the left side (Figure 1.1). Within the vascular tree, two main circulations can be identified: the systemic circulation and the pulmonary circulation. The systemic circulation brings nutrients and removes waste products from the organs such as liver, kidneys, skeletal muscles, cardiac muscle, brain, intestine, stomach, etc.; the pulmonary circulation perfuses the lungs enabling exchange of oxygen and carbon dioxide in the blood [1, 4].

Vessels in different parts of the vascular tree have different structures and different properties. Arteries, the vessels that carry the blood away from the heart, are compliant.

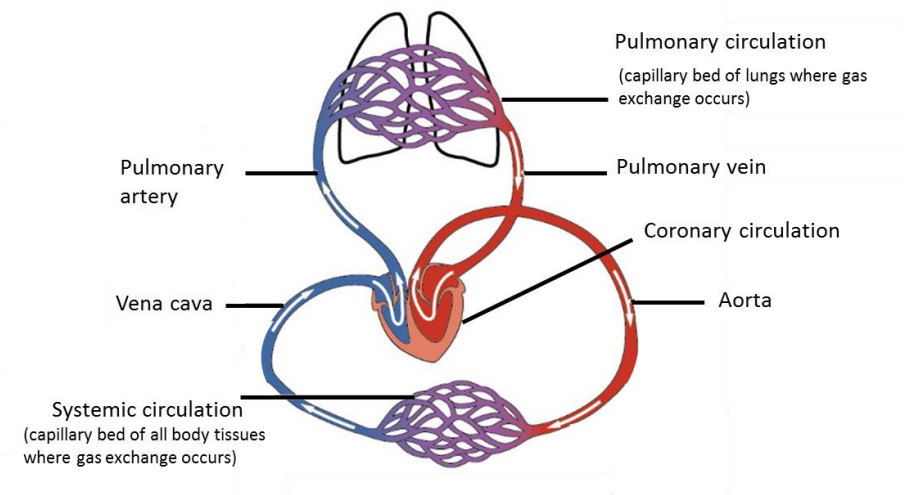

Figure 1.1: Simplified scheme of the cardiovascular system.
Figure adapted by OpenStax College [CC BY 3.0 (http://creativecommons.org/licenses/by/3.0)], via Wikimedia Commons- Creative Commons Attribution-Share Alike 4.0 International license copyright (https://commons.wikimedia.org/w/index.php?curid=30148235).

Whilst this generally results in a smoothing of the flow and damping of pressure pulses produced by the intermittent ventricular ejection [4, 14], there can also be local amplification of pulse pressures in the arteries associated with wave reflections. The typical range of vessel diameters is around 25 mm for the aorta decreasing, through a series of bifurcations, for the main arteries to 1-6 mm and for the arterioles to 30 μm. Capillaries are the small vessels within the tissues in which nutrients and waste are exchanged. They have a diameter of 5-6 μm [4]. Veins are very compliant vessels, which act as a blood reservoir and enable blood redistribution when physiological changes occur. They collect the blood from the upper body (superior vena cava) and lower body (inferior vena cava) returning it back to the heart. The diameter varies from 30 mm for the vena cava to about 0.5-5 mm for smaller veins [1, 4].

1.1.1.2 Coronary circulation

The coronary circulation provides nutrients to the heart muscle (the myocardium). Coronary arteries originate from the root of the aorta and branch to run over the surface (epicardium) of the cardiac muscle (myocardium). There are two main coronary arteries: the left and right (Figure 1.2). The left coronary artery divides into two branches to supply the left and the

anterior parts of the heart whilst the right coronary artery supplies the right and the posterior parts [1, 15]. Blood return from the coronary circulation is primarily via the coronary veins which drain into the right atrium [16, 17].

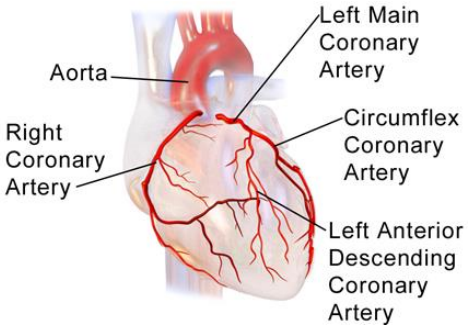

Figure 1.2: Anatomy of coronary circulation to the myocardium.
The left and right coronaries originate from the aortic root: the left supplies the left and anterior part of the heart, with its two main branches, circumflex and anterior descending, while the right supplies the right and the anterior part of the heart.
Figure by BruceBlaus (Own work) [CC BY 3.0 (http://creativecommons.org/licenses/by/3.0)], via Wikimedia Commons, via Wikimedia Commons- Creative Commons Attribution-Share Alike 4.0 International license copyright (https://commons.wikimedia.org/wiki/File%3ABlausen_0256_CoronaryArteries_02.png) .

1.2 PHYSIOLOGY

Blood circulation is a vital function: every cell in the body needs oxygen to carry out its functions and oxygen is supplied by the blood. Simultaneously, waste products derived from tissue metabolism need to be eliminated. Other functions of the cardiovascular system are: i) to maintain the fluid balance within the body; ii) to distribute the blood appropriately according to different activities; iii) to protect the body from infection and blood loss; iv) to maintain body temperature within the physiological range; v) to distribute hormones. In this project consideration of cardiovascular physiology is limited to the transport of oxygen and carbon dioxide and the regulation of blood flow and pressure to distribute blood volumes according to the adenosine stimulus.

1.2.1 System physiology

The cardiovascular system enables an appropriate blood supply to the different organs and tissues. The brain, a very delicate and vital organ, has high priority in terms of oxygen supply and, in consequence, cerebral blood flow is relatively constant. For other organs, blood flow is strongly related to need. For example, the skeletal muscles require more oxygen during exercise and the stomach and intestines are the most active organs during digestion; flow to these organs increases to meet these needs.

1.2.1.1 Physiology of regulatory pathways

The cardiovascular regulation acts to ensure the appropriate distribution of blood throughout the body and maintains appropriate blood pressures and flows [1]. There are two types of regulation: auto-regulation and neuro-regulation.

Auto-regulation is a process of local flow regulation. This has a higher impact and importance in delicate and vital organs such as the brain, heart and kidneys. The vascular tree in these organs responds intrinsically to changes in haemodynamics, aiming to maintain an appropriate flow and pressure. Auto-regulation is driven by myogenic and metabolic stimuli. The first of these is directly related to stretching of smooth muscles in the vessel wall which in turn controls the artery/arteriolar diameters, in order to create an appropriate pressure gradient and blood flow. The second is related to the minimum/maximum thresholds of concentration of nutrients/wastes and can increase or decrease the blood flow to meet local requirements.

Neuro-regulation is a more complex and sophisticated system involving the nervous system through the sympathetic and vagal pathways. In the cardiovascular system there are check points in the aortic arch and in the carotid artery, where baroreceptors check the pressure and chemoreceptors check the oxygen and carbon dioxide levels in the blood continuously. An afferent signal is sent from the receptors to the vasomotor centre in the medulla oblongata where, in response, an efferent signal is produced and sent back to the cardiovascular system

through the sympathetic and the parasympathetic systems. The chemoreceptor response is carried just by the sympathetic system, while the baroreceptor response involves both systems. The sympathetic system, responsible for the "flight-or-fight response", acts on the heart and vasculature, increasing the heart rate and changing the vascular resistance in order to increase the blood flow in the organs involved in activity.

The parasympathetic or vagal system, responsible for the "rest-and-digest" condition, compensates the effects of the sympathetic system by decreasing the heart rate (Figure 1.3). The system of regulation described thus far is classified as 'short-term' regulation, and acts over a timescale from a few seconds to a few minutes. There is also a 'long-term' mechanism which acts over hours and involves the kidneys and hormonal system. Since the focus of this thesis is on the short-term response to the administration of adenosine, a surrogate for an exercise state under which coronary flow is maximum, long-term regulation is considered to be out-of-scope and not discussed in detail here.

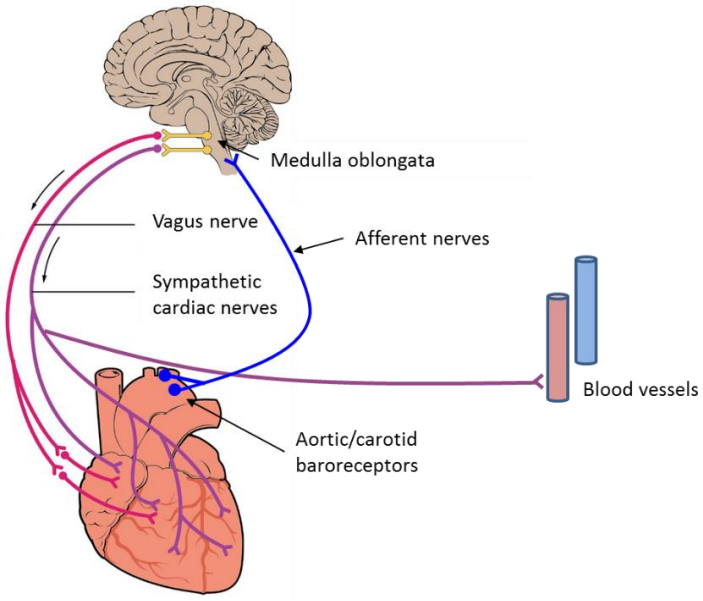

Figure 1.3: Scheme of baroreceptors reflex diagram on cardiovascular system.
Aortic sinus and carotid baroreceptors send signal to the vasomotor centre in the medulla oblongata through the afferent nerves. The information is integrated and the sympathetic and parasympathetic (vagal) systems transmit the signal to the effectors: the heart and vessels. The sympathetic system can create different effects depending on the target organ. Chemoreceptors act in a similar way, but are confined to the sympathetic response. Figure adapted from OpenStax College - Anatomy & Physiology, Connexions Web site. (http://cnx.org/content/col11496/1.6/), Creative Commons Attribution-Share Alike 4.0 International license copyright (https://commons.wikimedia.org/w/index.php?curid=30148235).

1.2.2 Coronary physiology

Coronary blood flow differs from the systemic blood flow in the aorta (Figure 1.4) because of the phases of cardiac contraction which generate compression of the coronary microvasculature. During systole (the ventricular contraction and ejection phase) blood is ejected through the aortic valve into the aorta and systemic arteries and pressure and flow in the systemic circulation reach a maximum. However, during this phase, the myocardium is contracted and the coronary microvasculature is compressed thus impairing coronary flow. This explains the diastolic predominance of the coronary flow, an effect which is more pronounced in the left coronary system than the right due to relatively high left-ventricular pressures [3, 18].

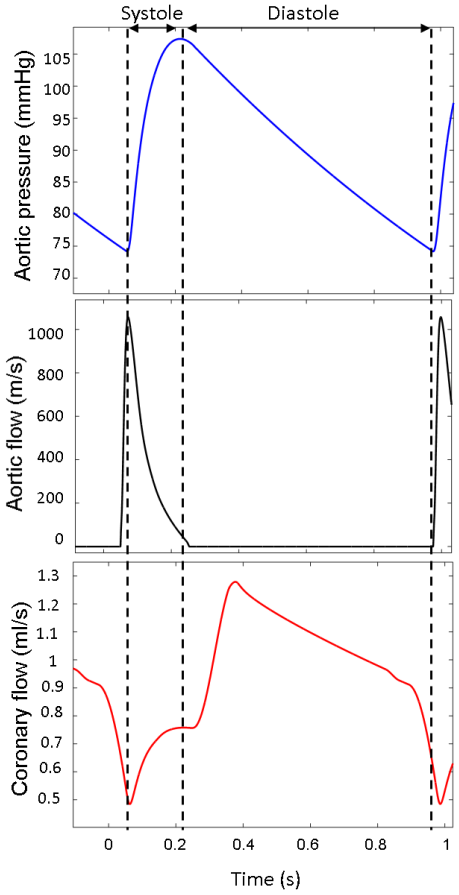

Figure 1.4: Coronary blood flow and aortic blood flow during cardiac cycle.
Typical coronary blood flow (red) wave shows a peak during diastole, due to contraction of the ventricle in systole, in contrast with the aortic flow that has a peak during systole.

1.2.2.1 Local regulation

While other tissues extract about 25% of oxygen from the blood at rest, because of the high density of capillaries (with approximately one capillary for each cardiomyocyte, i.e. the cardiac muscle cell), myocardial tissue is able to extract as much as 70% of the oxygen from the blood [15]. This high rate of extraction explains why, when the heart is working hard, during exercise for example, the myocardium needs access to more oxygen and nutrients and the only way to achieve this is to increase coronary blood flow.

Coronary blood flow (CBF) has been shown to be proportional to myocardial oxygen consumption [19-22] and it is driven by the regulation of the coronary resistance vessel tone, as the result of a huge number of vasodilator and vasoconstrictor signals. These signals are produced by several different mechanisms:

- the metabolic response in the coronary vessels is determined by pH, carbon dioxide concentration and adenosine-tri-phosphate (ATP) concentration. ATP reacts with adrenoreceptors to produce adenosine;
- the endothelium-derived response is sensitive to shear stress and pulsatile strain and therefore to blood flow;
- the autonomic nervous system innervates the coronary vasculature through its sympathetic and vagal pathways (the former is activated during exercise to contribute to vasodilation in a feed-forward manner, while the latter is the most active during the rest condition);
- aortic pressure, which determines the pressure gradient between the coronary arteries and the right atrium, where the coronary veins empty;
- myocardial extravascular compression;
- heart rate and cardiac output.

The dominant effect is the vasoconstriction/vasodilation of the small arteries and arterioles in the myocardium; these contribute 90% of the coronary resistance [20].

1.3 HAEMODYNAMIC MODELS

The working principles of the cardiovascular system have always fascinated scientists from the time of ancient populations [23]. The cardiovascular system can be represented as a closed-loop circuit (Figure 1.5), in which flow obeys the laws which apply to all physical fluid systems: the principles of conservation of mass and conservation of momentum [18].

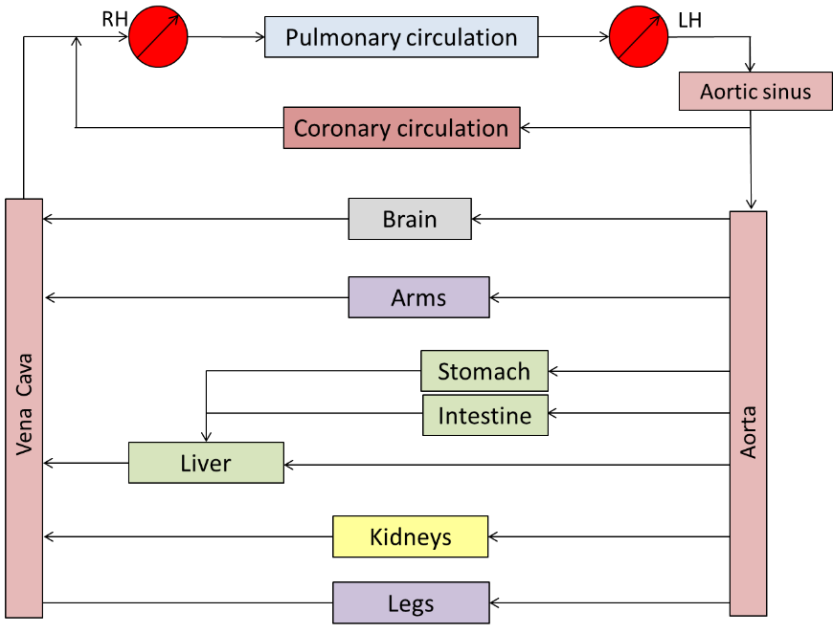

Figure 1.5: Basic representation of the cardiovascular system as a closed loop.

1.3.1 Physics of flow: governing equations

The principle of **mass conservation** asserts that the mass flow into a compartment must equal the sum of increase in mass in the compartment and the mass flow out. It is essentially expressed by the continuity equation (Eq.1.1), where ρ is the density of the fluid and v the vector of fluid velocity:

$$\frac{\partial \rho}{\partial t} + \nabla \cdot (\rho \boldsymbol{v}) = 0 \qquad \text{(Eq.1.1)}$$

The principle of **conservation of momentum**, which might be interpreted as an expression of Newton's second law, states that the rate of change of momentum of a fluid element is equal

to the forces acting on it and is expressed by Navier-Stokes equation for momentum (Eq. 1.2), where ρ is the density of the fluid, v is the fluid velocity vector, p is the pressure, μ is the fluid viscosity and f represents the external forces:

$$\rho\left[\frac{\partial \boldsymbol{v}}{\partial t} + (\boldsymbol{v}\cdot\nabla)\boldsymbol{v}\right] = -\nabla p + \mu\nabla^2\boldsymbol{v} + \rho\boldsymbol{f} \qquad \text{(Eq.1.2)}$$

Integrating the Navier-Stokes equation along a streamline and assuming a steady state condition with incompressible and inviscid fluid, the Bernoulli equation is obtained [24] (Eq. 1.3), where ρ is the flow density, v is the velocity of fluid, p is the pressure, g is gravitational acceleration and h is the elevation of the point above a reference plane:

$$p + \rho\frac{v^2}{2} + \rho g h = constant \qquad \text{(Eq.1.3)}$$

The vascular system can be represented as branching tree with each vessel defined by its length and radius. Each of the single vessels offers resistance to blood flow, which can be calculated by Hagen-Poiseuille's law (Eq. 1.4), where μ is the viscosity of blood, L is the characteristic length of the vessel and r is the vessel radius:

$$\Delta P = PR \cdot Q = \frac{8\mu L}{\pi r^4}\, Q \qquad \text{(Eq.1.4)}$$

Also the Hagen-Poiseuille law (Eq.1.4) can be derived from Navier-Stokes equation (Eq.1.2), assuming a Newtonian fluid, laminar flow, steady state condition in horizontal small tubes, where the gravity force can be ignored. These hypotheses can be valid in peripheral vessels, such as arterioles and capillaries, where the pulsatility is smoothed by the proximal high-compliance vessels, i.e. the main arteries.

From the Hagen-Poiseuille law (Eq.1.4) it is clear that the pressure gradient in the system is much more sensitive to a change in vessel radius than to a change in flow. Assuming μ and L to be relatively constant, a small variation of radius, which has exponent 4 in Eq.1.4, results in a significant variation in pressure gradient [25].

Another important principle applied to the cardiovascular system is the Frank-Starling law, which describes the relationship between the cardiac output and venous return. The main aim of this mechanism is to synchronise cardiac output and venous return, maintaining the blood pressure in the systemic and pulmonary circulations within physiological ranges and thus avoiding an unbalanced distribution of blood volume between the pulmonary and systemic circulations. The venous return changes according to particular stimuli: for example, it decreases when an individual stands up because the central venous pressure decreases; it increases during walking because the action of the calf muscles (calf muscle pump) helps to return the blood to the right ventricle. This variation of venous return brings about a change in left-ventricular filling pressure and, therefore, of stroke volume and cardiac output. The amount of blood filling the left ventricle determines the degree of stretch of the ventricular wall, which in turn influences the length of the contractile units (sarcomeres) within the cardiac muscle fibres. During systole the cardiac muscle fibres contract generating a force proportional to the initial stretched length [4, 26, 27]. An increase in contraction is related to an increase in myocardial metabolism which, in turn, is associated with an increase in demand for blood flow in coronary vessels.

Several physical quantities can be defined that characterise the operation of the cardiovascular system in a particular state, many of which might be measured clinically [28]. These include:

- heart rate (HR), the number of beats per minute;
- stroke volume (SV), the amount of blood volume ejected from the ventricle at each beat;
- cardiac volumes, in particular the end-systolic (ESV) and end-diastolic volumes (EVD) of the left ventricle, which provide information concerning the efficiency of the pumping heart;
- ejection fraction (EF), the ratio between SV and EVD;
- aortic pressure (P_{ao}), which can be distinguished in systolic, diastolic and mean aortic pressure (MAP);

- pulmonary pressure, the pressure in the pulmonary artery;
- cardiac output (CO), the volume of blood ejected into the systemic circulation in one minute. CO is related to the heart rate (HR) and stroke volume (SV) as shown below (Eq. 1.5):

$$CO = HR \times SV \quad \text{(Eq.1.5)}$$

- peripheral resistance (PR), the resistance offered to the flow by the vessels of the systemic circulation. A number of factors influence this parameter, including vessel compliance, vasoconstriction and vasodilation mechanisms. PR can be estimated from the ratio of the mean arterial pressure and the cardiac output (Eq.1.6):

$$PR = \frac{MAP}{CO} \quad \text{(Eq.1.6)}$$

- pulmonary resistance, the resistance of the pulmonary circulation. In a similar way, this can be estimated from the ratio of mean pulmonary pressure and the cardiac output relative to the right ventricle.

1.3.2 Models of cardiovascular system

Different type of models can be used to represent and study the cardiovascular system. The main categories are lumped-parameters (zero-dimensional, 0D) and distributed-parameters (one-dimensional, 1D; two-dimensional, 2D; three-dimensional, 3D models). It is necessary to select the most suitable type of model depending on what is the aim of the study, on what are the features of interest and, moreover, on what are the clinical data available (Table 1.1) [29-31].

0D models are usually used to study the global distribution of pressure, flow and volume of blood under different physiological states. They represent the cardiovascular system in compartments, lumping together parts of vasculature with similar characteristics, and their blood pressure, flow and volume are exclusively a function of time. A system of differential

equations solves the conservation of mass, the conservation of momentum and the equilibrium between pressure and volume.

1D models are mainly used to study the wave propagation effect in the vasculature, especially for large arteries. Blood pressure and flow are function of time and of the cross-sectional area of the vasculature. This type of model requires pressure and/or flow curves and cross sectional area of the vessel as boundary conditions.

Table 1.1: Types of cardiovascular models with the described features and the clinical data required for personalisation.

Model type	Described features	Clinical data required
0D	Pressure, flow and volume distribution in compartments P(t), Q(t), V(t)	Pressure and flow upstream the model
1D	Pulsatility and wave propagation P(t, x), Q(t, x), V(t, x)	Pressure and/or flow curves as boundaries, radius variation along the vessel
2D	Variation of velocity profile in radial direction in axis-symmetric conditions P(t, x, y), Q(t, x, y), V(t, x, y)	Images for geometrical properties, pressure and/or flow curves as boundaries
3D	Complex flow patterns in specific region of cardiovascular system P(t, x, y, z), Q(t, x, y, z), V(t, x, y, z)	Images for geometrical properties, pressure and/or flow for boundaries conditions

2D models enable the study of the velocity variation in the radial direction for an axis-symmetric vessel model and they are often used in multiscale modelling with 3D models.

3D models are the most accurate model, where blood pressure and flow have a spatial and temporal distribution. Computational Fluid Dynamics (CFD) simulations can capture complex flow patterns in small region of the cardiovascular system, such as ventricles, heart valves, bifurcations. These type of model require geometrical details of the area of interest and, therefore images need to be available and processed. Moreover, boundary conditions in terms of pressure and/or flow are essential to perform the simulations. The computational cost for these models and the amount of input data increase massively and this is the reason why they are used to represent only small portions of the cardiovascular system.

For the purpose of this project and for the type of clinical data available, the 0D models have been selected. In the following paragraph these model are therefore the focus and they are going to be described.

However, the parameters of the 0D representation of patient-specific coronary stenoses, described in Chapter 6, have been determined from three-dimensional computational fluid dynamics analyses that represent in particular the convective acceleration and viscous dissipation in the complex flow fields and capture the nonlinear relationship between pressure gradient and flow.

1.3.3 Zero-dimensional or lumped parameters models

Zero dimensional models (also known as *lumped-parameter* models) are based on a combination of resistive, compliant and inertial elements, arranged in series or in parallel, to represent the cardiovascular system or specific part of it (compartment). Within each compartment the quantities are assumed to be spatially invariant; only temporal variations are represented. Such models can be mono-compartmental, in which the different components are merged into a single compartment that includes the properties of each, or multi-compartmental, in which the vascular system is divided into separate modelled compartments between which it is also possible to evaluate the interactions [30]. The development of these models is based on an electric-hydraulic analogy (Table 1.2) and Ohm's and Kirchoff's laws.

Table 1.2: Analogies between hydraulic and electric quantities.

HYDRAULIC	ELECTRIC
Pressure (P)	Voltage (V)
Flow (Q)	Current (I)
Friction	Resistance (R)
Compliance	Capacitance (C)
Inertial mass	Inductance (L)

1.3.3.1 Mono-compartmental models

The simplest model is the *2-element Windkessel* (1889-Otto Frank), a parallel RC circuit (Figure 1.6-A). This model was used to study the arterial tree in terms of P-Q relationships during diastole, considering pressure decay as characteristic time decay of RC circuit, although it cannot represent high frequencies of the arterial load to the ventricle [32]. The resistor represents the resistance offered by the network of vessels and the capacitor the arteries' capacity for blood storage [30]. The circuit is described by the following system of equations:

$$\begin{cases} Q_{in} - Q_{out} = C\dfrac{dP}{dt} \\ P_{in} - P_{out} = Q_{out} \cdot R \end{cases}$$

In 1971 Westerhof [33] developed the *3-element Windkessel* (Figure 1.6-B), introducing in series the characteristic aortic impedance, Z_0, which represents the resistance of large conduit arteries [34, 35]. Its value is equal to the ratio between the oscillatory pressure and the flow rate in the absence of reflective waves: $Z_0 = \frac{P}{Q}$. However, in lumped-parameters models the characteristic impedance of main arteries, which consists about 5-7% of the peripheral resistance, is often represented as a resistor generating small errors at low frequencies [34]. The equations that describe the model are:

$$\begin{cases} Q_{in} - Q_{out} = C\dfrac{dP_C}{dt} \\ P_{in} - P_{out} = Q_{in} \cdot Z - Q_{out} \cdot R \end{cases}$$

Burattini in 1982 [36] proposed the *4-element Windkessel*, introducing an inductance, L, which represents the inertial behaviour of blood flow in the arterial vessel [37]. This can be inserted in series or in parallel with Z_0 and each circuit has different solving equations and different values of L (Figure 1.6- C, D). Whilst this model works well at all frequencies, it is difficult to estimate a value for the inductance. For this reason the 3-element Windkessel is often chosen

to represent the global behaviour of arterial system using physiologically estimated parameters, although it is not able to represent wave propagation [34].

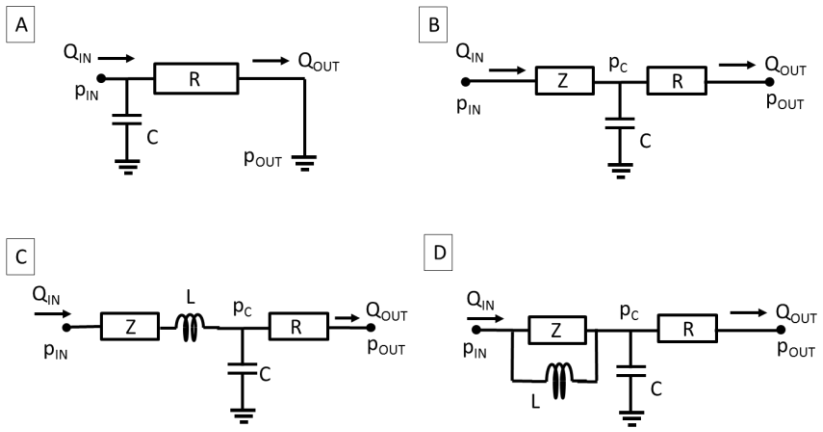

Figure 1.6: Most used lumped-parameter models.
A) 2 element- Windkessel electrical analogue model. B) Windkessel model with 3 elements. C) 4-element Windkessel model with the inductance L in series. D) 4-element Windkessel model with the inductance L in parallel.

More elements can be added to these models and arranged in different ways, aiming to represent parts of the vascular system with greater accuracy. Here it should be recognised that a value needs to be found for each additional element and often it is not a simple task to define or measure this.

A multi-compartmental model has been chosen as the basis for the current study (see Chapter 2 for more details).

1.3.3.2 Modelling cardiovascular system and regulatory pathways

Inspired by the work of Guyton [38], many scientists have developed different mathematical models to represent the cardiovascular system in terms of its multiple aspects and functions with the final aim of building a virtual model capable of including the entire human cardiovascular system. Several models of varying levels of complexity have been used to describe the physiology of the cardiovascular system. A mathematical model of the pumping left ventricle was developed by Suga *et al.* [39]. Both pressure and volume curves of the left ventricle were defined. The ratio between pressure and volume during the cardiac cycle

represents the contraction activity of the ventricle (E(t)). This depends on the highest value of the pressure and volume ratio (E_{max}) and its relative instant in the cardiac cycle (T_{max}). This model of the heart has subsequently been widely used by others and adapted for all the cardiac chambers.

Shi *et al.* [40] describe different models of closed-loop circulation, including the left and right heart with the systemic and pulmonary circulations. Both systemic and pulmonary circulations comprise different mono-compartmental elements, representing the arteries, arterioles, capillaries and veins, arranged in series. Each cardiac chamber is represented by a variable elastance with its specific contractility function. The cardiac valves, represented as diodes, guarantee unidirectional blood flow. This complete model describes the pressure curves in the arteries, veins and heart and the volume curves for the ventricles and atria. The results obtained are realistic and physiological in terms of pressure and flow in the atria and ventricles. Curated implementations of these models are publicly available from the CellML Model Repository [https://models.cellml.org/cellml]. This Repository, established and maintained by the Auckland Bioengineering Institute (ABI) [https://www.auckland.ac.nz/en/abi] in New Zealand, aims to support the biomedical modelling community by making available a series of published models, in a consistent format, that is curated to ensure that the produced results are consistent with the original published data.

A more complete model was developed by Liang *et al.* [41]. Here, the heart model includes the interaction between left and right heart and considers the ventricular inter-septal pressure [42]. The model includes different compartments: the vena cava, aorta, cerebral and upper limb circulations, pulmonary circulation, renal circulation, splanchnic circulation and lower limb circulation. The results are realistic for both the healthy system and that with heart dysfunction. One drawback of this model is the large number of parameters which must be defined, especially in regional segments of the circulation. This highlights a particular issue that is of

fundamental importance to the work that is presented in this thesis: the very simplest models are able only to represent the simplest responses, whilst increasing complexity in the model can represent more of the physiological phenomena and responses and provide an increasingly faithful representation of the systems physiology. This is excellent when the purpose of the model is to increase understanding of the system, and to evaluate the likely contributions of a multitude of parameters and effects to the system response. However, when the purpose of the model is to describe the physiological characteristics and responses of a specific individual, the sparsity of the available clinical data upon which the model can be personalised, especially if the intent is to use only data that is collected in the standard clinical pathway rather than under a research protocol, necessarily limits the number of parameters that can be included in the model.

In recent years, with increasing emphasis on the use of personalised models to describe individual cardiovascular physiology, there has been a renewed interest in the identification and operation of the simplest models that can be personalised from minimal clinical data [43]. It has been demonstrated that even the simplest models, when personalised to the individual, might have important diagnostic utility [44].

Within this thesis the aim is to select the simplest model that can describe the phenomena of interest, in order to facilitate the personalisation of parameters for an individual patient. The aim is to predict how an individual responds to a change of state.

Recently research focus has been concentrated on the definition of the cardiovascular regulatory system, or parts of it, with different models, simulating healthy individuals and patients with different disease under different conditions.

Ursino and co-workers [45-53] developed a number of different models to study how the blood pressure and the concentration of oxygen influence the response of efferent pathways and the local regulation of cardiovascular system. Aortic baroregulation, chemo-regulation as function

of the partial pressure of oxygen and carbon dioxide, metabolic regulation driven by the local effect of oxygen and carbon dioxide concentrations and the action of lung stretch receptors on tidal volume during respiration were implemented. The results obtained show a good representation of the effect of each regulatory system analysed for a generic individual, during simulation of haemorrhage and variation of the oxygen partial pressure in the aorta. Ursino's models were also used by Fresiello *et al*.[54] to develop a baroreflex cardiovascular model, which can represent the exercise condition in healthy individuals and patient with heart failure, providing an educational and clinical tool. In addition Fresiello *et al*.[55] developed a model that can be used for patient-specific purposes using some measured data, including patients with VAD devices, drug infusion representation and pre-set disease.

The same research group developed a 0-D model of cardiovascular system including the baroreflex model to study the general effects of early inflation, late inflation and length of inflation of the intra-aortic balloon pump (IABP) with particular regard to aortic receptors at the site where the device is located [56, 57].

Ursino's regulatory model focuses on a number of effectors (ventricle pumping function, systemic resistance, heart rate and venous unstressed volume), which are analysed in more depth in Chapter 2. This type of control is relevant for the study of the adenosine response, in terms of the aortic pressure and heart rate effects, and for its implementation in the cardiovascular model.

Other complex cardiovascular models with details of vascular compartments and regulation mechanisms were implemented with the purpose of understanding specific mechanisms, although here the representation of specific individuals is not possible.

In 2010 Cheng *et al.* [58] developed an integrated lumped cardio-respiratory model (PNEUMA) to study and understand the regulation of sleep in cases of obstructive or central sleep apnoea for a generic individual.

In 2011 Hester *et al.* [59] developed a integrative model of human physiology (HumMod), with more than 5000 variables to describe cardiovascular, respiratory, renal, musculo-skeletal system including the neural, endocrine and metabolic physiology. This complex model is based on empirical data from the peer-reviewed literature and the interface allows parameters and conditions to be modified manually. Although tuning 5000 variables is impossible for patient-specific applications, this model is a great tool for investigating the human body and for research and education purposes.

Blanco *et al.* [60] built a coupled 0D-1D-3D closed-loop cardiovascular model, with 0D model of baroreflex to simulate the generic response to haemorrhage, valvular disease and cerebral aneurism and understand the influence of the barocontrol in a generic individual or patient. Similarly, Neidlin *et al.* [61] developed a 3D aortic arch model coupled with a 0D baroreflex component to study the cerebral circulation during cardiopulmonary by-pass surgery with a 2-way coupled fluid-structure interaction.

Mantero *et al.* [25] developed a model of the complete circulation including coronaries and a control loop to regulate the effect of heart rate on aortic flow. The coronary circulation is represented as a single branch in parallel with the systemic circulation and, in order to represent the intra-myocardial pressure during systole, the myocardial compliance has a pressure generator. The control loop is able to represent different physiological conditions, such as rest and exercise, and the response of the heart rate, contractility and cardiac output to the oxygen demand, by comparing with a threshold for both coronary and aortic flows. Results show good agreement with the natural cardiovascular behaviour.

Other types of integrated cardiopulmonary models with regulation were published to represent the generic system of healthy individuals or groups of patients with certain pathologies in order to compare the response to different stimuli such as exercise [54, 62], orthostatic stress test [63, 64] and Valsalva manoeuvre [58, 65].

In summary, many lumped parameter models have been developed to describe and to represent the physiology of the cardiovascular system. The level of complexity, and processes represented in the model, depend on the question or hypothesis addressed. The majority of studies focus on the representation of physiological processes and the facility to describe known phenomena rather than on the operation for diagnostic or prognostic purposes for an individual. Complex models incorporating multiple parameters represent a major challenge; it is important to understand the sensitivity of the model outputs to its inputs so that an appropriate subset of parameters can be personalised to the individual physiology. For the current study it is important to understand which processes are important in this specific context of coronary physiology. This is the focus of the next section.

1.3.3.3 Modelling the coronary system and physiology

The coronary circulation has recently become a key area of interest for the application of lumped parameter models. Largely due to the high incidence of coronary pathologies [25, 66-75], the coronary circulation is an application of great interest, in which lumped parameter models have significant potential both to improve understanding and to represent changes of physiological state in an individual. Whilst some of these studies aim to reproduce pressure and flow in the coronaries (patient-specific and generic) with mathematical models and use them as a tool for understanding and diagnosis, others are more focused on the regulation of the coronary circulation.

Maasrani *et al.* [70, 72, 73, 76] aimed to simulate the patient-specific coronary blood flow before and after coronary bypass grafting. Main coronary branches are represented by mono-compartment models, using resistors, capacitors and inertances, with parameter values obtained from vessel geometry averaged data (length and diameter). These are assumed to be the same for all patients. In contrast, the myocardial resistance and aortic pressure are patient-specific. In this way by knowing the patient coronary artery stenosis location and setting the

corresponding values of parameters in relevant branches, it is possible to evaluate whether myocardial blood flow is sufficient before and after the treatment.

Kim *et al.* [74, 77, 78] developed a 3D model of the aorta coupled with 0D models at the outlets representing the different branches. The model also included the coronaries and the left ventricle. MRI images and measurements were used to define the patient-specific 3D geometry of the aorta and the patient-specific blood flow in some of the aortic branches with brachial pulse pressure measurements used to personalise the function of the left ventricle. In this model the simple coronary compliance, represented by an ordinary capacitor, was distinct by the ventricular contraction activity, represented by a second capacitor with the back pressure applied. Simulations at rest and exercise in both healthy and pathological (coronary stenosis) conditions were performed, including a number of assumptions with regards to the change of cardiac output, heart rate and the peripheral resistance of the coronary circulation. Results of pressure, flow and wall shear stress in the coronary circulation showed that the implemented model is useful for prediction of specific-patient conditions, although many hypotheses and assumptions need to be made to represent the exercise condition.

Geven *et al.*[66] developed an *in vitro* model and a mathematical model for a simplified cardiovascular system, which included the heart, the systemic and coronary circulations, in order to study and reproduce coronary pressures and flows for both baseline and hyperaemic conditions, validating them against invasive measurements in a conscious man.

Manor *et al.* [79] described the coronary circulation with a 0D model including the epicardial coronaries and the intra-myocardial compartments, where the ventricular pressure is applied. The model is able to auto-regulate in case of an obstruction in the epicardial coronaries or in case of increase of flow demand, varying the capacitances according to the cross-sectional area.

Cornelissen *et al.* [80, 81] studied the control of the blood flow in a generic coronary arterial tree consisting of 10 resistors in series, each representing the properties of a class of vessel size.

The model aims to study the interaction of the different control mechanisms (myogenic, metabolic and shear stress) governing the coronary blood flow.

1.4 CORONARY ARTERY DISEASE

The heart must pump blood continuously in order to avoid tissue ischemia. If blood flow to the myocardium is impaired due to pathology, the heart is unable to continue to pump effectively and myocardial ischemia and, ultimately in severe cases, death are the consequences.

The incidence of coronary artery disease (CAD) increases every year all over the world in both young and old. CAD is the most common type of heart disease and is related with the life style habits (e.g. smoking, a diet high in cholesterol) and with other pathologies such as hypertension and diabetes. CAD is caused by plaque formation inside the coronary lumen. This impairs blood flow and thus the myocardial tissue does not receive all the nutrients it needs [82].

1.4.1 Clinical investigation

It is important to diagnose CAD at an early stage in order to avoid complications and symptoms such as angina and myocardial ischemia. This is also supported by the huge growth of technology in the last century especially with regard to clinical applications. There are a number of diagnostic techniques available in clinical practice and each of these provides different qualitative and quantitative information. Some examples of these diagnostic techniques are angiography (3D angiography, Invasive Coronary Angiography, CT Angiography, Quantitative Coronary Angiography, Rotational angiography), Positron Emission Tomography (PET), Optical Coherence Tomography (OCT) and Cardiovascular Magnetic Resonance (CMR). This thesis focuses on Invasive Coronary Angiography.

1.4.1.1 Symptoms: Baseline vs Hyperaemia

It is important to define the impact of a coronary stenosis. The same stenosis might represent a different severity if patient has a sedentary lifestyle or an active one. Different lifestyles

generate different levels of oxygen demand by the tissues and, therefore, a different workload for the heart to achieve the appropriate cardiovascular function. A condition of exercise or hyperaemia is thus a valuable way of determining the effect of the stenosis during increased myocardial flow.

1.4.1.2 Invasive Coronary Angiography

The most common diagnostic method for CAD is Invasive Coronary Angiography (ICA) [http://www.nhs.uk/]. ICA is a clinical diagnostic technique used to study coronary vessels in symptomatic patients, who are believed to have a significant coronary stenosis. The technique consists of inserting a guiding catheter into a peripheral artery (femoral or radial), pushing it into the aorta, along the aortic arch and into one of the main coronary arteries. A contrast agent is injected through the catheter to make the vessel lumen visible to X-rays. In this way it is possible to identify regions where the lumen is reduced (stenosis) and to quantify the occlusion (Figure 1.7-left).

Invasive Coronary angiography produces 2D images of the single coronary and the major limitation concerns the overlapping or foreshortening during the acquisition, which does not provide a valuable way to estimate the severity of the stenosis.

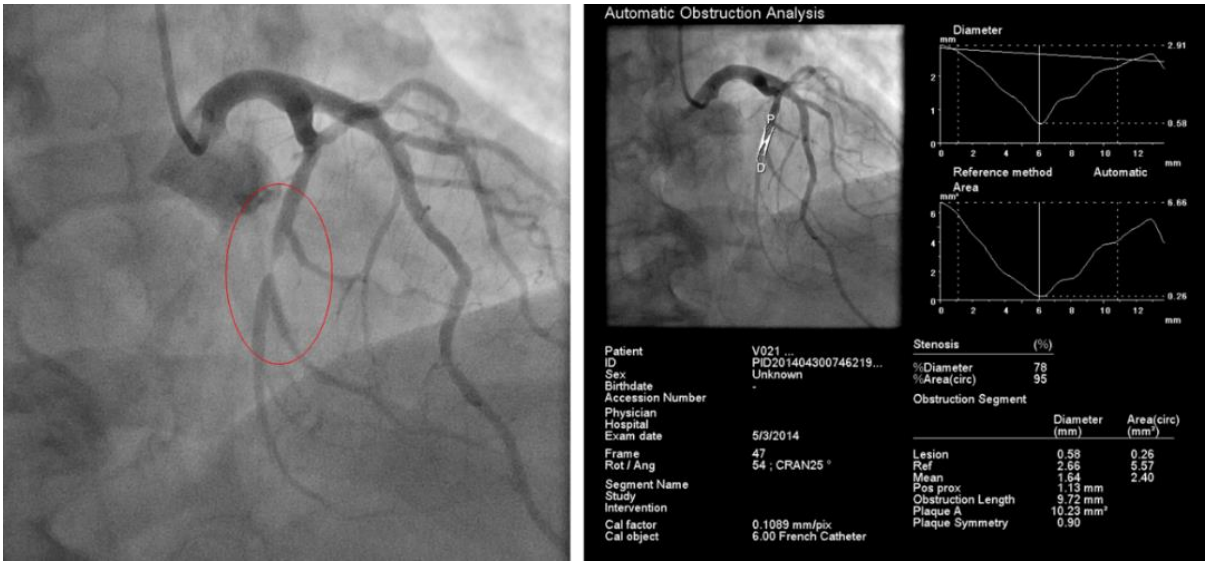

Figure 1.7: Coronary Angiography (left) and QCA (right) example in a case of stenosis of the circumflex coronary artery.

In the Quantitative Coronary Angiography (QCA), 2D images of the lumen of the vessel are provided as inputs to image reconstruction software in order to create 3D geometries of the coronary vessels, determining the contour of the lumen. This allows parameters related with the stenosis, such as the lesion length, the reference average vessel diameter, the minimal luminal diameter, the severity of stenosis, etc., to be estimated [83, 84] (Figure 1.7-right).

1.4.1.3 Fractional Flow Reserve index (FFR)

Following the publication of the results of the DEFER study in 2007, the Fractional Flow Reserve (FFR) index has been introduced into clinical practice to provide a more objective assessment of the lesions. FFR is a physiological index which gives information about the severity of the stenosis in the coronary arteries [5, 85-87]. FFR reflects the pressure drop across the stenosis: it is defined as the ratio between the maximum coronary flow in the presence of the stenosis and the maximum coronary flow that could be achieved if the stenosis was not present [10, 86].

The coronary stenosis can be represented as an electric circuit (Figure 1.8), in which P_A indicates the aortic pressure, P_V the venous pressure, P_D the distal pressure downstream the stenosis, R_S is the resistance offered by the occlusion and R is the physiological resistance in the coronary microcirculation.

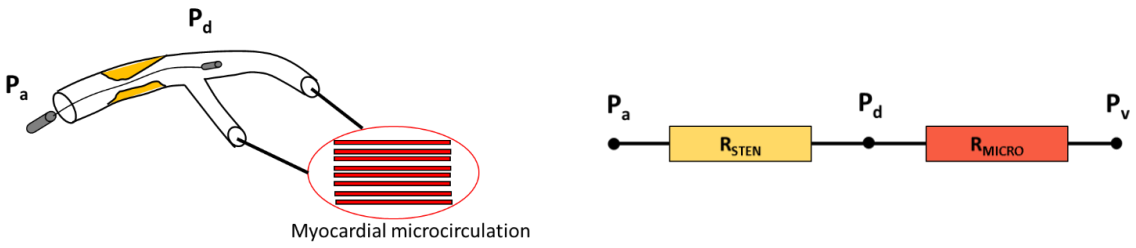

Figure 1.8: Representation of a coronary artery stenosis and myocardial microcirculation with corresponding lumped model.
The pressure guide measures the aortic pressure (P_a) and the distal (P_d) pressure across the stenosis when the microcirculation is vasodilated maximally. P_v represents the coronary venous pressure.

Considering the hypothesis that P_V is null, the resistance R has the same value irrespective of the presence of a stenosis and considering Poiseuille's law, FFR can be expressed as the ratio between the distal and the proximal blood pressure (Eq. 1.7):

$$FFR = \frac{Q_S^{max}}{Q_N^{max}} = \frac{(P_A - P_V)/(R_S + R)}{(P_A - P_V)/R} = \frac{R}{R + R_S} = \frac{P_D - P_V}{Q} \cdot \frac{Q}{P_A - P_V} \cong \frac{P_D}{P_A} \qquad \text{(Eq.1.7)}$$

During ICA, proximal and distal pressures across the stenosis are continuously recorded with catheters during intravenous infusion of adenosine, the drug routinely used to stimulate hyperaemic conditions. Hyperaemia refers to vasodilatation of myocardial microcirculation aiming to emulate the exercise condition, i.e. myocardial resistance decreases and coronary flow increases. The P_d/P_a ratio is continuously calculated from rest through to hyperaemia and the FFR is identified as the P_d/P_a during hyperaemia.

During the hyperaemic condition an increase, by a factor of 2, in coronary flow and a decrease of the P_d/P_a caused by the vasodilatory response of the myocardial microcirculation is observed when compared to resting condition. Myocardial resistance decreases to about 50% of the value observed at rest [10]. The variation of P_d/P_a demonstrates that the lesion has less effect at rest compared to the hyperaemic state, when the effect of the stenosis dominates and blood flow is mainly obstructed by the narrowing, reducing the influence of the microcirculation.

The cardiovascular auto- and neuro-regulatory mechanisms play primary roles in the hyperaemic response at pulmonary, systemic and coronary levels. Aortic pressure and heart rate increase as direct effect of adenosine response and the cardiovascular system responds by decreasing aortic pressure and heart rate. The evidence of this can be observed in the P_d/P_a behaviour, where peak and stable hyperaemic phases are normally achieved [10]. The FFR value is within the range [0; 1] with values between 0.75-0.80 indicating that the stenosis is responsible for significant myocardial ischemia [9, 10].

This index is used by clinicians to make decision about the treatment for each patient.

Different theories about the influence of haemodynamic conditions on FFR have been exposed. According to Pijls and De Bruyne [9, 10], pressure and FFR are independent, because of the linear relationship between pressure and flow (Poiseuille's law). However, Siebes *et al.* [87] demonstrated that in stenotic conditions, where there is likely to be turbulent flow, the pressure drop consists of viscous (A_V) and inertial (B) losses (Eq. 1.8):

$$\Delta P = A_V Q + B Q^2 \qquad \text{(Eq.1.8)}$$

Therefore, the stenosis resistance varies according to the blood flow and the approximation of FFR as P_d/P_a is imprecise. By calculating the FFR as ratio of resistances, its dependence on haemodynamic conditions becomes clearer (Eq. 1.9):

$$FFR = \frac{Q_S}{Q_N} = \frac{R}{R + R_S} \qquad \text{(Eq.1.9)}$$

where R and R_s are strictly related to the haemodynamic conditions determined by disease and the pressure gradient. Moreover, Siebes *et al.* [87] believe that other assumptions made in the calculation of FFR as P_d/P_a leads to an incorrect estimation. In particular, the downstream pressure P_V, which is assumed to be 0, actually depends on the aortic pressure, the venous pressure and the slope of the P-Q curve in coronary artery at maximum dilatation.

In this project the clinical FFR measurement is considered as the ratio between the distal and proximal pressure during stable hyperaemia and the resistance of the stenosis is described by the quadratic equation (Eq.1.8), which includes viscous and inertial losses.

1.4.2 Coronary Artery Disease models

As presented before, mathematical modelling is increasingly used to represent the cardiovascular system, whether considering the system as a whole or focusing on specific parts of it. In particular, models of coronary artery disease have been developed with different purposes, for example to study the wall shear stress, to estimate the myocardial microcirculation resistance, to predict the severity of the stenosis and to predict stent

deployment. A number of 0-D coronary circulation models have been already mentioned in paragraph *1.3.2.3 Modelling the coronary system and physiology*.

Image processing and Computational Fluid Dynamics (CFD) techniques have been integrated into a number of diagnostic examination processes such as angiography, Positron Emission Tomography (PET), Optical Coherence Tomography (OCT), Cardiovascular Magnetic Resonance (CMR). Using these techniques, the 3D structure of the vessel can be reproduced to be used in CFD and, thus, estimate different physiological parameters.

Wellnhofer *et al.* [88, 89] compared the wall shear stress in the right coronary artery in control patients, patients with CAD and patients with aneurysmatic CAD, employing a CFD analysis. The angiographic images from each patient were used to define the vessel geometry with the complete RCA side branches, with boundary conditions defined from Doppler measurement of the total blood flow, divided into branches proportionally to their respective diameters.

CFD analysis using patient-specific vessel geometries was also employed in the study carried out by Morris *et al.* [13]. Patient-specific geometries were obtained from 2D angiographic images from patients with CAD, stenoses were characterised in terms of viscous and inertial losses applying CFD analysis and a virtual FFR was estimated applying patient-specific pressures as the boundary conditions.

Li and co-workers [90] reconstructed the coronary geometries with branches using information from OCT and 3D-angiography to evaluate the effect of the branches, showing better accuracy for determining the blood flow and for shear stress evaluation with more complex models.

CFD can be also used for simulation of the implanted stent. Naghipoor *et al.* [91] studied drug release from a PLGA eluting stent using a computational study to investigate the growth of restenosis, the influence of the coated stent and the viscoelasticity of the arterial wall. This approach has the potential to be used as a predictive tool for the follow up-of stented patients.

This thesis considers a 0D model for the coronary circulation using the results of previous 3D CDF analyses, which characterised the stenosis pressure losses. This previous work was the subject of the thesis "*Computational Fluid Dynamics modelling of coronary artery disease*" submitted in 2016 by Dr Paul Morris [92].

1.5 CONCLUSIONS AND CLINICAL PERSPECTIVE

This chapter describes the project background in terms of its clinical and modelling aspects. The overall focus is the clinical investigation of coronary artery stenosis. Modelling is used to investigate the physiological effects of coronary obstruction under different conditions and predict the hyperaemic response to estimate FFR from a patient-specific model.

FFR has become a valuable tool in the clinical assessment of CAD and in guiding treatment decisions. FFR is able to identify ischemia causing lesions [93], improve clinical outcomes [94] and reduce long-term costs [95]. Despite these benefits, FFR remains underused (<10% patients have this treatment) due to increased procedural time/costs and lack of operator expertise; in general clinicians are more familiar with traditional angiography [11]. More recently, predictive models of FFR have been developed which provide the proven benefits of physiological coronary assessment without the factors limiting widespread use [13]. These have been relatively successful, but, because they make assumptions about coronary microvascular adenosine response (usually applying population-averaged data), a ceiling of accuracy appears to have been reached. The accuracy-defining step is how these models represent coronary microvascular physiology and response to adenosine on a patient-specific basis [96]. The focus of this thesis is on the development of a lumped-parameter model of the cardiovascular system. Features modelling the barocontrol system and the distribution of blood volume, adenosine and gases, all necessary to describe the adenosine response during hyperaemia, are also described. Clinical data from CAD patients undergoing Coronary Angiography are used as inputs for different analyses and classifications, including;

- tuning of the cardiovascular model at a systemic level and coronary level,
- identification of the minimum and stable FFR through an objective algorithm,
- classification of patient hyperaemic response.

The hypotheses and results associated with each topic will be presented in the rest of thesis.

1.6 THESIS OUTLINE

This PhD project has been organised into five main chapters plus introduction and conclusions.

This first chapter, *Introduction & Background*, provides a contextual overview of the relevant anatomical and physiological concepts of the cardiovascular system, of the clinical problem and of the state-of-the-art in 0D modelling.

Chapter 2, *Modelling the cardiovascular system*, provides a description of the 0-D cardiovascular model developed in this project in terms of the haemodynamics, the barocontrol system and the adenosine pharmacokinetics.

Chapter 3, *Modelling the response to the administration of adenosine*, describes the adenosine response in a generic individual considering what is reported in the literature. The relative influence between the systemic and the coronary circulation justifies the approach of personalising the two circulations separately.

The focus of Chapter 4, *Clinical data*, is entirely on the data collected during invasive Coronary Angiography, which have been processed to develop an algorithm to objectively identify maximal and stable hyperaemia and to classify patients on the type of adenosine response.

Chapter 5, *Personalisation of parameters of cardiovascular system*, illustrates the personalisation process of the global system, which allows to estimate the aortic adenosine concentration for each patient.

In Chapter 6, *Local tuning of coronary branches*, the focus moves on to the coronary personalisation providing a set of different patient-specific inputs to obtain myocardial adenosine concentration and resistance during adenosine injection, which have been considered to predict the adenosine response on patients' profile basis.

Chapter 7, *Conclusions and future work*, a final overview of the limitations and conclusions of this project in terms of results obtained is reported. Also future work and ideas for improvement are presented.

CHAPTER 2
MODELLING THE CARDIOVASCULAR SYSTEM

INTRODUCTION AND PURPOSE

The primary aim of the project is to construct and validate a computational lumped parameter model to represent the cardiovascular system in order to understand the effect of coronary lesions under different physiological conditions in a specific individual. The cardiovascular model to be introduced and developed in this chapter must include a representation of the coronaries and of myocardial flow. Ultimately, the model is applied to seek understanding of the physiological response of a specific individual and, because the measured clinical data available to support the model personalisation are sparse, the minimal set of parameters that need to be personalised to capture the basic characteristic measures of coronary physiology must be identified. The impact of the coronary stenosis is more evident during the short-term regulation mechanism where myocardial blood flow increases and the myocardial resistance decreases. An example of this is observed during the exercise condition, which is simulated metabolically during angiography by the infusion of adenosine.

In this chapter, the focus is on the development of an appropriate 0D model to represent the cardiovascular system, including the coronary arteries, to support the aims of the study. A published cardiovascular model, featuring representations of the heart and pulmonary and systemic circulations, has been extended to include the coronary circulation and the baro- and chemo-controls by the integration of other published models. Thus, the model developed is

able to represent the blood volume distribution and the species distributions in each compartment. The main components of this model are;

- the *cardiovascular circulation* described in terms of blood pressure, flow and volume,
- the *short-term regulatory mechanisms*,
- the *adenosine pharmacokinetics*.

This chapter provides a description of the implementation of these elements, justifying the choices that were made according to the challenges and the problems encountered.

2.1 LUMPED PARAMETER MODEL OF CARDIOVASCULAR SYSTEM

The lumped-parameter model is based on the electric-hydraulic analogy (see Table 1.1) and uses electric components such as resistances, capacitances, inertances and diodes to represent a hydraulic circuit.

This thesis is focused on the investigation of coronary flow under a range of physiological states, the latter described by a global circulation model operating under appropriate conditions. Starting from the global multi-compartmental model for a generic individual developed by *Korakianitis et al*.[40], which represents the whole cardiovascular system including the systemic circulation, pulmonary circulation and left and right heart, with respective cardiac valves, a coronary circulation divided into left and right branches was added in parallel with systemic circulation (Figure 2.1).

In order to represent the anatomy of the coronary circulation, the coronaries are introduced as an RCR circuit originating downstream of the aortic sinus compartment (SAS) and draining into the right atrium. To represent the ventricular contraction during systole, a back pressure proportional to the ventricular pressure was applied to the coronary compliance [25].

The distribution of volume in each compartment is a function of the initial volume and the difference of the inlet and outlet flow. The species distributions, in particular oxygen, carbon dioxide and adenosine, were estimated with a mass balance equation. Finally, the baro- and chemo-controls systems were introduced by adapting published models, as presented in the paragraphs which follow.

The reasons for this level of complexity in our cardiovascular model are firstly related to the implementation and curation in CellML repository and secondly because of its level of resolution which could eventually represent different physiological states.

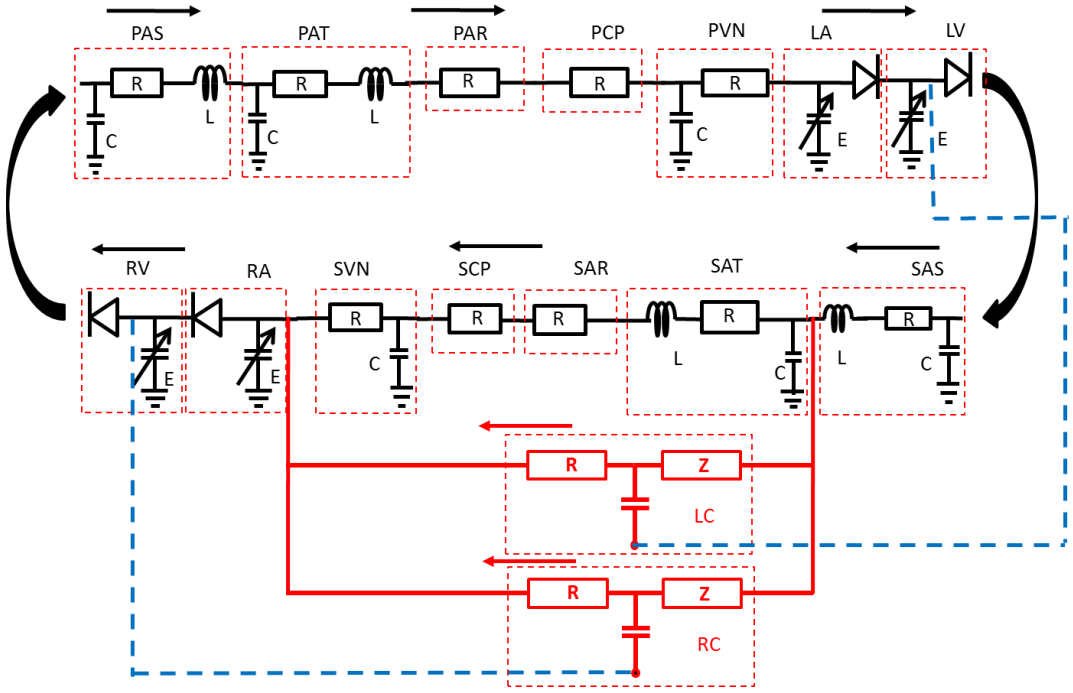

Figure 2.1: Zero dimensional cardiovascular model used in this project.
Compartments: systemic aortic sinus (SAS), systemic artery (SAT), systemic arteriole (SAR), systemic capillary (SCP), systemic vein (SVN), pulmonary artery sinus (PAS), pulmonary artery (PAT), pulmonary arteriole (PAR), pulmonary capillary (PCP), pulmonary vein (PVN), left and right ventricles (LV, RV), left and right atria (LA, RA). The coronary circulation comprises 2 branches (LC, RC) with the application of back pressure (blue line). Adapted from [40].

2.1.1 Haemodynamic system

This paragraph develops the equations which describe the haemodynamics for each compartment of the model, with respect to blood pressures, flows and volumes. As mentioned before, the global model including heart, systemic and pulmonary circulation was published in literature by *Korakianitis et al*. [40] and the equations of the model are reported.

2.1.1.1 Heart: chambers and valves

Each cardiac chamber (atria and ventricles) are defined as a variable elastance, which represents the contracting function, and a diode, which represents the valve (Figure 2.2).

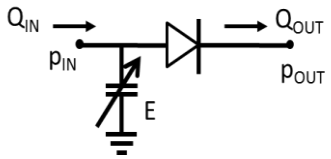

Figure 2.2: Variable elastance and diode for heart chamber.

The variable elastances, *E(t)*, are defined by a function of contractility, *e(t)*, as described in Eq.2.1:

$$E(t) = E_{min} + \frac{E_{min} + E_{max}}{2} \cdot e(t) \qquad \text{(Eq.2.1)}$$

where E_{MIN} and E_{MAX} are constants defined for each atrium and ventricle (Table 2.1).

For the atria *e(t)* is defined as in Eq.2.2:

$$e(t) = \begin{cases} 0 & if \quad 0 \le t \le T_{pwb} \\ 1 - \cos\left(\frac{t - T_{pwb}}{T_{pww}} \cdot 2\pi\right) & if \quad T_{pwb} \le t \le T_{pwb} + T_{pww} \\ 0 & if \quad T_{pwb} + T_{pww} \le t \le T \end{cases} \qquad \text{(Eq.2.2)}$$

where $T_{pww} = 0.09 \cdot T$, $T_{pwb} = 0.92 \cdot T$, considering T = 1 s.

For the ventricles e(t) is defined as in Eq.2.3:

$$e(t) = \begin{cases} 1 - \cos\left(\frac{t}{T_{s1}} \cdot \pi\right) & if \quad 0 \le t \le T_{s1} \\ 1 + \cos\left(\frac{t - T_{s1}}{T_{s2} - T_{s1}} \cdot \pi\right) & if \quad T_{s1} \le t \le T_{s2} \\ 0 & if \quad T_{s2} \le t \le T \end{cases} \qquad \text{(Eq.2.3)}$$

where $T_{S1} = 0.3 \cdot T$, $T_{S2} = 0.45 \cdot T$.

The outflow from each chamber or the flow through the valve at its outlet, Q_{out}, is determined by the trans-valvular pressure gradient, ΔP, modelled by a smooth diode for each cardiac valve. The pressure-flow relationship for a perfect diode is with a quadratic relationship between flow and pressure in the forward flow regime. The abrupt change at the origin tends to create instability in a numerical solver, and for this reason smoothing was introduced. The smoothing parameters were chosen to produce a reasonable behaviour in this region of the system, without impacting on the system behaviour during the main periods of systole and diastole. Each cardiac chamber is therefore described by the following system of equations:

$$\begin{cases} Q_{out} = \begin{cases} CV \cdot \sqrt{\Delta P} & \text{if } \Delta P \geq \text{th} \\ \frac{CV \cdot P_0}{2\sqrt{th}} \sin\left(\frac{\Delta P - th}{P_0}\right) + CV\sqrt{th} & if\ th - \frac{\pi}{2} < \Delta P < \text{th} \\ \frac{\left(\frac{CV \cdot P_0}{2\sqrt{th}} - CV\sqrt{th}\right)}{2}\left(\cos\left(\frac{\Delta P - th - \frac{\pi}{2}}{P_0}\right) - 1\right) & if\ th - \frac{3\pi}{2} < \Delta P < th - \frac{\pi}{2} \\ 0 & if \Delta P < th - \frac{3\pi}{2} \end{cases} \\ p_{in} = p_{ini} + E \cdot (V - V_{ini}) \\ \frac{dV}{dt} = Q_{in} - Q_{out} \\ \Delta P = p_{in} - p_{out} \end{cases}$$

where CV [ml s^{-1} $mmHg^{-0.5}$] represents the flow coefficient, p_{out} is the pressure downstream of the valve, p_{ini} and V_{ini} are respectively the pressure and blood volume always present within each specific chamber, Q_{in} is the flow in input in the chamber, th is the threshold used to define the smooth valve function, arbitrarily chosen below π/2 for the type of sinusoidal curves used to define the relationship in the region of null pressure gradient, P_0 is a reference value equal to 1 mmHg. Figure 2.3 shows the perfect diode and the smooth diode relationship obtained with th=0.25 and th=0.5. In this model a threshold value of 0.5 was selected.

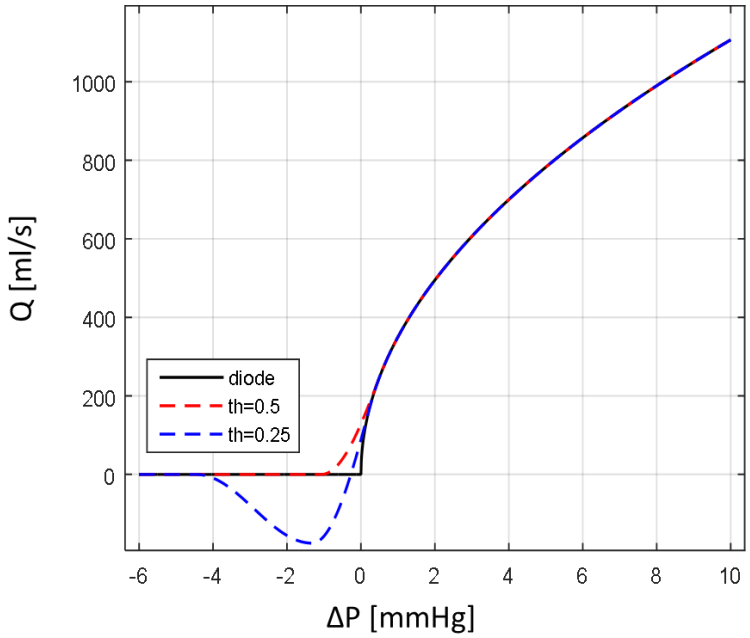

Figure 2.3: ΔP - Q relationship obtained with perfect diode and smooth diode.
ΔP and Q are respectively the pressure gradient and flow across the cardiac valve. The black line indicates the perfect diode, the blue and red dashed lines represent the smooth diode using two different thresholds (0.25 and 0.5 respectively).

2.1.1.2 Systemic and Pulmonary Vasculature

The systemic circulation is composed of several compartments (Figure 2.1): systemic aortic sinus (SAS), systemic arteries (SAT), systemic arterioles (SAR), systemic capillaries (SCP) and systemic veins (SVN). The pulmonary circulation has similar compartments: pulmonary artery sinus (PAS), pulmonary arteries (PAT), pulmonary arterioles (PAR), pulmonary capillaries (PCP) and pulmonary veins (PVN).

Both systemic and pulmonary sinuses and arteries are represented by a CRL circuit, the veins are represented by a CR circuit, arterioles and capillaries are represented by simple resistors. The resistances in the different compartments are considered to be linear and result in proportional pressure gradient and flow. Their values are not constraint by derivation from the Poiseuille's equation (Eq.1.4), but rather just to reproduce system measurements. The circuits and the systems of equations for each component are reported in Figure 2.4. Values used for each parameter in the model to represent a generic healthy individual are reported in Table 2.1,

except for the coronary parameters which are described in detail in the next paragraph (*2.1.1.3 Coronary modelling*).

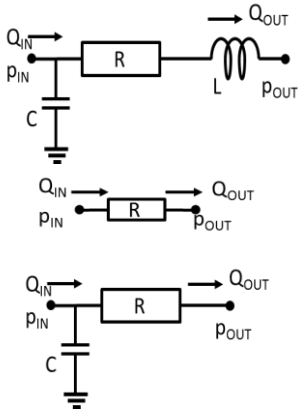

$$\begin{cases} C\dfrac{dp_{in}}{dt} = Q_{in} - Q_{out} \\ L\dfrac{dQ_{out}}{dt} = p_{in} - p_{out} - Q_{out} \cdot R \end{cases}$$

$$\begin{cases} p_{in} = Q_{in} \cdot R + p_{out} \\ Q_{in} = Q_{out} \end{cases}$$

$$\begin{cases} C\dfrac{dp_{in}}{dt} = Q_{in} - Q_{out} \\ p_{in} - p_{out} - Q_{out} \cdot R = 0 \end{cases}$$

Figure 2.4: Circuit components with relative system of equations. Artery sinus and main arteries (top), arterioles and capillaries (middle), vein (bottom).

Table 2.1: Values of constant parameters for the model parameters. Units: C [ml/mmHg], R [mmHg s/ ml], Z [mmHg s/ ml], L [mmHg s^2/ ml], V [ml], P [mmHg], E [dimensionless], CV [ml /s mmHg$^{0.5}$].

Left heart and systemic				Right heart and pulmonary			
C_{SAS}	0.08	V_{LVI}	500	C_{PAS}	0.18	V_{RVI}	0
R_{SAS}	0.003	V_{LAI}	400	R_{PAS}	0.002	V_{RAI}	0
L_{SAS}	0.000062	V_{LV0}	5	L_{PAS}	0.000052	V_{RV0}	10
C_{SAT}	1.6	V_{LA0}	4	C_{PAT}	3.8	V_{RA0}	4
R_{SAT}	0.05	P_{LV0}	1	R_{PAT}	0.01	P_{RV0}	1
L_{SAT}	0.0017	P_{LA0}	1	L_{PAT}	0.0017	P_{RA0}	1
R_{SAR}	0.5	E_{LAmax}	0.25	R_{PAR}	0.05	E_{RAmax}	0.25
R_{SCP}	0.52	E_{LVmax}	2.5	R_{PCP}	0.25	E_{RVmax}	1.15
C_{SVN}	20.5	E_{LAmin}	0.15	C_{PVN}	20.5	E_{RAmin}	0.15
R_{SVN}	0.075	E_{LVmin}	0.1	R_{PVN}	0.006	E_{RVmin}	0.1
P_{SAS0}	100	CV_{ao}	350	P_{PAS0}	30	CV_{pu}	350
P_{SAT0}	100	CV_{mt}	400	P_{PAT0}	30	CV_{tr}	400

2.1.1.3 Coronary modelling

The coronary circulation, in terms of left and right coronaries, was included in the 0D model as two Windkessel circuits which originate from the aortic sinus (SAS) and end in the right atrium (RA). In this generic model it is assumed that the left and right coronary parameters are equal. Each branch is represented by the circuit reported in figure 2.5 and described by the following system of equations:

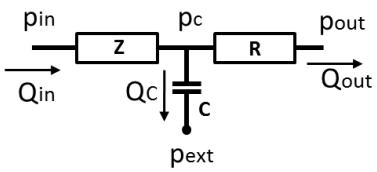

$$\begin{cases} p_{in} - p_c = Q_{in} \cdot Z \\ p_c - p_{out} = Q_{out} \cdot R \\ \dfrac{d(p_c - p_{ext})}{dt} = \dfrac{Q_{in} - Q_{out}}{C} \\ p_{ext} = \dfrac{P_{ventr}}{2} \end{cases}$$

Figure 2.5: 0D model of the coronary branches, using an external pressure on the capacitor.

The ventricular contraction effect on the coronaries was introduced with an external pressure, P_{ext}, set to half of the instantaneous left/right ventricular pressure for the left/right coronary. This was intended to represent grossly the spatial average of the pressure in the wall of the ventricle. The value of the total coronary resistance parameter was calculated with the hydraulic Ohm's law (Eq.2.4) using average values of pressure gradient and coronary flow for healthy adults. The pressure gradient is given by the difference of the aortic pressure (100 mmHg) and the right atrial pressure (15 mmHg), while the average coronary flow is around 1 ml/s per branch in baseline conditions [97]:

$$Z + R = \frac{\Delta P}{\bar{Q}} = \frac{100 - 85\ mmHg}{1 ml/s} = 85\ \frac{mmHg\ s}{ml} \qquad \text{(Eq.2.4)}$$

Typically, the arterial models represented with the 3-element Windkessel fit pressure and flow data distributing the total resistances as 10% in the proximal resistance, Z, and 90% in the distal one, R [98]. In the modelling of the coronary circulation, this distribution does not produce physiological flow results because of the back pressure applied to the capacitance. When the back pressure is active, it generates an outflow from the capacitor, forced to the direction of the proximal resistance because of its lower value compared to that downstream. To achieve typical coronary flow waveforms, with the characteristic diastolic dominance, the Windkessel model for coronary circulation works using the opposite distribution of the resistances. Thus, the values of the coronary parameters are:

$$Z = 76.5\ \frac{mmHg\ s}{ml} \qquad R = 8.5\ \frac{mmHg\ s}{ml}$$

The coronary capacitances were set to 0.9 ml/mmHg [25].

2.1.1.4 Blood volume distribution

An average adult male, with height of 1.70 m and weight of 80 kg, was considered to have about 5 litres of total blood volume, BV, according to Nadler formula [99] (Eq.2.5, Eq.2.6):

$$BV_{MALE}\ (l) = 0.3669\ \cdot Ht^3(m^3) + 0.03219 \cdot Wt\ (kg) + 0.6041 \quad \text{(Eq.2.5)}$$

$$BV_{FEMALE}\ (l) = 0.351\ \cdot Ht^3(m^3) + 0.03308 \cdot Wt\ (kg) + 0.1833 \quad \text{(Eq.2.6)}$$

In the cardiovascular system the total blood volume can be divided into:

- the unstressed volume, V_0, which fills the blood vessels without generating pressure;
- the stressed volume, which in the no-flow condition would generate an intravascular pressure of 7 mmHg [100], known as the mean systemic filling pressure (PMFC) [38, 101-104].

Blood volume (V) and pressure (P) in each compartment are proportional to the compliance (C) (Eq.2.7). The variation of the compartmental blood volume is calculated as the difference between the inlet flow, Q_{in}, and outlet flow, Q_{out}, (Eq.2.8).

$$V = C * P + V_0 \quad \text{(Eq.2.7)}$$

$$\frac{dV}{dt} = Q_{in} - Q_{out} \quad \text{(Eq.2.8)}$$

An initial value for V is required for the derivative equation (Eq.2.8) for each compartment. To select these values, data was obtained from the literature; the aim was to achieve a realistic distribution of blood volume in the system model and thus give realistic values for the distribution of the species of interest. The initial value of blood volume in each compartment is the average amount of blood that fills the specific compartment under pumping conditions. The specific example of the aorta (Figure 2.6) shows a change of volume between the end of systole (V_{max}) and the end of diastole (V_{min}), corresponding to the change of aortic pressure (120 and 80 mmHg respectively). The average value of blood volume (V_m) is the value used for the initialisation of the system, defined using different percentages of the total blood volume.

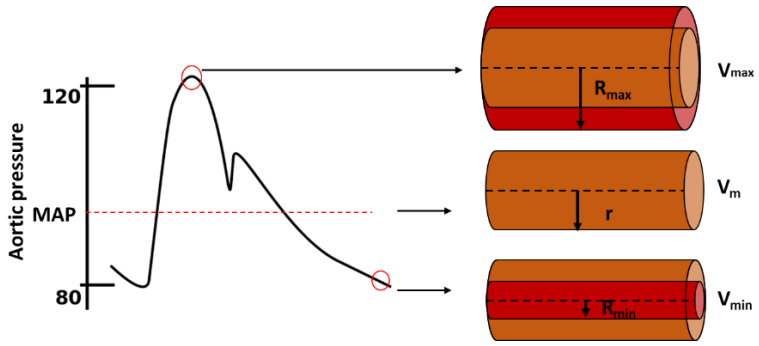

Figure 2.6: Representation of the change of the aortic volume during the systole and diastole. The mean aortic volume, V_m, is associated with mean arterial pressure, MAP (= 100 mmHg). The aortic volume increases during systole (P=120 mmHg) toward its maximum, V_{max}, and it decreases during diastole (P=80 mmHg) towards its minimum, V_{min}. Part of the figure is from Wikipedia Common (author Benutzer:Lupino, with public domain).

The blood volume was distributed based on data in the literature [1] (Figure 2.7), rearranging the percentages to take account of a difference in subdivisions of compartments.

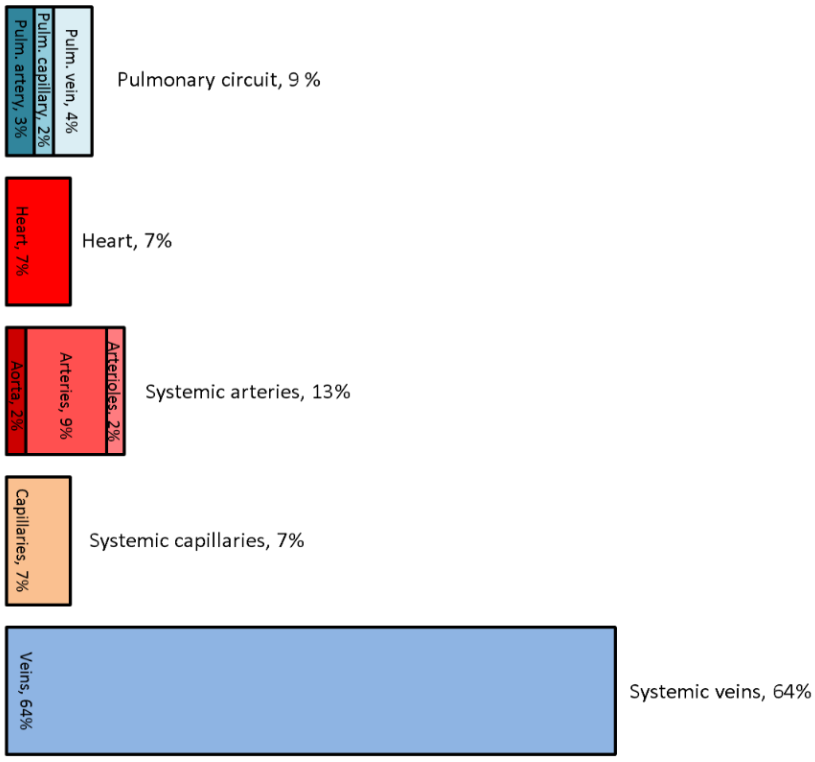

Figure 2.7: Distribution of blood volume in the cardiovascular system. (Blood volume distribution, Pearson Education, Inc.)

The total cardiac chambers volume was 387.5 ml, corresponding to 7.75 % of total volume. Coronary circulation is not included in the distribution in Figure 2.7. Data from the literature with regard to the amount of blood per 100 gr of LV (9 ml/100 gr LV, [105]) and the mass of

LV and RV [106, 107], allow the amount of blood volume in the whole myocardium of a generic adult to be estimated. If the heart muscle is represented as a hollow sphere (thickness of 7.5 mm [108]) filled by 350 ml of blood in the central cavity, which corresponds to the cardiac chambers, the mean radius can be estimated and, assuming that blood volume makes up 12% of the cardiac tissue [109], the computed volume of blood in the myocardial system is then 26 ml which corresponds to 0.52 % of the total blood volume.

The myocardial blood volume was sub-divided into left and right coronary circulation with 18 ml (0.36 %) and 8 ml (0.16 %) respectively, hypothesising a dominance of the left heart with a ratio between the left ventricle mass and the right ventricle mass of 2.3 [107].

The argument above provides a reasonable basis for the approximation of the volume of blood in the myocardium. This is an important parameter in the computation of the time-series response to adenosine infusion because it dictates the rate of blood 'turn-over' and concentration in the coronaries builds as the drug arrives in the aorta. Because this is important, a complementary estimate was determined by representing the coronary vasculature and microvasculature as an idealised branching tree (see Chapter 6). The geometrical branching rules were tuned to give an appropriate pressure gradient, based on Poiseuille's equation, and the volume computed. This gross approximation returned a computed volume that is similar to that estimated above. As mentioned previously, the initialisation volume in each compartment is necessary to provide a sensible distribution of blood volume in the cardiovascular system to calculate the concentration of species. The selection of such a complex cardiovascular model, which requires also the volume distribution, was made for different reasons. First, the aim was to develop a model from a CellML curated model which could be then shared in the repository. Second, if exercise needs to be simulated, this model could better represent the effects than a simple model.

For the systemic distribution, SAS, SAR and SCP compartments had 2%, 2% and 7% of total blood volume respectively. SAT volume was considered to be 9%, the sum of muscular and elastic arteries (4 and 5%).

The pulmonary arterial compartment has, in total, 3% of total blood volume and it is distributed among PAS, PAT and PAR compartments using the same proportions in the systemic compartment, with resulting percentage of 0.45%, 2.1 % and 0.45% respectively.

Moreover, starting from a value of 64%, the volume of the systemic veins, was set to 62.74% in order to redistribute a 0.76% excess in the heart and a 0.5% excess in coronary volume, ensuring that the sum of the percentages is 100%.

The blood distribution and the percentage for each compartment is summarised in Table 2.2.

Table 2.2: Distribution of blood volume (% BV) in each compartment of the cardiovascular model.

Compartment	% BV	Compartment	% BV	Compartment	% BV
LV	2.75	**SAS**	2.00	**PAS**	0.45
LA	1.22	**SAT**	9.00	**PAT**	2.10
RV	2.66	**SAR**	2.00	**PAR**	0.45
RA	1.13	**SCP**	7.00	**PCP**	2.00
LC	0.36	**SVN**	62.74	**PVN**	4.00
RC	0.16				

2.1.2 Oxygen and carbon dioxide distribution

2.1.2.1 Physiology

The most important and vital function of the blood is to carry nutrients and waste. In particular oxygen and carbon dioxide are transported between the cells and the lungs. Exchange of these gases occurs in the systemic and pulmonary capillaries by diffusion processes driven by pressure gradients. Although the specific focus of this thesis is on the representation of the response to infusion of adenosine as a pharmacological surrogate for the exercise condition, a longer-term goal is to simulate exercise itself. The model has been developed with the

possibility of this future extension in mind, and so a representation of oxygen concentration and its distribution has been included in the model formulation.

The concentration of a gas (C_{gas}) in a fluid is proportional to its partial pressure (P_{gas}) and the solubility coefficient specific for each gas/fluid combination (H) (Henry's law - Eq.2.9):

$$C_{gas} = H \cdot P_{gas} \qquad \text{(Eq.2.9)}$$

The value of H for oxygen/blood is 0.03 $\frac{ml\ O_2}{l_{blood} \cdot mmHg}$ [105]; the value of H for carbon dioxide/blood is 0.065 $\frac{ml\ CO_2}{l_{blood} \cdot mmHg}$ [110].

The relatively low solubility of oxygen in blood is compensated by the haemoglobin binding mechanism. Each molecule of haemoglobin, a protein found in the red cells in the blood, is able to bind 1.34 ml O_2 at the pulmonary level [111]. The blood concentration of oxygen is calculated considering both haemoglobin binding and Henry's law, as follows (Eq.2.10):

$$C_{O2} = 1.34\ [ml\ O_2] \cdot C_{haemo} \cdot SAT[\%] + H_{O2/blood} \left[\frac{ml\ O_2}{l_{blood}\ mmHg}\right] \cdot P_{O2}\ [mmHg] \qquad \text{(Eq.2.10)}$$

where C_{haemo} is the concentration of haemoglobin in blood and its value is 15 $\frac{g}{100\ ml_{blood}}$ [111]; SAT is the percentage saturation of haemoglobin depending on the partial pressure of oxygen. The relationship between the saturation of haemoglobin (SAT) and the partial pressure of oxygen (P_{O2}) (Figure 2.8) is described by Hill's equation [112] (Eq.2.11):

$$Sat(P_{O2}) = 100 \cdot \frac{1.39 \cdot 10^{-4} \cdot (P_{O2})^{2.7}}{1 + 1.39 \cdot 10^{-4} \cdot (P_{O2})^{2.7}} \qquad \text{(Eq.2.11)}$$

There are other parameters which influence haemoglobin saturation, but for the sake of simplicity these are not included in the model.

In the *pulmonary capillaries* oxygen is introduced into the blood from the alveolar air and carbon dioxide is eliminated from the blood. Typically, the partial pressure of oxygen (P_{O2}) in the alveolar air is 100 mmHg, whilst in the alveolar venous blood it is 40 mmHg, corresponding to a concentration of 15.2 ml O_2/ ml_{blood}; the partial pressure of carbon dioxide (P_{CO2}) in the

alveolar air is 40 mmHg, while that in the alveolar blood is 46 mmHg, corresponding to a concentration of 3 ml CO_2/ ml_{blood} [113].

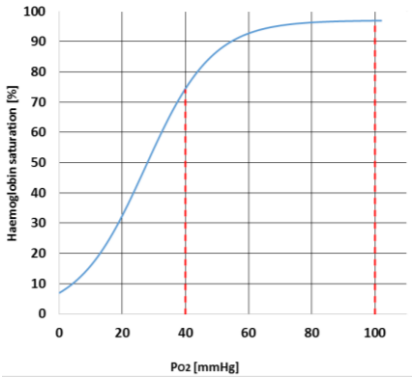

Figure 2.8: Haemoglobin dissociation curve.
The level of saturation of haemoglobin depends on the partial pressure of oxygen. The 2 red dashed lines represent the values of pressure and saturation in systemic capillaries (40 mmHg-75%) and pulmonary capillaries (100 mmHg-97%).

In the *systemic capillaries* the partial pressure of oxygen (P_{O2}) in the systemic arterial blood is 100 mmHg (i.e. a concentration of 20 $\frac{ml\ O_2}{ml_{blood}}$), while in the tissue it is less than 40 mmHg, the partial pressure of carbon dioxide (P_{CO2}) in the tissue is more than 46 mmHg, while in the blood it is 40 mmHg (a concentration of 2.6 $\frac{ml\ CO_2}{ml_{blood}}$) [113] (Figure 2.9).

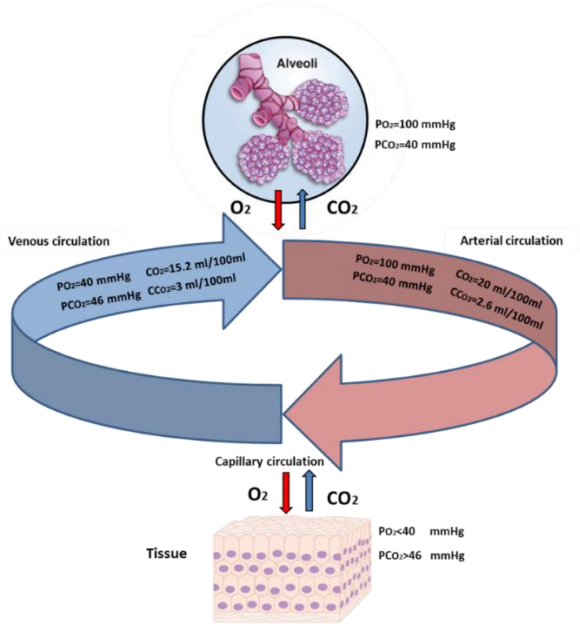

Figure 2.9: Oxygen and carbon dioxide partial pressures and concentrations in the cardiovascular system. The exchange of gases occurs only in the pulmonary and systemic capillaries, while the exchange in the vasculature is neglected. Part of the figure was adapted from Cancer Research UK / Wikimedia Commons and from UNSHAW/Wikipedia Common, both with Creative Commons Attribution-Share Alike 4.0 International license copyright.

2.1.2.2 Modelling

To represent the gases exchange and distribution, an equation of mass balance for each gas (Eq.2.12) was added to each compartment:

$$\frac{d\,(C \cdot V)}{dt} = \sum C_{in} \cdot Q_{in} - \sum C \cdot Q_{out} \qquad \text{(Eq.2.12)}$$

where C is the concentration of the species, V the blood volume of the compartment, Q_{in} and Q_{out} are respective the input and output flow in and from the compartment, C_{in} is the concentration of the species in the immediate upstream compartment. The assumption of instantaneous and homogeneous distribution of gases in each compartment is considered.

This derivative equation requires initial values for the amount of each species in each compartment. These were calculated as the product of the typical concentration in the compartment and its volume. For PVN, LA, LV, SAS, SAT, SAR compartments the partial pressure of oxygen was set equal to19.8 mlO_2/ml_{blood} and the partial pressure carbon dioxide equal to 2.6 $mlCO_2/ml_{blood}$. For SCP, RA, RV, PAS, PAT, PAR, PCP, LC and RC the partial pressure of oxygen was set equal 15.2 mlO_2/ml_{blood} and the partial pressure carbon dioxide equal to 3 $mlCO_2/ml_{blood}$.

A number of assumptions were made in order to represent the gas exchange mechanism in the model of the cardiovascular system:

- i) gas exchange/consumption at the level of the vasculature wall was neglected, and an assumption was made that this occurs in the capillaries (systemic, coronary and pulmonary) as represented in figures 2.9 and 2.10;
- ii) the amount of oxygen introduced in pulmonary capillaries (I) was equal to the amount of oxygen consumed in the tissues (E) and was calculated as the product between the SCP blood volume (V_{scp}, ml) and difference between the arterial and venous concentration (ΔC, ml_{specie}/ml_{blood}) (Eq.2.13):

$$I = E = V_{SCP} \cdot \Delta C \qquad \text{(Eq.2.13)}$$

- iii) the consumption of oxygen/emission of carbon dioxide in the systemic and coronary capillaries was constant, while in the pulmonary capillaries it was driven by the phase of respiration. During a breath, oxygen was introduced during the inspiration phase and the carbon dioxide was eliminated during the expiration phase. A respiration rate of 12 breaths/min (T_{breath}=5 s) was assumed, with inspiration and respiration phases equally distributed (T_{insp} = T_{exp} = 2.5 s). Therefore, the flow of oxygen introduced into the pulmonary capillaries during expiration is null and during inspiration is (Eq.2.14):

$$Q_{IN,O2} = \frac{V_{SCP} \cdot \Delta C}{T_{insp}} \qquad \text{(Eq.2.14)}$$

In the systemic and coronary capillaries, the flow of oxygen consumed is constant and equal to (Eq.2.15):

$$Q_{OUT,O2} = \frac{V_{SCP} \cdot \Delta C}{T_{insp}} * \frac{T_{insp}}{T_{breath}} \qquad \text{(Eq.2.15)}$$

The same approach was applied for carbon dioxide.

- iv) the elimination and introduction of gases at systemic and coronary capillaries levels was divided considering the proportions of their respective mean flows to the cardiac output (97.4% for systemic and 1.3% for each coronary) (Figure 2.10).

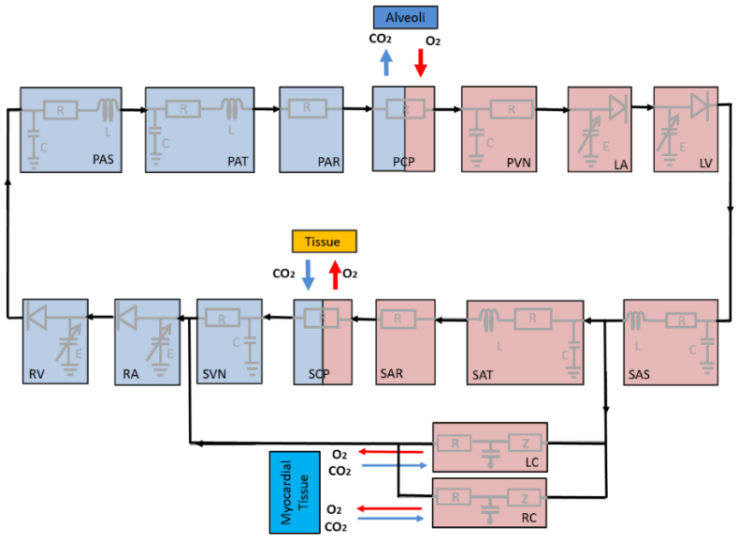

Figure 2.10: Cardiovascular model with gases exchange.
Oxygen and carbon dioxide are exchanged in pulmonary capillaries, systemic capillaries and coronary capillaries.

2.1.3 Neuro-regulatory and auto-regulatory systems

Regulation of the cardiovascular system occurs through the neuro-regulatory pathways, which involve sympathetic and vagal responses, and local auto-regulatory effect. The physiology of these systems has already been explained in Chapter 1 (Paragraph *1.2.1.1 Physiology of regulatory pathways*).

Ursino *et al.* [49, 52, 114] has developed controlled cardiovascular lumped-parameter models, distinguishing between splanchnic, extra-splanchnic, skeletal-muscle, brain and coronary compartments. The regulatory pathways implemented consist of the barocontrol and chemocontrol signals. The original model is in closed-loop with regard to the aortic pressure and therefore the barocontrol, while the chemocontrol is in open-loop, meaning that the partial pressures of the gases in blood are provided as an input to the model. Also the tidal volume for the respiratory compartment is just an output of the model, which does not influence the 0D elements of the pulmonary capillaries, where the exchange of gases is not implemented.

The barocontrol and chemocontrol were incorporated into the cardiovascular model by adapting the Ursino models as described in the following paragraphs. Figure 2.11 describes how the barocontrol and chemocontrol were implemented in the model, illustrating the effectors which were actually modified by the regulation.

Chemocontrol was implemented as closed-loop, providing the oxygen partial pressure in the aorta (SAS) as input for aortic chemocontrol, the oxygen partial pressure in the systemic capillary (SCP) for the systemic CSN hypoxic response and the average oxygen partial pressure in the left and right myocardium for the heart CSN hypoxic response.

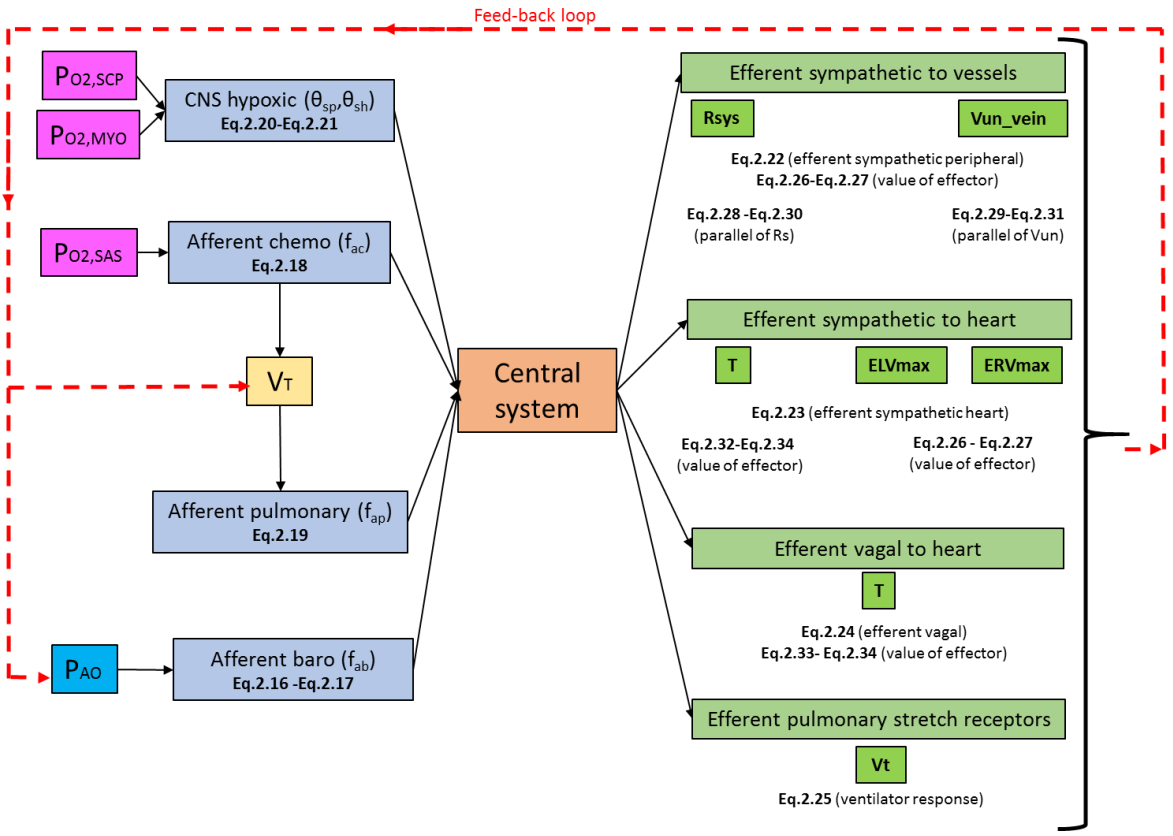

Figure 2.11: Scheme of barocontrol and chemocontrol system applied to the cardiovascular model. Each block is referenced to the describing equations listed in the following paragraph.
The central system receives the afferent signals from baroreceptors (influenced by the aortic pressure (P_{AO})), chemoreceptors and the CSN (central nervous system) for hypoxia (both driven by the partial pressure of oxygen (P_{O2})) and from pulmonary stretch receptors (indirectly influenced by the chemoreceptors through the tidal volume (V_T)). The central system then elaborates the efferent signals propagated through the sympathetic and vagal pathways. Sympathetic pathways act on systemic vessels in terms of resistances (R_{sys}) and venous unstressed volumes (V_{un_vein}), on the heart in terms of left ventricle elastances (ELV_{max}, ELV_{min}) and heart period (T) and on the pulmonary stretch receptors in terms of tidal volume. Vagal pathways act on the heart period (T). A feedback loop is sent back to P_{AO} and V_T.

2.1.3.1 Barocontrol and chemocontrol model

Following Ursino, the afferent signal to the central system includes:

- a baro-afferent signal (f_{ab}), expressed as a sigmoid curve (Eq.2.16) based on the first order derivative on the aortic pressure (P_{ao}) (Eq.2.17):

$$f_{ab} = \frac{f_{ab,min} + f_{ab,max} \cdot exp\left(\frac{\tilde{P} - P_n}{k_{ab}}\right)}{1 + exp\left(\frac{\tilde{P} - P_n}{k_{ab}}\right)} \qquad \text{(Eq.2.16)}$$

$$\tau_{p,b}\frac{d\tilde{P}}{dt} = P_{ao} + \tau_{z,b} \cdot \frac{dP_{ao}}{dt} - \tilde{P} \qquad \text{(Eq.2.17)}$$

$$\tau_{p,b} = 2.0760\ s \quad \tau_{z,b} = 6.37\ s \quad P_n = 92\ mmHg$$
$$f_{ab,min} = 2.52\ spikes/s \quad f_{ab,max} = 47.78\ spikes/s \quad k_{ab} = 11.76\ mmHg$$

- a chemo-afferent signal, f_{ac}, calculated as a first order derivative based on the partial pressure of oxygen in the aorta, Pa_{O2} (Eq.2.18):

$$\frac{df_{ac}}{dt} = \frac{-f_{ac} + \frac{f_{ac,max} + f_{ac,min} \cdot exp\left(\frac{Pa_{O2} - P_{O2,n}}{k_{ac}}\right)}{1 + exp\left(\frac{Pa_{O2} - P_{O2,n}}{k_{ac}}\right)}}{\tau_c} \quad \text{(Eq.2.18)}$$

$$\tau_c = 2\ s \qquad P_{O2,n} = 45\ mmHg$$

$$f_{ac,min} = 1.16\frac{spikes}{s} \quad f_{ac,max} = 17.07\frac{spikes}{s} \quad k_{ac} = 29.27\ mmHg$$

- a pulmonary-afferent signal, f_{ap}, calculated as a first order derivative based on the tidal volume, V_t (Eq.2.19):

$$\frac{df_{ap}}{dt} = \frac{-f_{ap} + G_{ap} \cdot V_T}{\tau_p} \quad \text{(Eq.2.19)}$$

$$\tau_p = 2\ s \qquad G_{ap} = 23.29\ l^{-1}spikes/s$$

- a central nervous system (CSN) hypoxic response for the peripheral vasculature (χ_{sp}, θ_{sp}) and for the cardiac circulation (χ_{sh}, θ_{sh}), since they have different threshold of minimum oxygen concentration ($P_{O2,n,sp}, P_{O2,n,sh}$) (Eq.2.20, Eq.2.21):

$$\frac{d\theta_{sp}}{dt} = \frac{-\theta_{sp} + \frac{\chi_{min,sp} + \chi_{max,sp} \cdot exp\left(\frac{Pa_{O2} - P_{O2,n,sp}}{k_{isc,sp}}\right)}{1 + exp\left(\frac{Pa_{O2} - P_{O2,n,sp}}{k_{isc,sp}}\right)}}{\tau_{isc}} \quad \text{(Eq.2.20)}$$

$$\frac{d\theta_{sh}}{dt} = \frac{-\theta_{sh} + \frac{\chi_{min,sh} + \chi_{max,sh} \cdot exp\left(\frac{Pa_{O2} - P_{O2,n,sh}}{k_{isc,sh}}\right)}{1 + exp\left(\frac{Pa_{O2} - P_{O2,n,sh}}{k_{isc,sh}}\right)}}{\tau_{isc}} \quad \text{(Eq.2.21)}$$

$$\chi_{min,sp} = 7.33\ \frac{spikes}{s} \qquad \chi_{max,sp} = 13.32\frac{spikes}{s} \qquad P_{O2,n,sp} = 30\ mmHg \qquad k_{isc,sp} = 2\ mmHg$$

$$\chi_{min,sh} = -49.38\frac{spikes}{s} \qquad \chi_{max,sh} = 3.59\ \frac{spikes}{s} \qquad P_{O2,n,sh} = 45\ mmHg \qquad k_{isc,sh} = 6\ mmHg$$

$$\tau_{isc} = 30\ s$$

The central system elaborates the afferent signals and produces:

- separate efferent sympathetic responses, for the peripheral vasculature (f_{sp}) (Eq.2.22) and for the heart (f_{sh}) (Eq.2.23):

$$f_{sp} = \begin{cases} f_{es,\infty} + (f_{es,0} - f_{es,\infty}) \cdot e^{[k_{es} \cdot (-W_{b,sp} \cdot f_{ab} + W_{c,sp} \cdot f_{ac} - W_{p,sp} \cdot f_{ap} - \theta_{sp})]} & if\ f_{sp} < f_{es,max} \\ f_{es,max} & if\ f_{sp} \geq f_{es,max} \end{cases} \quad \text{(Eq.2.22)}$$

$$f_{sh} = \begin{cases} f_{es,\infty} + (f_{es,0} - f_{es,\infty}) \cdot e^{[k_{es} \cdot (-W_{b,sh} \cdot f_{ab} + W_{c,sh} \cdot f_{ac} - \theta_{sh})]} & if\ f_{sh} < f_{es,max} \\ f_{es,max} & if\ f_{sh} \geq f_{es,max} \end{cases} \quad \text{(Eq.2.23)}$$

$$f_{es,\infty} = 2.1 \frac{spikes}{s} \qquad f_{es,0} = 16.11 \frac{spikes}{s} \qquad k_{es} = 0.0675\ s \qquad f_{es,max} = 60 \frac{spikes}{s}$$

$$W_{b,sp} = 1 \qquad W_{c,sp} = 5 \qquad W_{p,sp} = 0.34 \qquad W_{b,sh} = 1 \qquad W_{c,sh} = 1$$

- a parasympathetic response (Eq.2.24):

$$f_v = \frac{f_{ev,0} + f_{ev,\infty} \cdot e^{\left(\frac{f_{ab} - f_{ab,0}}{k_{ev}}\right)}}{1 + e^{\left(\frac{f_{ab} - f_{ab,0}}{k_{ev}}\right)}} + W_{c,v} \cdot f_{ac} - W_{p,v} \cdot f_{ap} - \theta_v \quad \text{(Eq.2.24)}$$

$$f_{ev,\infty} = 6.3 \frac{spikes}{s} \qquad f_{ev,0} = 3.2 \frac{spikes}{s} \qquad f_{ab,0} = 25 \frac{spikes}{s} \qquad k_{ev} = 7.06 \frac{spikes}{s}$$

$$W_{c,v} = 0.2 \qquad W_{p,v} = 0.103 \qquad \theta_v = -0.68\ spikes/s$$

- and a ventilator response (Eq.2.25):

$$V_T = V_{T,N} + \Delta V_T \qquad \frac{d\Delta V_T}{dt} = \frac{-\Delta V_T + G_V \cdot [f_{ac}(t - D_V) - f_{ac,n}]}{\tau_V} \quad \text{(Eq.2.25)}$$

$$G_V = 0.125 \frac{l}{v} \qquad \tau_V = 3\ s \qquad D_V = 6\ s \qquad V_{T,N} = 0.583\ l \qquad f_{ac,n} = 3.6\ spikes/s$$

The efferent signals were then transmitted to the effectors, considering specific delays (D_θ) gains (G_θ), constant times(τ_θ) and reference values (θ_0) for each. Sympathetic signals for the peripheral effectors (f_{sp}) were used to regulate the peripheral resistance and venous unstressed volume and those for the heart (f_{sh}) regulate cardiac elastance (Eq.2.26). The value of each effector was then calculated using a first order differential equation (Eq.2.27):

$$\frac{d\Delta\theta}{dt} = \begin{cases} \dfrac{-\Delta\theta + G_\theta \cdot \ln[f_{sp/sh}(t - D_\theta) - f_{es,min} + 1]}{\tau_\theta} & if\ \ f_{sp/sh} \geq f_{es,min} \\ \dfrac{-\Delta\theta}{\tau_\theta} & if\ f_{sp/sh} < f_{es,min} \end{cases} \quad \text{(Eq.2.26)}$$

$$\theta(t) = \Delta\theta(t) + \theta_0 \quad \text{(Eq.2.27)}$$

$$f_{es,min} = 2.66 \frac{spikes}{s}$$

As stated at the beginning of this paragraph, the model implemented in this thesis had a different compartmental structure to that published by Ursino: the systemic branch in the Ursino model consisted of more parallel branches representing different organs (splanchnic, extra splanchnic and muscles), whilst in the current project one single branch was considered. For this reason, an adaptation was made to the effectors of peripheral resistances and unstressed venous volume. In particular, both the capillary resistances and unstressed volume used in Ursino's model were considered in parallel, to give the single peripheral resistance and unstressed volume representation used in the current model (Eq.2.28, Eq.2.29):

$$R_{SYS} = \frac{R_{SP} \cdot R_{EP} \cdot R_{MP}}{R_{SP} + R_{EP} + R_{MP}} \quad \text{(Eq.2.28)}$$

$$UNven = Vu_{SP} + Vu_{EP} + Vu_{MP} \quad \text{(Eq.2.29)}$$

Coherently, the equivalent parallel was valid also for the controlled resistances and volumes values (Eq.2.30, Eq.2.31):

$$R_{SYS} = \frac{(\Delta R_{SP} + R_{SP0}) \cdot (\Delta R_{EP} + R_{EP0}) \cdot (\Delta R_{MP} + R_{MP0})}{(\Delta R_{SP} + R_{SP0}) + (\Delta R_{EP} + R_{EP0}) + (\Delta R_{MP} + R_{MP0})} \quad \text{(Eq.2.30)}$$

$$UNven = (\Delta Vu_{SP} + Vu_{SP0}) + (\Delta Vu_{EP} + Vu_{EP0}) + (\Delta Vu_{MP} + Vu_{MP0}) \quad \text{(Eq.2.31)}$$

For the heart period (Eq.2.34), both sympathetic (Eq.2.32) and vagal (Eq.2.33) pathways were involved in the calculation:

$$\frac{d\Delta T_S(t)}{dt} = \begin{cases} \dfrac{-\Delta T_S(t) + G_{T,s} \cdot \ln[f_{sh}(t - D_{T,s}) - f_{es,min} + 1]}{\tau_{T,s}} & if \;\; f_{sh} \geq f_{es,min} \\ \dfrac{-\Delta T_S(t)}{\tau_{T,s}} & if \; f_{sh} < f_{es,min} \end{cases} \quad \text{(Eq.2.32)}$$

$$\frac{d\Delta T_V(t)}{dt} = \frac{-\Delta T_V(t) + G_{T,v} \cdot f_v(t - D_{T,v})}{\tau_{T,v}} \quad \text{(Eq.2.33)}$$

$$T = \Delta T_S + \Delta T_V + T_0 \quad \text{(Eq.2.34)}$$

The constants used for each effector for gain, time constant, delay and reference value are reported in Table 2.3.

Table 2.3: Values of gain, time constant, delay and reference value for each effector.

Gain	Time constant	Delay	Reference value
$G_{Emax,lv} = 0.475\ mmHg\ \cdot ml^{-1} \cdot v^{-1}$ $G_{Emax,rv} = 0.282\ mmHg\ \cdot ml^{-1} \cdot v^{-1}$ $G_{Rsp} = 0.695\ mmHg\ \cdot ml^{-1} \cdot v^{-1}$ $G_{Rep} = 1.94\ mmHg\ \cdot ml^{-1} \cdot v^{-1}$ $G_{Rmp} = 2.47\ mmHg\ \cdot ml^{-1} \cdot v^{-1}$ $G_{Vu,sv} = -265.4\ ml/v$ $G_{Vu,ev} = -74.21\ ml/v$ $G_{Vu,mv} = -58.29\ ml/v$ $G_{Tv} = -0.13\ s/v$ $G_{Ts} = 0.09\ s/v$	$T_{Emax,lv} = 8\ s$ $T_{Emax,rv} = 8\ s$ $T_{Rsp} = 6\ s$ $T_{Rep} = 6\ s$ $T_{Rmp} = 6\ s$ $T_{Vu,sv} = 20\ s$ $T_{Vu,ev} = 20\ s$ $T_{Vu,mv} = 20\ s$ $T_{Tv} = 2\ s$ $T_{Ts} = 1.5\ s$	$D_{Emax,lv} = 2\ s$ $D_{Emax,rv} = 2\ s$ $D_{Rsp} = 2\ s$ $D_{Rep} = 2\ s$ $D_{Rmp} = 2\ s$ $D_{Vu,sv} = 5\ s$ $D_{Vu,ev} = 5\ s$ $D_{Vu,mv} = 5\ s$ $D_{Tv} = 2\ s$ $D_{Ts} = 0.2\ s$	$E_{max,lv0} = 2.392\ mmHg/ml$ $E_{max,rv0} = 1.412\ mmHg/ml$ $R_{sp0} = 2.49\ mmHg\ s/ml$ $R_{ep0} = 1.655\ mmHg\ s/ml$ $R_{mp0} = 2.106\ mmHg\ s/ml$ $V_{u,sv0} = 1435\ ml$ $V_{u,ev0} = 640.74\ ml$ $V_{u,mv0} = 503.26\ ml$ $T_0 = 0.58\ s$

In the current model the unstressed volume in systemic vein (SVN) was introduced based on the relationship between pressure (P) and volume (V) in a compliant system assuming that the compliance was a constant and was independent of the unstressed volume (Figure 2.12). For a certain unstressed volume V_0, the pressure P is null and for any volume V the pressure can be described as in Eq.2.35:

$$P = \frac{V - V_0}{C} \qquad \text{(Eq.2.35)}$$

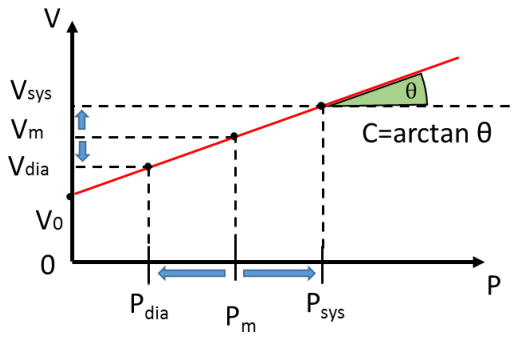

Figure 2.12: Pressure -Volume relationship with change of unstressed volume.

2.1.3.2 Validation of the adapted controlled cardiovascular model

In order to provide some verification that the adapted model of barocontrol is behaving as expected, a simulation of haemorrhage was run and the results compared with the original Ursino's results.

Haemorrhage causes a response which aims to maintain a constant cardiac output by increasing the heart rate to compensate for the decrease in stroke volume whilst increasing the peripheral resistance in order to maintain the blood pressure.

Simulation of haemorrhage can be achieved by introducing a volume leakage (10% of the total blood volume was chosen for the simulation reported) in the systemic venous compartment for a certain interval of time (5 s). The reaction of the barocontrol system is a short-term one; the cardiovascular system is not able to recover the normal condition, since the physiological systems required to model the long-term response (such as the kidneys and hormonal systems) were not included.

The model predicts that haemorrhage causes a rapid drop of systemic pressure by 21% (60 mmHg) of the baseline value. This activates the afferent and efferent pathways and the barocontrolled effectors respond as expected (Figure 2.13): both ventricular elastances (ELV_{max} and ERV_{max}) increase, together with the heart rate (HR) and the peripheral systemic resistance (R_{sys}) and, as a result, the cardiac output decreases. Comparing the results with those reported by Ursino [46], it can be seen that trends of change of R_{SYS}, HR, systemic pressure (P_{SYS}) and cardiac output (CO) are similar, although the absolute changes are not the same (Table 2.4).

This difference is assumed to be generated by the different compartmental structure of the model keeping the original barocontrol coefficients. Reproduction of the same results can be achieved tuning the coefficients of barocontrol. This particular point has been investigated for the adenosine response, as explained in the next chapter.

Table 2.4: Effect of haemorrhage stimulation in the barocontrolled model.
Changes of peripheral resistance (R_{SYS}), heart rate (HR), systemic pressure (P_{SYS}) and cardiac output (CO) during the simulation of haemorrhage are compared with results of Ursino's model [50, 52].

Parameter	HR	R_{SYS}	P_{SYS}	CO
Current model	15%	13%	−18%	−25%
Ursino's model	10%	10%	−10%	−17%

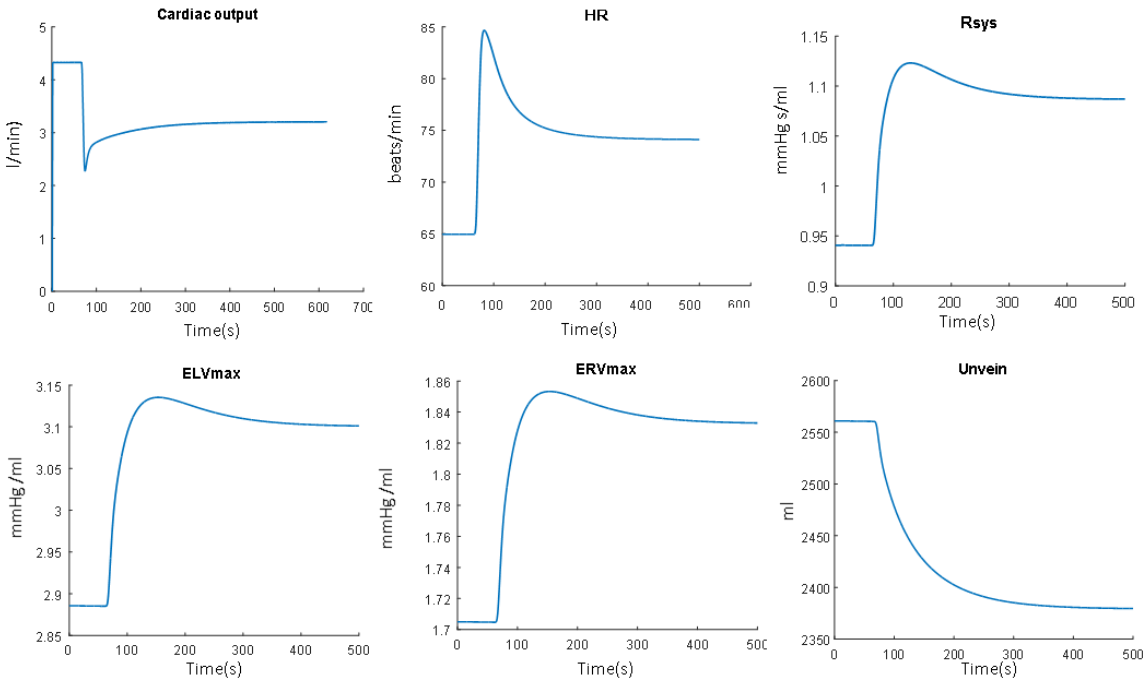

Figure 2.13: Effectors response to haemorrhage stimulus in an ideal patient model. Heart rate, HR; max left ventricle elastance, ELV_{max}; max right ventricle elastance, ERV_{max} ; peripheral systemic resistance, R_{sys}; Unstressed venous volume, Unvein).

2.1.4 Adenosine pharmacodynamics and pharmacokinetic model

Adenosine is a purine nucleoside which is present naturally within human body. It is an ubiquitous extracellular signalling molecule which is involved in many different physiological processes, such as energy production through ATP (Adenosine Tri-Phosphate) and blood flow regulation [115]. It is very relevant to this project since it is used during angiography to stimulate hyperaemia. The aim is to represent its distribution in the model and classify the different type of responses observed clinically.

2.1.4.1 Pharmacodynamics

Adenosine has different receptors, both intracellular and extracellular. Amongst the extracellular receptors 4 types of receptors, able to create different responses, have been recognised [115-117]:

- **A1** receptors are mainly located in myocardial cells and are responsible for a negative chronotropic effect (decrease of heart rate) and negative dromotropic effect (inhibition of AV node conduction and a prolongation of the refractory period);
- **A3** receptors are mainly located in peripheral compartments and their role is not completely known;
- **A2a** and **A2b** receptors are mainly located in the smooth muscle of the vasculature and are responsible for vasodilation in most vascular beds and for vasoconstriction in kidney and liver circulations.

Interest in adenosine metabolism has increased over the last 50 years since its effects on the cardiovascular system (use in treatment of cardiac arrhythmias and ischaemia for example) were discovered [115, 116, 118] and many experimental studies have been performed on animals [119-123]. Ventricular and atrial arrhythmias have been treated with the direct injection of exogenous adenosine into the heart circulation in order to stimulate dromotropic and chronotropic responses and to correct the heart rhythm [116].

With intracoronary and intravenous injection, adenosine generates hyperaemia, a condition of vasodilation and consequent increase of myocardial blood flow which aims to simulate this aspect of exercise. Pharmacological induction of hyperaemia is widely used therapeutically. In patients with CAD who undergo diagnostic angiography, the use of adenosine to stimulate hyperaemia is potentially less invasive than other hyperaemic stimulation methods such as vessel occlusion and, whilst exercise can be considered to be the least invasive method, patient movement limits the quality of acquired images [115].

2.1.4.2 Pharmacokinetics

During angiography the hyperaemic condition is induced by the intravenous administration of adenosine in to the medial cubital vein. A dose of 0.14 mg/ml per kg of patient body weight

(BW) is routinely used and the injected solution has an initial concentration (C_{INJ}) of 3 mg/ml [115]. The adenosine injection flow (Q_{AD}) is calculated as (Eq.2.36):

$$Q_{ad} = \frac{dose \cdot BW}{C_{INJ}} \quad \text{(Eq.2.36)}$$

In the model of the cardiovascular system, the flow of adenosine, Q_{ad}, is introduced into the systemic vein (SVN) and it is assumed that the drug is eliminated in all the vascular compartments with a half-life ($t_{1/2}$) of 7 s [116]. The clearance of the drug, CL, in each compartment is expressed as (Eq.2.37):

$$CL = \ln 2 \cdot \frac{Volume}{t_{1/2}} \quad \text{(Eq.2.37)}$$

A mass balance equation is implemented in each compartment to describe the adenosine concentration and its elimination (Eq.2.38). In the systemic vein (SVN) the injection of adenosine is also included (Eq.2.39).

$$\frac{d\,(C \cdot V)}{dt} = C_{in} \cdot Q_{in} - C \cdot (Q_{out} + Q_{el}) \quad \text{(Eq.2.38)}$$

$$\frac{d\,(C \cdot V)}{dt} = C_{in} \cdot Q_{in} - C \cdot (Q_{out} + Q_{el}) + Q_{ad} \cdot C_{INJ} \quad \text{(Eq.2.39)}$$

2.2 DISCRETISATION AND SOLUTION METHODS

Section 2.1 focused on the development of the systems of equations that describe the cardiovascular model.

As stated before, the starting point was a published model and, specifically a model that was available publicly from the CellML repository. This model represents an excellent starting point, because its implementation had already been curated by the managers of the repository. Furthermore, the CellML environment supports experimentation with the alternative solvers that might be appropriate for equation systems of this type. However, additions to the system that are a required for this specific study include a number of phenomena (neuro-regulation and the non-linearity of oxygen partial pressure and concentration relationship) that are not readily implemented in CellML. Further details are given in the paragraphs that follow.

Because of these limitations, the model was exported from CellML - Open Cor (http://www.opencor.ws/) into a MATLAB script, and the additional functionality was implemented within the MATLAB2015a environment (The MathWorks, Inc). The performance of the core model, as exported to MATLAB, was checked against results from the original CellML operation.

2.2.1 CellML- Open Cor

The analogue hydraulic model with the species distribution (adenosine, oxygen and carbon dioxide) was implemented within the open source software Open Cor (http://www.opencor.ws/). Open Cor has been specifically developed to represent physiological models and enables a system of differential equations and linear algebraic equations to be solved.

There are different solvers available: Forward Euler, 2nd order Runge-Kutta, 4th order Runge-Kutta and CVODE. The latter was selected to run the simulations.

Implementation of some of the features associated with the baro- and chemo-control and the oxygen concentration proved intractable in Open Cor. The first problem was encountered in equations for the effectors, where a delay was applied (Eq.2.40), the second in the non-linear equation for the calculation of oxygen partial pressure from the concentration (Eq.2.41).

$$\sigma_\theta = G_\theta \cdot \ln[f(t - D_\theta) - f_{min} + 1] \quad \text{(Eq.2.40)}$$

$$0.00417 \cdot (P_{O2})^{3.7} + (0.28 - 1.39 \cdot 10^{-4} \cdot C_{O2}) \cdot (P_{O2})^{2.7} - H_{O2-blood} \cdot P_{O2} - C_{O2} = 0 \quad \text{(Eq.2.41)}$$

However, since it proved possible to export the curated model directly as a MATLAB code and expand the functionality in the MATLAB environment, this was the solution chosen for the work described in this thesis.

2.2.2 MATLAB

In MATLAB 2015a there are a number of different functions to solve differential equations. The exported code from Open Cor provides the *ode15s* solver, based on the BDF 1-5. This solver uses a variable time-step to solve the differential and linear equations but, once again use of this specific solver gave rise to the problems in the introduction of the barocontrol delays. The original code with variable time-step was extended in order to store the algebraic quantities, checking the convergence by using a loop on the time-step values. Results from Open Cor were compared with the results of the post-processing of the algebraic equations in MATLAB, as shown in the example in Figure 2.14. Overall the results were unstable and unsatisfactory.

To address this limitation, the solver *ode4*, was chosen. This is an explicit solver with arbitrarily fixed time-step, using the 4th order Runge-Kutta method. The advantages of using a fixed time-step relate to the possibility of storing non-derivative quantities and manipulation of some quantities for averaging, as described in the next paragraphs.

A sensitivity analysis on the time-step length was carried out in order to find the right compromise between simulation duration and accuracy of the results. Different values of time-

steps (0.000025 s, 0.0001 s, 0.0005 s, 0.001 s, 0.002 s) were used for the simulation and the results were compared against the CellML solution. As expected, the smallest time-step produced results close to the original solution, while results with the largest time-step showed high inaccuracy and instability, especially during the closure of the cardiac valves. It is important to highlight that the ode4 solver was modified to allow the storage of variables not described by derivative equations (such as cardiac pressures and flows).

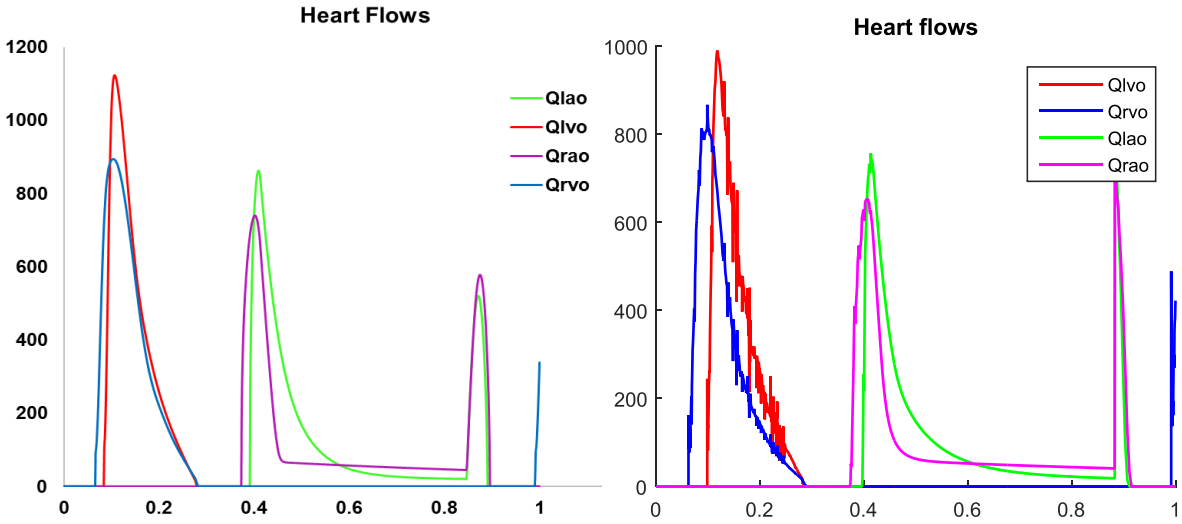

Figure 2.14: Comparison between Open Cor results and MATLAB results.
The MATLAB variable step solver was modified to allow the storage of the flows. Left) Results of heart flows obtained with OpenCor. Right). Results of heart flows obtained with MATLAB code using the modified ode15s. Legend: Qlao (left atrium output flow); Qlvo (left ventricle output flow); Qrao (right atrium output flow); Qrvo (right ventricle output flow). Units: flow in ml/s, x-axis in seconds.

These variables (for example the left ventricular output blood flow and pressure) are sensitive to the time-step and smaller time-steps produce a stable and accurate solution (Figure 2.15 A, B), while the derivative variables (for example left ventricular volume) do not show the same level of sensitivity (Figure 2.15 C). Interestingly when implementing the same smooth valve in Open Cor, the solver requires a time-step of 0.0001 s to run the model with both fixed and non-fixed time-step solver (CVODE and 4th order Runge-Kutta respectively), while using the diode valve requires a time-step of 0.01 s for the variable time-step solver (CVODE) and 0.0001 s for the fixed time-step one (4th order Runge-Kutta).

The time-step equal to 0.0001 s was selected for the simulation of the model in MATLAB. This provides stable left ventricular blood flow during all phases and close to the Open Cor solution.

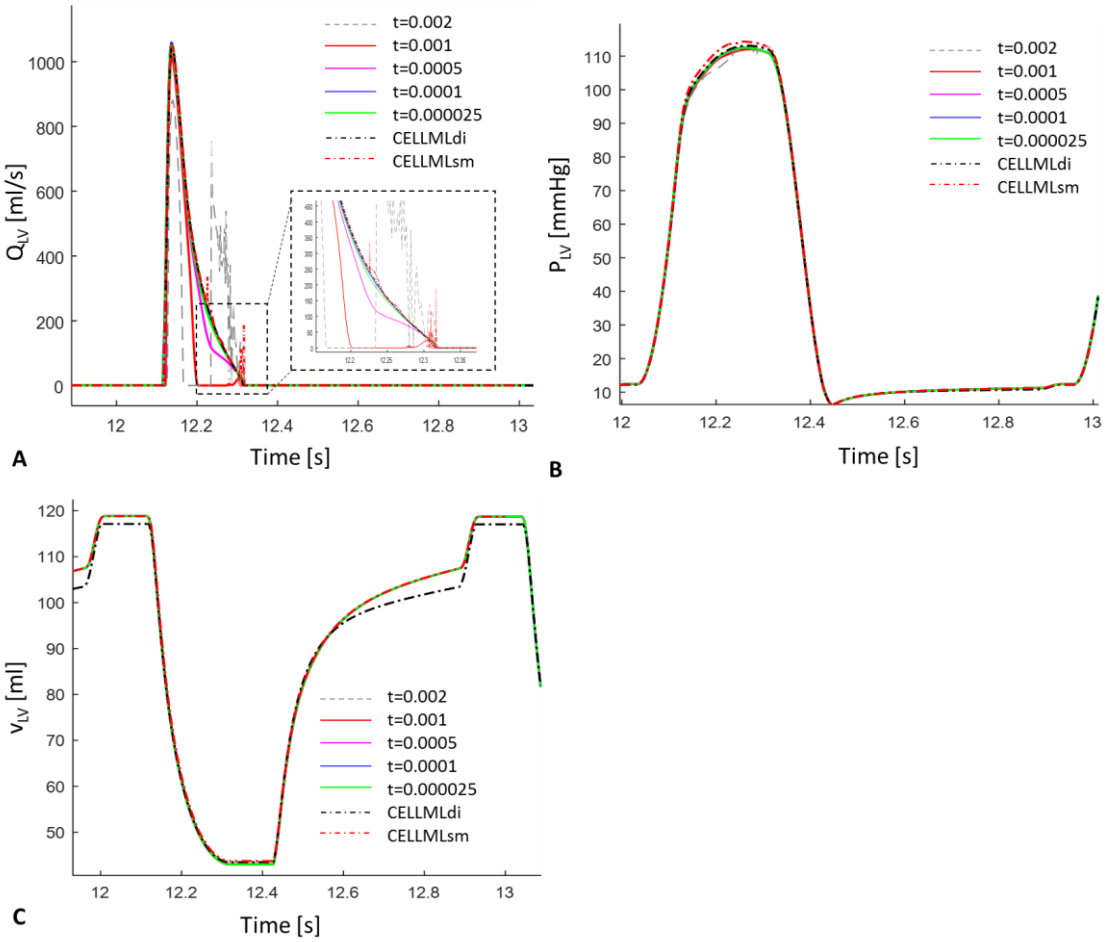

Figure 2.15: Open Cor VS MATLAB results of left ventricle blood flow, pressure and volume. A) Blood flow across the aortic valve, with a detail of the closure valve solutions. B) Left ventricular blood pressure. C) Left ventricle blood volume. MATLAB results are obtained with different time-steps (dashed grey 0.002 s, continue red 0.001 s, continue magenta 0.0005 s, continue blue 0.0001 s, continue green 0.000025 s) using the smooth valve. Open Cor results are obtained with diode valve (dashed black, 0.01 s time-step, CVODE solver) and with smooth valve (dashed red, 0.0001 s time-step, CDVODE solver).

2.2.2.1 Algorithms

The fixed time-step solver also introduces the possibility to implement different algorithms to represent the barocontrol system and to keep track of non-derivative quantities. The following sub-sections list, and briefly describe, the algorithms introduced within this type of solver.

2.2.2.1.1 Moving average calculation

The moving average concept was used to introduce the delay for the barocontrol, and smooth the response. Without this the control mechanism responds continually to the variations within the heart cycle, and the fact that the delay is not generally an integral multiplier of the heart period produces non-physiological oscillations in the response. The solution was to calculate an average value of a certain quantity across the last cardiac cycle. A detail of the implementation is that the average is accumulated based on the fraction of the cardiac cycle, even if the heart period changes.

The fraction of the cardiac cycle varies from 0 to 1 and increases at each instant. It is described as the sum of the last value of fraction ($Fract_{i-1}$) and the ratio between the time-step and the cardiac period at the current time (T_i). When the value of the cardiac fraction is equal or higher than 1, it is reset to 0, considering the fraction to be in excess (Eq.2.42):

$$Fract_i = Fract_{i-1} + \frac{timestep}{T_i} \qquad if\ Fract_i \geq 1 \quad Fract_i = 0 + (Fract_i - 1) \tag{Eq.2.42}$$

As described before, the efferent pathways are activated with a specified delay for each effector and, therefore, it is necessary to store these quantities in order to consider the value at the specified instant in the past. In figure 2.16, a generic signal A(t) is shown and the fractions of cardiac cycle are reported for 4 consecutive cardiac cycles with different periods (T_1, T_2, T_3, T_4). Ideally the delay, applied in the last cycle at a certain fraction of cardiac cycle, has to take into account the signal at the same fraction of cardiac cycle. The delay values do not guarantee that the same fraction of cardiac cycle is considered. For this reason, for each instant the efferent sympathetic signal is smoothed, based on the average of its values occurring during the last cardiac cycle.

A vector containing the signal during the last cardiac cycle was created using a length equal to $\frac{3s}{timestep}$, where 3 s was chosen as a maximum possible value of cardiac period. Assuming a

linear relationship of the signal within the time-step interval, a number of values of the signal within the time-step can be calculated at ft_k point (Figure 2.17).

The linear relationship is calculated as (Eq.2.43):

$$y = \frac{A_j - A_{j-1}}{fract_j - fract_{j-1}} \cdot (x - fract_{j-1}) + A_{j-1} \qquad \text{(Eq.2.43)}$$

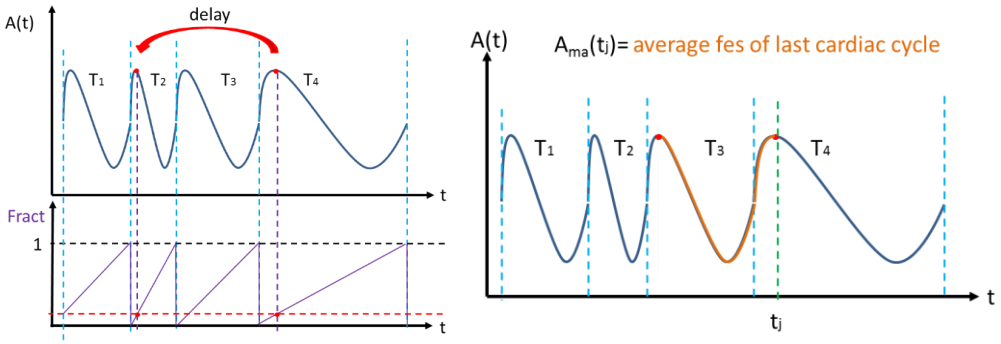

Figure 2.16: Implementation of the moving average to apply delays.
Left) Ideally the delay in A(t) (sympathetic efferent signal) should be applied considering the fraction of period in order to be in the same phase of the cardiac cycle. The values of delays do no guarantee to consider the same fraction of cardiac cycle. Right) For each instant A(t) is calculated considering the average of the last cardiac cycle (highlighted in orange).

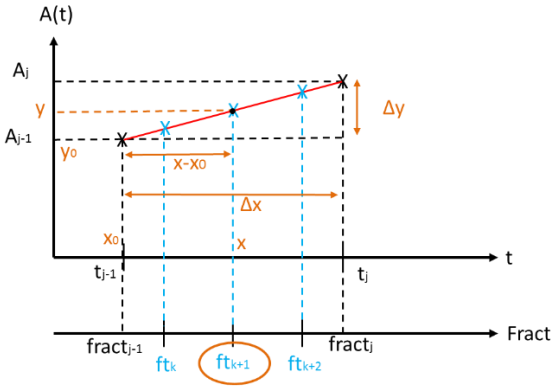

Figure 2.17: Scheme of the linear interpolation of the signal for intermediate fraction-steps.
The graph shows how the values of A(t) (X) are calculated for each intermediate fraction of heart period (ft_k) considering a linear relationship of A(t) within a time interval (t_j-t_{j-1}) or an equivalent fraction period interval ($fract_j$-$fract_{j-1}$). Knowing the coordinates of A(t) at time t_j and time t_{j-1} it is possible to define the straight line equation.

The moving average of the signals was then calculated as the mean within a cardiac cycle. This approach of smoothing was applied to the efferent sympathetic and vagal signals and to the afferent chemo-signal. Moreover, it can also be applied to the gas concentrations which could be used as inputs to the chemo regulation pathways.

2.2.2.1.2 Calculation of oxygen partial pressure: interpolation method

The distribution of oxygen in the cardiovascular system can be expressed as a concentration ($[O_2]$), calculated from the mass balance implemented in the model or as partial pressure (P_{O2}). There is a relationship between these two parameters which takes into account the solubility coefficient of the gas in blood (Eq.2.9) and its binding phenomena with haemoglobin (Eq.2.10, Eq.2.11). Combining all these equations together, the non-linear relationship between oxygen concentration and its partial pressure in blood is expressed as (Eq.2.44):

$$0.00417 \cdot (P_{O2})^{3.7} + (0.28 - 1.39 \cdot 10^{-4} \cdot [O_2]) \cdot (P_{O2})^{2.7} - H_{O2-blood} \cdot P_{O2} - [O_2] = 0 \qquad \text{(Eq.2.44)}$$

To solve this non-linear relationship and obtain the value of oxygen partial pressure, an interpolation function, *interp1*, was employed.

2.2.2.1.3 Cardiac output, stroke volume and ejection fraction for each cardiac cycle

To define the cardiac output (CO), the stroke volume (SV) and ejection fraction (EF) at each cardiac cycle, it is necessary firstly to identify the individual cardiac cycles, within which these quantities can be calculated. The concept of fraction of cardiac cycle was introduced in the previous paragraph (2.2.2.1.1 *Moving average calculation*).

The cardiac output was calculated as the ratio between the difference of the maximum and minimum left ventricular volume and the duration of the cardiac cycle (Eq.2.45):

$$CO = \frac{VLV_{max} - VLV_{min}}{T_{CC}} \qquad \text{(Eq.2.45)}$$

The stroke volume was calculated as the difference between the maximum and minimum left ventricular volume occurring within a cycle (Eq.2.46):

$$SV = VLV_{max} - VLV_{min} \qquad \text{(Eq.2.46)}$$

The ejection fraction was calculated as the ratio between the stroke volume and the maximum left ventricular volume (Eq.2.47):

$$EF = \frac{VLV_{max} - VLV_{min}}{VLV_{max}} \qquad \text{(Eq.2.47)}$$

The advantage of using the volume data to obtain these other variables is essentially the possibility to reduce the time-step for the optimisation process, which is explained in detail in Chapter 5, enabling the overall simulation time to be reduced.

2.3 Sensitivity Analysis

A sensitivity analysis aims at the definition of the influence of the independent variables (or inputs) on the dependent variables (or outputs) of the system. There are different methods of performing a sensitivity analysis [124, 125]. In this project the *One-at-a-time (OAT)* sensitivity measure was selected. With this method each input value is adjusted by a percentage of its original value, while all the other inputs are held constant, and the outputs are then compared with the original case values.

The sensitivity analysis was performed for the non-barocontrol and the barocontrol model. With the introduction of the barocontrol, some inputs become outputs and more inputs are introduced with the barocontrol constants. Table 2.5 summarises the input and output parameters for the non-barocontrolled model and the barocontrolled one in terms of the haemodynamic. The input parameters for the non – barocontrolled are:

- timing parameters related the ventricles and atria and heart period;
- unstressed cardiac volumes and correspondent pressures;
- active and passive cardiac elastances and valvular coefficients;
- resistances, capacitances, inertances;
- initial blood volumes in the different compartments;
- unstressed systemic venous volume.

The output parameters are divided in raw and derived. Among the raw or independent outputs there are: the time-discretised pressures, volume and flow in each compartment; the left-ventricular end diastolic and end systolic volumes. Among the derived or dependent

parameters, there are cardiac output, stroke volume, ejection fraction, systolic and diastolic pressure, mean arterial pressure and the adenosine concentration in each compartment.

With the barocontrolled model, the effectors ELV_{MAX}, ERV_{MAX}, R_{SCP}, UN_{vein}, and T are substituted by their respective reference values and their resulting values are outputs. In addition, a number of barocontrol constants are introduced as inputs, regarding the effectors gains, delays and the parameters describing the sigmoid functions of the afferent pathways and the logarithmic function describing the efferent pathways.

The input parameters were changed by a certain percentage of the initial value and the normalised variation was calculated for each output parameter, as explained below.

Each input parameter value (P_i) was modified adding or subtracting a percentage from its initial value ($P_{i,ORIG}$) as described in Eq.2.48:

$$P_i = \frac{P_{i,ORIG}(100 \pm X\%)}{100} \qquad \text{(Eq.2.48)}$$

where X% is a percentage chosen equally to 10%, 20%, 30%, 40%, 50%, 60%,70%, 80%.

The normalised variation (NV) for each output, P_o, and for each $\pm$X% was calculated as shown in Eq.2.49.

$$NV_{X\%} = \frac{\sqrt{\sum_1^n \left(\frac{P_{o,+X\%} - P_{o,ORIG}}{P_{o,ORIG}}\right)^2} + \sqrt{\sum_1^n \left(\frac{P_{o,-X\%} - P_{o,ORIG}}{P_{o,ORIG}}\right)^2}}{\frac{2}{X\%}} \qquad \text{(Eq.2.49)}$$

where N represents the number of time-steps for the time-discretised outputs (pressures, flows and volumes) and it is equal to 1 for the outputs discretised over a cardiac cycle.

Finally a total NV (NV_{TOT}) was calculated as the average of the $NV_{X\%}$ for each couple of input/output with the different X% of the input.

A similar approach was taken to calculate the influence of the heart period on the outputs of the model. Different values of heart period (T) within physiological range have been considered, in particular 0.54 s, 0.6 s, 0.7 s, 0.8 s, 1 s, 1.1 s, 1.2 s, 1.3 s, 1.4s, 1.5s. The variation

of the heart period required an interpolation to produce a uniformly-sample signal for the comparison of time-discretised outputs over cardiac cycle.

The sensitivity analysis described for the parameters above have been run in absence of barocontrol for a time of 1 s. Results of the sensitivity analysis are reported in figure 2.18, where, among the output, are reported pressures (Panel A), flows and some of the derived outputs (CO, SV, EF, P_{SYS}, P_{DIA}) (Panel B), more clinically relevant as explained later.

The same approach was also used to perform the sensitivity analysis for the barocontrolled model increasing the time simulation to 30 seconds, including in the inputs parameters the barocontrol constants and the reference values for the effectors, consistent with the list of inputs and outputs provided in Table 2.5. Results of the sensitivity analysis of the barocontrol effectors and results of the sensitivity analysis of a selection of the barocontrol constants are reported in figure 2.19. This selection was made based on the focus of Chapter 3, where the adenosine response is implemented for a generic individual.

Table 2.5: List of the input and output parameters for the non-barocontrolled and barocontrolled model. The barocontrolled model replaces the effectors values with their reference value (in red) and introduces the barocontrol constants.

NON-BAROCONTROL			BAROCONTROL		
INPUTS	OUTPUTS		INPUTS	OUTPUTS	
	RAW	DERIVED		RAW	DERIVED
Timing parameters: **T**, Ts1, Ts2, Tpw1, Tpw2 Elastances: **ELVmax**, ERVmax, ELVmin, ERVmin Unstressed cardiac volume and pressures: Vlvini, Plvini, Vrvini,Prvini Vlaini, Plaini, Vraini, Praini Valvular coefficients: CVao, CVmi, CVtr, CVpo Capacitances: Csas, Csat, Csvn, Cpas, Cpat, Cpvn, Clc, Crc Resistances: Rsas, Rsat, Rsar, **Rscp**, Rsvn, Rpas, Rpat, Rpar, Rpcp, Rpvn, Zrc, Zlc , Rrc, Rlc Inhertances Lsas, Lpas Initial volumes: Vlai, Vlvi, Vrvi, Vrai, Vlci, Vrci, Vsasi, Vsati,Vsari, Vscpi, Vsvni, Vpasi, Vpati, Vpari, Vpcpi, Vpvni, **Unveini**	Pressures: Plv(t), Pla(t), Pra(t), Prv(t), Psas(t),Psat(t),Psar(t), Pscp(t),Psvn(t), Ppas(t), Ppat(t),Ppar(t), Ppcp(t),Ppvn(t) Flows: Qlvo(t), Qlao(t), Qrvo(t), Qrao(t) Qsas(t), Qsat(t), Qsar(t), Qscp(t), Qsvn(t), Qpas(t), Qpat(t), Qpar(t), Qpcp(t), Qpvn(t), Qlc(t), Qrc(t) Volumes: Vla(t), Vlv(t), Vrv(t), Vra(t),Vlc(t), Vrc(t), Vsas(t) , Vsat(t), , Vsar(t), Vscp(t), Vsvn(t), Vpas(t), Vpat(t), Vpar(t), Vpcp(t), Vsvn(t) LV- end diastolic volume LV- end systolic volume	CO EF SV Psys Pdia MAP	Timing parameters: **T_ref**, Ts1, Ts2, Tpw1, Tpw2 Elastances: **ELVmax_ref, ERVmax_ref,** ELVmin, ERVmin Cardiac initial values: Vlvini, Plvini, Vrvini,Prvini Vlaini, Plaini, Vraini, Praini Valvular coefficients: CVao, CVmi, CVtr, CVpo Capacitances: Csas, Csat, Csvn, Cpas, Cpat, Cpvn, Clc, Crc Resistances: Rsas, Rsat, Rsar, **Rscp_ref**, Rsvn, Rpas, Rpat, Rpar, Rpcp, Rpvn, Zrc, Zlc , Rrc, Rlc Inhertances Lsas, Lpas Initial volumes: Vlai, Vlvi, Vrvi, Vrai, Vlci, Vrci, Vsasi, Vsati,Vsari, Vscpi,Vsvni, Vpasi, Vpati, Vpari, Vpcpi, Vpvni, **Unveini_ref** Barocontrol constants: **G_{ELVMAX},G_{ERVMAX}, G_{RSCP}, G_{UNVEIN}, G_{TS},G_{TV} D_{ELVMAX}, D_{ERVMAX}, D_{RSCP}, D_{UNVEIN}, D_{TS}, D_{TV}, Pn, fabmin, fabmax, kab, Tpb, Tzb fes0, fesinf, fesmax kes, Fevinf, fev0, fab0, kev,**	Barocontrolled parameters: **ELVmax, ERVmax, Rscp, T Unvein** Pressures: Plv(t), Pla(t), Pra(t), Prv(t), Psas(t),Psat(t),Psar(t),Pscp(t) , Psvn(t), Ppas(t),Ppat(t), Ppar(t),Ppcp(t),Ppvn(t) Flows: Qlvo(t), Qlao(t), Qrvo(t), Qrao(t), Qsas(t), Qsat(t), Qsar(t), Qscp(t), Qsvn(t), Qpas(t), Qpat(t), Qpar(t), Qpcp(t), Qpvn(t) Qlc(t), Qrc(t) Volumes: Vla(t), Vlv(t), Vrv(t), Vra(t),Vlc(t), Vrc(t), Vsas(t) , Vsat(t), Vsar(t), Vscp(t), Vsvn(t), Vpas(t), Vpat(t), Vpar(t), Vpcp(t), Vsvn(t) LV- end diastolic volume LV- end systolic volume	CO EF SV Psys Pdia MAP

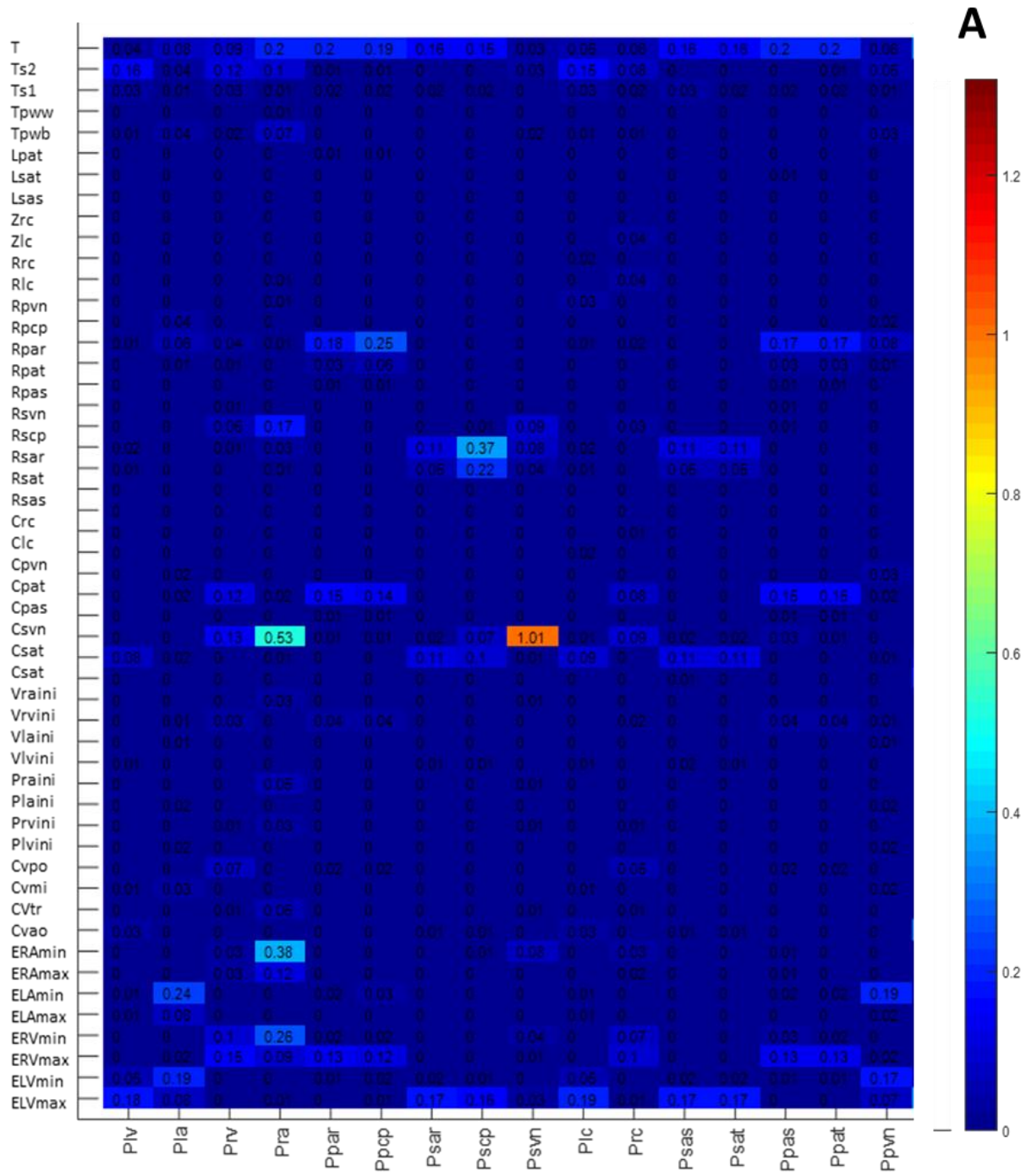
A
T
Ts2
Ts1
Tpww
Tpwb
Lpat
Lsat
Lsas
Zrc
Zlc
Rrc
Rlc
Rpvn
Rpcp
Rpar
Rpat
Rpas
Rsvn
Rscp
Rsar
Rsat
Rsas
Crc
Clc
Cpvn
Cpat
Cpas
Csvn
Csat
Csat
Vraini
Vrvini
Vlaini
Vlvini
Praini
Plaini
Prvini
Plvini
Cvpo
Cvmi
CVtr
Cvao
ERAmin
ERAmax
ELAmin
ELAmax
ERVmin
ERVmax
ELVmin
ELVmax
Plv
Pla
Prv
Pra
Ppar
Ppcp
Psar
Pscp
Psvn
Plc
Prc
Psas
Psat
Ppas
Ppat
Ppvn
1.2
1
0.8
0.6
0.4
0.2
0

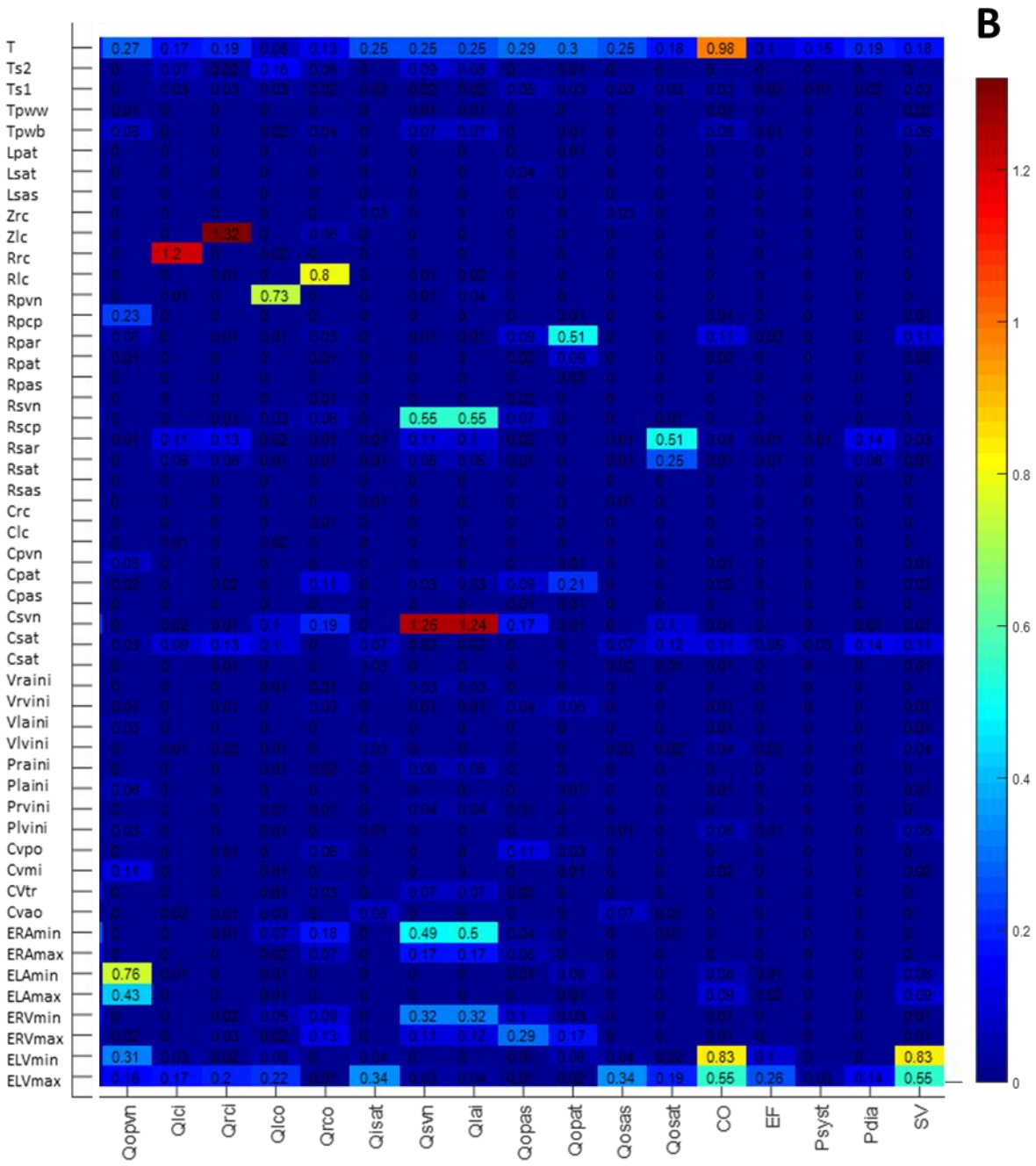

Figure 2.18: Sensitivity analysis results for the non barocontrol model.
Panel A shows the sensitivity analysis with respect to the pressure outputs, Panel B shows the sensitivity analysis with respect of the flows outputs and other derivate clinical outputs (CO, EF, Psys, Pdia, SV). The X-axis reports the outputs and the Y- axis the inputs. The numbers indicate the NV for each couple of input/output.

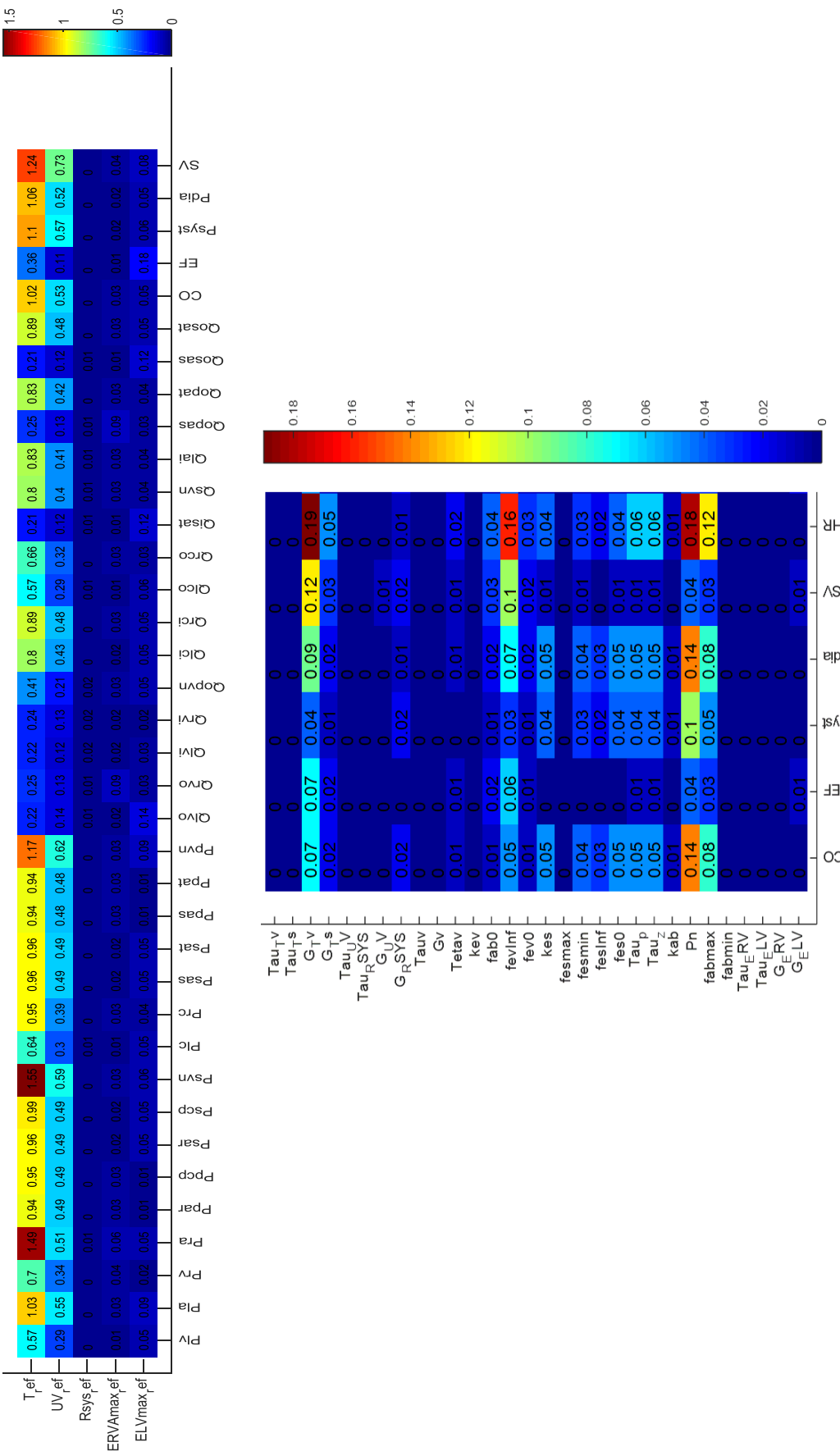

Figure 2.19: Sensitivity analysis results of the barocontrol model.

Top Panel shows the sensitivity of the effectors constants with respect to the pressure, flows and clinical outputs (CO, EF, Psys, Pdia, SV). Bottom panel show the sensitivity of the barocontrol constants with respect to the clinical outputs (CO, EF, Psys, Pdia, SV, HR). The X-axis reports the outputs and the Y- axis the inputs. The numbers indicates the NV for each couple of input/output.

2.4 MODEL OUTPUTS

The model was operated, for a generic individual, from an initialisation state for 100 s to allow the barocontrol to stabilise. The simulation run-time on a normal office desktop was above 24 hours.

2.4.1 Blood pressures, flows and volumes

In this section the results of detailed beat-to-beat blood pressure, flow and volume are reported for each compartment of the cardiovascular model. Figure 2.20 shows the results of blood pressure, flow and volume in the cardiac chambers (A), the results of blood pressures (B), flows (C) and volume (D) in each compartment of the systemic circulation and in the coronary circulation. Note the physiological diastolic dominance of the coronary flow waveforms.

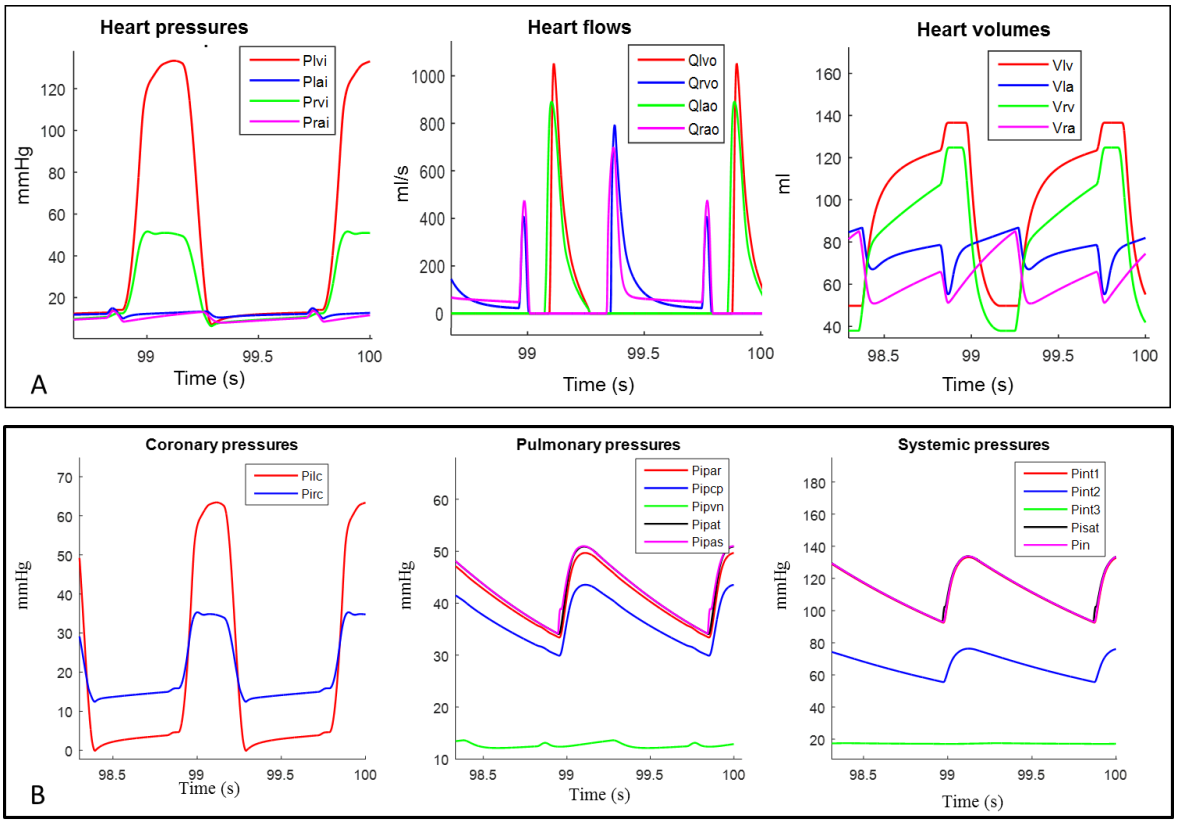

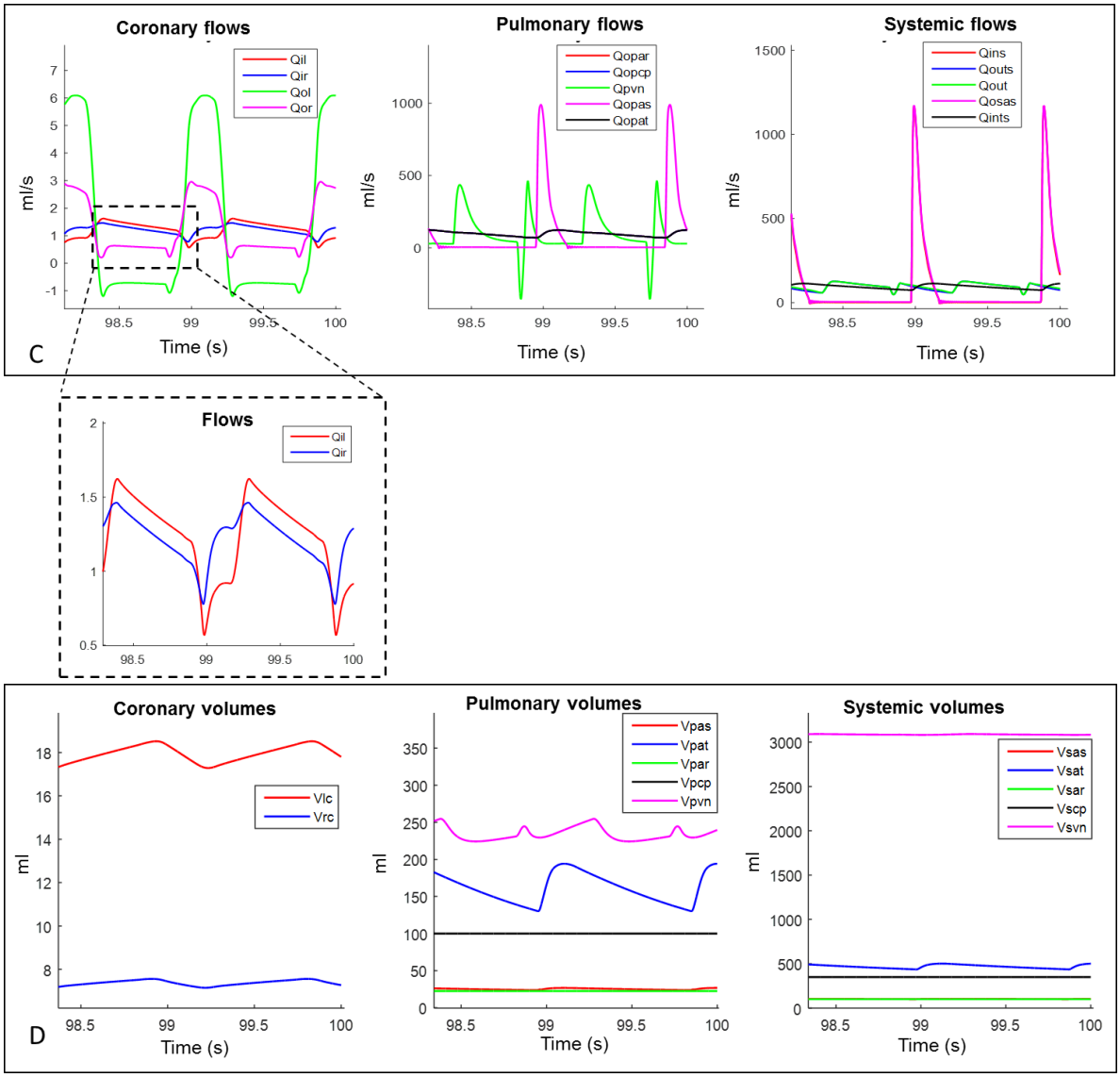

Figure 2.20: Results of beat-to-beat blood pressures, flows and volumes in each compartment. The results presented are for a generic individual model of cardiovascular system. Panel A) Pressures, volumes and flows in the heart chambers. Panel B) Pressures in coronary, pulmonary and systemic circulations. Panel C) Flows in coronary, pulmonary and systemic circulations. A detail of inlet coronary flows is shown. Panel D) Volumes in coronary, pulmonary and systemic circulations.

2.4.2 Barocontrol effectors

Barocontrol becomes active 5 s [49] after the simulation starts, allowing to calculate the barocontrol effect on effector with highest delay. After an initial settling down period, the barocontrol brings the entire system to a stable condition. Figure 2.21 shows the results of the change of the six effectors implemented in the model, under barocontrol.

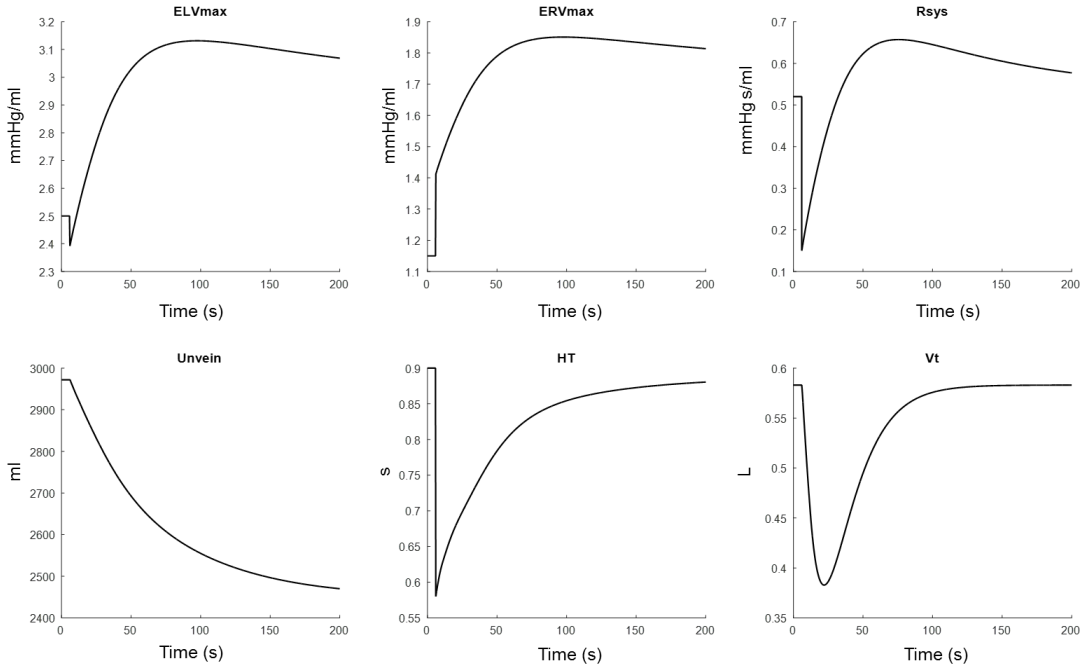

Figure 2.21: Barocontrol effectors under activation of the barocontrol in the model. From the top left: maximal left-ventricular elastance, maximal right ventricular elastance, systemic resistance, venous unstressed volume, heart period, tidal volume.

2.4.3 Oxygen and carbon dioxide distribution

For selected compartments (SAS, SCP, SVN, LC, RC), oxygen concentration and its cardiac cycle averaged value, partial pressure and saturation are shown in figure 2.22, while carbon dioxide concentration and pressure are shown in figure 2.23.

Values of concentrations, pressures and saturation are consistent with physiological values described in paragraph *2.1.2 Oxygen and carbon dioxide distribution*.

The variation of the concentration in both species is caused by the assumption of the instantaneous mixing within each compartment.

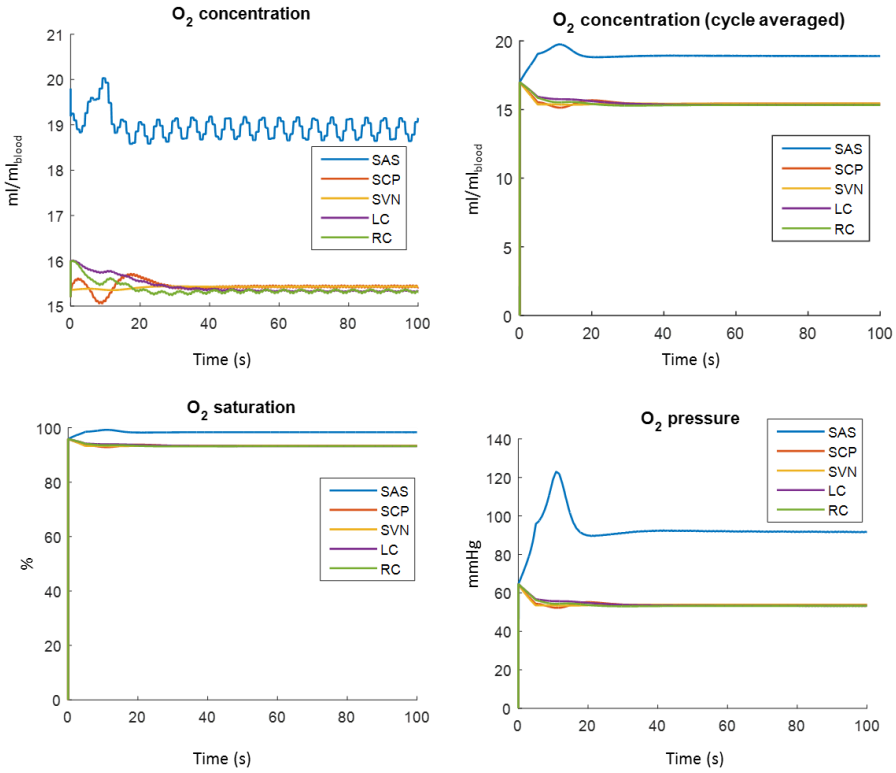

Figure 2.22: Results of oxygen distribution in selected compartments.
Oxygen concentration, cycle-averaged concentration, saturation and partial pressure in SAS, SCP, SVN, LC, and RC.

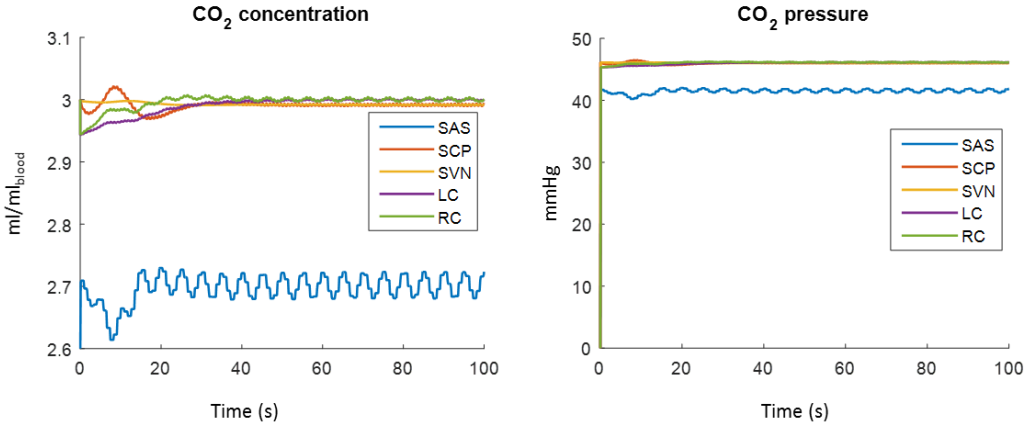

Figure 2.23: Results of carbon dioxide distribution in selected compartments.
Carbon dioxide concentration and partial pressure in SAS, SCP, SVN, LC, and RC.

2.4.4 Cardiac output, stroke volume and ejection fraction

Cardiac output, stroke volume and ejection fraction are clinically relevant parameters. With echocardiography, clinicians measure these parameters to establish the efficiency and performance of the heart. The model can also produce these values as output.

Figure 2.24 shows the cardiac output, stroke volume and ejection fraction obtained from the barocontrolled cardiovascular model for a generic individual. The stable values achieved for cardiac output (5.6 l/min), stroke volume (87 ml/s) and ejection fraction (64%) are within the physiological range.

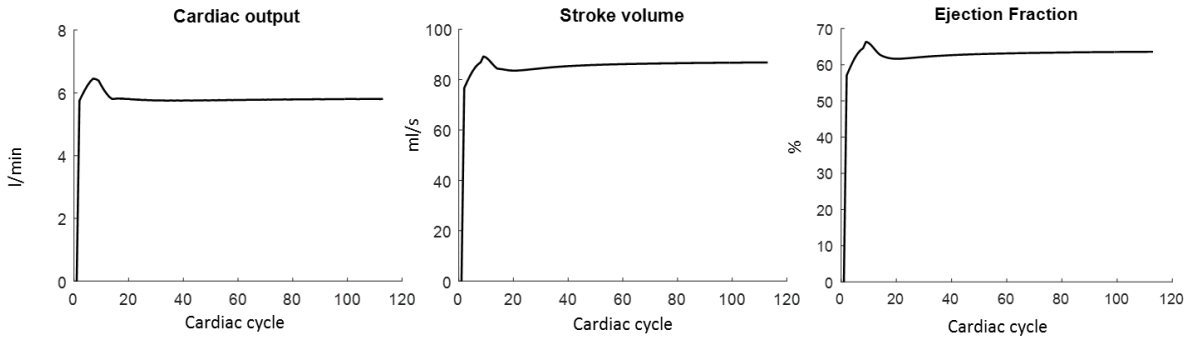

Figure 2.24: Generic model results of cardiac output, stroke volume and ejection fraction. Results were obtained with the barocontrolled cardiovascular model for a generic adult.

2.5 LIMITATIONS

The major limitation of the model is that it represents only some of the features of the cardiovascular control system, while others have been ignored. Lumped parameter-model represent a significant simplification of the cardiovascular system, compared to more accurate modelling approaches, such as 1D and 3D, which are capable to reproduce wave propagation of blood pressure and flow and more detailed results of pressure and flow distribution.

A limitation in this part of the model development is relative to the initialisation of the blood volume in each compartment, which is based on data from the literature and not validated directly. It is important to mention that the amount of blood in each compartment is not an easy parameter to measure.

The necessity to store the non-derivative variables gave rise to the problem of time-step sensitivity, forcing the reduction to a time-step of 0.0001 s for a stable solution. This inevitably increases the simulation time in MATLAB.

A limitation of the barocontrolled model is that it is relatively expensive in computational time. For any particular physiological state it is necessary to run the barocontrolled model until it reaches stability, since the initial condition is not necessarily the stable one.

This introduces limitations especially if the model needs to be operated iteratively as part of a process of personalisation of a model to fit measured clinical parameters. This is discussed further in the next chapters.

2.6 CONCLUSIONS

The 0D model described in this chapter represents the cardiovascular system for a generic individual.

The purpose of this chapter was to extend an existing, published and curated model, to include a representation of the coronary arteries and of the species transport that will support the modelling of physiological changes under exercise conditions in the following work.

A closed-loop model of barocontrol was implemented. The effectors respond to any perturbation of the blood pressure, and a verification of the operation of the model in the context of haemorrhage was performed.

Results for blood pressure, flow and volume for each compartment can be described. The model also enables the calculation of some clinically relevant outputs, such as cardiac output, stroke volume, ejection fraction, end-diastolic and end-systolic volumes, and the description of the distribution of oxygen and carbon dioxide in terms of concentration and partial pressure and saturation.

The modelling of the adenosine distribution has been mentioned in the current chapter in terms of implementation within the model and, in the next chapters, the focus will be on the representation of the adenosine response for individuals with a coronary artery stenosis.

CHAPTER 3

MODELLING THE RESPONSE TO THE ADMINISTRATION OF ADENOSINE

INTRODUCTION AND PURPOSE

In this chapter the model is extended to include a stenosis in the coronary system and to represent the cardiac/cardiovascular response to the administration of adenosine, which is used in the Catheterisation Laboratory to stimulate hyperaemia. The aims are:

- to demonstrate that the model is able to reproduce the observations reported in the literature related to the intravenous infusion of adenosine;
- to examine whether simplifications to the model might be possible to facilitate the process of personalisation of the model parameters to describe the response of an individual based on measured clinical data.

The extended model predicts systemic pressure and flow distributions, as well as heart rate (under barocontrol), and also the time series history of the pressures proximal and distal to the coronary stenosis. The latter is used to characterise the transient dynamics of the hyperaemic response.

It is hypothesised that the dynamics of the systemic circulation has significant influence on the coronary flow response, because it controls both the proximal (aortic) pressure, driving the coronary flow, and the rate at which the adenosine, administered in the veins, reaches the coronary inflow. Conversely, the coronary dynamics might have relatively low influence on

the system dynamics, because the coronaries take a relatively small proportion of the flow and, therefore, it might make small perturbations to the global pressure and flow distributions. If this hypothesis is proven, then a one way coupling, in which proximal pressure and adenosine concentration are computed in a system model and applied as a boundary condition to a local coronary model, might be more tractable for recursive operations as part of a parameter fitting optimisation process.

In this chapter also the influence of the proximal, distal pressure and heart rate on the FFR, hypothesising different stenosis severity, the influence of the barocontrolled hyperaemic response on the adenosine concentration and the influence of the stenosis severity on the delay to reach stable hyperaemia are analysed.

3.1 LITERATURE ON ADENOSINE RESPONSE

As introduced in the previous chapter (*Paragraph 2.1.4 Adenosine pharmacodynamics and pharmacokinetics model*), adenosine is naturally present in the human body. From the cardiovascular system point of view, adenosine has 4 types of cellular receptors, which can decrease the heart rate, prolong the refractory period of the cardiac cycle, vasodilate the peripheral circulation and vasoconstrict some organs such as kidneys and liver.

Adenosine can produce different effects depending on the method of administration (*bolus, infusion*), the location of administration (*intracoronary*-IC, *intravenous*-IV *femoral* or *radial*) and the dose [116, 126].

Recently several experimental studies have sought to understand and to quantify the effect of adenosine on the cardiovascular system, especially when it started to be used as part of treatment of cardiac arrhythmias and ischaemia.

In the bolus injection, adenosine concentration rapidly increases and decreases because of its short half-life (<10s) and acts mainly on the electrical signals of the heart, exerting negative chronotropic effects on the sinus node and negative dromotropic effect on AV node [116].

In contrast, infusion allows the concentration of adenosine to reach a stable value for a longer period of time and, therefore, other physiological processes related to cardiovascular regulation can be stimulated, including haemodynamic effects. The presence of cyclic response can be observed for lower doses, due to cyclic variation of adenosine concentration [126].

As mentioned beforehand, intravenous infusion of exogenous adenosine is the gold standard method used to induce hyperaemia in patients with CAD to assess the severity of the lesion. For this application, adenosine is commonly administrated by femoral infusion with a dose of 140 μg/kg/min, which is considered the optimal to achieve maximum hyperaemia: above this dosage the level of vasodilation does not increase [126, 127].

In the next paragraphs, the effect of adenosine response during intravenous infusion is described, distinguishing between the systemic and the coronary effects.

3.1.1 Systemic effects

Clinical and experimental results have shown different types of systemic adenosine response in conscious humans, and also in animals. Variability of the responses can be observed between different species and within individuals of the same species.

Infused adenosine causes vasodilation of the microcirculation (arterioles and small arteries) in most of the organs. It is expected then a decrease in the blood pressure, which stimulates the barocontrol to restore the baseline condition, increasing the heart rate, as several studies in patients and healthy humans have reported [126, 128-133]. Chronologically the pulmonary vasodilation occurs first, probably with an immediate stimulation of the reflex regulation which

changes the respiratory rates and volumes. Experimental and clinical studies report this type of theoretical response.

Biaggioni *et al.* [134-136] studied the cardiovascular effects of adenosine on healthy volunteers and on patients with severe autonomic failure, in a state of consciousness, aiming to identify the importance of the sympathetic reflex and the contribution of the lungs. Results showed that IV infusion of adenosine (140 μg/kg/min) in healthy volunteers caused an increase of heart rate (30-35 beats/min), an increase of the systolic pressure (10-16 mmHg), an increase of the pulse pressure (10-20 mmHg) and a decrease of the diastolic pressure (5-6 mmHg), whilst maintaining the mean arterial pressure constant. Also the respiratory rate was constant, although the minute ventilation (the ventilation per minute) increased from 7.8 to 14.7 l/min. In patients with severe autonomic failure, a different response was observed: the heart rate increased by less than 10 beats/min, and both systolic and diastolic blood pressure decreased by 40 mmHg. These results suggest the vasodilatory effects of adenosine are regulated by the sympathetic system. This was also demonstrated by the measurement of the right peroneal nerve activity which showed an increase from 198 to 452 units/min. The study confirmed the dose- and site-dependence of the adenosine response in conscious humans. From the obtained results, observations were made to attempt a description of the influence of the respiratory stimulation by the adenosine. Considering the short half-life of the drug, the concentration of adenosine should be higher in the right circulation than the systemic circulation, and, therefore stretch-receptors in heart and lungs and carotid chemoreceptors should be responsible for the sympathetic response.

Pelleg [116] reviewed the adenosine effect on humans, reporting that the infusion of adenosine on average increases heart rate by 33 beats/min, systolic blood pressure by 13 mmHg and decreases diastolic blood pressure by 8 mmHg. At a pulmonary level, it also increases the minute ventilation and decreases the partial pressure of carbon dioxide. Systemic infusion of

adenosine causes also a renal effect with reduction of urine production, which might be the consequence of the blood pressure drop or a direct vasoconstrictor effect of the adenosine.

During the hyperaemia stimulated to measure FFR, heterogeneous responses to IV adenosine have been observed, although the reason for this diversity is not clear. Adenosine produces a dose-dependent decrease in vascular resistances, linked to significant decreases in central venous and LV end-diastolic pressures, which stimulate a reflex discharge of the sympathetic system in order to increase the cardiac output [129].

Fuller et al. [117] studied the effects of adenosine infusion at different consecutive doses on 6 male subjects monitoring the cardiovascular and respiratory effects and the skin temperature. Results, considering the dosage of 100 μg/kg/min, showed an increase of heart rate by 25 beat/min, a non-significant increase in both systolic and diastolic pressure, an increase of skin temperature by about 1°C, an increase of tidal volume by 19%, of minute ventilation by 15%, a decrease of CO_2 partial pressure by 4% and an increase of mean respiratory flow by 22%. The insignificant effect on the blood pressure compared with other studies might be related with the method of measurement used or the protocol used in terms of duration and dose of the infusion. The increase on the skin temperature suggests an activation of the microcirculation, while the respiratory effects should be related with the carotid chemoreceptors. A central effect was excluded as the adenosine is not able to pass the brain barriers. With regard to the increase of heart rate, it might be caused by a compensatory effect for the vascular relaxation, without barocontrol activation since the blood pressure is only slightly affected.

Ogilby et al. [137] compared the haemodynamic effect of adenosine in normal subjects and in patients with CAD. Heart rate and systolic blood pressure followed the same trend in both categories with similar changes (+20 beats/min, -28 mmHg respectively), cardiac output increased slightly more for healthy subjects (3.1 l/min against 2.4 l/min), the total systemic vascular resistance decreased by 35% and 42% respectively. In this study also pulmonary

pressure data were measured reporting an increase of both mean pulmonary capillary wedge (72 % and 127% respectively for normal subjects and patient with CAD) and mean pulmonary arterial pressures (55% for normal subjects and 50% for patients with CAD).

The literature on human response shows contradictory results with respect to the measured systemic pressure: some studies show an increase in aortic pressure, others a decrease and others a non-significant change. It is therefore challenging to establish categorically what the actual effect will be on the aortic pressure for an individual patient. The only certainty is the vasodilatory effect of adenosine on the microcirculation of the heart. The vasodilatory effect of adenosine on other parts of the systemic circulation is documented, but it appears that arterioles in the brain and kidneys are not affected.

3.1.2 Coronary effects

It is evident the importance of myocardium behaviour in the diagnostic use of adenosine, such as the assessment of FFR. Normally the coronary blood flow is well controlled by the myocardial resistances, driven by the autoregulation mechanism. The most important parameters to determine coronary blood flow are coronary arterial pressure and myocardial oxygen consumption [115, 138, 139].

The coronary circulation comprises different compartments: main coronary arteries, small arteries and arterioles, capillaries and ultimately the venous system. In normal physiology in resting condition, 60% of the resistance is given by the arteriolar level, 25% by the capillaries and 15% by the venous compartment. Epicardial arteries are considered to have no resistance. During hyperaemia the total resistance drops by approximately 65% (86% in the arteriolar compartment and 98% in the venular) and the capillaries offer the maximum resistances. For the assessment of coronary stenosis, hyperaemia is generated in order to have a minimal

resistance and counteract the autoregulation [115]. The direct consequence of myocardial vasodilation is the increase of myocardial blood flow (MBF), which is dose dependant, as shown by Wilson et al. [126], and can reach even 4 times the baseline MBF.

Overall it is possible to state that the only coronary effect of adenosine is the vasodilation of the myocardial microcirculation, although the actual mechanisms are not known yet.

3.2 MODELLING ADENOSINE EFFECTS ON A GENERIC INDIVIDUAL

In this paragraph the description of the modifications of the model with regard to the IV infusion of adenosine effects are explained.

The systemic response is the most complex one because it involves different mechanisms and some are still unknown. The mechanism of vasodilation effect at arterial level is the most certain and documented, although it does not happen in all the organs, depending on the type of receptors. Arterial vasodilation should cause a decrease in the aortic pressure, which then stimulates the barocontrol and chemocontrol system to restore to baseline condition. This is what it is expected considering the known effects of adenosine, although experiments have demonstrated the existence of other effects. Different types of response have been identified in patients and not all of them have a physiologically known explanation.

Supported by the literature mentioned before, and by our own clinical data, it is assumed that the first effect happens in the pulmonary circulation, where arterioles are vasodilated and this could potentially cause:

i) an increase in pulmonary blood volume and consequent decrease in oxygen concentration in the pulmonary capillaries, which stimulates the chemoreceptors and therefore the respiration. This can be observed in the increase of tidal volume, which aims to restore

the oxygen partial pressure. The stimulation of respiration involves also the relaxation of lung stretch receptors, allowing a higher airflow in input;

ii) a pulmonary pressure drop which is then reflected in a lower left ventricular pressure, which then activates barocontrol receptors in the aorta.

The increase in heart rate during adenosine IV infusion might be caused by multiple components of its regulation:

i) the activation of the barocontrol system to compensate the pressure drop and maintain a constant cardiac output;

ii) the activation of chemocontrol system to restore the oxygen concentration;

iii) the increase of respiration activity linked to the stretch receptors stimulation;

iv) a compensation of the negative chronotropic and negative dromotropic effects caused by the cardiac A1 receptors of adenosine;

v) "fight-or-flight" response emotionally driven by the side effects of the adenosine which might lead patients to panic.

Our cardiovascular model, described in the previous chapter, attempts to represent the observations in real patients considering the generic individual, conscious of the limitation in the representation of the full effects of the cardiovascular response, since the model does not include every mechanism.

The model response to adenosine is represented as a vasodilation in the pulmonary and systemic circulations and in the myocardium, each as a function of the adenosine concentration in the respective compartments, as explained in the following paragraphs.

3.2.1 Inclusion of coronary stenosis

Since in this project the primary investigation is that of the effect of adenosine on a CAD patient, the model is extended to include a mild stenosis in the left coronary branch (R_{sten}),

represented as a resistance in series with the RCR circuit, representing the left myocardial compartment, as shown in figure 3.1.

The ratio between the distal (P_d) and proximal (P_a) pressure across the stenosis is calculated for each time-step during all the simulation to determine then the FFR at stable hyperaemia.

The value of the stenosis resistance, R_{sten}, was set to 16 mmHg s/ml, generating P_d/P_a ratio close to 0.8, which represents the cut-off value for clinical intervention. A long-term aim is to use the model in the diagnosis of clinically significant lesions, and so it is important that its performance is investigated closely in the threshold region.

3.2.2 Vasodilation in systemic, pulmonary and coronary compartments

As mentioned before, literature data suggest that adenosine generates total systemic vasodilation and myocardial vasodilation, with a respective drop in the resistances of 30-42% and of 70%, acting in the arterioles.

It is necessary at this point to make a comment on the adaptation of Ursino's neuro-regulatory model onto the one described in this project. Ursino described the systemic circulation as an arterial compartment from which develop parallel branches, consisting of the peripheral and the venous circulation for the splanchnic and extra-splanchnic circulation. The peripheral circulation is the target of the regulatory pathways. In contrast, in the model developed in this thesis, the systemic circulation was represented as one single branch but with greater differentiation between the vasculature compartments (aorta, arteries, small arteries, arterioles, capillaries and veins). The barocontrol is applied on the capillaries compartment, although the vasodilation/vasoconstriction is dominant in compartments such as arterioles and small arteries. The review of the literature indicated that the adenosine-induced vasodilation is understood to act on the arterioles and arteries, and, therefore, it was applied to these compartments in the model. Specifically, the vasodilatory effect was applied on the following

compartments: the systemic arterioles (SAR), the pulmonary arterioles (PAR) and the left (LC) and right (RC) myocardium (Figure 3.1). The vasodilation is assumed to produce a 50% decrease in the resistance for all the target compartments (SAR, PAR, LC and RC). This is consistent with the results of the experimental studies in literature [140-143], where the arterioles' diameter on average increases by 15-20% when stimulated by adenosine. Approximating the arteriolar resistance with Poiseuille's law, the power to the 4 of the change in diameter will determine about 50% decrease in the resistance (Eq.3.1).

$$\frac{R_D}{R_B} = \frac{\frac{1}{(1+v)^4 \cdot D_{art.,B}^4}}{\frac{1}{D_{art.,B}^4}} = \begin{cases} 0.57 & if\ v = 0.15 \\ 0.48 & if\ v = 0.2 \end{cases} \qquad \text{(Eq.3.1)}$$

where R_D is the vasodilated arterial resistance, R_B is the baseline arterial resistance, $D_{art,B}$ the average diameter of the arterioles at baseline and v represent the variation of the baseline diameter due to vasodilation.

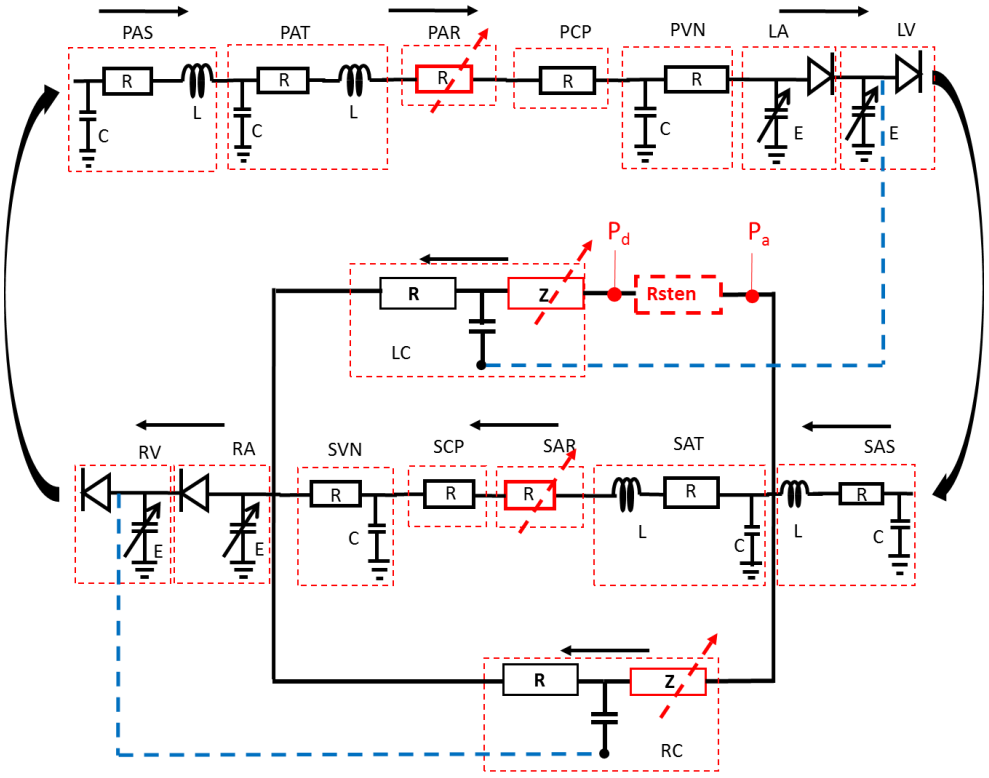

Figure 3.1: Model adapted to include adenosine-induced vasodilation.
Pulmonary arterioles, systemic arterioles and left and right myocardium resistances are dependent on the adenosine concentration in the relative compartment.

Literature data are not explanatory on how the arteriolar resistances vary *in vivo* as a function of the adenosine concentration. It was observed on humans that adenosine (administrated through venous infusion) has a saturation level, beyond which the effects are no longer dependent on the concentration [127]. This is also intuitive considering that *in vivo* arterioles cannot physically continuously vasodilate. For these reasons in this model the arteriolar resistances, R_x, were described as a linear function of the adenosine concentration in every compartment, $C_{ADE,x}$, until a saturation value of adenosine concentration, $C_{ADE,th}$, is reached above which the resistances were stable (Eq.3.2- Figure 3.2), where $R_{x,0}$ is the baseline arteriolar resistance, FR_{th} is the vasodilation coefficient set to 0.5.

$$R_x(C_{ADE,x}) = \begin{cases} R_{x,0}\left(1 - \dfrac{(1 - FR_{th}) * C_{ADE,x}}{C_{ADE,th}}\right) & if\ C_{ADE,x} < C_{ADE,th} \\ R_{x,0} * (1 - FR_{th}) & if\ C_{ADE,x} \geq C_{ADE,th} \end{cases} \quad \text{(Eq.3.2)}$$

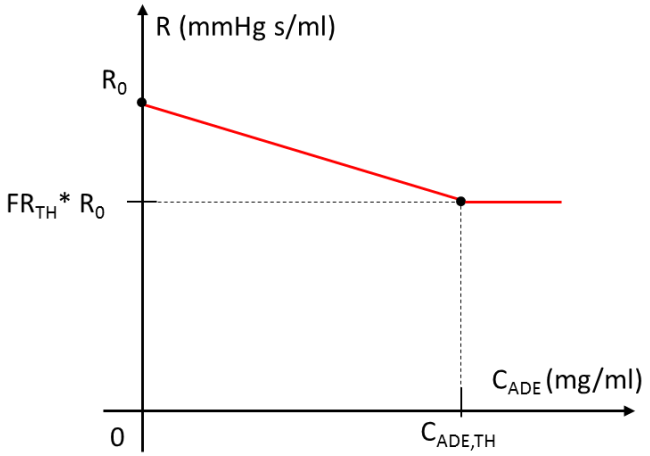

Figure 3.2: Relationship between adenosine concentration and vascular resistance.
Adenosine concentration and resistance of the compartments where occurs vasodilation are linearly dependent. After a concentration threshold value, a saturation is observed when the resistance stays stable at its minimum value.

It is assumed that the IV infusion of adenosine used in the clinical protocol for the FFR assessment stimulates the maximum hyperaemia and therefore the $C_{ade,th}$ was selected observing the maximum concentration in the coronary compartments. Figure 3.3 shows the maximum adenosine concentration in the compartments, starting from the systemic vein where

the drug is injected. As suggested by some literature data [134], the steady state response shows maximal adenosine concentration at the location at which the adenosine is introduced (SVN), and a gradual reduction away from this location. Because of its short half-life (7 s), adenosine never achieves a relatively uniform distribution across the system. Table 3.1 reports the respective baseline resistance and maximum adenosine concentration for the target compartments (SAT, PAT, LC and RC).

Table 3.1: Values of baseline resistances and maximum adenosine concentration for target compartments.

Compartment	R_0 [mmHg s/ml]	$C_{ADE,th}$ [mg/ml]
SAR	0.5	$1.29*10^{-4}$
PAR	0.05	$3.43*10^{-4}$
LC	76.5	$0.90*10^{-4}$
RC	76.5	$0.97*10^{-4}$

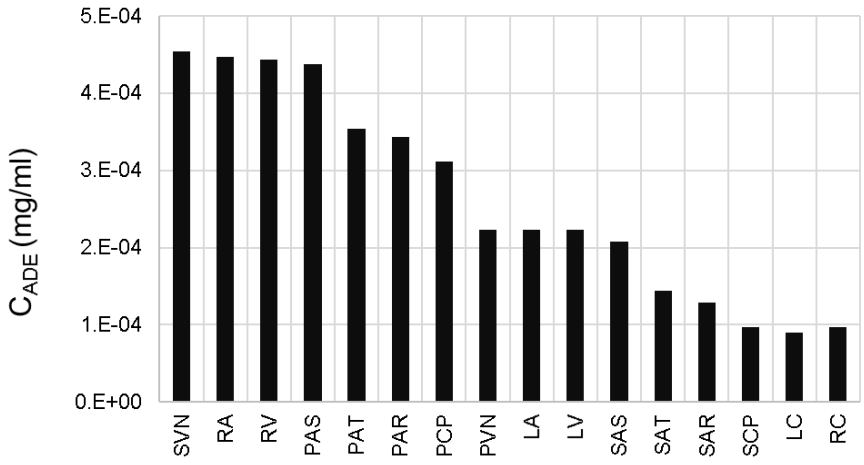

Figure 3.3: Steady state adenosine concentration in each compartment.

3.2.3 Sensitivity analysis

As stated before, this thesis is focused on the model-based representation of the adenosine response for each individual, which as observed both in the literature [120, 129, 144] and in

the collected data of the Wellcome study (STH 16467 *Wellcome study: an angiogram is all you need*) can be different from patient to patient.

To quantify the influence of the parameters in the global circulation model on the local coronary circulation, and vice versa, a sensitivity analysis was performed. It is hypothesised that, because the coronary flow is a small proportion of the total systemic flow, the system model is not strongly influenced by the coronary parameters whilst, in contrast, the coronary flow is driven by the aortic pressure and the supply of adenosine to the coronaries is driven by the concentration in the aorta and, thus, a strong dependence of coronary flow on system parameters is expected. The aim of this section is to prove this hypothesis by quantifying the associations between model inputs and model outputs.

3.2.3.1 Relative influence between the global and local circulation: a sensitivity analysis

The focus of this paragraph is to study how a change in aortic pressure and heart rate, correspondent to the clinical measurements during assessment of FFR, influences the distribution of the adenosine and its relative vasodilatory effect in a cardiovascular model for a generic individual.

The sensitivity analysis presented in Chapter 2 (Figure 2.18) already suggests that the coronary parameters only influence the coronary outputs, while the systemic output are not sensitive to these parameters. As can be seen in the results of the sensitivity analysis of the barocontrolled model described in Chapter 2 (Figure 2.19), the central pressure of the sigmoid function of the barocontrol, P_n, has high sensitivity with regards to both the aortic pressure and the heart rate, although there are barocontrol parameters which have an effect on these, such as the reference capillary resistance and the gains of the variation of the effectors.

To study the heart and the aortic pressure sensitivity, the input parameters selected for this specific sensitivity analysis are the P_n for the global system and the stenosis, R_{sten}, and the myocardial, $R_{myo,}$ resistances for the local system.

Table 3.2 reports the values used for each variable, which were changed, one at a time, to determine the changes in the outputs associated with these changes in inputs. The reference model had P_n equal to 85 mmHg, R_{sten} equal to 16 mmHg s/ml and R_{myo} equal to 76.5 mmHg s/ml. The considered output parameters were, for the global model, aortic pressure P_{AO}, heart rate HR, cardiac output CO, aortic concentration of adenosine $C_{ADE,AO}$, systemic arteriolar, R_{SAR}, and capillary resistance, R_{SCP}, pulmonary arteriolar resistance, R_{PAR}, and finally, for the local model, distal pressure P_D and left and right myocardial upstream resistances, Z_{LC} and Z_{RC}. The P_D/P_A ratio dependent on both parts of the model was also considered.

Table 3.2: Values of parameter of the systemic and the local coronary circulation used for the simulation in a generic patient.

Parameters	Reference values	Values changed OAT	
P_n (mmHg)	**85**	75	95
R_{sten} (mmHg s/ml)	**16**	8	32
R_{myo} (mmHg s/ml)	**76.5**	50	100

Each simulation time was set to 380 s allowing the barocontrol to reach stability, the adenosine injection to last 90 s and to restore to baseline conditions. The simulation results regarding the CO are reported for each cycle, as explained in the previous chapter, while signals of HR, pressures, adenosine concentrations and resistances are represented in time.

With respect to the analysis of the time course of the response to adenosine, the variations over the cardiac cycle are not important and so, for presentation of the results in the next section, the time series signals have been smoothed with a window of 2 s. The period of numerical stabilisation from the initial conditions is not important, and so in the figures the results of the simulation are presented from t=240 s, 10 seconds before the adenosine starts to be infused.

For comparison, the CO signal was normalised on the x-axis with respect to the number of cycles.

The comparison between the reference model results, Y_m, and the ones where one single input parameter X was increased, Y_{+X}, and decreased, Y_{-X}, was described by a root mean square change (RMS), calculated from the average normalised sum between the reference results and the changed parameters results, and divided by the difference in percentage of the input change. Since for each parameter a higher and a lower value have been considered, the final RMS_X is the average between the two comparisons with both values for the same parameter. Equation 3.3 describes the RMS for each parameter.

$$RMS_X = mean\left(\frac{\frac{\sum_{t=240}^{t=380}\left|\frac{Y_m(t)-Y_{+X}(t)}{mean(Y_m)}\right|}{N}}{\left|\frac{X_{ref}-X_+}{X_{ref}}\right|} \quad , \quad \frac{\frac{\sum_{t=240}^{t=380}\left|\frac{Y_m(t)-Y_{-X}(t)}{mean(Y_m)}\right|}{N}}{\left|\frac{X_{ref}-X_-}{X_{ref}}\right|}\right) \quad \text{(Eq.3.3)}$$

where N is the number of sample per signal, X_{ref} is the reference value for each input parameter. A similar approach was used to compare the peak values of the global and local outputs at the variation of each of the input parameter, as described in Eq.3.4.

$$RMS_{X,peak} = mean\left(\frac{\frac{\left|Y_{m,peak}-Y_{+X,peak}\right|}{Y_{m,peak}}}{\left|\frac{X_{ref}-X_+}{X_{ref}}\right|} \quad , \quad \frac{\frac{\left|Y_{m,peak}-Y_{-X,peak}\right|}{Y_{m,peak}}}{\left|\frac{X_{ref}-X_-}{X_{ref}}\right|}\right) \quad \text{(Eq.3.4)}$$

where $Y_{m,peak}$ is the value of the output parameter at peak from the reference model and $Y_{\pm X,peak}$ is the value of the output parameter at peak obtained when one of the parameters was changed. To identify the peak values for each output the following approach was used. For the outputs HR, CO and systemic capillaries resistances (R_{SCP}) the global maximum value was considered; for the outputs P_a, pulmonary resistances (R_{PAR}) and systemic arterioles resistances (R_{SAR}) the global minimum was considered. For the remaining outputs (P_d, C_{ao}, C_{RC}, C_{RC}, Z_{LC}, Z_{RC} and FFR) if the global maximum or minimum would have been considered, the peak value would

have been wrong, since these outputs have a small negative slope during all the hyperaemia. To overcome this problem, a reference value after 50 s the adenosine infusion starts, $X(t_{50})$, was selected observing the output results of the model and making sure that 50 s were sufficient to reach stable response for all these outputs. The identification of the starting of the peak response consists of a comparison of the relative reference value at t_{50} with the value of the considered output at previous time-steps since the difference is below a threshold value specific for each output: respectively of 0.75 mmHg for P_d, 0.00001 mg/ml for C_{ao}, 0.000002 mg/ml for C_{RC} and C_{RC}, 0.6 mmHg s/ml for Z_{LC} and Z_{RC} and 0.002 for FFR. These thresholds were arbitrarily chosen after a trial and error approach to get satisfactory results visually examined. The delays (in time for all the outputs, except in cardiac cycle for CO) necessary for each output to reach the peak value in the period following the start of adenosine administration have been then considered for comparison.

3.2.3.2 Influence of the barocontrol on the coronary boundaries outputs

The coronary boundaries outputs signals calculated with the barocontrolled model (Y_{BARO}) and with the non-barocontrolled model ($Y_{NO\text{-}BARO}$) were compared as shown in Eq.3.5. The signals were considered between 240s and 380s time interval, with N samples.

$$RMS_{BARO} = \frac{\sum_{t=280}^{t=380} \left| \frac{Y_{BARO}(t) - Y_{NO-BARO}(t)}{mean(Y_{BARO})} \right|}{N} \qquad \text{(Eq.3.5)}$$

As explained already in the previous paragraph, for CO, expressed in cardiac cycles, a similar index was calculated, where the number of samples is the number of cardiac cycles and the signal have been considered proportional to the time interval.

3.2.4 Change of barocontrol parameters

It has already been demonstrated (*Paragraph 2.1.3.2 Validation of the adapted controlled cardiovascular model*), that the current barocontrolled model can reproduce the observed peak pressure drop of about 40 mmHg and peak response of heart rate increase of 20 beats/min in a haemorrhagic condition. Operation of the model with the same numerical values of the barocontrol parameters as those used to simulate haemorrhage does not reproduce the typical decrease of aortic pressure of about 10 - 15 mmHg and increase of heart rate of about 25 beats/min that is reported in the literature under the administration of adenosine.

The parameters that require to be changed are the ones related with the heart rate and therefore its reference value and its gains related with the sympathetic and vagal ways.

It was assumed that the same barocontrol processes govern the response to adenosine, but that the control parameters should be adjusted to produce the observed magnitude of response. Compared with the haemorrhage simulation, the aortic pressure drop is reduced and the variation of heart rate is higher. Intuitively, then, the heart rate gain (in absolute value) should be increased. The baseline condition should still stabilise at a normal heart rate, and so the reference value of the heart period was also adjusted. The original barocontrol parameters of reference value and sympathetic and vagal response gains were respectively 0.58 s, -0.13 s/*v* and 0.09 s/*v*. To obtain the desired behaviour, the reference heart period was set to 0.48 s, corresponding to 125 beats/min, and the sympathetic and vagal gains respectively to -0.75 s/*v* and 0.25 s/*v*. These values were obtained with a trial and error approach.

3.3 RESULTS

Results of the barocontrolled cardiovascular model representing an average individual with a stenosis in the left branch of the coronary, generating a nominal FFR of 0.8 in the reference state, are presented in this first part of this section. As discussed previously, this was chosen because it is the threshold for the intervention decision and so the region of greatest interest for operation of the model.

Because of the requirement to reach stability, each simulation runs for about 8 hours on a normal office desktop (DELL, Intel i5). A process of optimisation of the code could reduce the simulation time and potentially move it closer to clinical application.

3.3.1 Analysis of aortic pressure and heart rate response to adenosine

The cardiovascular model with the barocontrol was tuned to represent the average response during IV infusion of adenosine reported by experiments reported in the literature. Figure 3.4 illustrates the time course of the aortic pressure and heart rate responses computed by the model. A decrease of aortic pressure by about 7 mmHg (7%) and a consequent increase of heart rate by 15 mmHg (23%) is observed, based on a vasodilation effect in the pulmonary and systemic arterioles and in the left and right myocardium of 50% dependant on the adenosine concentration in the compartments. These results show agreement with typical literature data on these two parameters, and thus it is demonstrated that, with the selection of appropriate parameters, the model is able to reproduce a plausible generic response to the administration of adenosine. The effects of the adenosine are still not completely known; different responses among different individuals have been reported.

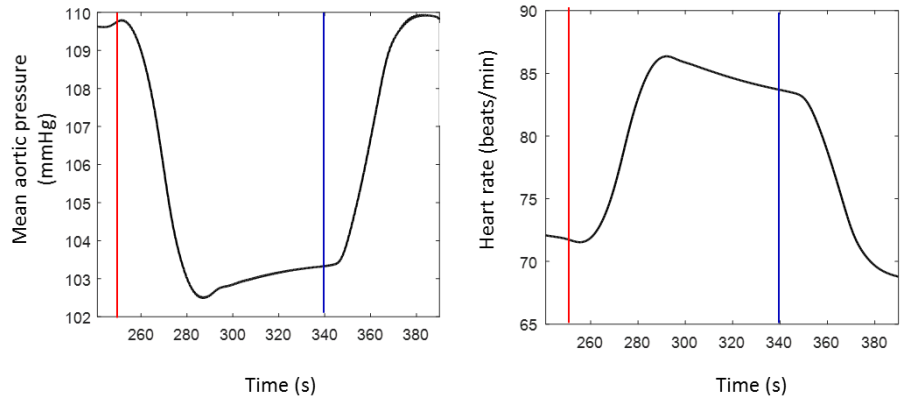

Figure 3.4: Mean aortic pressure and heart rate response to adenosine.
The red vertical line indicates when the adenosine starts to be infused and the blue lines when it stops.

3.3.2 Influence between the global model and the local circulation and interpretation of the results

The sensitivity analysis results are reported in Figure 3.5. The inputs (vertical axis) and the outputs (horizontal axis) have been clustered into systemic and coronary elements, with the outputs at the boundary between the systems, and part of both, explicitly identified.

Figure 3.5-A shows the sensitivity considering the entire signal (from t=240 to 380s). As expected, it is observed that the influence of the systemic inputs is high for the systemic outputs and for some of the coronary outputs, whilst the coronary inputs have high influence only on the coronary outputs. The influence of the coronary inputs on the systemic outputs is low. In particular, the barocontrol parameter P_n is the one having the most effect on all the outputs. It changes the baseline value of the heart rate and therefore influences the cardiac output. It also affects the systemic capillary resistance.

The aortic pressure is also dependent on the P_n value, as well as the coronary pressure distal to the lesion. The high value of the dependence of distal pressure on P_n is explained by the fact that the distal pressure is dependent on the aortic pressure, which is in turn dependent on the P_n. The aortic adenosine concentration is slightly influenced by the P_n and this suggests that

also the myocardial adenosine concentrations are slightly influenced by the aortic pressure, as reflected also in the myocardium resistances, since the change of adenosine concentration in the myocardium changes also the vasodilation curve and values. The highest dependence of the left myocardium resistance might be cause by the back pressure from the left ventricle which is intuitively more influenced by the P_n compared with the right ventricle pressure applied to the right myocardium.

The FFR is independent of the P_n, consistent with expectation, and it is dependent on the myocardium resistance and the stenosis resistance inputs.

The coronary inputs related to the stenosis and myocardium resistance have very little influence on all the systemic outputs and higher influence on the coronary outputs. In particular, the stenosis resistance has impact on the distal pressure and on FFR. The initial value of myocardial resistance (set equal for left and right branches) has influence on all the coronary outputs, with a high value for the myocardial resistances during the adenosine response as expected. Similar results were obtained considering the comparison between the peaks of the outputs (Figure 3.5-B).

Figure 3.5- C shows the difference between the delays to peak from the reference state and the results varying the inputs (in seconds for all the outputs, except CO which is expressed in cardiac cycles) necessary for each output to reach the peak value after the adenosine starts.

It is observed that the pulmonary arterioles resistance is the first to respond with a reference delay of 2.94 s, since the adenosine hits them first.

The P_n input parameter is the most influencing parameter in terms of the speed of the response for all the outputs parameters, both systemic and coronary. The reason for that might be related with the fact that an increase/decrease of P_n determines an increase/decrease of the aortic pressure, of the heart rate and the cardiac output so that the adenosine distributes quicker/slower.

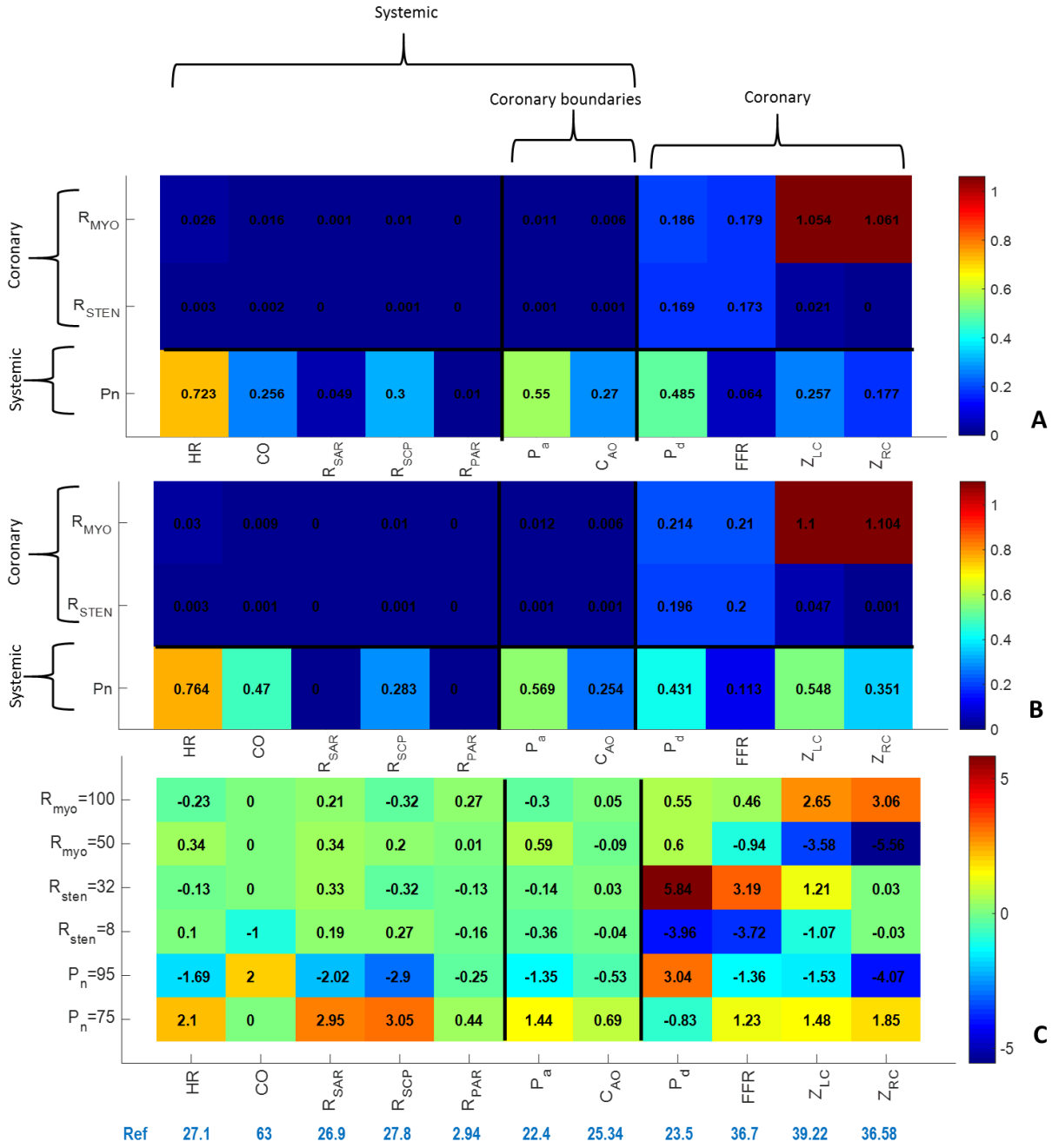

Figure 3.5: Sensitivity analysis results about the relative influence of the local and global model. A) RMS considering the time series signals. B) RMS considering the peak values. C) Difference of the delay to peak for each output to reach the peak value since the adenosine starts. Time necessary to reach peak for the reference state (P_n=85 mmHg, R_{sten}=16 mmHg s/ml, R_{myo}=76.5 mmHg s/ml) is indicated in the bottom-row (in blue) in s, except for CO in cycles.
Inputs clustered in systemic (P_n) and coronary (R_{sten}, R_{myo}). Outputs clustered in systemic (HR, CO, R_{SAR}, R_{SCP}, R_{PAR}), coronary boundaries (P_a, C_{AO}) and coronary (P_d, FFR, Z_{LC}, Z_{RC}).

The aortic adenosine concentration delay in the peak response is mostly influenced by the aortic pressure, and slightly influenced by the coronary inputs. The difference in the delay to reach the peak compared to the reference is 0.69 s (2.7% slower) for P_n= 75 mmHg and -0.53 s (2.1

% quicker) for P_n= 95 mmHg. With regards to the coronary inputs the difference in the aortic adenosine concentration delay in peak response is less than 0.1 s (0.4 %).

The FFR delays are dependent on the stenosis severity: -3.72 s (10% quicker) for non-severe stenosis, and +3.19 s (8.7 % slower) for the severe stenosis. This can be explained by the reduction of flow to the myocardium caused by the lesion, which in turn means that the local adenosine concentration needs more time to stabilise. This hypothesis seems to be also confirmed by the influence of the R_{myo} input on the left and right coronary resistance delay: for a smaller baseline value of the myocardial resistance the peak response in the right myocardium happens 5.56 s (15.2%) before the reference situation, and for a stiffer baseline myocardium the peak happens 3.06 s after (8,4%) the reference delay. Again, this is associated with the proportional amount of blood flow, relative to the compartment volume, determined by the myocardial and the stenosis resistance. The FFR delays in the peak response is also slightly influenced by the myocardial resistance: -0.94 s (2.5% quicker) for R_{myo}=50 mmHg s/ml and +0.46 s (1.2 % slower) for R_{myo}=100 mmHg s/ml. Similarly happens with the variation of P_n: +1.23 s (3.3% slower) for P_n= 75 mmHg and -1.36 s (3.7 % quicker) for P_n= 95 mmHg. The concentration of adenosine in the myocardium requires a different amount of time to get to stable values.

The P_d delay is strongly associated with the stenosis severity: +5.84 s (24% slower) for severe stenosis and -3.96 s (16.8% quicker) for the non-severe stenosis. P_d peak delay is also influenced by P_n with +3.04 s (13% slower) for P_n= 75 mmHg and -0.83 s (3.2% quicker) for P_n= 95 mmHg.

For some of the outputs parameters (R_{SAR}, R_{PAR} and P_a) the delay to reach the peak with the variation of the coronary parameters show a concordant sign for both the input values. These are dependent on how the peaks have been calculated. However, their values are less than a third of a second and therefore very small compared with other delays above 2 s.

Figures 3.6, 3.7 and 3.8 report the time-series response for each output parameter, under the variation of each input (P_n figure 3.6, R_{sten} figure 3.6, R_{myo} figure 3.8). The x axis of all graphs is time (s), except the CO expressed in number of cardiac cycles. The y axis represents different units according to the parameter represented (mmHg for pressures, beats/ min for heart rate, mmHg s/ml for resistances, mg/ml for concentration, l/min for cardiac output).

Figures 3.6, 3.7 and 3.8 show the concentration in the aorta and in the coronaries. It is observed that the time to reach maxima hyperaemia in the coronary circulation is highly dependent on the delay of the aortic concentration. The time to reach maximum concentration in the aorta is about 25 s in all the cases with different pressure, severity of stenosis and myocardial resistance. The myocardial concentration in the myocardium reaches its maximum about 10 s after the peak within the aorta. The time to reach maximal hyperaemia is therefore 70% determined by the global system and 30 % by the local system.

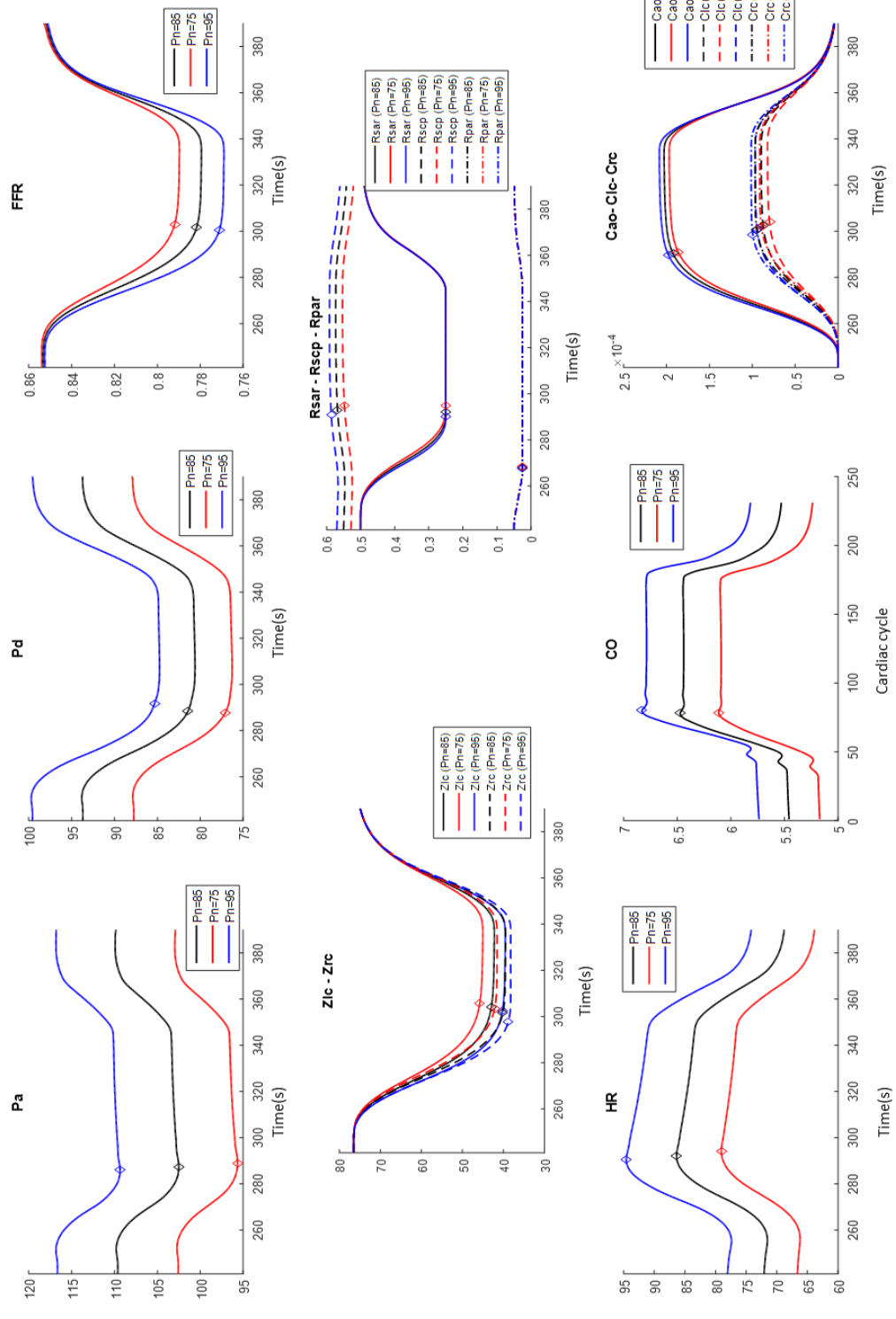

Figure 3.6: Outputs results at the variation of P_n from its reference value of 85 mmHg to 75 and 95 mmHg.
From the top left: mean aortic pressure (P_a, mmHg), mean distal pressure (P_d, mmHg), FFR, left and right myocardial resistances (Z_{LC} and Z_{RC}, mmHg s/ml), systemic arterioles, systemic capillaries and pulmonary arterioles resistances (R_{sar}, R_{scp}, R_{par} mmHg s/ml), heart rate (HR, beats/min), cardiac output (CO, l/min), aortic and left and right myocardium adenosine concentration (C_{AO}, C_{LC}, C_{RC} mg/ml). Units of x axis are second for all except CO in cardiac cycle.

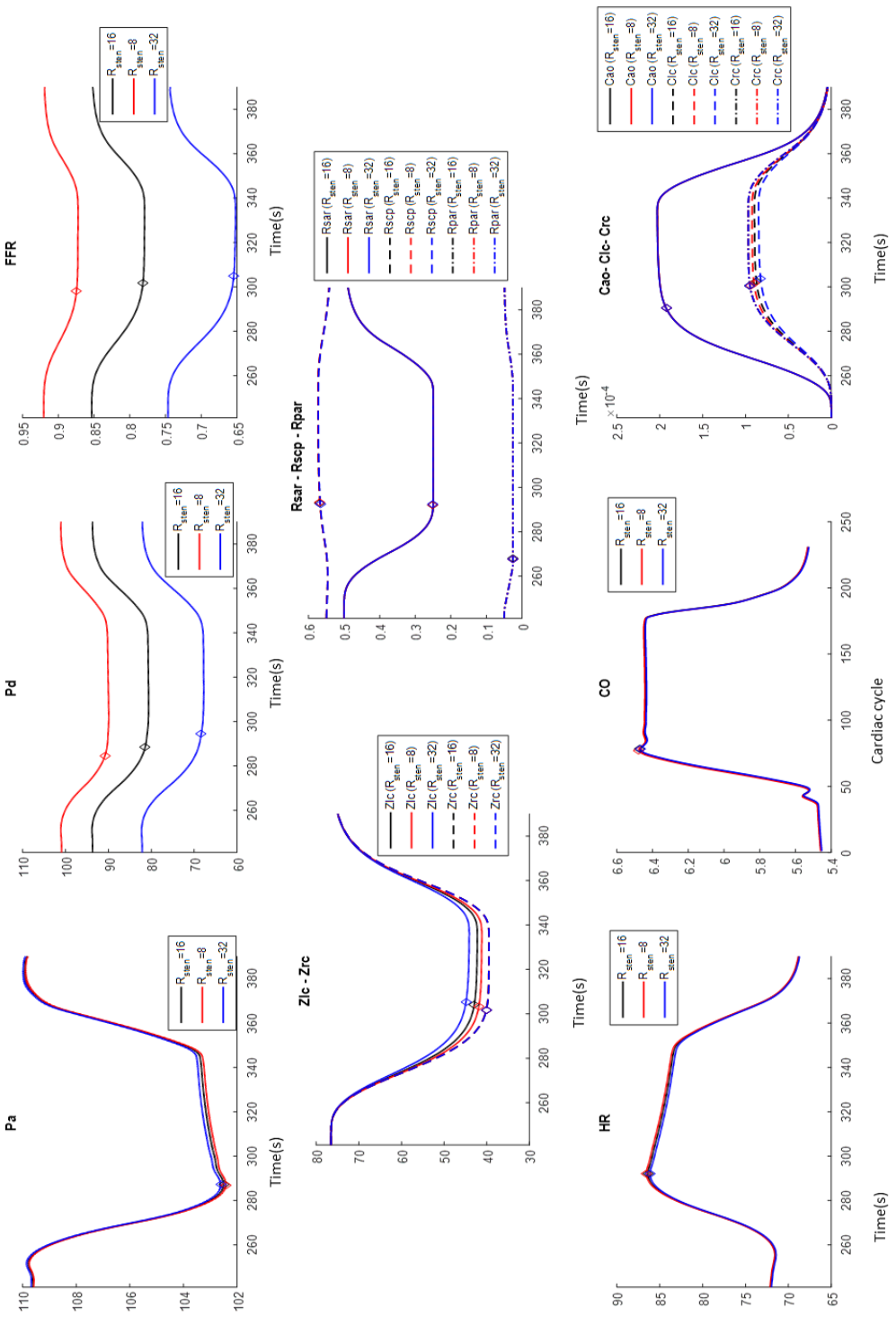

Figure 3.7: Outputs results at the variation of R_{sten} from its reference value of 16 mmHg s/ml to 8 and 32 mmHg s/ml. From the top left: mean aortic pressure (P_a, mmHg), mean distal pressure (P_d, mmHg), FFR, left and right myocardial resistances (Z_{LC} and Z_{RC}, mmHg s/ml), systemic arterioles, systemic capillaries and pulmonary arterioles resistances (R_{sar}, R_{scp}, R_{par} mmHg s/ml), heart rate (HR, beats/min), cardiac output (CO, l/min), aortic and left and right myocardium adenosine concentration (C_{AO}, C_{LC}, C_{RC} mg/ml). Units of x axis are second for all except CO in cardiac cycle.

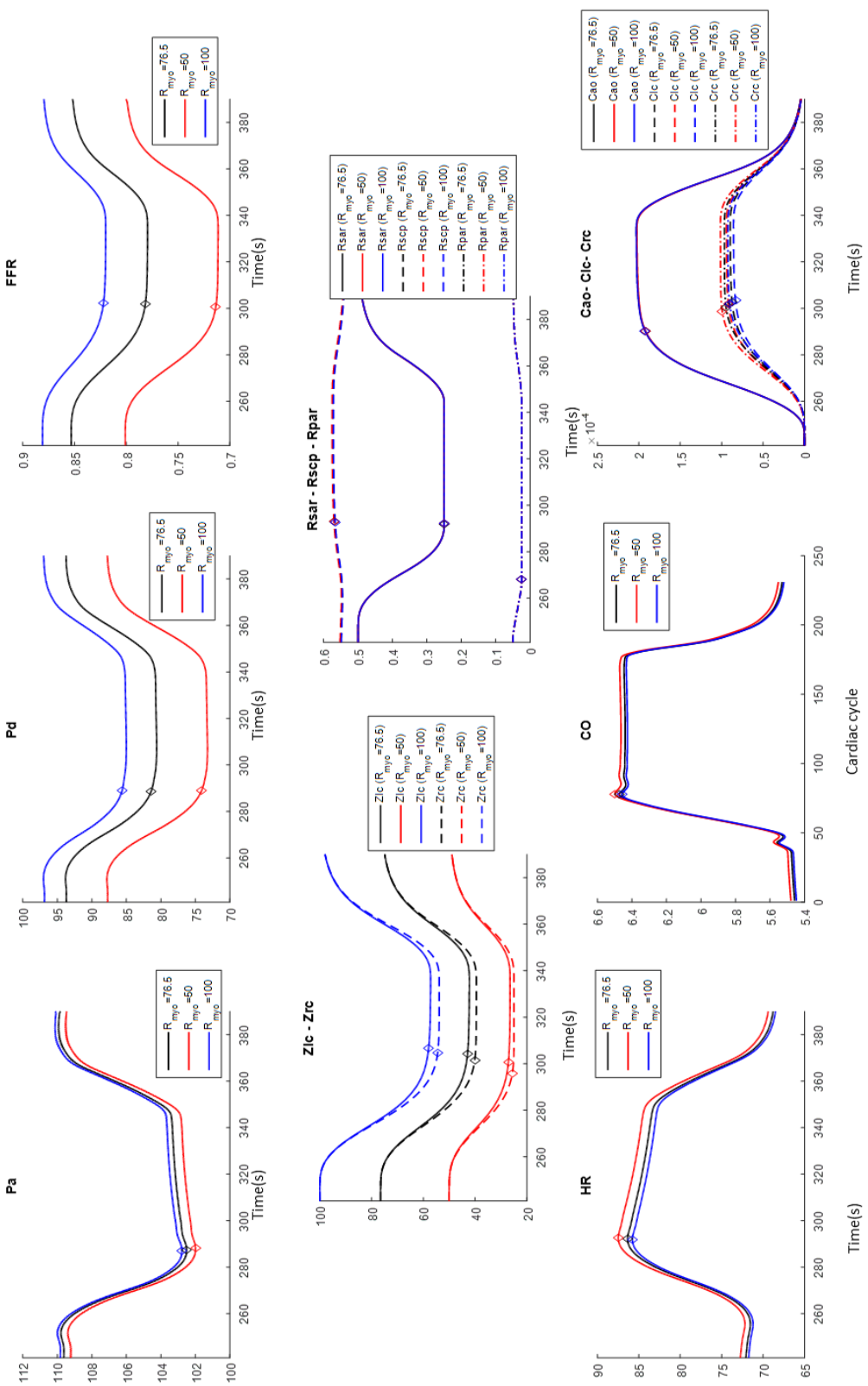

Figure 3.8 Outputs results at the variation of R_{myo} from its reference value of 76.5 mmHg s/ml to 50 and 100 mmHg s/ml.
From the top left: mean aortic pressure (P_a, mmHg), mean distal pressure (P_d, mmHg), FFR, left and right myocardial resistances (Z_{LC} and Z_{RC}, mmHg s/ml), systemic arterioles, systemic capillaries and pulmonary arterioles resistances (R_{sar}, R_{scp}, R_{par} mmHg s/ml), heart rate (HR, beats/min), cardiac output (CO, l/min), aortic and left and right myocardium adenosine concentration (C_{AO}, C_{LC}, C_{RC} mg/ml). Units of x axis are second for all except CO in cardiac cycle

3.3.3 Influence of barocontrol on the coronary boundaries

The comparison between the outputs obtained with the barocontrolled model and the non-barocontrolled model is focused on the coronary boundaries output: aortic pressure and aortic adenosine concentration. It is intuitively expected that, having the barocontrol activated, the heart rate, the left ventricular elastances, the peripheral resistance and the unstressed venous volume will be controlled and different from the non-barocontrolled model. This causes a difference in all the outputs described previously. As an example, in figure 3.9, the comparison of the cardiac output is shown. This output shows different value at baseline (+12% with barocontrol) and different amplitude (+0.3 l/min with barocontrol, +1.1 l/min) in the response the adenosine vasodilation.

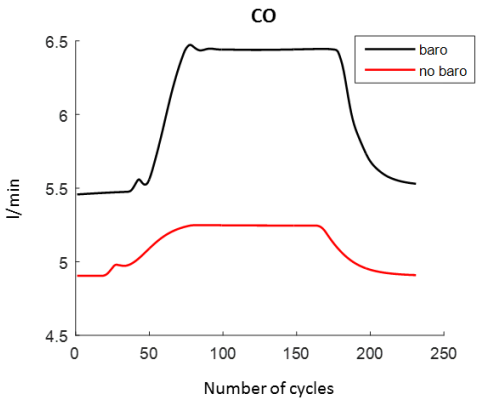

Figure 3.9: Example of model output (CO) obtained with a without barocontrol.

The coronary boundaries parameters will be used for the coupling of the global and local model, as explained in the following paragraphs, and therefore the focus of our discussion of results will be on these two. Figure 3.10 shows the mean aortic pressure and the aortic adenosine concentration obtained with and without barocontrol. As expected, there is a different aortic pressure signal with a different value at baseline and a different response to adenosine vasodilation in the barocontrolled and non-barocontrolled model results. The drop in pressure is higher for the non-barocontrolled model, where the effectors involved in the regulation are

not changed according to the pressure drop to restore a natural condition as happens with the barocontrol model. The baseline value of the aortic pressure is 16% higher in the barocontrolled model and the pressure drop is of about 7 mmHg and 16 mmHg respectively for the barocontrolled and the non-barocontrolled model.

Clearly the absolute value of the aortic pressure is strongly influenced by the barocontrol mechanism. This is not surprising given the location of the baroreceptors.

With regards to the aortic adenosine concentration, the time to reach the plateau concentrations since the adenosine starts is slightly different by about 3 seconds (44.2 s for the non-barocontrolled and 47.5 for the barocontrolled). The value of the plateau concentration is also different by $0.26*10^{-4}$ mg/ml ($2.05*10^{-4}$ mg/ml for the barocontrolled and $1.79*10^{-4}$ mg/ml for the non-barocontrolled). This corresponds to an increase of the plateau aortic adenosine concentration of 12.6%.

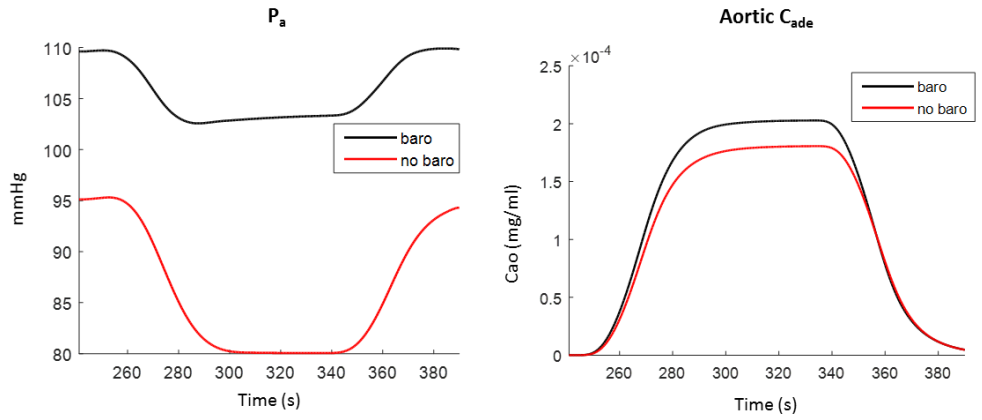

Figure 3.10: Mean aortic pressure (left) and aortic adenosine concentration (right) results with the barocontrolled (black) and the non-barocontrolled (red) model.

The concentration of adenosine in the coronaries is not so strongly influenced. The shape and period of the response are very similar with or without barocontrol. In later chapters, when the model is personalised to represent individual patients, the systolic and diastolic pressure are known. The purpose of the system model is to derive estimates of the concentration because these are not measured in the clinical protocol.

3.4 LIMITATIONS

The cardiovascular model used in this project did not include all the compartments in a real cardiovascular system. Many physiological/anatomical components were lumped into larger compartments, a characteristic of all lumped-parameter models, and overall this particular model consists of 16 compartments (Figure 2.1) each of which represents a part of the cardiovascular system, as summarised in table 3.3.

Therefore, it cannot represent the different effect of the adenosine response in different organs where different receptors can cause vasodilation or vasoconstriction.

Table 3.3: Model compartments and their equivalent in the cardiovascular system.

Compartment	Equivalent in cardiovascular system
LV, LA, RV, RA	4 chamber of the heart respectively: left ventricle, left atrium, right ventricle, right atrium
SAS	Aortic sinus
SAT	Systemic main arteries of the different organs in parallel
SAR	Systemic arterioles of the different organs in parallel
SCP	Systemic capillaries of the different organs in parallel
SVN	Systemic veins
PAR	Main pulmonary artery sinus
PAT	Pulmonary main arteries
PAR	Pulmonary arterioles
PCP	Pulmonary capillaries
PVN	Pulmonary veins
RC	Right coronary circulation
LC	Left coronary circulation

The model simulated only the vasodilation in the compartments that were most important for the achievement of coronary hyperaemia, which is the main goal of this PhD project, and for which clinical data is available from the study cohort that is examined in subsequent chapters. As described in the introduction of this chapter, the adenosine mechanisms is not yet completely understood and therefore it is difficult to represent faithfully the adenosine response in all its mechanisms. In this model the representation of the adenosine effects has been based

on the literature data about its effects in parts of the vasculature and on the observed measured effects in terms of the blood pressure and heart rate. In addition, the model described only the barocontrol to determine the adenosine response, ignoring the effect of the chemoreceptors at pulmonary and aortic level. One of the stated hypothesis with regards to the pulmonary response in this chapter was that the vasodilation of the pulmonary arterioles could create changes of the oxygen and carbon dioxide concentration, which could stimulate the chemocontrol.

Another limitation in this implementation is about the assumption of the linear relationship between myocardial resistance and the adenosine concentration in the myocardium, up to a saturation threshold. In a real patient it is known that if the baseline resistance is high it means that the myocardium is stiff and its capacity of vasodilation is reduced. Therefore, a different slope in the linear relation of the model should be used in order to include this physiological aspect. Nevertheless, for the purposes of this chapter, the model is shown to capture the basic responses reported in the literature.

Finally, the length of the simulation was about 8 hours to represent 380s of results, to achieve stabilisation from an initial state and to represent the period of adenosine administration. Optimisation of execution time was not a focus in this work, but it is a limitation both for the use of the model to examine the pharmacodynamics of the system and certainly for any potential clinical application for individual patients.

3.5 CONCLUSIONS

The main outcomes of the work presented in this chapter are:

- the extension of the model to include a coronary artery stenosis and specifically to represent the response to the administration of adenosine;
- the demonstration that the model is able to describe the responses reported in the literature;
- the quantification of the relative influence of global and local coronary model parameters on global and local coronary outputs.

The complete model, including the barocontrol that is activated by the adenosine administration, was able to represent the typical behaviour of the cardiovascular system during the administration of the drug through IV infusion, according to the observations reported in the literature, with regard to the changes of heart rate and aortic pressure.

Further improvements could be introduced, such as tuning of chemocontrol in closed-loop to take in account other adenosine effects on the oxygen and carbon dioxide variations; the variation of the myocardial vasodilation based on the initial value of the myocardial resistance, in order to take into account the reduced vasodilatory abilities of a stiff myocardium.

Moreover, it was demonstrated that the influence of the global system parameters on both global and local coronary outputs is strong, whilst local coronary parameters influence only local coronary outputs. This information justifies the approach adopted in subsequent chapters of this thesis, which assumes that the global model is not dependant on the local model and that the boundary conditions in terms of the input concentration of adenosine can be computed by a global model and then applied to a local coronary model (i.e. there is a one-way coupling). The parameters in the global model can be personalised using individual patient data, and the resulting computed adenosine concentrations used to study and to interpret the local coronary response.

The study of the influence of the barocontrol model on the coronary boundaries outputs shows that both heart rate and aortic pressure changes are controlled by this mechanism, but that the adenosine concentration in the aorta is less strongly influenced and the shape and timing of the response is well-represented even without barocontrol. This is relevant for the current study because the number of parameters for a barocontrolled model inevitably increases and therefore the tuning for a specific patient requires a higher number of input data to solve the higher number of unknowns of the global model.

In this study the aortic pressure was measured during the angiogram and therefore this information is directly available both to personalise the global model and to provide the boundary of the coronary model. Other parameters were also measured, but not their response to adenosine during hyperaemia. This makes challenging the realisation of a global patient-specific model with barocontrol. The following chapters explain and develop one-way coupling of the global and the local model to identify patient specific parameters, after an analysis of the available clinical data of the CAD patients.

CHAPTER 4
CLINICAL DATA

INTRODUCTION AND PURPOSE

This chapter introduces, and analyses, the clinical data collected from patients with CAD who underwent angiography in study STH16467.

General demographic data, comorbidities, echocardiographic data and invasive pressure data measured during adenosine infusion were collected. Pressure data were post-processed to define proximal and distal pressures, heart rate and FFR at baseline, peak and stable hyperaemia, together with the time-response for each patient.

The adenosine response was classified, based on the outputs of post-processing to ultimately identify any relationship between comorbidities and the adenosine response.

Part of the motivation for this study was to explore whether it might be possible to predict *a priori* the hyperaemic response for the patient, from information about the rest state combined with other clinical data, without the need for administration of adenosine.

A further outcome relates to the development of an algorithm which can identify the peak and stable hyperaemic response in a more objective way when compared with the subjective evaluation routinely carried out by the clinician during the procedure. The experience and subjectivity of the operator have a high impact on the clinical and economic outcomes [145].

4.1 CLINICAL DATA

Clinical data used to explore model-tuning were collected in the course of the development of a computational tool for the measurement of FFR [92] for which the work reported in this thesis was a contributory element. Informed consent was obtained from patients recruited to the study (STH16467) and a cohort of 100 CAD patients, who underwent angiography during the period 2013-2016 were recruited. Pseudonymisation was performed prior to gaining access to the data; no identifiable data were used in the execution of this study.

4.1.1 Invasive pressure data

As discussed in Chapter 1 (Paragraph *1.4.1 Clinical Investigation*), during Invasive Coronary Angiography, the FFR index is determined as the ratio between the distal and proximal pressure across the lesion during hyperaemia. Pressures are measured via catheters inserted through the radial or femoral artery. In this specific study adenosine was injected from the radial access. The proximal pressure (P_a) is measured at the ostium of the coronary vessel with a manometer fitted to the guide catheter, whilst the distal pressure (P_d) is measured by a pressure wire that can be moved along the vessel to position the pressure transducer (located 3 cm from the catheter tip) downstream of the lesion (Figure 4.1-left). P_a and P_d are measured simultaneously with either a Primewire PRESTIGE® (Volcano Corporation, CA, USA) or a PressureWire™ X Guidewire (St Jude Medical, MN, USA) system and recorded at sampling frequencies of 200 Hz and 100 Hz respectively.

After measuring P_d/P_a at baseline, adenosine is injected to bring about the hyperaemic condition. The P_d/P_a ratio is calculated continuously within the software considering the average pressures across a number of cardiac cycles; the number cycles can be chosen by the operator but the default number is set to 3. P_a and P_d are displayed on a monitor, together with the P_d/P_a (Figure 4.1-right).

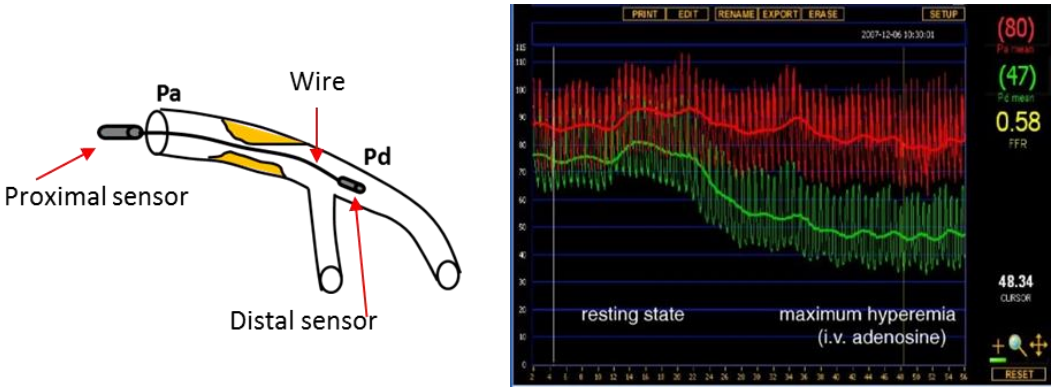

Figure 4.1: Representation of the pressure measurements across a stenosis.
(Left) Representation of the pressure wires across the lesion and (Right) the Volcano software interface. Proximal pressure, P_a, measured with the proximal sensor, is indicated in red in the Volcano software; distal pressure, P_d, measured with the distal sensor, is indicated in green in the Volcano software. The pressures are reported both as a mean value, at top right, and transient measurements as the continuous signal in the main window. The P_d/P_a is shown in yellow on the right.

During the injection of adenosine, the operator must identify the stable hyperaemic condition to, thus, obtain the appropriate value of FFR. This is not always a straight-forward task and there is often an element of subjectivity involved as the operator moves the cursor on the signal to re-visit the P_d/P_a ratio and select the value which best represents the FFR. For this reason, operator variability has an important influence both within this phase of estimation of lesion severity and may have an impact on the subsequent decision-making process.

Pressure data were post-processed in two ways: first to obtain the transient pressure signal over a cardiac cycle and, second to analyse the transient adenosine response in the local system and to identify stable hyperaemia and the variability of the FFR.

4.2 PROCESSING INVASIVE PRESSURE DATA

This paragraph describes the post-processing applied to the proximal and distal pressure signals for each lesion to i) obtain the pressures averaged over a cardiac cycle and ii) identify the phases of adenosine response within the P_d/P_a ratio signal.

4.2.1 Average pressure signal over a cardiac-cycle

The moving-average signal process requires identification of individual cardiac cycles and of rest and hyperaemic periods. It should be noted that the effect of extraneous factors, respiration for example, can be seen clearly within the signals, but are not represented in the model.

Two software tools able to perform the filtering into individual cardiac cycles were available: one was embedded in an early implementation of the GIMIAS environment (Graphical Interface for Imaging Analysis and Simulation, GIMIAS, 2015), and one in the VIRTUheart environment (VIRTUheart^{TM}). Both essentially perform the same operations as shown in figure 4.2, but for the purpose of illustration, the GIMIAS environment is shown. Pressure data collected over a recording period of several minutes were loaded into the software and displayed. Shorter windows, identified manually with reference to the patient's Cathlab notes, were extracted to represent baseline and hyperaemic periods (step 1). Within these windows the signal was divided into individual cardiac cycles, abnormal cycles (e.g. ectopic beats) were rejected (step 2), and the remaining cycles averaged (step 3).

The period of the cardiac cycle (T) extracted from this analysis was also used in Eq.4.1 to compute the average heart rate (HR), expressed in clinical units of beats per minute:

$$HR = \frac{60}{T} \qquad \text{(Eq.4.1)}$$

The outputs of the first post-processing method are the heart rate and the time series of aortic pressure over one cardiac cycle at baseline from which systolic and diastolic pressures were obtained.

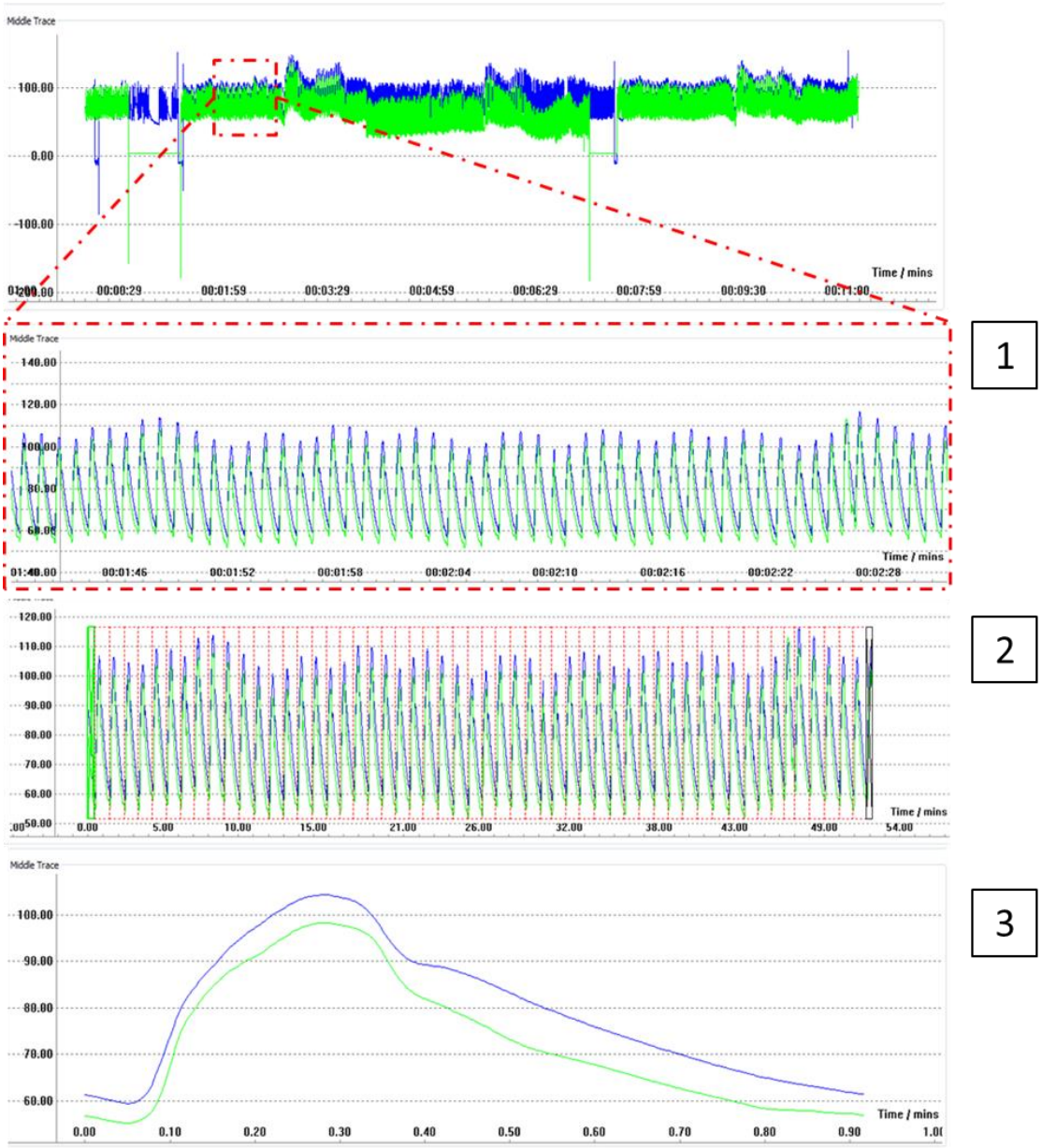

Figure 4.2: Example of the process to obtain the average pressures over a cardiac cycle in GIMIAS. Step 1) The region of interest (baseline or hyperaemia) is selected. Step 2) Data is split into cardiac cycles with elimination of abnormal cycles, if necessary. Step 3) The pressure signals are averaged over a cardiac cycle.

4.2.2 Algorithm to identify minimum (FFR_{MIN}) and stable (FFR_{ST}) FFR

Currently the clinical decision protocol for FFR assessment defines a threshold of 0.8; above this value the lesion does not need treatment. Typically, the P_d/P_a ratio falls, reaches its lowest value, and then stabilises at a very slightly higher level to give a period of stable maximal hyperaemia [120, 144], but this 'overshoot' of the P_d/P_a ratio is not easily identified in all cases.

Furthermore, present guidelines do not specify whether the *minimum* or the *stable* P_d/P_a should be considered as "the true" FFR [86, 144, 146].

The second post-processing method aims to analyse the P_d/P_a ratio signal in order to automatically identify the phases of the adenosine response, peak and stable hyperaemia, which are typically observed during adenosine infusion after the baseline condition (identified as the instant when adenosine starts to be administered), defined as follows:

1) **Peak response**, when P_d/P_a ratio reaches its minimum value (FFR_{MIN}) generated by the adenosine-induced vasodilation;
2) **Stability**, when the P_d/P_a ratio is stable (FFR_{ST}). This occurs when the cardiovascular system responds to adenosine-induced vasodilation with short-term regulation (baro and chemocontrol) bringing it to a balanced response resulting in a flat P_d/P_a.

The minimum P_d/P_a is easier to identify in the Cathlab, although it is still highly dependent on operator interpretation, making sure that there are not artefacts in the pressure signals due to the patient coughing or to movement of the wires.

The algorithm described below identifies the minimum P_d/P_a (FFR_{MIN}) and stable P_d/P_a (FFR_{ST}). To identify FFR_{MIN} and FFR_{ST} two methods were selected to smooth the signal: a moving average method (with a window size of 1 beat, 2 beats and 3 beats) and a Fast Fourier Transform (FFT) filter. The outputs of these analyses were then compared to the FFR measured in the Cathlab (FFR_{CL}), in particular, with regards to the impact on treatment. Table 4.1 summarises the different processing methods and their respective results.

Table 4.1: Processing methods and relative results of FFR_{MIN} and FFR_{ST}.

	FFR_{MIN}	**FFR_{ST}**
Clinical	FFR_{CL}	
Moving average:1 beat	$FFR_{MIN,1B}$	-
2 beats	$FFR_{MIN,2B}$	-
3 beats	$FFR_{MIN,3B}$	-
FFT filter	-	$FFR_{ST,F}$

4.2.2.1 Moving average

Moving average smoothing over 1 beat, 2 beats and 3 beats requires the identification of the cardiac cycles within the pressure signals. The ECG signal could have been used in this context, but this was not available for all patients.

4.2.2.1.1 Identification of the cardiac cycle

Identification of the cardiac cycles was based on the proximal pressure signal for each vessel investigated. Diastolic pressure was used as the identifier for the start of the cardiac cycle. In MATLAB 2015a, the function 'extrema' allows all local minima in a signal to be identified. However, it cannot distinguish between the real minima of the pressure signal corresponding to the diastolic pressure at the end of systole and other minima that might occur due to the aortic notch or pressure catheter- induced artefacts.

For the reasons above, two conditions had to be satisfied in order to select the minima corresponding to the diastolic pressure: the minimum values had to fall below a threshold (between 65 and 100 mmHg) and must occur within a time interval between 0.54 and 0.70 s. The results were inspected visually to ensure that the diastolic pressures were captured correctly. In certain cases, adjustment of the thresholds was required.

Distance in time between minima was stored as the heart period, from which the heart rate was calculated. A further output is, thus, the change in heart rate during the adenosine infusion and heart rates at baseline and stable hyperaemia were used to analyse the adenosine response. Once the cardiac cycles were identified, the P_d/P_a ratio is calculated in each cycle using the averaged distal and proximal pressures.

4.2.2.1.2 P_d/P_a ratio over N beats

The moving average of the P_d/P_a over N cardiac cycles was then calculated as shown in Eq. 4.2 with different values of N set to 1, 2 and 3.

$$\left(\frac{P_d}{P_a}\right)_i = \frac{\sum_{i-N}^{i}\left(\frac{P_d}{P_a}\right)_i}{N} \quad \text{(Eq.4.2)}$$

Figure 4.3 shows an example of a real patient data, the different P_d/P_a over N beats can be observed and compared against the raw P_d/P_a.

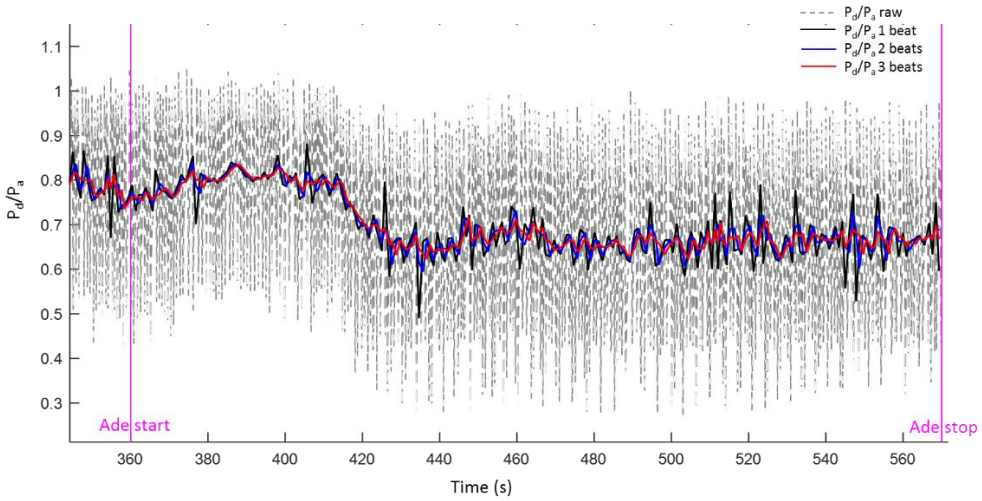

Figure 4.3: Comparison between the raw P_d/P_a and P_d/P_a averaged over N beats.
The graph shows the original raw P_d/P_a, calculated as the instantaneous ratio of pressures (in grey), and the averaged P_d/P_a ratio over 1 cardiac cycle (in black), 2 cardiac cycles (in blue) and 3 cardiac cycle (in red). Vertical lines in magenta represents the start and stop of adenosine infusion.

4.2.2.2 Fast Fourier Transform filter

Pressure signals measured invasively during angiography can be very noisy. Two principal frequencies are usually observed: one with a frequency of about 1.1 Hz (65 beats/min) related to the cardiac cycle and respiratory movements with a frequency of 0.2-0.25 Hz (12-15 breaths/min). An example is shown in Figure 4.4, where the proximal and distal pressures are reported.

Smooth P_d and P_a signals were obtained with the following process using MATLAB 2015a:

- Fast Fourier Transform (FFT) was applied to decompose the signals in the frequency domain;
- A low band-pass filter was applied using cut-off frequencies of 0.04 and 0.5 Hz, corresponding to periods of 25 s and 2 s respectively. The first cut-off value eliminates

extraneous frequencies (e.g. cardiac and respiratory oscillations), whilst preserving physiological frequencies relating to the hyperaemic response. The second cut-off instead eliminates only the cardiac oscillations.

- An inverse FFR to rebuild the signal in the time domain.

An example of the results of this signal processing against the original input is shown in figure 4.5. The filtered signal was used to define the $FFR_{ST,f}$.

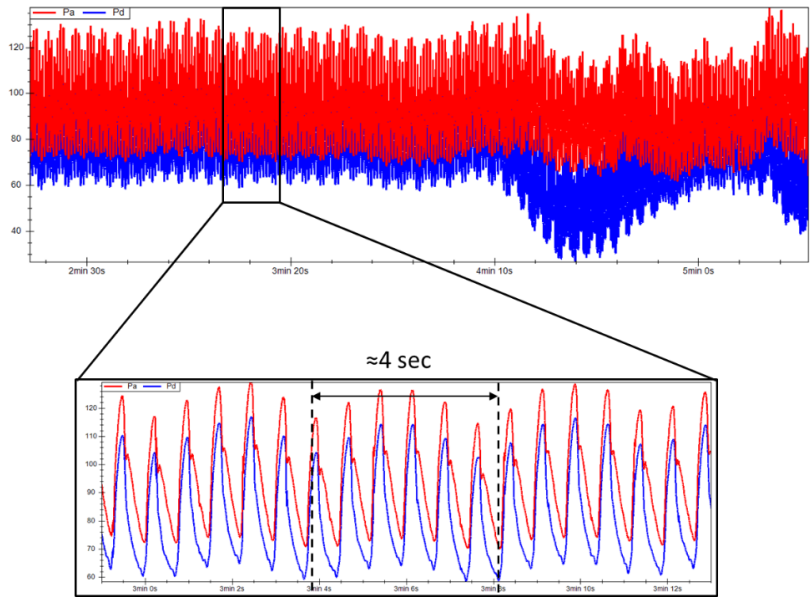

Figure 4.4: Proximal and distal pressures signals contain cardiac and respiratory oscillations
The top graph shows the pressures measured for about 4 minutes and an oscillation at a constant frequency is observed. Zooming in for details, the period is about 4 seconds, which is compatible with the respiratory movements.

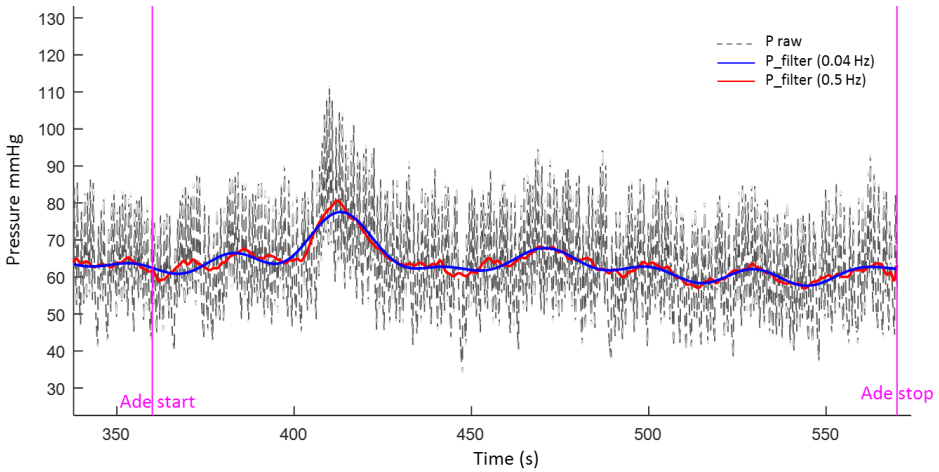

Figure 4.5: Example of real and filtered result on a pressure signal.
In dashed grey is reported the real pressure signal, in blue the filtered pressure signal with cut-off of 0.04 Hz, in red the filtered pressure signal with cut-off of 0.5 Hz.

4.2.2.2.1 Identification of the peak response: the minimum P_d/P_a (FFR_{MIN})

The minimum P_d/P_a value for the cycle-averaged P_d/P_a was calculated as the global minimum over the averaged signal. The results obtained for N equal to 3 will be considered to define the $FFR_{MIN,3B}$, as this is considered to be closest to the Cathlab signal where the default averaging window of the software is set to 3 cardiac cycles. The minimum value of P_d/P_a calculated from the averaged signals over 1 beat ($FFR_{MIN,1B}$) and 2 beats ($FFR_{MIN,2B}$) were also calculated to compare their values. These show the variability of the signal with the smaller averaging windows.

The time response to the peak is calculated as the difference between baseline and peak times.

4.2.2.2.2 Identification of the stable response: the stable P_d/P_a (FFR_{ST})

Stable P_d/P_a was calculated from the FFT-filtered signal (FFR_{ST}) using the process described below.

A finite central difference scheme was used to calculate the first derivative with a 4th order accuracy, as described in Eq.4.3.

$$f'(x) = \frac{f(x-2h) - 8 \cdot f(x-h) + 8 \cdot f(x-h) - f(x-2h)}{12\,h} \qquad \text{(Eq.4.3)}$$

where h is the sampling interval, arbitrarily set to 7 seconds. As a smaller sampling interval captures the signal variation, it makes it difficult to identify the stable part, i.e. when the first derivative is null.

The FFR_{ST} was identified as the average value of P_d/P_a ratio during the stable period, identified between the first and last instants where the derivative was below a threshold, after the peak response.

The threshold for the first derivative was set to 10^{-5} and was increased by 5% with an upper limit of 10^{-3}.

Figure 4.6 shows an example of the graph produced in MATLAB 2015a with all the information related to the specific case including:

- the FFRs measured in the Cathlab,
- the FFR_{MIN} from the 3 beat moving-average signal, $FFR_{MIN,3B}$;
- the FFR_{ST} from the filtered signal with cut-offs of 0.04Hz and 0.5 Hz ($FFR_{ST,F\ 0.04Hz}$, $FFR_{ST,F\ 0.5Hz}$) represented as a straight line which indicates the length of the stable period identified;
- a time indicator of the start and stop of adenosine.

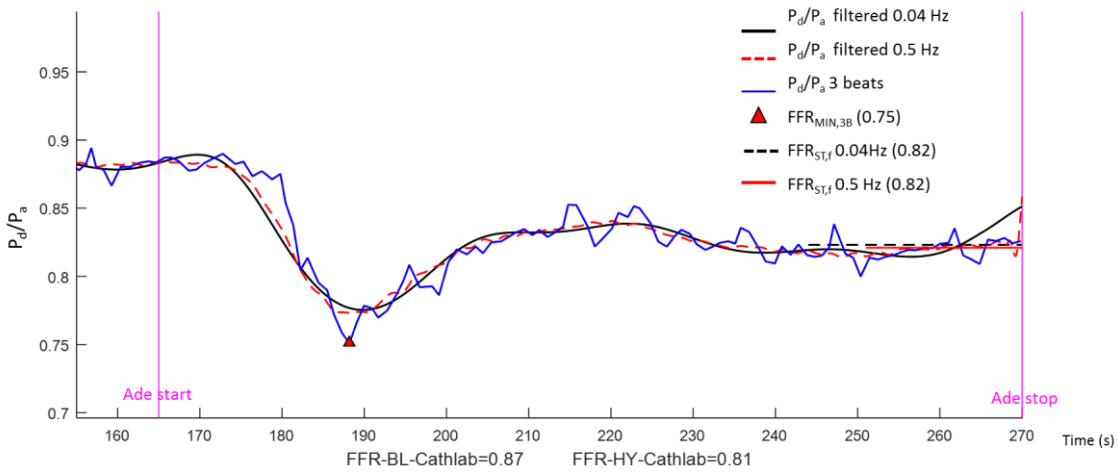

Figure 4.6: Example of algorithm results for the FFR_{MIN} and FFR_{ST}.
The graph reports the FFR measured in Cathlab at baseline (FFR-BL-Cathlab) and at hyperaemia (FFR-HY-Cathlab), the P_d/P_a signal processed with the 3 beats moving average (blue), and with the FFT filter with cut off 0.04Hz (black) and 0.5Hz (dashed red), $FFR_{MIN,3B}$(▲), $FFR_{MIN,f}$ 0.04 Hz (◆), $FFR_{MIN,f}$ 0.5 Hz (◆), and $FFR_{ST,f}$ 0.04 Hz (- - -) and $FFR_{ST,f}$ 0.5 Hz (----). The start and end of e adenosine infusion is indicated by vertical lines.

4.2.2.3 Statistical analysis

FFRs measured in the Cathlab (FFR_{CL}) and the calculated minimum and stable P_d/P_a ($FFR_{MIN,3B}$, $FFR_{ST,F\ 0.5\ Hz}$, $FFR_{ST,F\ 0.04\ Hz}$) were compared using a 2-tailed paired T-test for each group, assuming a normal distribution.

The variables were compared statistically calculating the mean delta (bias) and the standard deviation (SD) and represented graphically by a Bland-Altman plot with limits of agreement

of ±1.96 SD. The correlation coefficient between the variables was also calculated. The same approach was used to compare $FFR_{MIN,3B}$ with $FFR_{ST,F\ 0.5\ Hz}$ and $FFR_{ST,F\ 0.04\ Hz}$ to demonstrate the common error of overestimation of the lesion severity in choosing the minimum P_d/P_a. The statistical analysis was performed in IBM SPSS (IBM Analytics, USA).

4.2.3 Variability of P_d/P_a at baseline and hyperaemia

During assessment of stenosis severity, clinicians have to interpret the P_d/P_a signal and choose the best representation of the FFR. This often results in the minimum value with the resulting overestimation of lesion severity. Volcano and St.Jude software, employed in angiography, report by default the minimum value for P_d/P_a, averaging the pressure signals over a number of cardiac cycles, which can be selected to be between 3 and 5 by the operator.

To calculate the variability of the P_d/P_a during baseline and hyperaemia, the cycle-averaged signals over 1 beat, 2 beats and 3 beats, calculated as described in paragraph *4.2.2.1.1 Identification of the cardiac cycl*e, were considered. For this purpose, the baseline period was identified over 5 consecutive cycles after the start of adenosine infusion. For all three averaging regimes ($FFR_{1B,}$ FFR_{2B}, FFR_{3B}), hyperaemia is defined as occurring over the period from the minimum to the end of the signal.

Patients were also classified by heart rate (HR), i.e. as bradycardic (HR<60 beats/min), tachycardic (HR>100 beats/min) or normal (60<HR<100 beats/min) and by the presence of atrial fibrillation (AF).

4.2.3.1 Statistical analysis

P_d/P_a ratio signal variability was estimated by calculating the coefficient of variation (CoV) during the period of hyperaemia for each case and for each type of analysis with 1 beat, 2 beats and 3 beats and then averaging the results for all cases. The coefficient of variation was calculated as the ratio between the standard deviation and the mean value.

4.3 CLASSIFICATION OF ADENOSINE RESPONSE

The proximal and distal pressures recordings were analysed to seek out any trends which could be used to classify patients into groups with a similar response and to attempt to link this to their profiles in terms of the general demographic data. Instantaneous proximal and distal pressures at baseline, peak and stable hyperaemia were calculated with the algorithm described previously.

The average response to adenosine for all patients/lesions was determined by calculating the averaged proximal and distal pressures at baseline and hyperaemia across the entire dataset. Patient groups were classified from the trends of proximal and distal pressures with respect to their respective baseline values, in terms of identifying negative or positive changes for each phase.

The heart rates, at baseline and hyperaemia obtained using the algorithm, were examined to determine the average response to adenosine based on this parameter and to understand the effects and importance of the barocontrol system.

A second classification was also made as a result of analysing the P_d/P_a ratio curves by eye and identifying groups of patients with similar behaviour.

4.4 RESULTS

4.4.1 Patient demographic

One hundred and sixty-three independent coronary lesions were studied in 93 patients. Demographic information for these patients is reported in Table 4.2.

Table 4.2: Demographic data and comorbidities for 93 patients.
BMI - Body Mass Index, PVD - Peripheral Vascular Disease, COPD - Chronic Obstructive Pulmonary Disease, MI - myocardial infarction.

Patient demographic	**Num% - mean (SD)**
Male	75%
Age (years)	64.7 (SD 10.2)
BMI	29.3 (SD 4.7)
Hypertension	65.5 %
PVD	5.4 %
Previous MI	40.9 %
Type II diabetes	22.6 %
Hyperlipidaemia	77.4 %
COPD	6.9 %

Eighty-one lesions were physiologically significant (FFR ≤ 0.80) and 82 were non-significant (FFR > 0.80). The mean FFR measured in the Cathlab was 0.78 (SD 0.15).

Lesions included: 72 in left anterior descending (LAD) arteries; 40 in right coronary arteries (RCA); 33 in circumflex arteries (LCX); 13 in diagonal arteries (DX); 5 in left main stem (LMS).

4.4.2 FFR measurements and algorithm results: impact on treatment

The distribution of FFR_{CL}, $FFR_{MIN,1\ B}$, $FFR_{MIN,2B}$, $FFR_{MIN,3B}$, $FFR_{ST,F\ 0.5\ Hz}$ and $FFR_{ST,F\ 0.04\ Hz}$ are shown in terms of their means, and standard deviations in Table 4.3.

$FFR_{MIN,1\ B}$ and $FFR_{MIN,2B}$ are reported to demonstrate that, as expected, the minimum value of P_d/P_a is influenced by the number of cycles over which the data was averaged. This issue has not been considered in terms of its impact on treatment since, in the Cathlab, the operators would choose to average over 3 beats, as they are aware of the beat-to-beat variability of the signal.

Table 4.3: Distribution of FFR_{CL}, $FFR_{MIN,3B}$, $FFR_{ST,F\ 0.5\ Hz}$ and $FFR_{ST,F\ 0.04\ Hz}$ for 163 vessels in 93 patients.

	Mean (SD)
FFR_{CL}	0.781 (0.15)
$FFR_{MIN,1\ B}$	0.748 (0.17)
$FFR_{MIN,2B}$	0.758 (0.15)
$FFR_{MIN,3B}$	0.762 (0.16)
$FFR_{ST,F\ 0.5\ Hz}$	0.799 (0.15)
$FFR_{ST,F\ 0.04\ H}$	0.806 (0.15)

The FFR values measured in the Cathlab during hyperaemia (FFR_{CL}) prior to PCI were compared with the results obtained with the algorithm implemented in MATLAB ($FFR_{MIN,3B}$, $FFR_{ST,F\ 0.5\ Hz,}$ $FFR_{ST,F\ 0.04\ Hz}$) and the stable FFRs ($FFR_{ST,F\ 0.5\ Hz,}$ $FFR_{ST,F\ 0.04\ Hz}$) were compared with $FFR_{MIN,3B}$. The resulting intra-class correlation coefficients indicate high correlation for each pair of variables:

- 0.99 (95% CI: 0.987-0.993, P-value < 0.001) for FFR_{CL} - $FFR_{MIN,3B}$;
- 0.987 (95% CI: 0.983-0.991, P-value < 0.001) for FFR_{CL} - $FFR_{ST,F\ 0.04\ Hz}$;
- 0.941 (95% CI: 0.920-0.956, P-value < 0.001) for FFR_{CL} – $FFR_{ST,F\ 0.5\ Hz}$;
- 0.943 (95% CI: 0.922-0.958P-value < 0.001) for $FFR_{MIN,3B}$ – $FFR_{ST,F\ 0.5\ Hz}$;
- 0.986 (95% CI: 0.980-0.989P-value < 0.001) for $FFR_{MIN,3B}$ – $FFR_{ST,F\ 0.04\ Hz}$;
- 0.949 (95% CI: 0.930-0.962P-value < 0.001) for $FFR_{ST,F\ 0.04\ Hz}$ – $FFR_{ST,F\ 0.5\ Hz}$.

Using the accepted threshold value of 0.8 for PCI intervention, lesions could be reclassified based on the different FFRs.

With $FFR_{MIN,3B}$ as the arbiter, 92 lesions (56 %) were classified as significant, and 71 (44 %) as non-significant. When $FFR_{ST,F\ 0.04\ Hz}$ was chosen as the arbiter, 27 significant lesions (16.5 % lesions -24 % patients) were reclassified as non-significant, resulting in 65 (40 %) significant and 98 (60 %) non-significant lesions (Figure 4.7-a). When $FFR_{ST,F\ 0.5\ Hz}$ was used 19 significant lesions (11.6 % lesions -17 % patients) were reclassified as non-significant (Figure 4.7-b), resulting in a total of 74 (45%) significant and 89 (55%) non-significant lesions.

Comparing FFR_{CL} and $FFR_{MIN,3B}$, 9 lesions (5.5 % of lesions, 7.5% of patients) were reclassified as significant and 1 lesion (0.6 % of lesions, 1.1 % of patients) was reclassified as non-significant (Figure 4.7-c).

Comparing FFR_{CL} and $FFR_{ST,F\ 0.5\ Hz}$, 12 lesions (7.3 % of lesions, 11 % of patients) were reclassified as non-significant and 1 lesion (0.6 % of lesions, 1.1 % of patients) was reclassified as significant (Figure 4.7-d) and, finally, comparing FFR_{CL} and $FFR_{ST,F\ 0.04\ Hz}$, 19 lesions (11.6 % of lesions, 18 % of patients) were reclassified as non-significant (Figure 4.7-e).

These results are summarised in Table 4.4.

Table 4.4: Impact on treatment results across pairs of FFR values.

		FFR_{CL} / $FFR_{MIN,3B}$	FFR_{CL} / $FFR_{ST,F}$ 0.5 Hz	FFR_{CL} / $FFR_{ST,F}$ 0.04 Hz	$FFR_{MIN,3B}$ / $FFR_{ST,F\ 0.5\ Hz}$	$FFR_{MIN,3B}$ / $FFR_{ST,F\ 0.04\ Hz}$
SIGN-->NON SIG	**LMS**	-	2	2	2	2
	LCX	-	5	9	8	12
	LAD	1	3	4	5	6
	RCA	-	2	4	4	7
	DX	-	-	-	-	-
	#lesions	**1 (0.6%)**	**12 (7.3%)**	**19 (11.6%)**	**19 (11.6%)**	**27 (16.5%)**
	#patients	**1 (1.1%)**	**11 (11%)**	**17 (18%)**	**16 (17%)**	**23 (24%)**
NON SIG-->SIG	**LMS**	-	-	-	-	-
	LCX	3	-	-	-	-
	LAD	3	-	-	-	-
	RCA	3	1	-	-	-
	DX	-	-	-	-	-
	#lesions	**9 (5%)**	**1 (0.6%)**	**-**	**-**	**-**
	#patients	**7 (7.5%)**	**1 (1.1%)**	**-**	**-**	**-**

A paired T-test (2-tailed, 95% CI) was performed for each pair of variables in order to identify the average difference between the paired values (bias) and the standard deviation (Figure 4.8):

- $FFR_{MIN,3B} - FFR_{ST,F\ 0.04\ Hz}$: bias =-0.04, SD=0.03, ($p<0.0001$) (Figure 4.8-a);
- $FFR_{MIN,3B} - FFR_{ST,F\ 0.5\ Hz}$: bias =-0.04, SD=0.03, ($p<0.0001$) (Figure 4.8-b);
- $FFR_{CL} - FFR_{MIN,3B}$: bias =+0.02, SD=0.03, ($p<0.0001$) (Figure 4.8-c);
- $FFR_{CL} - FFR_{ST,F\ 0.04\ Hz}$: bias =-0.02, SD=0.03, ($p<0.0001$); (Figure 4.8-d);
- $FFR_{CL} - FFR_{ST,F\ 0.5\ Hz}$: bias =-0.02, SD=0.03, ($p<0.0001$); (Figure 4.8-e).

The Bland-Altman plots show the impact on treatment as well. Both stable FFRs ($FFR_{ST,F\ 0.04\ Hz}$, $FFR_{ST,F\ 0.5\ Hz}$) are, on average, higher by 0.02 compared to FFR_{CL} and by 0.04 compared with $FFR_{MIN,3B}$, with a P-value < 0.001, indicating high statistical significance. The average difference between FFR_{CL} and $FFR_{MIN,3B}$ is 0.02 with P-value < 0.001. These results suggest that the FFR measured in Cathlab falls in between the minimum and the stable values and therefore, if the stable FFR is taken to be the gold standard, the severity of some lesions will be overestimated.

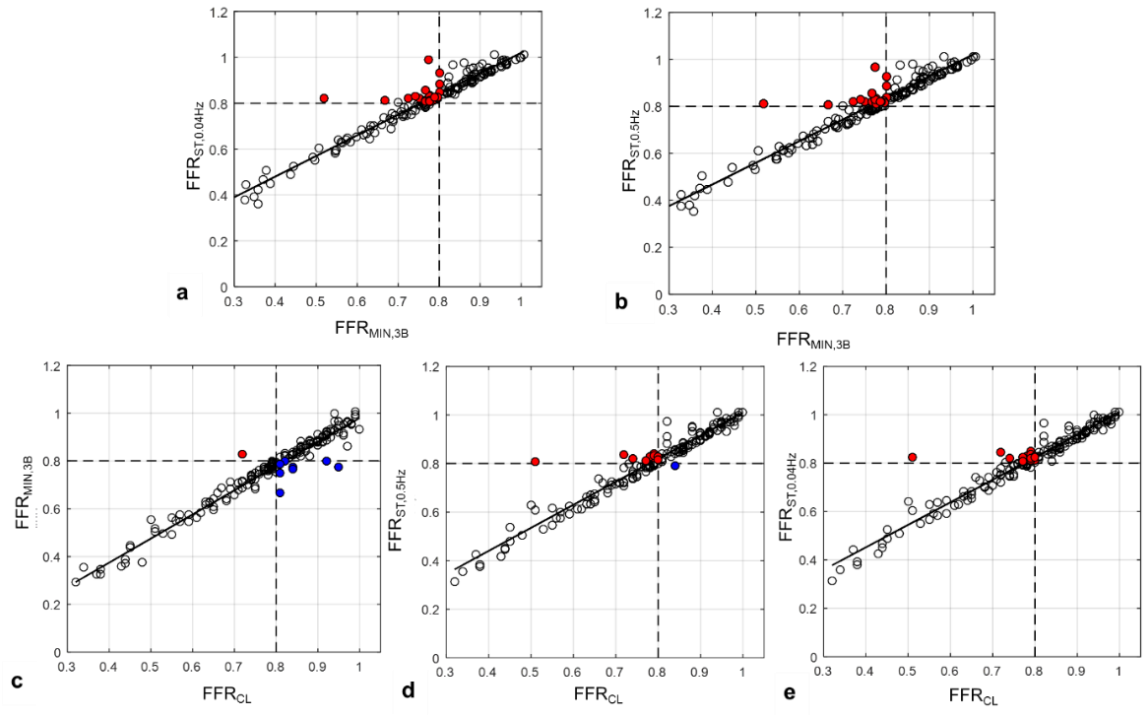

Figure 4.7: Impact on treatment decision based on the different FFRs.
a) $FFR_{MIN,3B}$ VS $FFR_{ST,F\ 0.04\ Hz}$. b) $FFR_{MIN,3B}$ VS $FFR_{ST,F\ 0.5\ Hz}$. c) FFR_{CL} VS $FFR_{MIN,3B}$. d) FFR_{CL} VS $FFR_{ST,F\ 0.5\ Hz}$. e) FFR_{CL} VS $FFR_{ST,F\ 0.04\ Hz}$. Red indicates lesions reclassified as non-significant and blue lesions reclassified as significant.

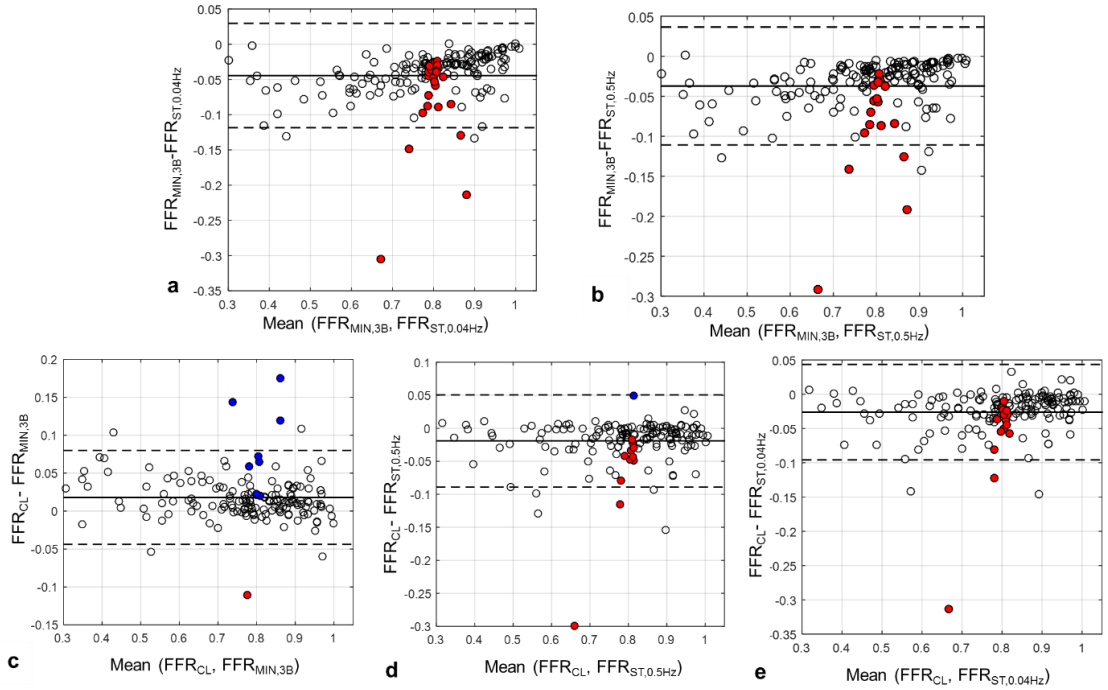

Figure 4.8: Bland-Altman plots for the each pair of variables.
a) $FFR_{MIN,3B}$ VS $FFR_{ST,F\ 0.04\ Hz}$. b) $FFR_{MIN,3B}$ VS $FFR_{ST,F\ 0.5\ Hz}$. Panel c) FFR_{CL} VS $FFR_{MIN,3B}$. d) FFR_{CL} VS $FFR_{ST,F\ 0.5\ Hz}$. e) FFR_{CL} VS $FFR_{ST,F\ 0.04\ Hz}$. Red indicates lesions reclassified as non-significant and blue lesions reclassified as significant.

Further analysis of those cases showing the largest differences between the FFR recorded in the Cathlab and results obtained using the algorithm revealed two underlying issues. In some cases, the FFR measured in the Cathlab did not correspond to the P_d/P_a seen in the signal, in this situation, the algorithm was able to identify correctly the minimum and stable FFRs. In other cases there was no stable period within the hyperaemic response: after reaching a minimum value, the P_d/P_a rose again toward the baseline. In such situation, the Cathlab operator selects the minimum value, but the algorithm reports a higher value as the period of stable FFR is occurring during the recovery transition to baseline. Two explicative examples of these are presented in Figure 4.9.

These results demonstrate the importance of a standard approach for the calculation of FFR, but are not able to provide information on whether FFR_{MIN} or FFR_{STABLE} should be chosen as the gold standard. The algorithm described could assist in the standardisation process and, since its processing time is about 2 seconds, it would be easy to incorporate this within software commonly used to assess FFR. However, here must be also noted that stable hyperaemia must

be achieved during adenosine infusion, for the algorithm to work correctly. This is especially important for those cases close to the threshold for the correct decision to be made.

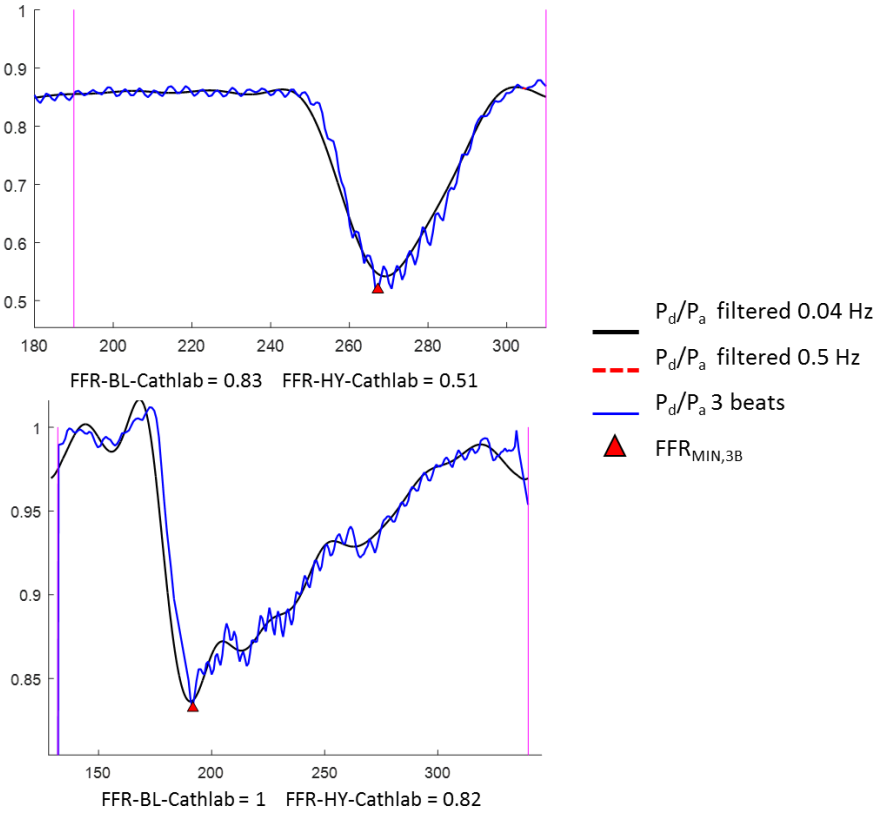

Figure 4.9 Examples of cases with large differences between FFR_{CL} and algorithm results. FFR measured in Cathlab at baseline (FFR-BL-Cathlab) and at hyperaemia (FFR-HY-Cathlab), the P_d/P_a signal processed with the 3 beats moving average (blue), and with the FFT filter with cut-off 0.04Hz (black) and 0.5Hz (dashed red), the $FFR_{MIN,3B}$(▲),the $FFR_{MIN,f\ 0.5\ Hz}$ (◆). Vertical lines indicate start and end of adenosine infusion.

4.4.3 Timing of adenosine peak response and stability

Clinically different types of response are observed in terms of pressure behaviour and time. The average time taken from the start of adenosine and the peak response is 55.3 (SD 19) s. Here, the range is wide from a minimum of 17.55 s to a maximum of 131.42 s.

Also in the Cathlab, this variability is observed and earlier and later responders are recognised. A visual analysis of the P_d/P_a traces obtained with the algorithm was performed in order to identify the average time to reach stable hyperaemia. 11 lesions have been excluded from the groups of patients described in Paragraph *4.4.1 Patient demographic*, because stable

hyperaemia was not reached during the recording period. The average time to reach stable hyperaemia was 69.41 s with a range of 18.6 s -140 s and standard deviation of 18.6 s.

The results are consistent with published data [144] on analysis of the P_d/P_a ratio. In particular, Tarkin *et al*. [120] identified different types of adenosine response observing pressure behaviour based on the minimum FFR reached within 60 s of the start of adenosine injection. With the algorithm used in the current work, the minimum FFR can be identified at any time. This is especially relevant for later responders.

4.4.4 FFR variability at baseline and hyperaemia

The coefficient of variation (CoV) was calculated for 1beat FFR variability (CoV1), 2beat FFR variability (CoV2) and 3beat FFR variability (CoV3) for both baseline and hyperaemia.

As expected for both baseline and hyperaemic conditions, the mean CoV1 has highest value and CoV3 the smallest, due to the different averages used to define the P_d/P_a. It is evident that, by increasing the number of beats, the resulting P_d/P_a traces are smoothed.

For 83% of lesions studied patients had a normal heart rate, for 4.5 % patients had tachycardia, for 9.8% patients had bradycardia and for 4.5 % patients suffered from atrial fibrillation.

For patients with multiple lesions, the heart rate classes were very similar in terms of tachycardia, bradycardia, arrhythmia and normal, with a high reproducibility of the heart rate in the different lesion assessment. In 2 patients the heart rate class varied between the 2 (or more) lesions' assessments. This is likely to be caused by the residual effects of adenosine.

At baseline CoV1 had an average value of 0.013 (range: 0.00053 – 0.538), for CoV2 the average value fell to 0.011 (range: 0.00022 – 0.536), and CoV3 increased again to an average value of 0.017 (range: 0.00021 – 0.173).

At hyperaemia an average CoV1 of 0.0257 (range: 0.0025 – 0.1018), average CoV2 of 0.0191 (range: 0.0023 – 0.0809) and averaged CoV3 of 0.0153 (range: 0.0017 – 0.0637) were observed. During hyperaemia, the number of patients with a variability of above 5% fell as the

number of beats average increased from 1 to 3: 14 (12.5 %) patients, 9 (8 %) patients and 7 (6.3 %) patients for 1 beat, 2 beats and 3 beats respectively.

CoVs values for each analysis with different beats were averaged for the patients' groups identified based on heart rate, as shown in table 4.5.

The variability of FFR is always greater for patients with AF, irrespective of the number of beats over which the analysis was performed. Differences are less evident between the other 2 condition, bradycardia and tachycardia. For patients with normal HR, the degree of variability of the FFR lies between that of patients with tachy/bradycardia and those with AF.

When it comes to selecting the value of FFR which best represents lesion severity, because of the continuous high variability of P_d/P_a during stable hyperaemia, patients with AF prove to be the most challenging from a clinical decision-making perspective.

Table 4.5: Averaged CoVs calculated for 1 beat, 2 beats, and 3 beats for all lesions and for groups with Atrial Fibrillation (AF), Bradycardia, Tachycardia and normal Heart Rate.

	Baseline			Hyperaemia		
	Mean CoV1	Mean CoV2	Mean CoV3	Mean CoV1	Mean CoV2	Mean CoV3
All lesions	0.013	0.011	0.017	0.026	0.019	0.015
AF	0.021	0.016	0.013	0.038	0.027	0.022
Bradycardia	0.006	0.0075	0.0062	0.02	0.013	0.01
Tachycardia	0.030	0.02	0.02	0.016	0.013	0.011
Normal HR	0.013	0.011	0.0065	0.026	0.02	0.016

In each group, the variability of FFR might be sufficient to lead to misinterpretation, especially for those cases around the cut-off value.

The increase of variability of CoV3 for baseline variability might be caused by the selection of the baseline period just after the infusion starts. The P_d/P_a might oscillate for a number of different reasons, such as movement of the pressure wires or the starting of the adenosine response.

The analysis of baseline variability is important with respect to a recently-developed stenosis severity assessment index, the intensity wave-free fractional reserve (iFR). iFR is calculated

during baseline as the ratio of the mean distal pressure to the mean proximal pressure during the wave-free period within the cardiac cycle. This is automatically identified during diastole and, more precisely, between 25% of the way into diastole and 5 ms before the end of diastole. During this period pressure and flow are linearly related and the myocardial resistance is minimal [147-149]. The iFR was used as part of a hybrid approach where both indices are used or it could substitute for FFR, as shown in the clinical trials DEFINE-FLAIR [149] and iFR-SWEDEHEART[148] and its cut-off value is set to 0.83 . The main advantages of iFR are the reduced procedural time and, since no vasodilatory drugs are used, its cost efficiency and less pain/discomfort in patients [150]. This physiological index looks very promising so far and it could provide an improved measurement protocol that is not compromised by the variability of response given by the adenosine administration.

4.4.5 Classification of the adenosine response

Processing and analysis of the invasive pressure data enable the patient response to adenosine to be classified based on the pressure behaviour and the P_d/P_a ratio curve measured before PCI.

4.4.5.1 Average adenosine response: pressures and heart rate changes

Pressures and heart rate at peak and stable hyperaemia identified with the algorithm were compared with the baseline condition in order to calculate the change of pressure and of heart rate in terms of absolute value and of percentage. Figure 4.10 shows the distributions of change of proximal pressure, distal pressure and heart rate between baseline and peak hyperaemia and baseline and stable hyperaemia.

The average proximal pressure at baseline is 94.91 (SD 12.08) mmHg, during the peak hyperaemia is 92.59 (SD 12.31) mmHg and at stable hyperaemia is 90.05 (SD 12.76) mmHg. Our data therefore suggest that the change in proximal pressure is minimal with a decrease of 2.32 mmHg (2.37 %) at peak and 4.86 mmHg (3.63 %) at stable hyperaemia. These results are

in disagreement with what was published in the literature, where the proximal pressure decreases about 10-13 mmHg [116].

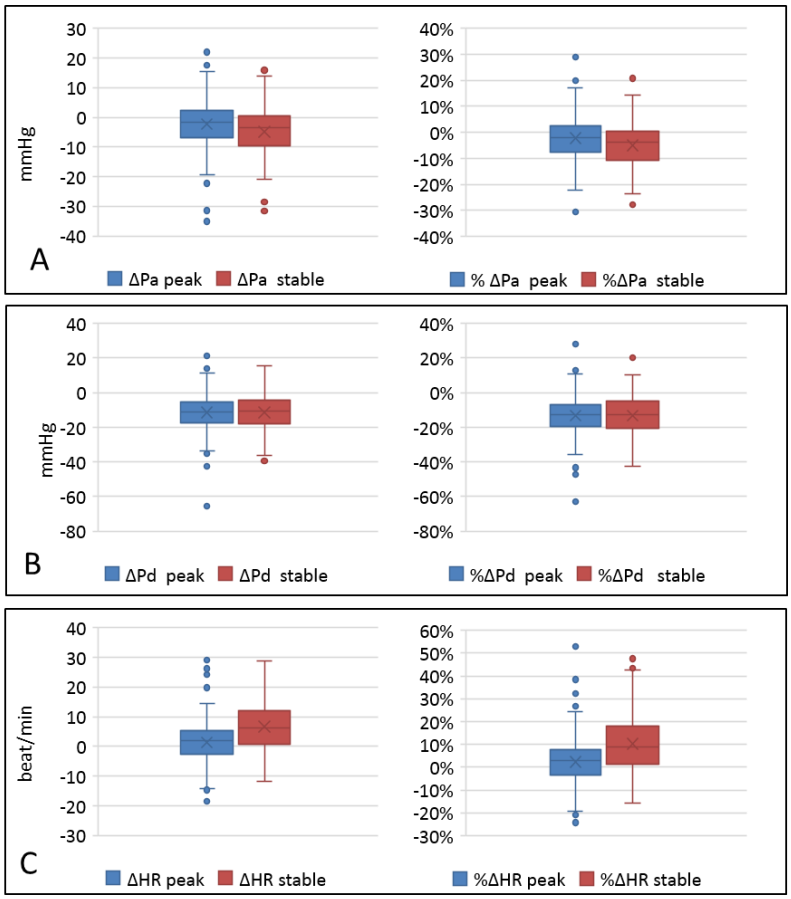

Figure 4.10: Distribution of proximal, distal pressure and heart rate to describe the adenosine response. Change of proximal pressure P_a (A), distal pressure P_d (B) and heart rate HR (C) between baseline and peak and between baseline and stable hyperaemia. Results are reported as absolute values (left) and percentages (right).

With regards to distal pressure, the average value at baseline is 86.21 (SD 15.33) mmHg, at peak hyperaemia is 74.93 (SD 16.51) mmHg and at stable hyperaemia is 74.88 (SD 16.38) mmHg. Therefore, the distal pressure decreases by 11.28 mmHg (13 %) and with minimal changes between peak and stable conditions. The distal pressure is primarily dependent on the severity of stenosis and on the myocardial resistance.

The average heart rate is 68 (SD 9.94) beats/min at baseline, increases slightly to 69.72 (SD 11.25) beats/min at peak hyperaemia, increasing further to 75.05 (SD 11.68) beats/min during stable hyperaemia. Our observations suggest HR increases of about 1.7 beats/min (2.34 %) at

peak and about 13 beat/min (10.35 %) during stable hyperaemia. This is less than the increase of about 30 beats/min reported in the literature [116].

The discrepancy in effect could be related to duration of adenosine infusion. In most studies adenosine was infused for several minutes, or even hours, and, in consequence, long-term neurocontrol mechanism may have been simulated. For patients in the present study, the infusion lasted between 90 and 120 s and thus probably not affecting long-term neuro-regulatory system.

4.4.5.2 Pressure trends between baseline, peak and stable hyperaemia

Based on proximal and distal pressure at peak and stable hyperaemia, seven types of response have been identified (Table 4.6). The seven groups are described in the list which follows in terms of average and standard deviations of the change of proximal, P_a, and distal, P_d, pressure at peak and stable hyperaemia:

- **Group A**: P_a and P_d showed the same trend with a decrease during the peak followed by restoration during stable hyperaemia. On average P_a decreased by 6.9 (SD 5.34) mmHg at peak and was restored during stable hyperaemia to 1.33 mmHg (SD 3.9) above the baseline. P_d decreased by 17.1 mmHg (SD 9.5) at peak and was restored at stable hyperaemia to 4.2 mmHg (SD 9.7) above the baseline. This response was seen in 65 lesions (46 patients); 31 LAD, 10 LCX, 16 RCA, 6 DX and 2 LMS.
- **Group B**: P_a increased slightly at peak and stabilised during stable hyperaemia, while P_d decreased and then was restored to baseline. On average P_a increased by 3.8 (SD 3.6) mmHg at peak and decreased during stable hyperaemia to 3.5 mmHg (SD 4.5) below the baseline. P_d decreased by 8.4 mmHg (SD 6.1) at peak and was restored at stable hyperaemia to the baseline condition (SD 3.6). This response occurred in 44 lesions (38 patients); 21 LAD, 10 LCX, 8 RCA, 4 DX and 1 LMS.

- **Group C**: P_a decreased at both peak and stable hyperaemia, while P_d decreased and then attempted to recover to baseline. On average P_a decreased by 2.7 (SD 2.3) mmHg at peak and decreased further at stable hyperaemia by 7.6 mmHg (SD 5.0). P_d decreased by 14.4 mmHg (SD 9.1) at peak and increased at stable hyperaemia to 3.5 mmHg (SD 5.3) below the baseline. This response occurred in 20 lesions (19 patients): 6 LAD, 3 LCX, 9 RCA and 2 DX.
- **Group D**: P_a increased at peak and then dropped during stable hyperaemia below the baseline, P_d followed the same trend. On average P_a increased by 9.4 (SD 6.3) mmHg at peak and decreased during stable hyperaemia to 6.1 mmHg (SD 7.2) below the baseline. P_d increased by 6.1 mmHg (SD 6.3) at peak and decreased during stable hyperaemia to 4.1 mmHg (SD 6.3) below baseline. This response occurred in 12 lesions (11 patients): 5 LAD, 5 LCX and 2 RCA.
- **Group E**: P_a increased at peak and then dropped below baseline at stable hyperaemia, while P_d decreased at peak and continued to decrease during the stable hyperaemia. On average P_a increased by 4.8 (SD 3.7) mmHg at peak and decreased during stable hyperaemia to 10.9 mmHg (SD 7.1) below the baseline. P_d decreased by 4.8 mmHg (SD 3.6) at peak and decreased further during stable hyperaemia to 7.5 mmHg (SD 3.3) below the baseline. This response occurred in 9 lesions (7 patients): 4 LAD, 3 LCX and 2 RCA.
- **Group F**: P_a increased slightly at both peak and stable hyperaemia, while P_d decreased at peak and then was restored above baseline. On average P_a increased by 1.1 (SD 0.8) mmHg at peak and increased further during stable hyperaemia to 3.5 mmHg (SD 1.9) above the baseline. P_d decreased by 12.4 mmHg (SD 9.0) at peak and was restored during stable hyperaemia to 5.6 mmHg (SD 3.1) above the baseline. This response occurred in 5 lesions (4 patients): 3 LAD and 2 LCX.
- **Group G**: both P_a and P_d decreased at peak and more at stable hyperaemia, again showing the same trend. On average P_a decreased by 2.3 (SD 2.5) mmHg at peak and continued to

decrease during stable hyperaemia to 12.6 mmHg (SD 5.2) below the baseline. P_d decreased by 6.5 mmHg (SD 4.3) at peak and decreased further during stable hyperaemia to 10.9 mmHg (SD 4.3) below the baseline. This response occurred in 2 lesions (2 patients): 1 LAD and 1 RCA.

Comparing these results with those in the published literature, some similarities can be seen with the classification made by Tarkin *et al*. [120]. Tarkin also identified seven types of response within 310 cases, although not all of them are consistent with the findings of the current work in terms of the average values of pressure changes at peak and stable hyperaemia compared to baseline conditions and in terms of the frequency of each type of response. One of the limitations of the study by Tarkin *et al.* is related to the definition of the peak phase as the minimum P_d /P_a ratio within 60 s from the start of adenosine infusion, whereas in the current algorithm the minimum is detected at any time after the start of the infusion. This enables the later responders to also be identified correctly.

In the classification, 2 types of response proposed here (Group E and Group F) occurred for a very limited number of patients. This could be related to a particular reaction within these patients (panic, movement, fear) or to movements of the pressure wires by the clinicians during the procedure and to the catheter position.

In the classification proposed in this work, a number of patients with multiple lesions presented similar adenosine response in all lesions. In other case patients responded differently for each of the lesions and this might be related to a residual effect of adenosine from a previous infusion for the earlier assessment of another lesion.

Table 4.6: Groups of adenosine response, based on the proximal (black) and distal pressure (red) at peak and stable hyperaemia compared with baseline.

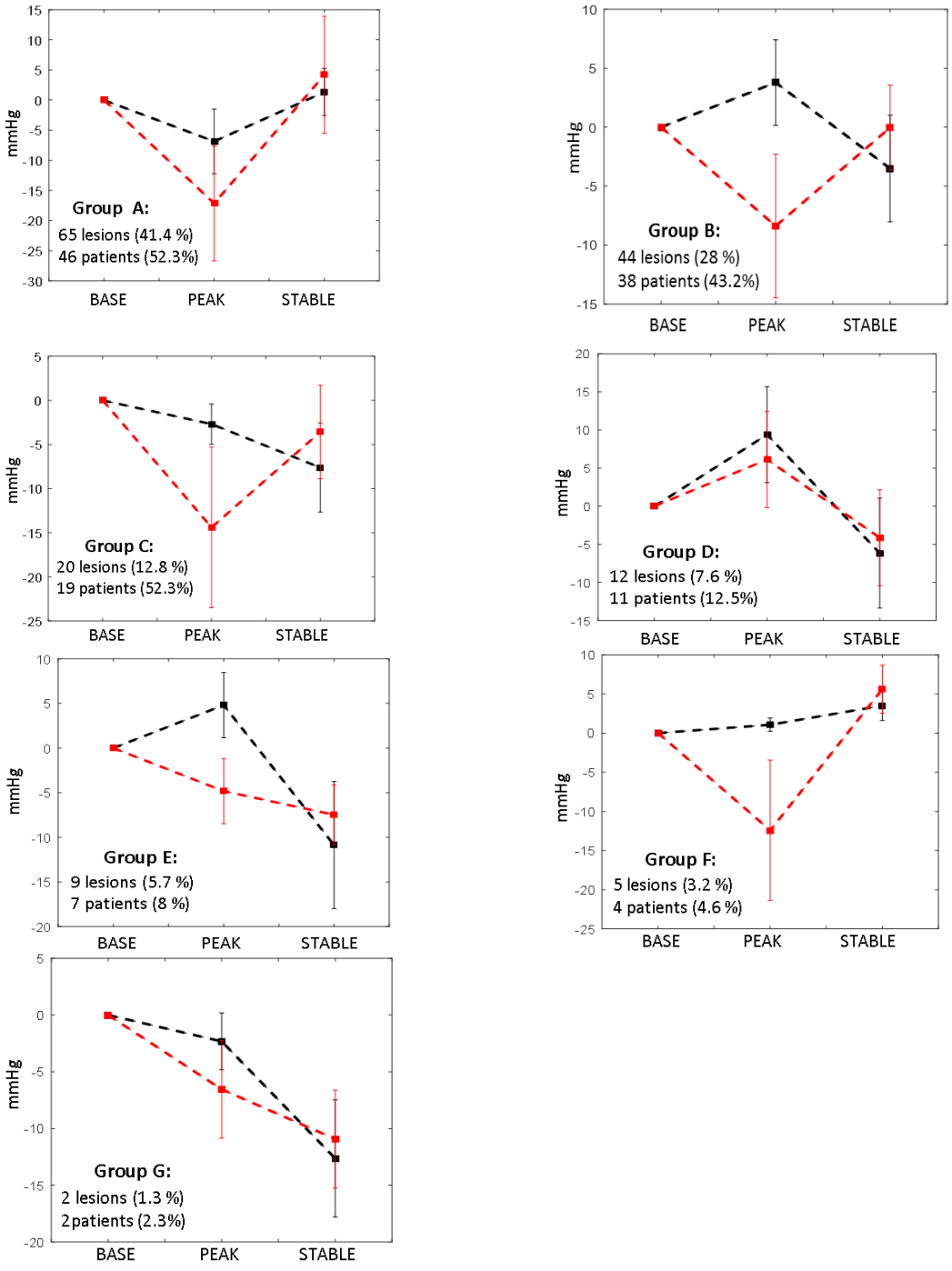

4.4.5.3 Groups response and patients' profiles

The profiles of each patient were analysed for each group of patients based on adenosine response, in order to identify any possible correlation with the adenosine response and patient condition.

Table 4.7 reports the patient profiles for each group in terms of gender, mean and standard deviation of age and BMI, number of obese, overweight and normal weight patients, smoking status (current, ex-smoker, never, unknown) and comorbidities with regards to: diabetes II, hyperlipidaemia, peripheral vascular disease (PDV), atrial fibrillation (AF), hypertension, asthma, chronic obstructive pulmonary disease (COPD), myocardial infarction and its location with respect to the treated lesion. Figures 4.11 - 4.13 show the graphs of the single patient profile in each of the response groups, classified by gender, BMI (overweight, obese and normal), age (>70, between 60 and 70, between 45 and 60 and between 35 and 45), smoking status (never, given up, current, unknown), and the pathologies described above. These results do not suggest any particular relationship between the group response and the patients' profiles. There is no evidence of any cloud of colours representing the different patients' characteristics with regards of each group. The characteristics of each group are similar with no relevant differences, making challenging the prediction of the adenosine response based on the patient profile and the pressure trends.

It is evident that most patients had hyperlipidaemia and hypertension for which they were treated and therefore it is not surprising that these two pathologies are not seen to influence the type of response. On the other hand, the other comorbidities considered were rare in our cohort and it is difficult to make a distinction between those with and without the pathologies. Greater numbers of patients with, and without, each comorbidity need to be recruited to detect any possible influences on the adenosine response. Another aspect that is not taken into account is

the potential effect of a combination of the comorbidities. This would be difficult to assess for each single patient depending on the severity of each pathology.

Table 4.7: Description of the patient profile in each group of adenosine response. Peripheral Vascular Disease (PDV), Atrial Fibrillation (AF), Chronic Obstructive Pulmonary Disease (COPD).

		Group A	Group B	Group C	Group D	Group E	Group F	Group G
	M/F	52/13	38/6	15/5	8/4	8/1	3/2	1/1
	Age	62.4 (10.4)	65.1 (8.5)	66.3 (10.7)	66 (10)	67.5 (13)	66.4 (7.1)	62.5 (6.4)
	BMI	28.7 (3.0) 17 obese 41 ow 7 normal	27.8 (4.0) 13 obese 20 ow 11 normal	28.1 (5.3) 7 obese 6 ow 7 normal	29.2 (4.3) 5 obese 4 ow 3 normal	27.6 (7) 2 obese 4 ow 3 normal	29.7 (7.2) 2 obese 0 ow 2 normal	29.1 (5.3) 1obese 1 ow 0 normal
Smoking	*Current*	4	8	3	1	1	0	0
	Ex-smokers	35	24	7	7	6	4	2
	Never	22	9	10	4	2	1	0
	Unknown	4	3	0	0	0	0	0
Comorbidities	*Diabetes II*	7	8	5	1	1	1	0
	Hyperlipid.	54	34	16	11	5	3	2
	PDV	4	2	1	2	0	0	0
	AF	2	3	0	0	0	0	0
	Hypertension	36	28	14	11	6	4	1
	Asthma	1	0	0	0	0	0	0
	COPD	3	5	2	1	0	0	0
	MI total	31	15	8	4	3	0	1
	MI same reg.	7	0	1	0	1	0	0
	MI elsewhere	17	9	2	1	2	0	0
	MI unknown	7	6	5	3	0	0	1

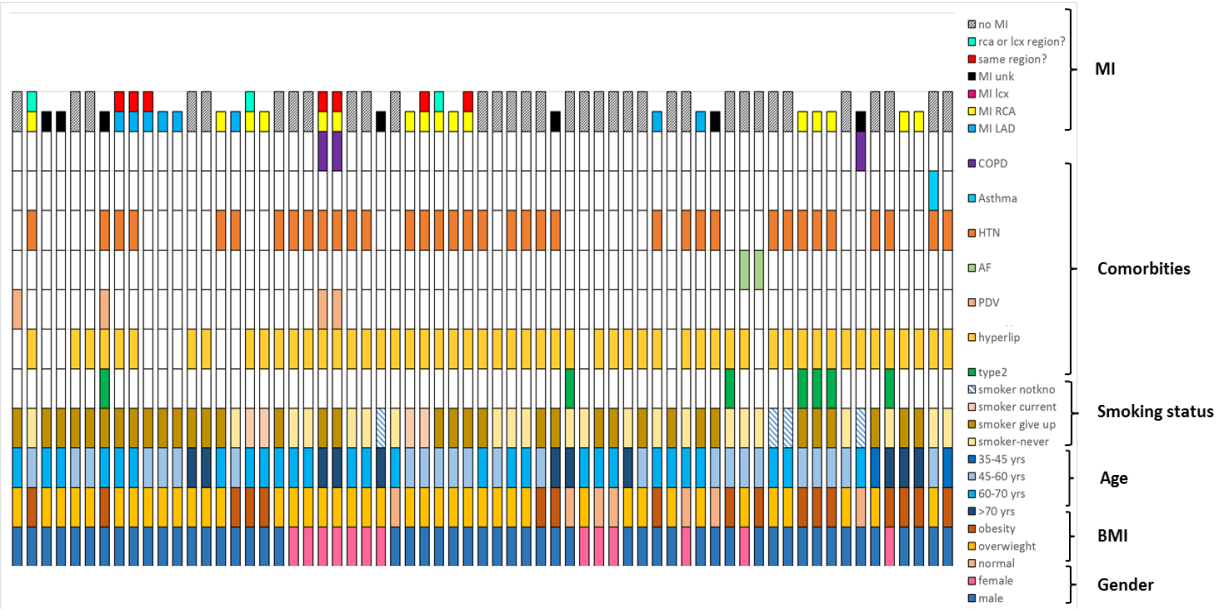

Figure 4.11: Patients' profiles of Group A.
Each column represents a single lesion. Each raw represents a specific characteristic of the patient, starting from the bottom: gender (male-female), BMI (normal-overweight-obese), age (35 to 45, 45 to 60, 60 to 70, over 70), smoking status (never-given up-current), comorbidities (type II diabetes, hyperlipidaemia, peripheral vascular disease, atrial fibrillation, hypertension, asthma, COPD, myocardial infarction and location.

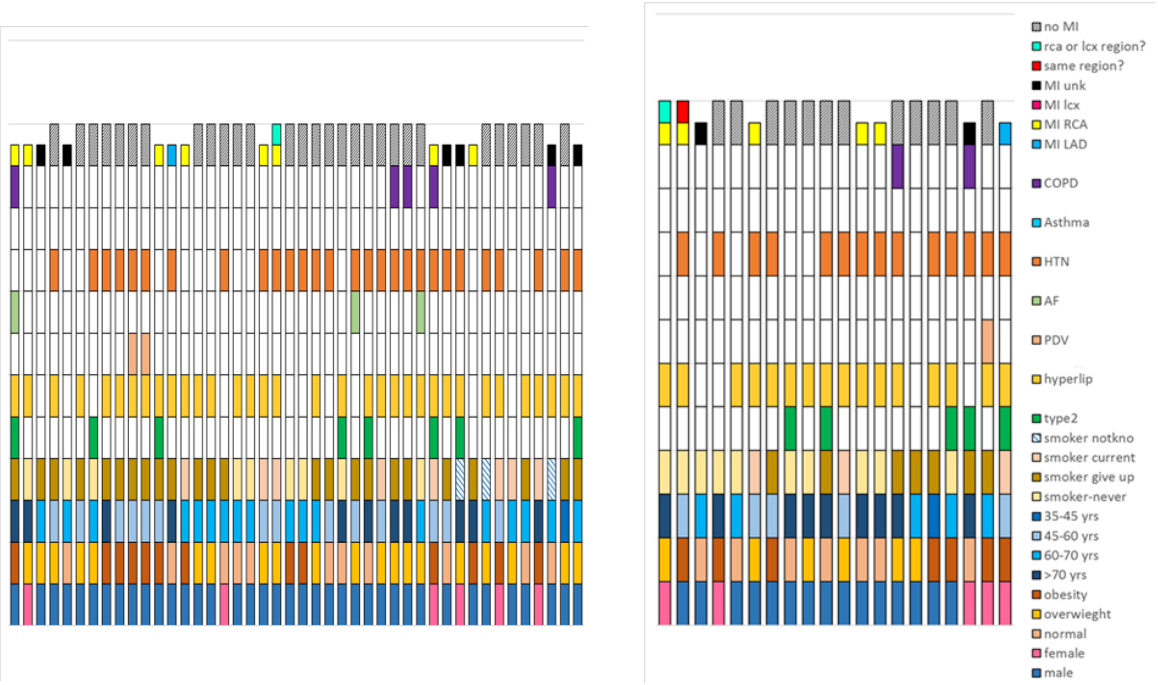

Figure 4.12: Patients' profiles of Group B (left) and C (right).
Each column represents a single lesion. Each raw represents a specific characteristic of the patient, starting from the bottom: gender (male-female), BMI (normal-overweight-obese), age (35 to 45, 45 to 60, 60 to 70, over 70), smoking status (never-given up-current), comorbidities (type II diabetes, hyperlipidaemia, peripheral vascular disease, atrial fibrillation, hypertension, asthma, COPD, myocardial infarction and location.

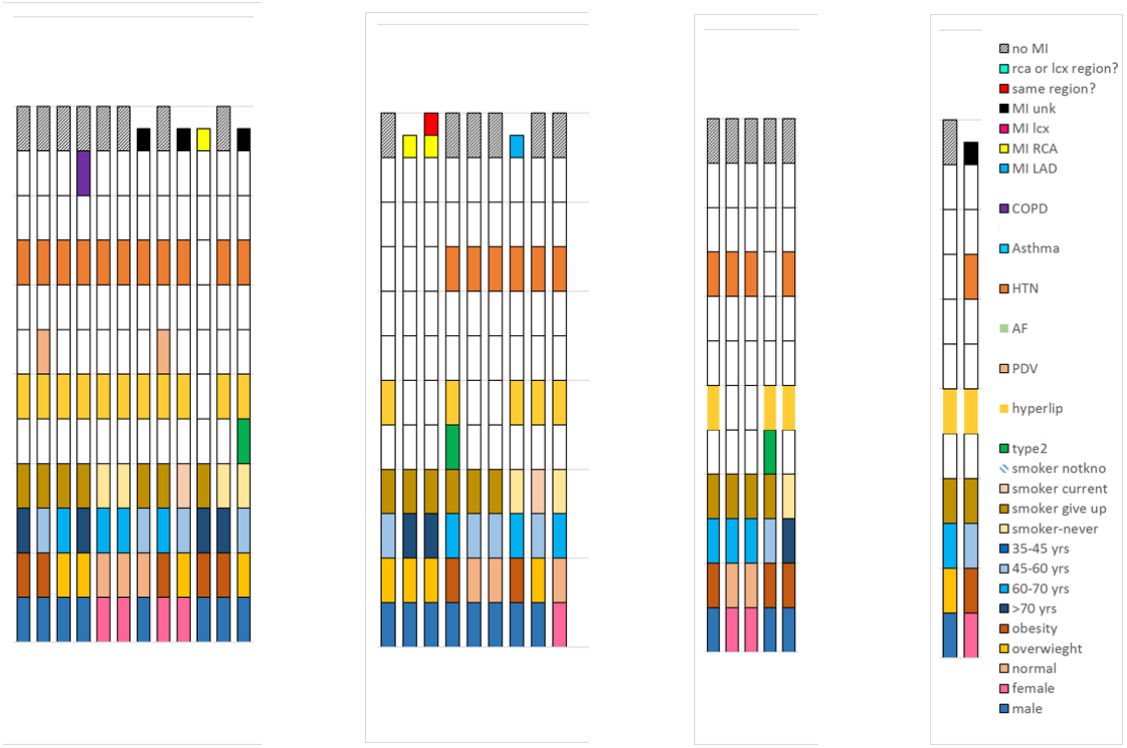

Figure 4.13: Patients' profiles of Group D, E, F, G (from left to right).
Each column represents a single lesion. Each raw represents a specific characteristic of the patient, starting from the bottom: gender (male-female), BMI (normal-overweight-obese), age (35 to 45, 45 to 60, 60 to 70, over 70), smoking status (never-given up-current), comorbidities (type II diabetes, hyperlipidaemia, peripheral vascular disease, atrial fibrillation, hypertension, asthma, COPD, myocardial infarction and location.

4.4.5.4 P_d/P_a ratio curves

The algorithm developed to analyse the raw clinical pressure data produced a P_d/P_a ratio curve for each lesion (total 163) and analysis by eye identified five trends:

- **Type 1**: decrease followed by a small bump and then a stable state;
- **Type 2**: decrease and then stable;
- **Type 3**: decrease and the recovery;
- **Type 4**: flat.
- **Type 5**: decrease followed by multiple bumps;

Table 4.8 represents the type of response and reports the number and the vessel of lesions. Figures 4.14 – 4.15 show the overall patient profiles in each of the groups identified on the basis of the P_d/P_a ratio as described for the previous classification based on the pressures.

In this classification, it is also not easy to identify any particular group characteristic which might aid the prediction of the adenosine response and the limitations are essentially the same reported for the previous classification based on pressure behaviour.

Johnson et al. [144] studied the repeatability of FFR in 190 cases using an algorithm which identified the "smart minimum" as the lowest average FFR across five consecutive cardiac cycles. Their observations suggest 3 types of response: 'humped', 'classic' and 'unusual'. The 'classic' response corresponds to type 2 and type 3 response in the current work and the 'humped' response includes types 1 and type 5, whilst the 'unusual' corresponds to the type 4. Similar percentages of the humped responses (type 1 and 5), while the classic one has a smaller percentage, due to a higher number of patients with flat response (type 4 or unusual) were found in the work by Johnson *et al.* and in the current work.

Table 4.8: 5 types of response based P_d/P_a ratio, with the total number of lesions and the distinction in type of vessels per type of response, with the respective percentages.

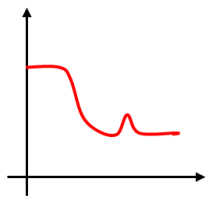	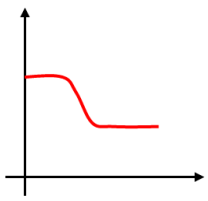	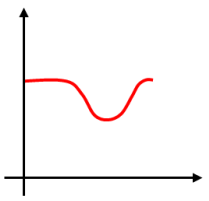	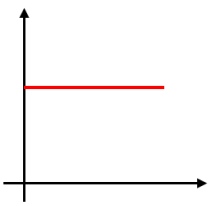	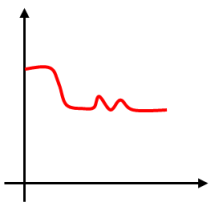
Type 1	**Type 2**	**Type 3**	**Type 4**	**Type 5**
TOT 98 (60%)	**TOT 43 (26.4%)**	**TOT 11 (6.8%)**	**TOT 7 (4.3%)**	**TOT 4 (2.5%)**
LAD 46 (28 %)	LAD 22 (13.5%)	LAD 6 (3.7%)	LAD 1 (0.6%)	LAD 2 (1.2%)
RCA 29 (18 %)	RCA 6 (3.7%)	RCA 2 (1.2%)	RCA 3(1.8%)	RCA - (- %)
LCX 18 (11%)	LCX 9 (5.5%)	LCX 2 (1.2%)	LCX 2 (1.2%)	LCX 2 (1.2%)
DX 5 (3%)	DX 6 (3.7%)	DX 1 (0.6%)	DX 1 (0.6%)	DX - (-%)

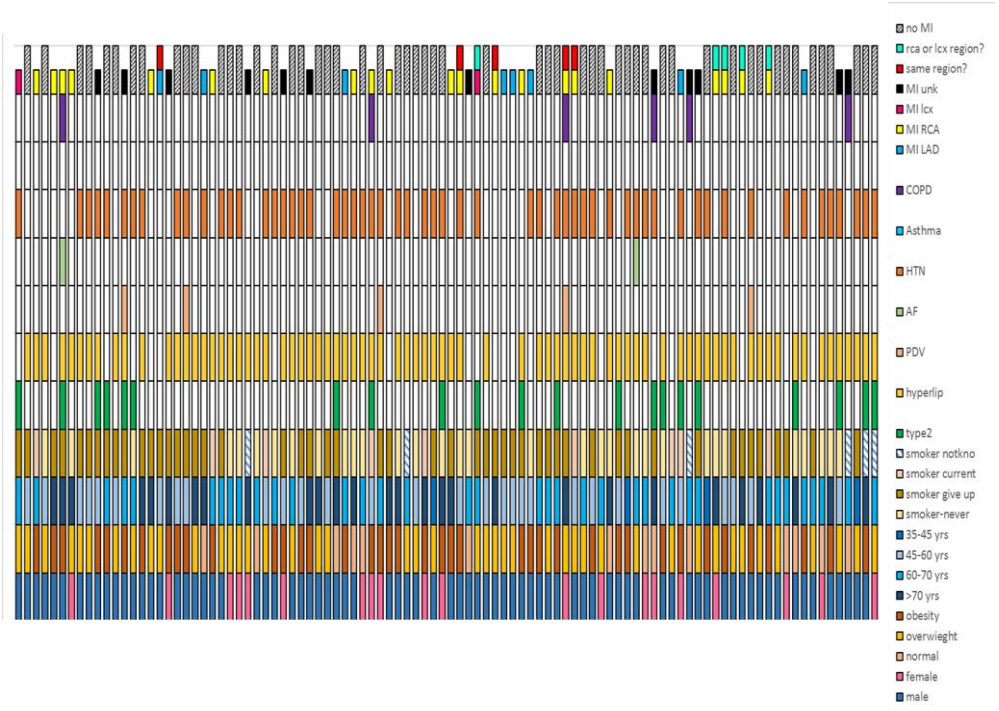

Figure 4.14: Patients' profile of response type 1.

Each column represents a single lesion. Each raw represents a specific characteristic of the patient, starting from the bottom: gender (male-female), BMI (normal-overweight-obese), age (35 to 45, 45 to 60, 60 to 70, over 70), smoking status (never-given up-current), comorbidities (type II diabetes, hyperlipidaemia, peripheral vascular disease, atrial fibrillation, hypertension, asthma, COPD, myocardial infarction and location.

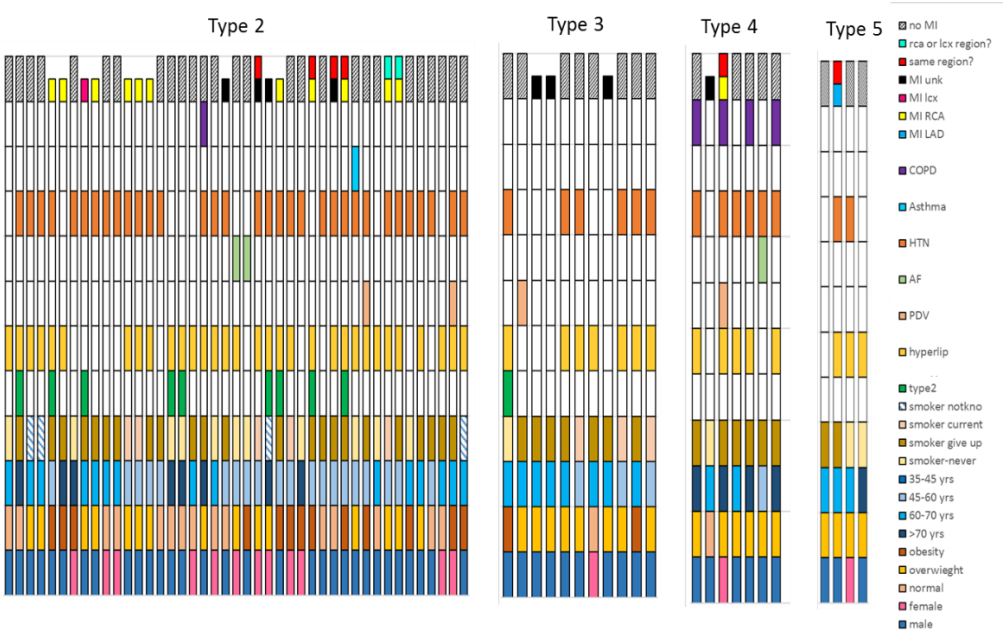

Figure 4.15: Patients' profile of response type 2, 3 ,4 and 5.

Each column represents a single lesion. Each raw represents a specific characteristic of the patient, starting from the bottom: gender (male-female), BMI (normal-overweight-obese), age (35 to 45, 45 to 60, 60 to 70, over 70), smoking status (never-given up-current), comorbidities (type II diabetes, hyperlipidaemia, peripheral vascular disease, atrial fibrillation, hypertension, asthma, COPD, myocardial infarction and location.

4.5 CONCLUSIONS AND LIMITATIONS

The algorithm developed for post-processing the clinical data provides an objective tool which can be incorporated within software used routinely in the Cathlab to assess FFR, eliminating the inter- and intra- operator variability in the interpretation of P_d/P_a ratio. A further standardisation is necessary as to whether to choose the minimum or the stable P_d/P_a ratio as the clinical diagnostic index upon which the treatment decision is based. From analysis of the cases in this study, the minimum is shown to be easier to identify in all patients, including cases where the hyperaemic response did not follow the typical trend and a stable phase was not reached.

The use of the algorithm also provided results in terms of pressure trends and heart rate changes during the adenosine response. Pressures were used to classify the patient responses to adenosine in terms of systemic and coronary circulations.

Trends in P_d/P_a ratio were also analysed to identify similar responses to adenosine which, in turn, can be used to group patients.

The patient profile for each group of response (based on pressure trends and based on P_d/P_a ratio curves) were also analysed to identify any relevant comorbidity or characteristic of the patients which could be related with the type of response. Unfortunately, since all the groups presented similar characteristics, without any particular difference between them, prediction of adenosine response based on patient profiles remains a challenge.

The results of the classification might be improved through the recruitment of a greater number of patients with and without defined comorbidities or characteristics in order to have a high statistical impact on the results.

A limitation of this type of classification may be the lack of consideration of severity and combination of more comorbidities in the same patient.

CHAPTER 5

PERSONALISATION OF PARAMETERS IN THE CARDIOVASCULAR MODEL

INTRODUCTION AND PURPOSE

The physiological status of a patient with coronary artery disease should be taken into account in the decision-making process. The same coronary lesion can have different impacts on different patients. As the anatomical accuracy of personalised computational models has increased with increasing spatial resolution and other improvements in the quality of medical images, there is increasing emphasis on the appropriate representation of the boundary conditions for the individual, describing their own 'physiological envelope'. This envelope is quantitively represented by the operation of lumped parameter models of the type described in Chapter 2.

The aim of this chapter is to develop a process for personalising a lumped parameter model to represent the physiology of an individual patient, especially in the context of diagnostic or prognostic application of such a model for a patient with coronary artery disease. The likelihood of short term clinical translation and impact for a model is increased if it can operate using the data that is already routinely collected in the clinical pathway. Generally, the available physiological data is relatively sparse, and therefore the number of parameters that can be individually personalised is limited, and it is important to identify both the sensitivity of the model to the individual parameters and the outputs that the model must reproduce

faithfully to be of clinical value. Specifically, the focus of this and the next chapter is on the patient-specific personalisation of a lumped parameter cardiovascular model, which includes the global cardiovascular system, in terms of left and right heart and pulmonary and systemic circulation, and the local coronary circulation.

It was demonstrated in Chapter 3 that the local coronary flow characteristics are strongly influenced by the global systemic parameters, but not vice versa. It is, therefore, practical to separate the model into a global model to represent the system response and to compute the parameters at the coronary inlet, and a separate model to analyse the coronary flow with the computed inlet boundary condition.

The idea of using simpler, patient-specific, cardiovascular models as a central component in the translation of computational tools to clinical application, driven by the recognition of the limitations and general sparsity of routine clinical physiological data that might be available for the personalisation process, is gaining traction. An example is the study of Hann *et al.* [43], in which a multi-compartment cardiovascular model was simplified and divided into sub-systems which were studied independently. Hann described the identification and selection, based on sensitivity analysis, of the significant model elements to fit the available data from a minimal clinical dataset (although even this, which is based on recordings in the intensive care unit, is relatively rich compared with routine clinical data), reducing therefore the parameters to be personalised. Another relevant example is the work of Sughimoto *et al.* [44], in which it is shown how the cardiovascular function can be assessed by a cardiovascular model combined with clinical data routinely measured, providing an extremely useful tool to the clinicians.

Schiavazzi *et al*. [151] developed a similar approach with the sub-model for the heart in patients with congenital HLHS (Hypoplastic Left Heart Syndrome) who undergo the Norwood procedure to improve the perfusion and the blood oxygenation through surgical intervention

[152]. The model consists of the heart model and an RCRCR branch for the systemic and pulmonary circulations and the shunt is also included.

In this thesis, in a first stage, the global cardiovascular model is personalised aiming to obtain and reproduce patient-specific outputs during baseline conditions, corresponding to the data collected during echocardiography and angiography. In the target application of the study of coronary flow changes under the intravenous administration of adenosine, the principal relevant output of the global system model is the distribution of the adenosine in all the compartments: no measurements of this parameter were made during the clinical process. In particular, the concentration in the aortic sinus compartment (SAS) is used, together with measured aortic pressure, as the input for the local model of the coronary artery.

The focus of this chapter is on the personalisation of the global model, with the specific aim of estimation of the adenosine distribution during the period of infusion and clearance. In a second stage, explained in detail in Chapter 6, the focus moves onto the local system, aiming to describe the local response to adenosine correlating the myocardial resistance to the adenosine concentration. Data from 3D simulations of the coronary stenosis together with proximal and distal pressure were used to characterize the lesion and to calculate the coronary flow and the myocardial resistance. Moreover, the adenosine concentration in the coronary compartment is estimated in order to establish a relationship between the myocardial resistance and the adenosine distribution. Optimisation processes was employed in both global and local system using the respective available data.

5.1 CLINICAL DATA: INCONSISTENCY AND STRATEGY

5.1.1 Clinical data

Patients with Coronary Artery Disease usually undergo pre-admission appointment, followed by echocardiography and finally angiogram. During each of these phases, different patient data are measured.

5.1.1.1 General data

During the Pre-Admission appointment for their PCI, patients were asked some general information, followed by a medical examination. The patient data available from the Pre-Admission appointment are:

- Gender, Age and Ethnicity;
- Height, Weight and Body Mass Index (BMI);
- Heart rate (HR), Systolic (P_{SYS}) and Diastolic (P_{DIA}) pressure measured with a cuff pressure monitor, from which mean arterial pressure (MAP) can estimated (Eq.5.1) [153];

$$MAP = \frac{P_{SYS} + 2 \cdot P_{DIA}}{3} \quad \text{(Eq.5.1)}$$

- Medical history with regards of Hypertension, Hyperlipidaemia, Pulmonary hypertension, Chronic obstructive pulmonary disease (COPD), Asthma, Atrial fibrillation, Diabetes type I, Diabetes type II, myocardial infarction (MI);
- Smoking status.

5.1.1.2 Echocardiography and Electrocardiography

Before angiogram, patients usually undergo simultaneously echocardiography and electrocardiography. Echocardiography, widely used in diagnosis, is a non-invasive technique which produces images of the heart using Doppler ultrasound and provides useful information

about the heart and its pathologies, such as cardiomyopathies, heart failure, congenital diseases, endocarditis, cardiac valves pathologies, location and extension of damaged tissue from heart attack. Electrocardiography is a non-invasive technique to measure heart rate.

The quantitative data provided by the echo- and electrocardiography are:

- End-systolic left ventricular volume, ESV;
- End-diastolic left ventricular volume, EDV;
- Velocity of blood across the aortic valve, $V_{ao}(t)$;
- Area of aortic valve, A_{ao};
- Heart rate, HR.

From these measured data, the following are derived:

- Ejection fraction is calculated from the left ventricular volume measurements (ESV and EDV) visualizing 2 chambers and 4 chambers (EF, Eq.5.2);
- Stroke volume can be calculated from left ventricular volume measurements (ESV and EDV) visualizing 2 chambers and 4 chambers (SV_{2CH}, SV_{4CH} - Eq.5.3) and from the product between the aortic valve area and the integral of the blood velocity over one cardiac cycle (SV_{LVOT} – Eq.5.4);
- Cardiac output is obtained as the product between SV and HR (CO, Eq.5.5).

$$EF_{2CH/4CH} = \frac{EDV_{2CH/4CH} - ESV_{2CH/4CH}}{EDV_{2CH/4CH}} \quad \text{(Eq.5.2)}$$

$$SV_{2CH} = EDV_{2CH} - ESV_{2CH} \qquad SV_{4CH} = EDV_{4CH} - ESV_{4CH} \quad \text{(Eq.5.3)}$$

$$SV_{LVOT} = A_{ao} \cdot \int_0^T V_{ao} \quad \text{(Eq.5.4)}$$

$$CO = SV \cdot HR \quad \text{(Eq.5.5)}$$

5.1.1.3 Invasive pressure measurements

During the angiogram, proximal and distal pressures were measured invasively as described in Chapter 4 (*Paragraph 4.1.1 Invasive pressure data*). The proximal pressure during baseline

was cycle averaged using GIMIAS or VIRTUheart (see *Paragraph 4.2.1 Average pressure signal over a cardiac-cycle*) and the length of signal provides the heart rate (HR) during angiography, consistent with the pressure curve used for the optimisation. The maximum value of the signal represents the systolic pressure (P_{SYS}), while its minimum the diastolic pressure (P_{DIA}). MAP can be estimated using the systolic and diastolic pressure (Eq.5.1) or as the real mean value of the pressure signal.

5.1.2 Inconsistency and strategy

Table 5.1 summarises the available data from each patient, distinguishing between invasive and non-invasive data with raw measurements and derived data.

Table 5.1: Invasive and non-invasive data measured and derived for CAD patients.

	Non -Invasive										**Invasive**	
	Pre-admission		ECG		ECHO 2ch		ECHO 4ch		DOPPLER		Angiogram	
	Raw	Der.	Raw	Der.	Raw	Der.	Raw	Der.	Raw	Der.	Raw	Der.
Gender	✓											
Ethnicity	✓											
Age	✓											
Height	✓											
Weight	✓											
BMI		✓										
Comorbidities	✓											
HR	✓		✓									✓
P_{SYS}	✓											✓
P_{DIA}	✓											✓
MAP		✓										✓
CO						✓		✓		✓		
SV						✓		✓		✓		
ESV				✓	✓		✓					
EDV				✓	✓		✓					
EF						✓		✓				
$P_a(t)$											✓	
A_{ao}									✓			
$V_{ao}(t)$									✓			

There is some redundancy in the fields because same parameters were measured with different techniques and in different moments. Of course it is impossible for a model to reproduce the measured outputs if they are not mutually consistent, which will often, or always, be the case when they are measured separately in clinical processes. This emphasises the need for careful design of the data protocol to support a modelling study and is discussed further at the end of the current chapter. In the following pages, the method employed to adjust the data is described and discussed.

5.1.2.1 Expected physiological ranges of echocardiographic data

Typical physiological ranges for the clinically measured parameters were derived from the literature [154-159]. A summary of the reported ranges of cardiac output, stroke volume, end-systolic volume, end-diastolic volume and heart rate data at baseline in health and disease (MI, Hypertension, CAD, angina) is presented in table 5.2.

5.1.2.2 Strategy

Invasive data of aortic pressure are the richest information provided in this work and provides a cycle-averaged pressure signal in time. Heart rate, systolic and diastolic pressure can be recovered from the trace respectively from the length of the cycle and the maximum and minimum pressure. The mean arterial pressure (MAP) could be recovered from average of the pressure signal but, consistent with clinical practice when only cuff pressures are available, it is computed using Eq.5.1.

Therefore, the measurements of these data during pre-admission and ECG were not considered. As mentioned previously, the stroke volume is estimated in different ways during the echocardiography and the results are generally inconsistent, because of the limitations of the echocardiogram itself.

Table 5.2: Literature data for cardiac output (CO), stroke volume (SV), heart rate (HR), end-systolic volume (ESV) and end-diastolic volume (EDV).

Parameter	Values	Source
CO [l/min]	1.9 - 21 with Doppler mitral method 1.2 - 9.6 with Doppler EDV method healthy/pathologic 2.4 - 9.5 with thermodilution method	F.Lewis *et al.*, 1984 [157]
	6.44 ± 1.26 normal patients 6.98 ± 0.95 patients with angina 5.71 ± 153 patients with previous MI	R.Mcdonough *et al.*,1974 [158]
	6.0 ±1.3 for healthy patients 5.4 ± 1.2 Significant single vessel CAD 5.7 ± 1.5 Significant multiple vessel CAD	K.Reryich *et al.*,1978 [159]
	6.9 ± 1.4 for healthy patients 5.3 ± 1.8 for patients with heart failure	K.Laskey *et al.*, 1990 [156]
SV [ml]	17 - 190 with Doppler mitral method 13 - 171 with Doppler EDV method healthy/pathologic 24 - 89 with thermodilution method	F.Lewis *et al.*, 1984 [157]
	92 ± 12 normal patients 109 ± 21 patients with angina 79 ± 31 patients with previous MI	R.Mcdonough *et al.*,1974 [158]
	76 ± 20 for healthy patients 63 ± 12 Significant single vessel CAD 76 ± 18 Significant multiple vessel CAD	K.Reryich *et al.*,1978 [159]
	99 ± 12 for healthy patients 60 ± 21 for patients with heart failure	K.Laskey *et al.*, 1990 [156]
	37-112 male and females age 61-70	P.A.Cain *et al.*, 2009 [154]
	92 ± 22 for normotensives 78 ± 14 for hypertensives	A.Cohen-Solal *et al.*, 1994 [155]
HR [beats/min]	69 ± 14.8 normal patients 65 ± 6.3 patients with angina 76 ± 16.3 patients with previous MI	R.Mcdonough *et al.*,1974 [158]
	81 ± 13 for healthy patients 87 ± 13 Significant single vessel CAD 75 ± 15 Significant multiple vessel CAD	K.Reryich *et al.*,1978 [159]
	75 ± 10 for normotensives 85 ± 13 for hypertensives	A.Cohen-Solal *et al.*, 1994 [155]
	73 ± 12 for healthy patients 95 ± 15 for patients with heart failure	K.Laskey *et al.*, 1990 [156]
EDV [ml]	116 ± 31 for healthy patients 93 ± 20 Significant single vessel CAD 138 ± 62 Significant multiple vessel CAD	K.Reryich *et al.*,1978 [159]
	72-185 male and females age 61-70	P.A.Cain *et al.*, 2009 [154]
ESV [ml]	40 ± 15 for healthy patients 30 ± 15 Significant single vessel CAD 62 ± 50 Significant multiple vessel CAD	K.Reryich *et al.*,1978 [159]
	22 - 88 male and females age 61-70	P.A.Cain *et al.*, 2009 [154]

On examination of the study data, it was observed that the calculation of the HR from the CO measured with Doppler, where available, and the SV yielded values within the expected physiological range based on the SV_{LVOT} from left ventricular outflow tract measurements, but not based on the $SV_{2CH/4CH}$ chamber volume measurements (Table 5.3). This suggested that

SV_{LVOT} is the most reliable between the two and it was selected for the optimisation. This leads to the inability to consider the values of ESV and EDV as they were measured in the echo, considering the average between the 2 chamber and 4 chamber views.

The approach used to resolve this inconsistency and enable use of all the echo parameters as target in the optimisation was to consider the data of SV_{LVOT} from the echo, the heart rate from the pressure signal at baseline (HR_{SIG}) and the ejection fraction (EF), to estimate the cardiac output (CO_{opt}) (Eq.5.6), the end systolic and diastolic left ventricle volumes (ESV_{opt}, EDV_{opt}) (Eq.5.7, Eq.5.8).

$$CO_{opt} = SV_{LVOT} * HR_{SIG} \quad \text{(Eq.5.6)}$$

$$EDV_{opt} = \frac{SV_{LVOT}}{EF} \quad \text{(Eq.5.7)}$$

$$ESV_{opt} = EDV_{opt} - SV_{LVOT} \quad \text{(Eq.5.8)}$$

Table 5.3: Comparison between the heart rate (HR) obtained with the $SV_{2CH/4CH}$ and with SV_{LVOT} and the cardiac output from echocardiography.

Case	HR =$CO_{echo}/SV_{2CH/4CH}$	HR =CO_{echo}/SV_{LVOT}	Case	HR =$CO_{echo}/SV_{2CH/4CH}$	HR =CO_{echo}/SV_{LVOT}
1	57.63	56.40	***15***	192.64	73.59
2	133.72	63.64	**18**	89.80	60.11
3	79.93	74.24	**20**	51.82	74.60
4	133.33	83.77	***23***	217.39	67.63
5	135.64	95.15	***24***	112.00	49.47
6	178.93	61.62	***25***	114.50	64.79
7	46.44	61.64	***26***	140.66	61.19
8	139.24	74.73	***27***	129.27	60.43
9	162.16	52.33	***28***	141.32	67.99
10	56.54	53.46	***29***	101.05	77.33
11	79.69	59.40	***30***	148.34	69.38
12	67.74	52.56	***31***	125.23	59.64
13	116.33	61.69	***32***	342.39	82.25
14	110.34	43.96	***33***	121.76	77.69

From the overall study cohort of 100 patients with coronary artery disease, a sub-cohort of 37 patients with a complete dataset of (pseudonymised) general clinical data, including echocardiographic data and including pressure signals during angiography, were identified. The selection criteria were:

- echocardiography performed (many patients did not undergo echocardiography before angiogram for reason of time and limited number of personnel in the ward);
- availability of measured stroke volume (SV_{LVTOT}) based on flow through aortic valve, considered the most reliable measure of this parameter, and ejection fraction;
- pressure data were properly collected during angiography.

Table 5.4 briefly describes this sub-cohort in terms of demographic data, comorbidities and smoking status (as an identified risk factor). These data were not used for the model personalisation process, but are used later to seek associations between the clinical phenotype and the measured response to adenosine.

Table 5.4: Demographic data, comorbidities and risk factors in the sub-cohort (37 patients). Demographic information is gender, age, BMI (Body Mass Index). Comorbidities are: type II diabetes, hyperlipidaemia, Peripheral Vascular Disease (PVD), Hypertension, Chronic Obstructive Pulmonary Disease (COPD), and previous myocardial infarction (MI). Risk factor is smoking status.

Patient demographic		**Num% - mean (SD)**
Male		73%
Age (years)		65 (SD 11)
BMI		29.26 (SD 4.9)
Hypertension		62.1 %
PVD		8.1 %
Previous MI		51.3 %
Type II diabetes		8.1 %
Hyperlipidaemia		67.5 %
COPD		5.4 %
Smoking status:	*Never*	24 %
	Ex-smoker	64.8 %
	Current	8.1 %

Raw data used for the parameter personalisation of the cardiovascular model for each individual in the sub-cohort included:

- gender, height and weight measured during the pre-angiogram medical examination;
- stroke volume estimated with Doppler (SV_{LVTOT});
- average ejection fraction measured during echocardiography visualising 2 and 4 chambers;
- heart rate, systolic pressure and diastolic pressure and mean arterial pressure calculated from the cycle-averaged proximal pressure signal.

Derived data from the listed above are: cardiac output, end diastolic left ventricle volume and end systolic left ventricle volume. Table 5.5 shows in red which data were chosen as input for the optimisation. Table 5.6 reports all the data and summarises them with the respective mean, median, standard deviation, range, minimum and maximum of each parameter.

The optimisation was performed for all the 37 patients and the obtained results were compared with the original data, used as target. The simulations were run considering the baseline proximal pressure as target. Optimising the hyperaemic condition requires another type of cost function, but there were not measurements available during the hyperaemic state, except of pressures. It is not possible therefore to use the echocardiographic data which were measured in absence of adenosine effect.

Table 5.5: Clinical data used for the optimisation process in red.

	Non -Invasive										**Invasive**	
	Pre-admission		ECG		ECHO 2ch		ECHO 4ch		DOPPLER		Angiogram	
	Raw	Der.	Raw	Der.	Raw	Der.	Raw	Der.	Raw	Der.	Raw	Der.
Gender	✓											
Ethnicity	✓											
Age	✓											
Height	✓											
Weight	✓											
BMI		✓										
Comorbidities	✓											
HR	✓		✓									✓
P_{SYS}	✓											✓
P_{DIA}	✓											✓
MAP	✓											✓
CO						✓		✓		✓		
SV						✓		✓		✓		
ESV				✓	✓		✓					
EDV				✓	✓		✓					
EF						✓		✓				
$P_a(t)$											✓	
A_{ao}									✓			
$V_{ao}(t)$									✓			

Table 5.6: Optimisation input data of 37 patients in the sub cohort.
Columns report: gender, height (cm), weight (kg); systolic pressure, diastolic pressure and MAP (mmHg); heart rate (HR- beats/min); stroke volume (SV_{LVOT} -ml); ejection fraction (EF-%); cardiac output (CO_{opt}-l/min), end diastolic left ventricle volume (EDV_{opt}-ml) and end systolic left ventricle volume (ESV_{opt}-ml).

Case	*Gen.*	*Height*	*Weight*	*P_sys*	*P_dia*	*MAP*	*HR_{sign}*	*SV_{LVOT}*	*EF*	*CO*	*EDV*	*ESV*
1	M	179	88.3	158	64	95.32	52.9	73.4	70	3.88	104.86	31.46
2	F	159	69.1	139.8	71.3	94.15	57.7	55	38.2	3.17	143.98	88.98
3	M	179	103	111.2	72.4	85.34	64.8	62.1	52.5	4.02	118.29	56.19
4	M	169	82.3	122.4	73	89.47	81.63	57.3	35.8	4.68	160.06	102.8
5	M	173	68.7	150.9	84.7	106.8	90.6	53.6	71.5	4.86	74.97	21.37
6	F	160	87.8	151.1	75.4	100.6	68.8	81.3	56.4	5.59	144.15	62.85
7	F	158	89	177.3	71.43	106.7	61.2	75	53.45	4.59	140.32	65.32
8	M	175	103	112.1	52.7	72.52	64.1	39.1	57.7	2.51	67.76	28.66
9	M	170	81.2	121.2	65.3	83.94	60.5	73.6	29.5	4.45	249.49	175.9
10	M	179	84.1	126.6	52.1	76.94	49.6	103.2	59.6	5.12	173.15	69.95
11	M	176	89.6	109.7	60	76.57	71.3	88.1	61.6	6.28	143.02	54.92
12	M	168	92.6	98.9	56.5	70.67	63	122.9	71	7.74	173.1	50.2
13	M	185	107	104.5	57.9	73.47	62.8	72.3	53.3	4.54	135.65	63.35
14	M	170	80.8	158.7	68.2	98.37	59.4	92.4	46.6	5.49	198.28	105.9
15	M	182	83	151.8	76	101.2	49.6	109.2	44.9	5.42	243.21	134.0
16	M	183.1	113.1	108.7	64.11	78.97	56.06	110.2	65.8	6.18	167.48	57.28
17	F	152	57.9	102.1	70.94	81.32	77.62	60.6	52.75	4.7	114.88	54.28
18	M	190	140	122.5	77.5	92.51	67.7	110.2	55	7.46	200.36	90.16
19	M	175	75	120.1	70.7	87.22	62.03	73.3	58.4	4.55	125.51	52.21
20	M	166	83.1	140	60.4	86.92	66.1	73.2	49.3	4.84	148.48	75.28
21	M	180	82	124.1	62.18	82.79	65.72	85.9	68.2	5.65	125.95	40.05
22	F	162	59	151.8	68.24	96.11	61.5	53.1	47.9	3.27	110.86	57.76
23	M	168	126	114.1	69.5	84.35	83.2	49.6	70.5	4.13	70.35	20.75
24	F	157	72.1	184	58	100.0	61.9	103.5	61.7	6.41	167.75	64.25
25	F	156	68.2	151.8	76.6	101.7	74.5	56.6	56	4.22	101.07	44.47
26	F	152	62.2	161.4	64	96.46	80.4	46.3	58.8	3.72	78.74	32.44
27	M	183	78	125.3	63.5	84.08	73.7	119.3	63.8	8.79	186.99	67.69
28	M	182	91.8	174.1	79.7	111.2	51.8	87.7	42.7	4.54	205.39	117.69
29	M	183	96.1	126.4	72.3	90.37	67.8	116.2	55.9	7.88	207.87	91.67
30	F	168	92.2	122.9	69.1	87.01	75.1	75	67.4	5.63	111.28	36.28
31	M	187	92	106	58.5	74.35	75.1	83.6	57.2	6.28	146.15	62.55
32	M	183	110	116.7	64.4	81.85	54.4	115.7	48	6.29	241.04	125.34
33	M	161	55.9	98.1	70.6	79.75	80	76.6	42.8	6.13	178.97	102.37
34	M	172	109	157.5	53.7	88.32	73.4	60.5	54.9	4.44	110.2	49.7
35	M	168	73.6	109.18	65.37	79.98	65.13	44.1	51.6	2.87	85.47	41.37
36	F	155	68.9	148.37	73.61	98.54	63.5	60.6	54	3.85	112.22	51.62
37	M	185	89.4	90.87	65.46	73.93	80.68	56.5	25.7	4.56	219.84	163.34
Mean	-	171.6	86.6	131.1	67.0	88.37	66.9	77.8	54.3	5.1	148.3	70.5
Median	-	172.0	84.1	124.0	68.2	86.97	65.1	73.6	55.0	4.7	144.0	62.6
Std.D	-	10.8	18.6	24.5	7.8	10.6	10.1	23.8	11.1	1.4	49.8	37.1
Range	-	38.0	84.1	93.1	32.6	40.54	41.0	83.8	45.8	6.3	181.7	155.1
Min	-	152.0	55.9	90.9	52.1	70.67	49.6	39.1	25.7	2.5	67.8	20.8
Max	-	190.0	140.0	184.0	84.7	111.2	90.6	122.9	71.5	8.8	249.5	175.9

5.2 GLOBAL TUNING OF CARDIOVASCULAR MODEL

Despite its apparent simplicity and limitations, the cardiovascular model described in Chapter 2 and in Chapter 3 contains a high number of parameters:

- 54 parameters are related to the hemodynamic part, including the initial blood volumes, resistances, compliances, inertances, cardiac elastances, valvular coefficients;
- 45 parameters are related to the barocontrol system.

It is evident that the development of a personalisation process for a model with so many parameters is not trivial. It is likely to be unstable numerically, especially given the sparsity of relevant clinical physiological information.

In this chapter a subset of the parameters of the basic systems physiology model, excluding both chemocontrol and barocontrol, is personalised to each individual in the sub-cohort using the sparse clinical data available. The justification for omitting the barocontrol is that two of the key parameters that are governed by the barocontrol mechanism, heart rate and aortic pressure, are directly measured during the period of administration of the adenosine.

The tuning of the global model parameters aims to reproduce the echocardiographic data and the invasive proximal pressure data during baseline. The first step is to select the personalisation inputs and outputs and the second step is the optimisation process.

5.2.1 Selection of inputs and outputs for parameter personalisation

The non-barocontrolled model is provided with inputs and produces outputs which can be classified as raw and derived. The parameters personalisation considers some of the input model to be defined, and therefore to be classified as unknown-outputs, and some of the model outputs to be known for each patient and therefore classified as input of the personalisation.

Table 5.7 indicates the inputs and outputs (raw and derived) from the non-barocontrol model and those for the parameter personalisation process.

The heart rate is an input parameter for both the model and the personalisation. The parameter personalisation process used 9 inputs which were model-outputs. These were: ejection fraction (EF), stroke volume (SV), from which cardiac output (CO), left ventricle end-systolic (ESV) and end diastolic (EDV) blood volumes were derived. An additional input was the invasive measurement of the aortic pressure signal over a cardiac cycle ($P_{sat}(t)$), from which aortic systolic (P_{SYS}) and diastolic (P_{DIA}) pressures and mean arterial pressure (MAP) were derived. The pressure signal provides a rich set of information and potentially is possible to personalise a number of parameters equal to the number of samples. However, in truth, it is not known how the model parameters influence the single sampling points of the signal and how they are related between themselves. Moreover, the model is a non-linear system and this causes an even higher complexity of the definition of independent parameters to define the outputs.

The outputs of the parameter personalisation were selected from the model inputs with sensitivity value (NVs, Chapter 2- Figure 2.18) above an arbitrarily selected threshold of 0.1 with regards of the inputs chosen for the parameter personalisation: heart period (T), passive (ELV_{min}) and active (ELV_{max}) left ventricle elastances, systemic (R_{scp}) and pulmonary (R_{pcp}) capillary resistances, systemic arterial capacitance (C_{sat}), initial blood volumes in left atrium (V_{lai}), left ventricle (V_{lvi}), systemic vein (V_{svni}) and unstressed systemic venous volume (Un_{veini}).

The threshold of 0.1 has selected based on the values of sensitivities obtained with the sensitivity analysis, in order to not select too few or too many variables for the personalisation process, according to the available clinical data.

Furthermore, a second selection was done to reject some of these input data for different reasons:

- the initial blood volumes in systemic vein (V_{svni}), left atrium (V_{lai}), left ventricle (V_{lvi}) and unstressed systemic venous volume (Un_{veini}) were already estimated as proportion of the total blood volume as shown later in *Paragraph 5.2.2.3.1 Preliminary tuning* and therefore they cannot be changed to keep constant to total blood volume;
- the heart period T was known from the patient data;

In conclusion, the optimisation process aimed to personalise ELV_{max}, ELV_{min}, R_{scp}, C_{sat} and R_{pcp} at baseline condition. This is in agreement with published data on sensitivity analysis of cardiovascular models [125, 160-163]. These five parameters are indicated in red in the outputs of the parameter personalisation of table 5.7.

Table 5.7: List of inputs and outputs (raw and derived) of the non-barocontrolled model and the parameter personalisation.
In red are indicated the model input parameters with sensitivity value above 0.1 (see Figure 2.18 about sensitivity analysis results). From these parameters only 5 were selected to be output for the parameters personalisation: ELV_{max}, ELV_{min}, R_{pcp}, R_{scp}, C_{sat}. In blue are indicated the clinical data which are model outputs and were used as input in the parameter personalisation.

NON-BAROCONTROL		
INPUTS	OUTPUTS	
	RAW	DERIVED
Timing parameters: **T** (or **HR**), Ts1, Ts2, Tpw1, Tpw2 Elastances: **ELVmax,** ERVmax, **ELVmin,** ERVmin Unstressed cardiac volume and pressures: Vlvini, Plvini, Vrvini,Prvini Vlaini, Plaini, Vraini, Praini Valvular coefficients: CVao, CVmi, CVtr, CVpo Capacitances: Csas, **Csat,** Csvn, Cpas, Cpat, Cpvn, Clc, Crc Resistances: Rsas, Rsat, Rsar, **Rscp,** Rsvn, Rpas, Rpat, Rpar, **Rpcp,** Rpvn, Zrc, Zlc , Rrc, Rlc Inhertances Lsas, Lpas Initial volumes: **Vlai, Vlvi,** Vrvi, Vrai, Vlci, Vrci, Vsasi, Vsati,Vsari, Vscpi,**Vsvni,** Vpasi, Vpati, Vpari, Vpcpi, Vpvni, **Unveini**	Pressures: Plv(t), Pla(t), Pra(t), Prv(t), Psas(t),**Psat(t),**Psar(t),Pscp(t), Psvn(t), Ppas(t),Ppat(t),Ppar(t), Ppcp(t),Ppvn(t) Flows: Qlvo(t), Qlao(t), Qrvo(t), Qrao(t) Qsas(t), Qsat(t), Qsar(t), Qscp(t), Qsvn(t), Qpas(t), Qpat(t), Qpar(t), Qpcp(t), Qpvn(t), Qlc(t), Qrc(t) Volumes: Vla(t), Vlv(t), Vrv(t), Vra(t),Vlc(t), Vrc(t), , Vsas(t) , Vsat(t), , Vsar(t), Vscp(t), Vsvn(t), Vpas(t), Vpat(t), Vpar(t), Vpcp(t), Vsvn(t) **EDV** **ESV**	**CO** **EF** **SV** **Psys** **Pdia** **MAP**

PARAMETER PERSONALISATION		
INPUTS	OUTPUTS	
	RAW	DERIVED
Clinical data: **CO, EF, SV, HR, EDV, ESV, Psys, Pdia, MAP, Psat(t)** Timing parameters: Ts1, Ts2, Tpw1, Tpw2 Elastances: ERVmax, ERVmin Valvular coefficients: CVao, CVmi, CVtr, CVpo Unstressed cardiac volume and pressures: Vlvini, Plvini, Vrvini,Prvini Vlaini, Plaini, Vraini, Praini Capacitances: Csas, Csvn, Cpas, Cpat, Cpvn, Clc, Crc Resistances: Rsas, Rsat, Rsar, Rsvn, Rpas, Rpat, Rpar, Rpvn, Zrc, Zlc , Rrc, Rlc Inhertances Lsas, Lpas Initial volumes: **Vlai, Vlvi,** Vrvi, Vrai, Vlci, Vrci, Vsasi, Vsati,Vsari, Vscpi,**Vsvni,** Vpasi, Vpati, Vpari, Vpcpi, Vpvni, **Unveini**	Personalisation parameters: **ELVmax, ELVmin, Rscp, Csat, Rpcp** Pressures: Plv(t), Pla(t), Pra(t), Prv(t), Psas(t), Psar(t),Pscp(t), Psvn(t), Ppas(t),Ppat(t),Ppar(t), Ppcp(t),Ppvn(t) Flows: Qlvo(t), Qlao(t), Qrvo(t), Qrao(t) Qsas(t), Qsat(t), Qsar(t), Qscp(t), Qsvn(t), Qlc(t), Qrc(t), Qpas(t), Qpat(t), Qpar(t), Qpcp(t), Qpvn(t) Volumes: Vla(t), Vlv(t), Vrv(t), Vra(t),Vlc(t), Vrc(t), , Vsas(t) , Vsat(t), , Vsar(t), Vscp(t), Vsvn(t), Vpas(t), Vpat(t), Vpar(t), Vpcp(t), Vsvn(t)	

5.2.2 Optimisation process

The second step of the global personalisation, and the most challenging, is the optimisation process. It consists, in turn, of two main phases: the definition of an objective function and the selection of a suitable algorithm to solve the problem.

5.2.2.1 Definition of the objective function

The objective function is used to evaluate the difference between the model outputs (m) and the clinical data (t). In this project the objective function had to take in account the 9 patient-specific parameter personalisation inputs: stroke volume (SV), ejection fraction (EF), cardiac output (CO), the left-ventricle end systolic blood volume (ESV) and the left ventricle end diastolic blood volume (EDV), measured aortic pressure (P_a (t)) during baseline over one cardiac cycle and the correspondent systolic pressure (P_{SYS}), diastolic pressure (P_{DIA}) and mean arterial pressure (MAP). Among these outputs, there were some dependent ones, which were obtained from the others:

- systolic (P_{SYS}) and diastolic (P_{DIA}) pressures were calculated as the maximum and the minimum pressure of the signal of aortic pressure over one cardiac cycle, obtained as described in paragraph *4.2 Invasive pressure data processing;*
- MAP, estimated as clinical definition (Eq.5.1).
- CO, ESV and EDV are function of SV, EF and HR as described in Eq.5.6, Eq.5.7, and Eq.5.8.

The objective function, fc, was defined as the sum of the normalized root mean square errors for each output as shown in Eq.5.9:

$$fc = \left(\frac{CO_m - CO_t}{CO_t}\right)^2 + \left(\frac{SV_m - SV_t}{SV_t}\right)^2 + \left(\frac{EF_m - EF_t}{EF_t}\right)^2 + \left(\frac{LVES_m - LVES_t}{LVES_t}\right)^2 + \left(\frac{LVO_m - LVO_t}{LVO_t}\right)^2 + \frac{\sum_{i=1}^{N}\left(\frac{Pa_{i,m} - Pa_{i,t}}{MAP_m}\right)^2}{N} + \left(\frac{MAP_m - MAP_t}{MAP_t}\right)^2 + \left(\frac{P_{SYS,m} - P_{SYS,t}}{P_{SYS,t}}\right)^2 + \left(\frac{P_{DIA,m} - P_{DIA,t}}{P_{DIAt}}\right)^2 \quad \text{(Eq.5.9)}$$

where the subscripts m and t indicate the origin of the data respectively from the model outputs and from the clinical data.

The aortic pressure in a cardiac cycle both from the model and the target were considered in terms of fraction of cardiac cycle, where N is the number of fraction-step of the pressure signal. This will be useful in a second step when aiming to introduce the barocontrol system, because, as observed in the sensitivity analysis, changing some parameters can cause also a change in the heart period and it will be difficult to compare the signals of different length.

Moreover, an interpolation was used to up sample or down sample the output from the model and have the same length of the patient data, again to compare them.

The cost function described in Eq.5.9 implicitly contains weights due the relationships between the dependent and independent parameters.

5.2.2.2 Searching algorithm

MATLAB Optimisation Toolbox provides a large number of options and solvers for optimisation problems considering constraints, number of variables, type of objective function, linearity of the problem. These functions require an initial state, which is not easy to define for all the parameters. In case of a solution space with multiple local minimums, the solution is obviously dependent on the initial state.

There are other algorithms that do not require an initial state and they will explore the solution space in order to find the minimum. Even so, these algorithms can produce different solution for the same problem. Examples are the Genetic Algorithm and the Multistart.

Another alternative to these algorithms is the Unscented Kalman Filter (UKF), which belongs to the family of the Kalman Filters. These are used to estimate unknown variables using measurements data over the time for non-linear systems.

In a published study from Lungu *et al*. [164], a combination of algorithms were used in order to overcome the limitations of each of them, with very positive results. In this study a similar

approach was, therefore, applied, using firstly the genetic algorithm to provide an initial guess to the optimisation solver selected.

5.2.2.2.1 Genetic algorithm

The genetic algorithm (GA) is a method for solving optimisation problems using the concept of natural selection: a population of individual solutions is generated at each step and the algorithm selects the best to be parents of the next generations using concepts of selection, mutation and crossover. In this way over generations, the solution evolves toward the optimal. GA creates randomly an initial population. For each step the fitness value for each individual is calculated and the best are selected as parents for the next generation using mutation and crossover factors to combine them. GA requires as input the *objective function* (described in Paragraph 5.*2.2.1 Definition of the objective function*) and the *number of variables* involved in the process. It is possible to define also *lower and upper boundaries* in order to limit the solution space within physiological ranges and therefore the simulation time. Other options can be defined in the GA:

- the function tolerance (TolFun) equal to 10^{-6} by default;
- the population size (PopulationSize) set to 5;
- the number of generations (Generations) set to 20;
- the crossover factor (0.8 by default);

The advantage of the GA is that it is not necessary to supply an initial guess which can be misleading in the condition of multiple local minimum.

A limitation of the use of GA is related with the solutions, which can be different if the simulation runs multiple times, especially in cases of flat solution space. For this reason, the solution of GA can be refined using it as initial guess for a specific solver that aims to identify the minimum.

5.2.2.2.2 *"fminsearch" and "fminsearchbnd"*

MATLAB provides a number of implemented functions designated to minimize problems. One of those is "*fminsearch"*, used for unconstrained non-linear optimisation with multiple parameters. The method used by this specific function is derivative-free and uses the simplex search method of Nelder-Mead, which explores the solution space around the provided initial guess, x_0. Comparing the fitness values between the different points individuated in the space, the algorithm investigates around the initial guess using different approaches: reflection, expansion, contraction outside or inside, or shrink.

The solution of GA was used as initial guess for *"fminsearch"* and the maximum number of iterations was set to 100.

"fminsearchbnd" is a modified version of *"fminsearch"* which includes the possibility to define the boundaries for the parameters to tune and produce a solution within the physiological ranges.

5.2.2.3 Simulation details

Each simulation produced the results for 30 s, necessary time for the model to reach stability from the initial condition provided, and the last complete cardiac cycle was used to compare with the target output values.

The lower and upper boundaries (LB, UB) for the variables were defined considering values from studies published in the literature [155, 156, 165, 166] and are shown in table 5.8.

Table 5.8: Lower and upper boundaries used for the variables. ELV: ml/mmHg; C: ml/mmHg; R: mmHg s/ml.

Variable	*LB*	*UB*
ELV_{MAX}	1	6
ELV_{MIN}	0.01	0.99
C_{SAT}	0.05	2
R_{SCP}	0.1	2.3
R_{PCP}	0.05	1

5.2.2.3.1 Preliminary tuning

Among the general patient data (Paragraph *5.1.1.1 General data*), gender, weight (Wt in kg) and height (Ht in m) were used to calculate the total blood volume (BV) of each patient using Nadler formula [99] (Eq.5.10, Eq.5.11):

$$BV_{MALE}\ (l) = 0.3669\ \cdot Ht^3(m^3) + 0.03219 \cdot Wt\ (kg) + 0.6041 \qquad \text{(Eq.5.10)}$$

$$BV_{FEMALE}\ (l) = 0.351\ \cdot Ht^3(m^3) + 0.03308 \cdot Wt\ (kg) + 0.1833 \qquad \text{(Eq.5.11)}$$

The total blood volume is used to define the distribution of blood volume, V, in all the compartments (Eq.5.12) and the capacitance values, C, (Eq.5.13) using the proportions of the generic model:

$$V_{i,specific} = \frac{V_{tot,specific} \cdot V_{i,generic}}{V_{tot,generic}} \quad for\ i = all\ compartments \qquad \text{(Eq.5.12)}$$

$$C_{i,specific} = \frac{V_{tot,specific} \cdot C_{i,generic}}{V_{tot,generic}} \quad for\ i = SAS, SVN, PAS, PAT, PVN \qquad \text{(Eq.5.13)}$$

where the subscripts *i,specific* and *i,generic* indicate the value of blood volume or capacitance in each compartment respectively for a specific patient and for a generic individual, while the subscripts *tot,specific* and *tot,generic* are referred to the total volume respectively for the specific patient and for the generic individual.

The cardiac output (CO) was used to define the total systemic resistance, in order to redistribute it using the same proportions of the generic model. The total systemic resistance in the generic model, $R_{sys,tot,G}$, was previously calculated as the ratio between the mean arterial pressure (MAP) and the cardiac output (CO) (Eq.5.14).

$$R_{sys,tot,G} = \frac{MAP_G}{CO_G} = \frac{P_{SYS,G} + 2 \cdot P_{DIA,G}}{3 \cdot CO_G} = \frac{107.6 + 2 \cdot 74\ mmHg}{3 \cdot 4.62\ l/min} = 1.107\ mmHg\frac{s}{ml} \qquad \text{(Eq.5.14)}$$

Using the same equation, the total systemic resistance is calculated for each patient (Eq.5.15) and then redistributed among the systemic compartments (Eq.5.16):

$$R_{sys,tot,sp} = \frac{MAP_{sp}}{CO_{sp}} = \frac{P_{SYS,sp} + 2 \cdot P_{DIA,sp}}{3 \cdot CO_{sp}} \quad \text{(Eq.5.15)}$$

$$R_{i,specific} = \frac{R_{tot,specific} \cdot R_{i,generic}}{R_{tot,generic}} \quad for\ i = SAS, SAT, SAR, SVN \quad \text{(Eq.5.16)}$$

The mean arterial pressure, MAP, obtained as a function of the systolic and diastolic pressures (Eq.5.1), is an estimation of the real mean of the pressure signal. This might generate an underestimation of the overall systemic resistance. On the other hand, systolic and diastolic pressures can be non-invasively measured and therefore these definition of MAP increases the number of patients on which the personalisation can be applied, without an invasive pressure measurement.

5.3 RESULTS AND DISCUSSION

5.3.1 Ideal patient: validation of the optimisation process

An ideal patient (male, 180 cm, 80 kg) was considered to validate and test the optimisation with the forward problem, knowing already all the parameters value and the outputs (Chapter 2, *Paragraph 2.1.1 Haemodynamic system*).

The set of input parameters for the optimisation (EF, SV, CO, HR, EDV, ESV, $P_A(t)$, P_{SYS}, P_{DIA}, MAP) were calculated as result of the original values of all the input parameters of the model.

Results of the fitness value of GA and *fminsearchbnd* are reported graphically in figure 5.1. The fitness value obtained with GA reaches its minimum at 0.82 and with *fminsearchbnd* solver it decreases at 0.099. Comparing the pressure curve over a cardiac cycle after the stabilization of the model, it is observed that the solution of *fminsearchbnd* is closer to the original one (Figure 5.2).

Table 5.9 reports the comparison between the model inputs and outputs against the optimisation results of inputs and outputs.

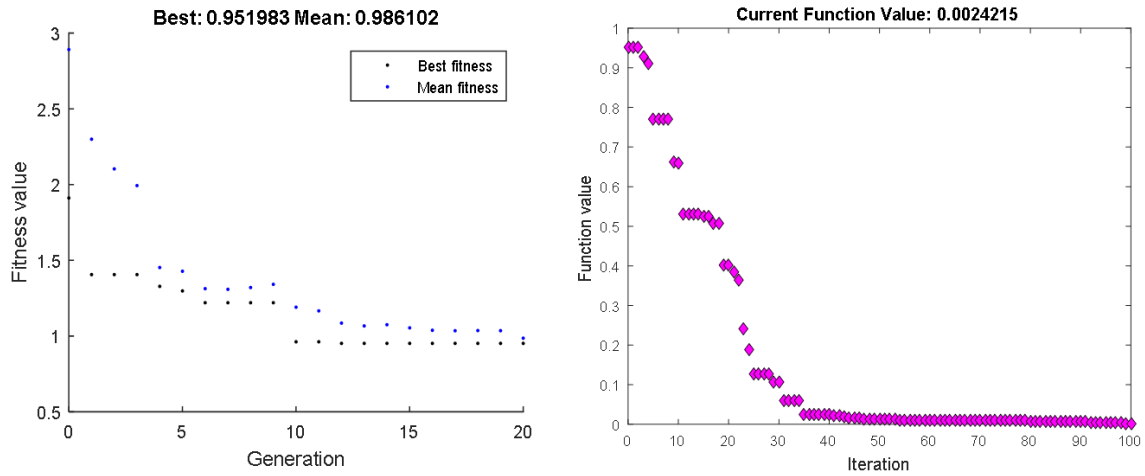

Figure 5.1: Results of the optimisation used for the validation on the ideal patient. Left) Genetic Algorithm fitness values. Right) "*fminsearchbnd*" fitness values.

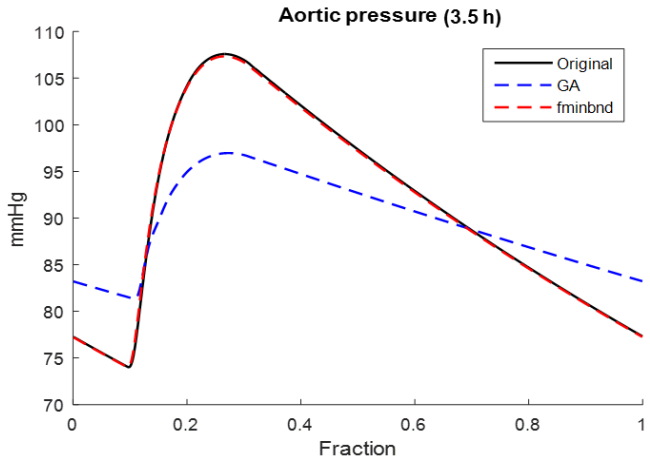

Figure 5.2: Comparison between the original aortic pressure of the ideal patient over one cardiac cycle and the results obtained with GA and then refined with *fminsearchbnd.*
The simulation lasts about 3.5 hours.

Table 5.9: Original values of tuned and target parameters for the ideal patient model were compared with the solution of the optimisation and the error in % was reported.

Parameters	Original value	Optimized value	Error %
R_{PCP}	0.25 [mmHg s/ml]	0.1 [mmHg s/ml]	-59%
R_{SCP}	0.52 [mmHg s/ml]	0.57 [mmHg s/ml]	9.9%
C_{SAT}	1.6 [ml/mmHg]	1.6 [ml/mmHg]	0%
ELV_{MAX}	2.5 [ml/mmHg]	2.5 [ml/mmHg]	0%
ELV_{MIN}	0.1 [ml/mmHg]	0.13 [ml/mmHg]	30%
CO	4.62 [l/min]	4.6 [l/min]	0.51%
SV	71.13 [ml]	70.77 [ml]	0.51%
EF	60%	60%	0%
P_{SYS}	107.6 [mmHg]	107.4 [mmHg]	-0.18%
P_{DIA}	74 [mmHg]	74.1 [mmHg]	0.12%
MAP	85.2 [mmHg]	85.3 [mmHg]	0.12%
HR	65 [beats/min]	65 [beats/min]	0%
ESV	47 [ml]	47 [ml]	0%
EDV	118.15 [ml]	117.73 [ml]	-0.35%

Figure 5.2 suggests that the number of generations and populations of GA are small, and therefore it cannot analyse in detail the solution space. A simulation with 50 populations and 1000 generation was run in order to prove that the GA would find a closest solution when the solution space is better explored. Figure 5.3 shows the comparison between the results with

'original' GA (5 populations - 10 generations) and with a 'wider' GA (50 populations - 1000 generations). As expected, the solution with higher number of population and generation provided the GA solution very close to the original pressure curve. Despite the accurate exploration of the solution space, the simulation time increases about 5.5 times. The optimisation with the 'original' GA lasted about 3.5 hours, while the use of 'wider' GA rose the simulation time to 19.5 hours.

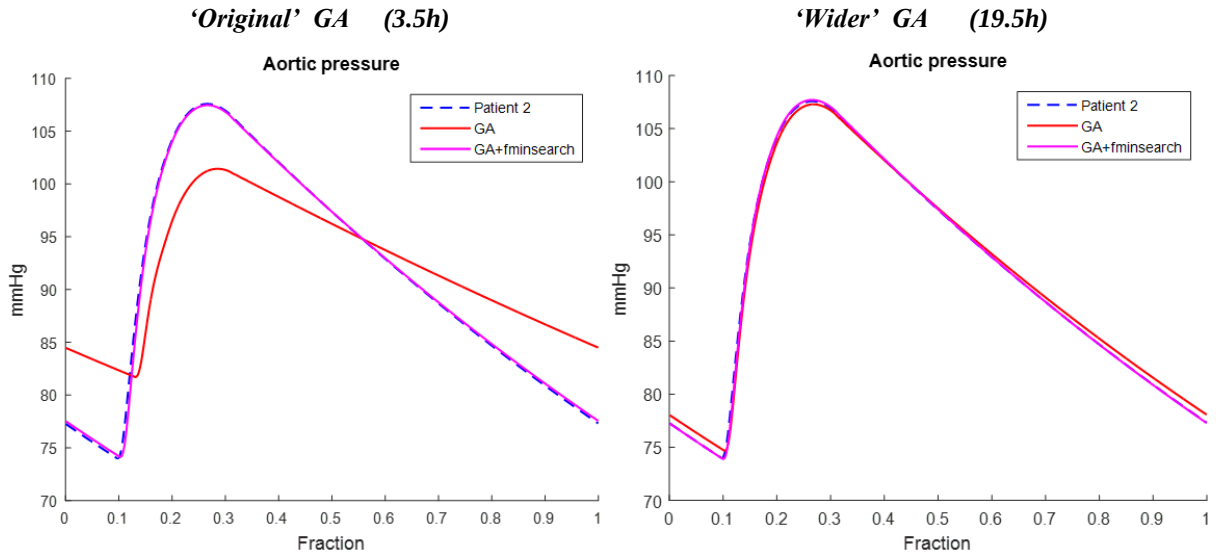

Figure 5.3: Comparison of GA solutions obtained with different number of populations and generations. Left) Optimisation results with 'original' GA (5 populations, 20 generations); Right) Optimisation results with 'wider' GA (50 populations, 1000 generations).

In conclusion, from the results it can be seen that the optimisation process provides a solution close enough to the original one for the ideal patient, with a maximum error of the tuned parameters of -59% regarding the pulmonary capillary resistance, 30% for the ELV_{min} and about 10% for the R_{scp}, while for the target parameters the errors are all close to 0 (Table 5.9). The high error for R_{PCP} is due to its relatively low sensitivity. In figure 2.18 in Chapter 2, its NV values for all the output parameters were reported and they were smaller than the other 4 parameters. A few simulations were run with different value of R_{PCP} to verify how influent it is on the output parameters and results are shown in table 5.10.

Table 5.10: % error measured for each output (CO, SV, EF, P_{SYS}, P_{DIA}, ESV, and EDV) whit different values of R_{PCP}.

R_{PCP} [mmHg s/ml]	CO	SV	EF	P_{SYS}	P_{DIA}	ESV	EDV
0.06	-1.30%	-1.30%	0.04%	-1.45%	-1.71%	-1.39%	-1.33%
0.10	0.48%	0.48%	0.16%	0.19%	-0.05%	0.09%	0.32%
0.15	2.63%	2.63%	0.31%	2.16%	1.74%	1.88%	2.33%
0.20	3.98%	4.69%	0.46%	4.01%	3.56%	3.60%	4.26%
0.40	-0.11%	12.12%	1.04%	10.83%	10.17%	9.80%	11.19%

The high error for the ELV_{min} is contradictory with the sensitivity results obtained in chapter 2. This parameter resulted in a high sensitivity with the regards of the cardiac output and stroke volume and, yet, despite the value 30% higher of what expected, our input data were recovered, suggesting that CO and SV were not sensitive to $ELV_{min.}$ An analysis more detailed of the sensitivity results of chapter 2 showed that for values above the initial value of ELV_{min} the sensitivity for CO and SV was lower, while for values below it, the sensitivity was high. Therefore, the average reported in the results show a high sensitivity for this parameter.

With regards of the systemic capillary resistance, the error of 9.9% between the optimisation results and the original model is due by the underestimation of the total resistances and consequently of the systemic resistances defined as a proportion of the total resistance as described in the paragraph *5.2.2.3.1 Preliminary tuning*. The calculation of the total systemic resistance as in Eq.5.15 and Eq.5.16 considers null the venous pressure. In addition, the mean arterial pressure calculated as in Eq.5.1 is slightly different from the mean value of the pressure signal.

5.3.2 Real patients' cases

The parameter personalisation was then applied to the real patient data, always considering a non-controlled cardiovascular system and the manipulated clinical data for consistency.

The mean fitness value was 0.16 (range: 0.11 - 0.23). Table 5.11 shows the comparison of the model results with the target values in terms of mean, maximum, minimum, median and

standard deviation. Figure 5.4 shows the distribution of the error for each parameter with a Box-and-Whisker plot. The highest mean errors of 2.68% and 1.23 % were obtained respectively by the diastolic pressure (P_{DIA}) and the systolic pressure (P_{SYS}). The reason of some relative high errors in this cohort of 37 patients' simulation for some outputs might be due to the range of the boundaries conditions imposed for all patients. Some parameters values resulted too close to the boundaries extremes, indicating that it was probably necessary a wider range of solutions to explore. To define a wider solution space for each variable it is necessary a study of the relative uncertainty.

Table 5.12 reports the results of the personalised parameters for each patient obtained with the optimisation process. As can be observed, boundaries ranges for some patients were already modified considering the poor result with the previous ones. In blue are highlighted the values obtained with wider boundaries for some parameters. In red are highlighted those which might need to use wider boundaries to improve the tuning reducing the errors. For the R_{PCP}, its small influence compared to the other parameters was also demonstrated in the ideal patient model and, therefore, it might not change the results or the errors were already small.

As an example, figure 5.5 shows the comparison of pressure signal over one cardiac cycle obtained for patient 9 with the GA and the *fminsearchbnd*.

Table 5.11: Results of parameter personalisation using consistent data.
Mean, minimum, maximum, median and standard deviation of the comparison between the clinical data and the results of the optimized model. Cardiac output (CO), stroke volume (SV), ejection fraction (EF), systolic pressure (P_{SYS}), diastolic pressure (P_{DIA}), end diastolic left ventricle volume (ESV), end systolic left ventricle volume (EDV).

	CO	*SV*	*EF*	P_{SYS}	P_{DIA}	*MAP*	*ESV*	*EDV*
Mean	0.34%	0.35%	0.52%	1.23%	2.68%	1.80%	-1.17%	-0.19%
Min	-0.69%	-0.68%	-2.96%	-2.49%	-5.18%	-2.20%	-16.77%	-3.92%
Max	1.73%	1.73%	4.93%	4.28%	15.76%	6.73%	5.90%	3.25%
Median	0.28%	0.31%	0.59%	1.34%	2.21%	1.54%	-0.92%	-0.24%
ST.Dev	0.53%	0.53%	1.23%	1.35%	5.12%	2.36%	3.46%	0.98%

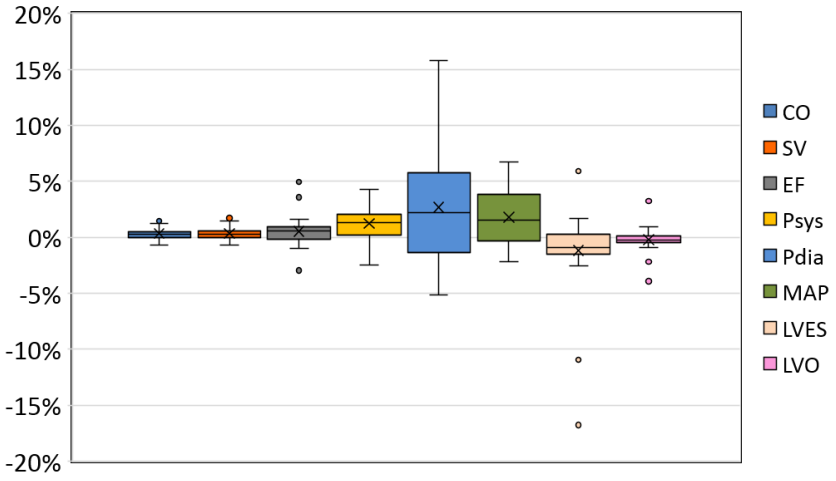

Figure 5.4: Box-and-Whisker distribution of errors between the consistent clinical data and the model results obtained with the parameter personalisation.
The boxes represent the lower and upper quartiles, the error bars represent the range between 1.5 times the first and third interquartile range and the dots outside the boxes represent the extreme outliers, i.e. the data out of the range between 1.5 times the first and the third interquartile range.

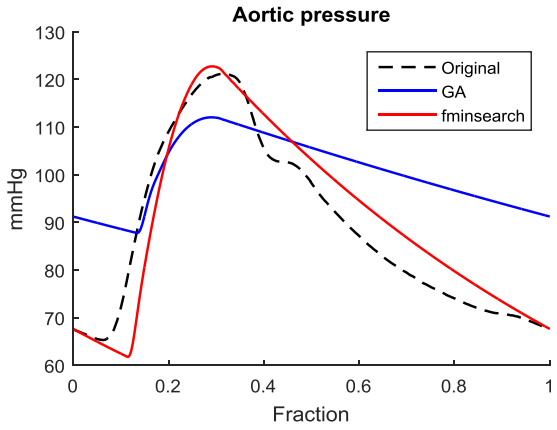

Figure 5.5: Aortic pressure results from optimisation for patient 9.
(Dashed black) Original aortic pressure signal over one cardiac cycle; (blue) aortic pressure result from GA; (red) aortic pressure result of *fminsearchbnd*.

Table 5.12: Results of the personalisation of the model for each patient.
ELV_{MAX} and ELV_{MIN}: ml/mmHg; C_{SAT}: ml/mmHg; R_{SCP} and R_{PCP}: mmHg s/ml. The percentage indicate the errors.

Pat.	*ELV MAX*	*ELV MIN*	C_{SAT}	R_{SCP}	R_{PCP}	*%CO*	*%SV*	*%EF*	*%P_{SYS}*	*%P_{DIA}*	*%MAP*	*%ESV*	*%EDV*
1	5.32	0.11	0.50	0.56	1.13	0.49	0.59	0.93	3.60	4.64	-0.12%	-2.51	-0.34
2	1.58	0.11	0.59	1.17	0.97	0.32	0.30	0.75	2.75	0.07	4.07%	-0.92	-0.45
3	2.09	0.17	1.21	0.77	0.95	0.17	0.17	0.66	0.23	-1.27	1.39%	-1.22	-0.49
4	1.22	0.06	0.93	0.71	0.99	0.04	0.05	0.45	0.88	-3.19	-0.62%	-0.66	-0.41
5	7.00	0.34	0.68	0.91	0.22	1.24	1.20	4.93	4.28	-5.18	-1.33%	-16.7	-3.92
6	2.46	0.03	0.71	0.64	1.00	0.24	0.37	0.82	1.84	5.77	-0.72%	-1.53	-0.46
7	2.76	0.08	0.42	0.88	0.93	0.39	0.39	0.90	2.12	9.70	3.81%	-1.55	-0.52
8	4.39	0.49	0.40	1.17	1.00	0.51	0.62	1.06	2.01	0.87	5.50%	-1.89	-0.44
9	0.71	0.03	0.89	0.67	0.81	-0.06	0.01	-0.34	-0.99	4.79	1.46%	0.49	0.35
10	1.88	0.03	0.86	0.46	0.99	-0.69	-0.68	-0.97	1.62	12.9	2.01%	1.72	0.29
11	2.05	0.17	1.34	0.43	0.18	0.51	0.49	0.76	2.24	-0.99	6.73%	-1.51	-0.28
12	2.15	0.10	1.99	0.29	0.23	0.63	0.64	-0.27	-0.45	2.78	0.55%	1.58	0.91
13	1.77	0.26	1.01	0.59	0.09	0.07	0.07	-0.64	-0.05	2.94	1.27%	1.44	0.71
14	1.56	0.10	0.63	0.66	0.07	-0.49	-0.49	-1.02	0.54	9.72	1.52%	1.40	0.52
15	1.13	0.01	0.99	0.62	0.84	-0.29	-0.29	-0.18	2.19	7.88	4.79%	0.04	-0.10
16	1.95	0.05	1.89	0.39	0.88	0.08	0.11	0.40	2.38	0.87	5.04%	-1.07	-0.29
17	1.96	0.07	1.86	0.61	1.00	0.22	0.22	0.66	1.55	-4.90	1.57%	-1.19	-0.45
18	1.38	0.09	1.93	0.43	0.39	1.23	1.23	0.87	1.45	-2.00	-2.20%	-0.71	0.36
19	2.41	0.16	1.09	0.70	0.41	0.32	0.32	0.52	1.82	1.81	-0.48%	-0.93	-0.20
20	1.86	0.10	0.67	0.71	0.58	0.86	0.86	1.42	2.72	-3.69	1.82%	-1.97	-0.57
21	3.37	0.07	0.92	0.50	0.89	0.02	0.02	-0.05	1.07	5.49	-0.25%	0.19	0.07
22	2.76	0.17	0.39	1.16	0.70	0.15	0.15	0.30	1.22	8.23	3.29%	-0.42	-0.15
23	6.00	0.39	0.81	0.78	0.92	1.47	1.47	3.58	2.02	-1.53	4.54%	-10.9	-2.19
24	2.95	0.03	0.46	0.54	0.64	-0.43	-0.43	-0.27	0.87	15.7	0.07%	0.28	-0.16
25	3.65	0.12	0.49	0.94	0.97	0.48	0.48	0.80	1.09	3.96	6.63%	-1.33	-0.32
26	5.54	0.37	0.29	1.16	0.09	0.84	0.84	0.94	0.63	-0.29	2.53%	-1.44	-0.10
27	1.95	0.03	1.34	0.32	0.44	-0.04	-0.04	0.08	-0.75	0.77	0.22%	-0.25	-0.11
28	1.50	0.11	0.59	0.94	0.06	-0.23	-0.23	-0.55	1.87	7.16	0.02%	0.72	0.31
29	1.42	0.06	1.55	0.38	0.28	0.00	0.00	-0.12	1.15	2.61	4.40%	0.28	0.13
30	3.67	0.18	1.06	0.58	0.56	1.13	1.13	0.95	1.83	-3.01	1.93%	-1.79	0.18
31	1.81	0.19	1.14	0.41	0.14	-0.09	-0.09	-0.18	-0.78	3.77	-0.73%	0.34	0.09
32	1.00	0.08	1.52	0.42	0.24	0.39	0.39	-2.96	1.18	4.91	1.61%	5.90	3.25
33	1.00	0.01	2.00	0.45	0.81	1.73	1.73	1.60	-2.49	-0.22	3.14%	-1.06	0.14
34	3.37	0.16	0.29	0.75	1.00	0.18	0.18	0.47	0.16	10.9	-1.15%	-0.85	-0.29
35	2.80	0.28	0.83	1.09	0.86	0.41	0.41	0.78	3.16	-3.38	4.54%	-1.21	-0.37
36	3.02	0.18	0.51	1.02	0.50	0.43	0.41	1.34	-0.02	5.85	-0.40%	-2.53	-0.94
37	0.55	0.13	2.00	0.58	0.05	0.03	0.03	0.42	1.64	-2.52	2.90%	-0.54	-0.40

5.3.3 Results of aortic adenosine concentrations

The personalised model was run to produce the aortic adenosine concentration specific for each patient. The hypothesis is that different heart rate, pressure and cardiac output might influence the delay and the maximum value of plateau adenosine concentration, and that this might be responsible for the different myocardial responses observed clinically.

For each patient with the personalised model, the maximum aortic concentration and the time to reach plateau were calculated.

The average value of C_{AO} was 3.03 $\cdot 10^{-4}$ mg/ml (SD 7.83$\cdot 10^{-5}$, range: 1.09$\cdot 10^{-4}$ - 4.59 $\cdot 10^{-4}$ mg/ml) and of the time to reach plateau was 56.3 s (SD 8.2). The concentration necessary to reach hyperaemia is not defined in the literature. Measure of the adenosine concentration in vivo is not simple, because of the short half-life. A number of protocols were developed involving *ad hoc* syringes and adenosine blockers [116, 167-169]. Inconsistency was found between the results, caused eventually by the technique or the species involved in the study (dogs, humans, pigs). In particular, Biaggioni *et al*.[167] measured in men the plasma concentration of adenosine in the arterial blood at hyperaemia of 1.1 ± 5 $\cdot 10^{-4}$ mg/ml. Our patient-specific results produced a higher value on average of the maximal aortic concentration, although of the same order of magnitude. Considering the short half-life of the drug also the location from where the sample is taken influences the results.

The protocol of adenosine infusion is designed to allow all individuals to reach hyperaemia: a dose proportional to the body weight of the individual and the duration of the infusion is usually of 90-120 minutes. Results of the time to reach plateau from the patient-specific model suggest that a major component of the response time during adenosine infusion is largely influenced by the systemic cardiovascular system, as already studied also in Chapter 3. This highlight the importance of a global cardiovascular system able to represent the specific individual to study the adenosine response, extremely dependent on it.

From the modelling it can be identified that some patient-specific parameters determine the maximum aortic concentration and the time to reach the maximal hyperaemia. The results suggest that an infusion of 90 seconds is long enough to stimulate the maximum hyperaemia in all patients.

Figure 5.6 shows the relationship with the clinical parameters: HR (A), CO (B), MAP (C), ESV (D) and EDV (E). It is observed that the maximum concentration is directly proportional to CO, ESV and EDV, while less influence is observed for MAP and HR. The time to reach the plateau is on the other hand indirectly proportional to HR and CO, and directly dependent on MAP and EDV.

The correlation coefficients in all the relationships are less than 0.5, with a maximum value of 0.35 between maximum concentration and CO (Panel B-left). This indicates that the correlations are weak.

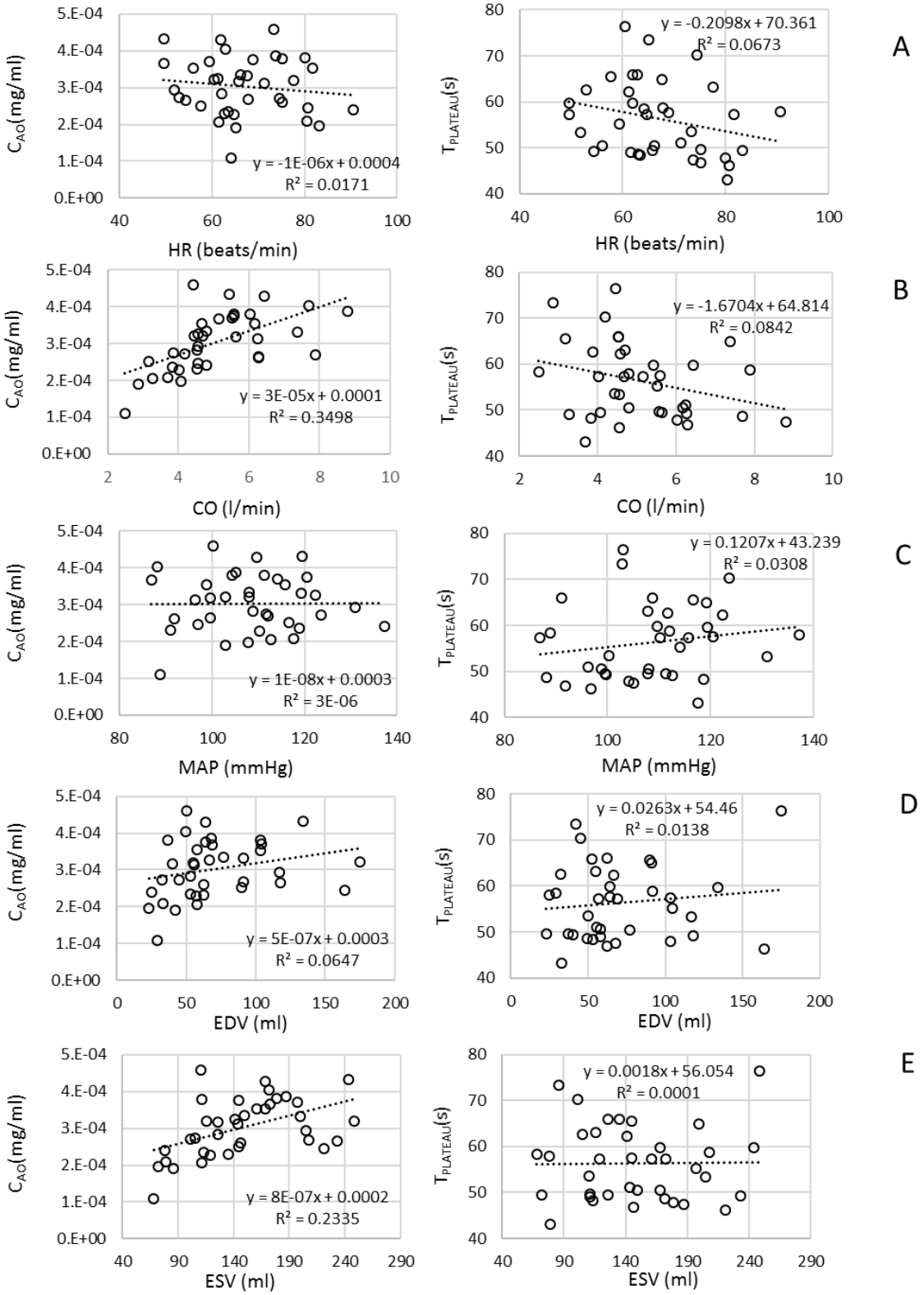

Figure 5.6: C_{AO} and time to plateau for each patient modelled with the personalised model. Panel A) HR (beat/min). Panel B) CO (l/min). Panel C) MAP (mmHg). Panel D) EDV (ml). Panel E) ESV (ml).

5.3.4 Limitations

The major limitation of the model is related to the incomplete representation of the real physiology in the cardiovascular system, such as neglecting the regulation system, limiting therefore the possibility of an accurate prediction and personalisation of the adenosine response.

Secondly in order to simplify the process of personalisation, the cardiovascular model was divided into global and local systems under certain assumptions, which bring furthermore lack of physiological representation.

With regards of the global personalisation, the most important limitation is represented by the clinical data from echocardiography which were not in themselves consistent. Several approximations were considered to bring consistency within the clinical data. It might be arguable the selection of the ejection fraction to define the other parameters, because it is itself calculated from the ratio of the left-ventricular volume, which were not considered. Another possibility would be to consider the measured EDV and calculate the other parameters, although it may happen that the stroke volume is equivalent or higher than the EDV and, therefore, non-physiological ejection fractions could be obtained.

Moreover, the inconsistency of the patients' data is also produced by the non-simultaneous measurements of echocardiographic data and invasive baseline pressures.

The coronary circulation was considered equal for everyone, since the focus in this chapter was on the global model.

Other limitations are related to the simulation time. As shown in the results, some cases produced high errors in the comparison the target values and the model results. This can be caused by the boundaries conditions, which may need to be wider for some cases, or by the number of populations and generations used for the GA and the number of iterations for *fminsearchbnd*. An increase of these parameters will certainly increase the possible

combinations of values and determine a better solution. These parameters were limited to a certain value respectively in order to obtain results for each case in about 3.5 hours in a normal office desktop.

With regards to the pharmacokinetic model of the adenosine, the assumption of an instantaneous distribution of the drug in each compartment represents an important limitation for the representation of the real physiological phenomenon. The assumption of a null adenosine concentration before the start of injection is another limitation of the model, given by the lack of measurement of this parameter. The subdivision in compartments and such small half-life of the drug produces plateaus of concentration in each compartment towards different values, while physiologically a homogenous concentration in the blood after a certain time elapse is expected.

With regards to the maximal adenosine concentration, literature data do not provide information of what adenosine concentration is necessary to generate hyperaemia and therefore it is difficult to validate the model results.

5.4 CONCLUSIONS

The patient-specific model developed in this project allowed to represent baseline conditions of patients, aiming to reproduce the aortic pressure and the echocardiographic data measured during baseline/rest.

The personalised model suggests that each patient shows a different maximum of aortic adenosine concentration and it is mainly dependent on the HR, CO and EDV. Therefore, when investigating the response to adenosine, it is important to have an associated systemic cardiovascular system representing the specific patient and his/her adenosine infusion transient profile in the systemic circulation.

The time to reach plateau has also been analysed, considering that this might be an important parameter in the protocol of administration of adenosine to reach maximal hyperaemia. It is mainly dependent on the HR and shows a range of values between 45 and 90 s.

The model results suggested that the adenosine infusion protocol should provide a time of infusion long enough to reach maximal hyperaemia in all individuals, although it is difficult to conclude if also the maximal concentration is sufficient to generate the maximal hyperaemia in all the patients.

The main outcome of this part of project is the concentration of adenosine in the aorta which is used as input in the local coronary model of the specific patient, as shown in the next chapter.

As future work, the patient-specific model needs to be improved in terms of the barocontrol parameters, which requires a higher number of measurements to set a parameter personalisation process with a higher number of variables to personalise.

The optimisation process requires quite long time to run and therefore an improvement in the code is necessary to bring the model into clinical usage.

CHAPTER 6

LOCAL TUNING OF CORONARY BRANCHES

INTRODUCTION AND PURPOSE

Personalising the local coronary circulation is the aim of this part of the project. The main objective is to define the relationship between the myocardium resistance and the adenosine concentration in the myocardium to classify the different adenosine responses in each patient. As discussed in chapter 4 patients were classified based on the pressure trend and the P_d/P_a ratio, as shown also in other studies published in the literature [120, 144].

In this chapter the aims are to define for each patient the parameters that better describe the myocardial vasodilation and the adenosine distribution and to classify patients based on these parameters. This requires a description of the myocardial blood volume and its change during adenosine vasodilation, in order to describe the distribution of the drug within the compartment. The blood volume change is estimated using a tree structure to describe the myocardium and its vasodilation during hyperaemia.

The patient - specific condition in terms of the demographic information and the comorbidities are also investigated in order to find any relationship with the adenosine response, focusing on those factors which are expected to have the strongest influence on the myocardium properties.

6.1 MODELLING LOCAL CIRCULATION: INPUTS AND OUTPUTS

The adenosine response of the local coronary circulation is studied in isolation, taking as an inlet condition the computed adenosine concentration in the aorta, to identify the relationship between the myocardial resistance and the adenosine concentration.

6.1.1 Hypotheses

6.1.1.1 Model of the coronary branches

The coronary branch was modelled as 2 resistances in series (Figure 6.1): R_{STEN} representing the stenosis and R_{myo} for the myocardial microcirculation. The difference between aortic pressure (P_a) and distal pressure (P_d) represents the pressure gradient across the lesion and determine the blood flow through the branch. The pressure downstream of the myocardial resistance, corresponding to the peripheral venous pressure (2-8 mmHg [10, 105]) could have been taken from the personalised global model, but since its value is small compared to the proximal and distal pressure, it is was assumed to be null.

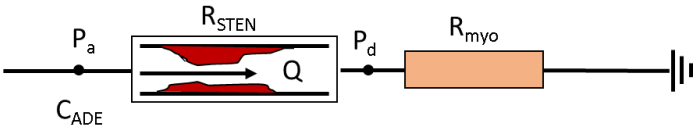

Figure 6.1: Model of local coronary circulation.
P_a and P_d are the pressures measured during angiogram, the stenosis and the myocardium are represented by resistances (R_{STEN} and R_{myo}), C is the myocardial compliance, C_{ADE} is the adenosine concentration, Q is the blood flow through the vessel.

A number of inputs to solve the model are listed below:

1. Patient-specific proximal and distal pressures as function of time, $P_a(t)$ and $P_d(t)$;
2. Aortic adenosine concentration, $C_{AO}(t)$, calculated within the global circulation (Chapter 5);
3. a simplified pressure-flow relationship for the specific stenosis, based on a quadratic fit to a pair of computational fluid dynamics analysis. The convective acceleration term might be

expected to be quadratic, as expressed by the Bernoulli equation whilst that associated with the viscous losses might be linear;

4. patient-specific body surface area (BSA) index, based on gender, height and weight used to estimate the myocardial blood volume.

The solution of this model for each lesion produced a time-series signal for the following:

1. the myocardial resistance, $R_{myo}(t)$, from which values at baseline and hyperaemia ($R_{myo,B}$ $R_{myo,H}$) were extracted considering the results of the algorithm presented in Chapter 4;
2. blood flow, Q(t);
3. myocardial blood volume, MBV(t);
4. myocardial adenosine concentration, $C_{myo}(t)$.

The main assumption considered for the local personalisation has already been discussed in Chapter 3. This consists of the consideration of a high influence of the global model on the local, but not vice versa. From the patient specific global model obtained in Chapter 5, the time-dependent aortic concentration of the adenosine was calculated and applied as input to the coronary branch to estimate the concentration of adenosine in the myocardium.

6.2 Haemodynamic inputs: pressure gradient and aortic concentration of adenosine

The pressure signals were smoothed in order to represent the average pressures, eliminating the variation during each single cardiac cycle. The pressure gradient for each lesion was smoothed with a window size of 5 seconds.

Following this preliminary signal processing, in some lesions the pressure drop across the lesion was negative, especially when there was only a small gradient. Measurements errors of the pressures might have been caused by an imprecise calibration of the pressure catheters or movements of the patient during the procedure.

To overcome this, the pressure gradient signals that contained a negative value were shifted upwards so that the temporal minimum of the signal is 1 mmHg. This is an arbitrary threshold but since it affects primarily only very mild lesions, for which the processing chain is in any case not well-suited, it is considered to be an acceptable process. It allowed the processing of data from lesions that had low gradients at rest but became significant under hyperaemic conditions. Some testing was performed to demonstrate that the selection of this particular threshold did not strongly affect the final results of the processing relative to the selection of a lower threshold. An example is reported in Figure 6.2.

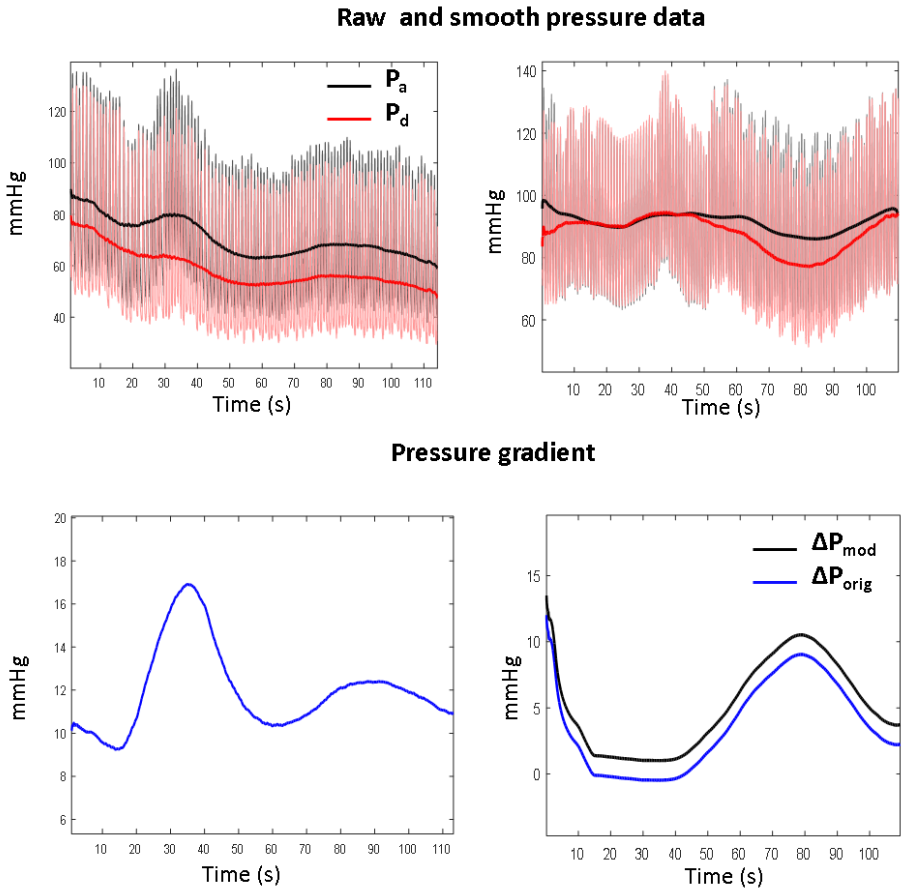

Figure 6.2: Examples of the post-processing results of the raw pressure data to obtain the pressure gradient across the lesion.
The example on the left is relative to a normal case without negative pressure gradients; the example on the right presented negative pressure gradient (ΔP_{orig}) and the signal was shifted on the y-axis (ΔP_{mod}). The top graphs show the raw proximal (P_a) and distal (P_d) pressure and the smooth pressure of proximal and distal pressure; the bottom graphs report the smoothed pressure gradient (on the right both original and modified signals).

The aortic concentration of adenosine obtained with the personalised global model was smoothed with a window of 2 s in order to eliminate the cardiac cycle variation, due to the approximation of instant homogenous mixing in each compartment.

6.2.1 Haemodynamic outputs: blood flow and myocardial resistance

The calculation of blood flow and myocardial resistance required the definition of the stenosis resistance, which is nonlinear and taken to have a quadratic and a linear component. The steady state pressure gradient across the stenosis as a function of flow is determined by a quadratic equation as reported in Eq.6.1.

$$\Delta P(t) = Z_1 \cdot Q + Z_2 \cdot (Q(t))^2 \qquad \text{(Eq.6.1)}$$

The coefficients Z_1 and Z_2 were computed based on the analysis of a pair of steady state 3D computational fluid dynamics (CFD) analyses for each patient-specific lesion. This was performed as part of a previous PhD project carried out by Dr. Paul Morris [92] in the Mathematical Modelling in Medicine Group at the University of Sheffield. The current project used the computed linear and nonlinear coefficients: further details on the method of computation are presented in the Appendix. Given the measured pressure gradient, ΔP(t), and the characteristic parameters for each lesion it was possible to evaluate the blood flow (Eq.6.2):

$$Q(t) = \frac{-Z_1 + \sqrt{Z_1^2 + 4 \cdot Z_2 \cdot \Delta P(t)}}{2 \cdot Z_2} \qquad \text{(Eq.6.2)}$$

And, assuming the myocardial resistance linear, it can be determined from Eq.6.3:

$$R_\mu(t) = \frac{P_d(t)}{Q(t)} \qquad \text{(Eq.6.3)}$$

It is recognised that this process for computation of flow, and therefore of myocardial resistance, is only robust when there is confidence in the measured pressure gradients. For very

mild lesions the pressure gradient measurements are unlikely to be sufficiently accurate, especially at baseline, to support a reliable estimate of myocardial resistance.

6.2.1.1 Myocardial resistance at baseline and at hyperaemia

The myocardial resistance at baseline ($R_{myo,BL}$) was obtained as the average value of the computed myocardial resistance during the 5 s before the adenosine infusion starts.

The myocardial resistance at hyperaemia ($R_{myo,HY}$) was considered as the myocardial resistance corresponding to the period of stable hyperaemia, described in Chapter 4.

6.2.2 Myocardial blood volume as function of myocardial resistance

The main challenge in this part of the project was related with the definition of the myocardial volume in time (MBV(t)) during the vasodilation to define the concentration of the adenosine in the myocardium as described in the next paragraph.

The myocardium has been object of studies for many years. Nevertheless, the quantification of the myocardial blood volume is still a challenging task, despite the extensive information available on myocardial blood flow, which has been largely studied using different techniques such as Doppler or contrast echocardiography, cardiovascular magnetic resonance (CMR), Positron Emission Tomography (PET), Single Photon Emission Computed Tomography (SPECT), Computed Tomography (CT), Thermodilution [170-179].

Experimental data on myocardial blood volume were mostly associated with invasive studies on animals [174, 180-184]. Other, less invasive, studies were conducted on patients or healthy volunteers, including some type of stimulation of the cardiovascular system to observe the response of the blood volume in the myocardium [175, 176, 185-188].

Several studies [181-183] identified the intracoronary blood volume as a function of myocardial blood flow and perfusion pressure in canine hearts. Myocardial blood volume is

usually reported as a volume per unit mass of myocardium, typically ml/100gr to normalise for heart size. The intracoronary blood volume varies between 7 to 20 ml\100gr with a respective perfusion pressure from 50 to 180 mmHg. Other experimental studies on dogs [174, 180, 184] demonstrated that the myocardial blood volume is also function of the myocardial oxygen consumption, the severity of stenosis in the coronary arteries, the specific coronary vessel and the condition (resting or hyperaemia). Reported values of the total blood volume in the coronary circulation in humans are within a range of 11 to 17.5 ml/100 gr of myocardium. Further studies on animals and humans [180, 187] demonstrated that the hyperaemic stimulus increased the myocardial blood flow due to the vasodilation, but the myocardial blood volume did not change substantially.

Experimental studies on dogs carried from Crystal *et al.* [180] studied the effect of adenosine on coronary open-capillary density. The estimated blood volumes in epicardial, middle and endocardial region of the ventricle wall were all about 4-5 ml/100g each and they were not influenced by the adenosine effect. On the other hand, the myocardial blood flow increased massively with the adenosine infusion.

Other studies on patients aimed to measure the myocardial blood volume. Indermühle *et al.* [187] studied the change of myocardial blood volume before and after angioplasty on 30 patients using contrast ultrasound. The blood volume increased after the angioplasty in the majority of the patients on average from 6.7 to 9.8 ml/100 gr.

Values of myocardial blood volume measured post mortem varied from 1.6 to 9.4 ml/100 gr of myocardium [105].

Other research groups worked on the modelling of the myocardium [109, 189, 190]. Briunsma *et al*. [189] employed 0D models (RCR) to represent the coronary circulation in the left ventricular wall divided into 8 layers from endocardium to the epicardium. The blood volume in the myocardium, proportional to the dimension of the vessels, was set to 9.4 ml/100gr LV

and it was proportionally distributed into the arteriolar, capillary and venular compartments for each of the 8 layers. The model simulates prolonged systole and diastole and evaluates the blood volume in each compartments of coronary circulation. In the prolonged systole, in veins and arteries the volumes reduced to zero, while in capillaries stayed almost stable to 4 ml/100gr LV.

The research group of J.Spaan and N. Smith [109, 190, 191] worked on the 3D reconstruction of coronary circulation of animals hearts using the cryomicrotome technique. This supports the study of the perfusion profile of a specific coronary circulation.

Other studies were conducted to invasively identify the level of vasodilation of the small arteries and arterioles in the myocardium under effect of adenosine infusion. The majority of the experiments were conducted in ex-vivo animals' hearts.

In 1989 Kanatsuka *et al.* [142] studied the vasodilatory effects on anesthetised dogs hearts. Adenosine acts on coronary vessels with diameter smaller than 150 μm. The study shows that, for higher doses, vessels with diameter of about 50 μm vasodilated by 55%, whilst vessels with diameter smaller than 150 μm vasodilated by 20-30 %. The change of diameter was dependent on the adenosine dose and on the initial vessel diameter itself, as demonstrated also by Yada *et al.* [169] in vessel with diameter between 100 μm and 40 μm.

Chilian *et al.* [140] measured a change in diameter of 30-40 % for vessels between 50 and 80 μm in dogs hearts. Hein *et al.* [192, 193] studied in ex-vivo pig coronary arterioles the adenosine induced-vasodilation associated with the arterial endothelium. Results showed a vasodilation dependent on the dose of adenosine and on the basal tone and in the control samples a change in diameter of 45 % in vessels of 85 μm diameter was observed.

According to Feliciano *et al.* [194] the vasodilatory response to adenosine involves different arterial compartments. Physiologically, when the myocardial oxygen demand increases, adenosine is released and its targets are primarily the small coronary arterioles with diameter

smaller than 100 μm. In particular, arterioles with diameter between 25-45 μm are dilated first, in a second phase arterioles with diameter between 50 and 80 μm are vasodilated due to metabolic and myogenic reaction. As consequence, arterioles (80-150 μm) and small arteries (140-400 μm) vasodilate as well since their endothelium responds to change in blood flow.

Cornelissen *et al.* [80, 81] developed a model for the coronary circulation (vessels with diameter between 20 and 400 μm), described by 10 compartments in series. An optimisation process was used to define a compartment-specific parameter as a function of the number and diameter of vessels, pressure, blood viscosity and vessel tone. They attempted to describe the coronary vasodilation in terms of myogenic, flow-induced and metabolic components, all combined together. Some discrepancy arose when comparing the model results with the experimental results, due to the approximations made on the vessel tone. Moreover, the coronary reserve of the model reached a value of 2, while in human is about 3-4.

In summary there are conflicting statements in the literature with regard to whether changes in myocardial blood volume are significant. Several papers provide measures of the dilation as a function of the diameter of the vessel, supporting the assumption that the volume does change, whilst others report that the volume changes are not significant.

For the purpose of this project the strategy is to employ a tree-structure model in which radius changes can be applied to each generation, according to the literature consensus, and to use an optimisation process to define the patient specific tree parameters that are consistent with the change of myocardial resistance. The personalised tree model was used to estimate the variation of myocardial blood volume during the hyperaemic response according to the variation of the myocardial resistance to estimate the myocardial adenosine concentration during hyperaemia.

6.2.2.1 Myocardium modelled as a tree-structure

A tree-like structure was developed to represent the circulation from a coronary artery to the capillaries of its perfused area (Figure 6.3).

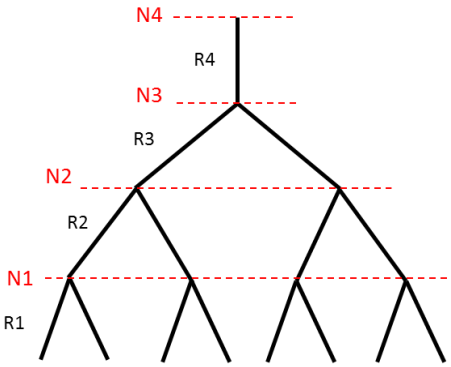

Figure 6.3: Tree-structure example with 4 generations.

A number of assumptions were made:

- each parent vessel divides into 2 symmetric daughter vessels;
- the starting radius for each specific vessel was obtained from the geometries obtained from the segmentation and 3D reconstruction used for the CFD simulation. When this data was unavailable, a starting radius of 2 mm [195] was considered.
- the minimum possible radius at the end of the tree-structure, corresponding to the capillaries, is 2.5 μm [4]
- length (l_d) and radius (r_d) of daughter vessels were defined on the radius of the parent vessel (r_p) as in Eq.6.4 and in Eq.6.5 [196, 197]:

$$r_d = \alpha \cdot r_p \quad \text{(Eq.6.4)}$$

$$l_d = \beta \cdot r_d \quad \text{(Eq.6.5)}$$

- a third parameter, γ, was introduced to represent the vasodilation as the change in radius for the target vessel of the metabolic vasodilation induced by adenosine as described in Eq.6.6:

$$r_{vaso} = \gamma \cdot r_{base} \quad \text{(Eq.6.6)}$$

where r_{vaso} is the radius at hyperaemia and r_{base} is the radius at baseline condition.

The target vessels for particular processes were chosen based on the literature data. Arterioles and small arteries, in the radius range 10 μm and 200 μm, were the target of metabolic vasodilation.

- the total resistance (Eq.6.7) was calculated solving the parallel and series parallel and series of vessels resistances, each of which is described by Poiseuille's formula.

$$R_{TOT} = \sum_{N=1}^{Nmax} \frac{1}{2^{N-1}} \cdot \left(\frac{8 \cdot \mu \cdot l_N}{\pi \cdot r_N^4} \right) \quad \text{(Eq.6.7)}$$

where l_N is the length of the vessel in the Nth generation, r_N is the radius of the Nth generation, μ is the blood viscosity ($3.5 \cdot 10^{-3}$ Pa·s), N_{max} is the last generation with smallest radius. This particular assumption does not allow to represent wave propagation and reflection effects in the coronary model. In this project the clinical data do not support the possibility to represent these phenomena and moreover the pressure data are considered averaged over the cardiac cycles and is out of the purpose of this project to represent the elasticity of these vessels and how this might affect the pressure and curve curves.

- the total volume was calculated by the sum of the volume of each vessel.

6.2.2.2 Optimisation for the tree-structure myocardial model

The optimisation aims to define the best combination of these 3 parameters: α, β and γ to reproduce the baseline resistance, $R_{myo,BL}$, and the hyperaemic (or minimum) resistance, $R_{myo,HY}$, measured for each patient as described above, and an estimate of the patient-specific blood volume, obtained as follows:

1. V_B (Eq.6.8) was computed as a function of the gender-dependent mass of the left ventricle indexed by the BSA (Body Surface Area index - Eq.6.9) and the density of blood volume per gram of tissue (9 ml/100 gr LV [105]):

$$V_B(ml) = \begin{cases} BSA(m^2) \cdot 73(\frac{gr}{m^2}) \cdot 0.09 \frac{ml}{gr\ LV} & if\ male \\ BSA(m^2) \cdot 63(\frac{gr}{m^2}) \cdot 0.09 \frac{ml}{gr\ LV} & if\ female \end{cases} \quad \text{(Eq.6.8)}$$

$$BSA\ (m^2) = \sqrt{\frac{ht\ (cm) \cdot wt(kg)}{3600}} \quad \text{(Eq.6.9)}$$

2. $R_{myo,HY}$ is obtained as described in the previous paragraph about the haemodynamic outputs in this current chapter (*Paragraph* 6.*2.1.1 Myocardial resistance at baseline and at hyperaemia).*

The objective function for the optimisation process takes in account the tree targets as described in Eq.6.10:

$$fc = \left(\frac{R_{myo,BL,m} - R_{myo,BL,t}}{R_{myo,BL,t}}\right)^2 + \left(\frac{V_{B,m} - V_{B,t}}{V_{B,t}}\right)^2 + \left(\frac{R_{myo,HY,m} - R_{myo,HY,t}}{R_{myo,HY,t}}\right)^2 \quad \text{(Eq.6.10)}$$

where m indicates the model results and t the target.

The optimisation was performed in MATLAB using *fminsearch* with boundaries for α, β and γ respectively of 0.6-0.9, 20-70, 1-1.8 [197, 198], and an initial solution for each parameter equal to 0.76, 52 and 1.2 respectively. The number of iterations was set to 5000, with default tolerance value which will automatically stop the simulation when it converges.

For a generic myocardium with starting radius of 2 mm, a volume of 13 ml and an overall resistance at baseline $R_{myo,BL}$ of 72 mmHg s/ml, obtained from a physiological pressure gradient of 80 mmHg between the main artery and the capillaries and a blood flow of 1.1 ml/s, and imposing the range of vasodilation target vessel published in literature (radii between 10 to 200 μm), for the generic model a vasodilation factor, γ, was computed that was out of the reported physiological range over 50%. Physiological ranges of vasodilation changes were obtained considering then a wider range between 7 and 200 μm and this range was used for all the patients' studies.

6.2.2.3 Relationship between myocardial resistance and myocardial volume

The myocardial blood volume and the myocardial resistance were considered to be related by a factor, $C_{BL\text{-}HY}$, which describes the proportion of variation of resistance and variation of volume between baseline and peak/stable hyperaemia as shown in Eq.6.11:

$$C_{BL-HY} = -\frac{\left(\frac{R_{myo,BL} - R_{myo,HY}}{R_{myo,BL}}\right)}{\left(\frac{V_{HY} - V_B}{V_B}\right)} \quad \text{(Eq.6.11)}$$

where the hyperaemic volume was computed from the personalised parameters in the tree model and the baseline volume and resistances are the inputs to the personalisation process.

Two coefficients $C_{BL\text{-}HY}$ were calculated considering the generic test model results and the results obtained with stable resistance and stable blood volume.

Substituting the value of stable myocardial resistance and blood volume with the respective values at the same instant of time, as expressed by Eq.6.12, the relationship between the myocardial resistance and the myocardial blood volume at each instant in time is obtained as in Eq.6.13:

$$C_{BL-HY} = -\frac{\left(\frac{R_{myo,BL} - R_{myo}(t)}{R_{myo,BL}}\right)}{\left(\frac{V(t) - V_{BL}}{V_{BL}}\right)} \quad \text{(Eq.6.12)}$$

$$V(t) = V_{BL} * \left(1 + \frac{\left(\frac{R_{myo,BL} - R_{myo}(t)}{R_{myo,BL}}\right)}{C_{BL-HY}}\right) \quad \text{(Eq.6.13)}$$

6.2.3 Myocardial pharmacokinetics

Under the hypothesis of an instant homogeneous mixing and an instantaneous constant myocardial blood volume, the concentration of adenosine within the myocardium (C_{myo}) was calculated with the mass balance (Eq.6.14), which is the same as the other compartments as explained in Chapter 2 (Paragraph *2.1.4 Adenosine pharmacodynamics and pharmacokinetic model):*

$$V_{myo}\frac{d(C_{myo})}{dt} = Q_{in}\cdot C_{SAS} - (Q_{out}+Q_{EL})\cdot C_{myo} \quad \text{(Eq.6.14)}$$

where C_{SAS} is the concentration in the aorta, Q_{in} and Q_{out} are respectively the input and output flow in the branch, Q_{EL} represents the amount of drug metabolized by the vessels (clearance) V_{myo} is the volume in the myocardium.

By definition, Q_{EL} is a function of the drug half-life time (thl) and the volume of blood in the myocardium (Eq.6.15).

$$Q_{EL} = \frac{V_{myo}\cdot \ln 2}{thl} \quad \text{(Eq.6.15)}$$

The half-life of the adenosine was considered equal to 7 seconds, as in the global model (Chapter 2- Paragraph *2.1.4 Adenosine pharmacokinetic and pharmacodynamics*).

The 1st order derivative equation for the C_{myo} (Eq.6.14) was solved using the Euler backward differentiation method, as indicated in Eq.6.16:

$$C_{myo,i} = \frac{V_{myo,i}\cdot C_{myo,i-1} + \Delta t\cdot Q_i\cdot C_{SAS,i}}{V_{myo,i} + \Delta t\cdot (Q_i + Q_{EL,i})} \quad \text{(Eq.6.16)}$$

6.2.4 Statistical analysis

Paired T-test analysis was performed to correlate the targets and the optimisation results in terms of myocardial resistance and myocardial blood volume. In particular, the results with peak and stable hyperaemic myocardial resistance were compared. Results are presented using linear correlation and Bland-Altman plots.

Results of α, β and γ are reported in terms of average value and standard deviation and graphically with Whisker plots.

6.3 CLASSIFICATION OF ADENOSINE RESPONSE

6.3.1 Classification based on the myocardial resistance trends

Using the characteristics of the stenosis, Z_1 and Z_2, and the pressure gradient at baseline, peak and stable hyperaemia, obtained from the measured pressure signals using the algorithm described in chapter 4, the corresponding values of the myocardial resistance during the response to adenosine infusion was computed, solving the equations reported in Eq.6.2 and Eq.6.3. The absolute and percentage changes in myocardial resistance under the infusion of adenosine were identified. The aim was to classify the patients' response, ultimately to determine whether the hyperaemic pressure gradient can be predicted reliably from baseline measurements given the broader information in the patient record. The lesions were also divided into four groups based on the location (LAD, DX together, RCA, LCX and LMS) to explore whether the response might be artery-dependent.

A common method for distributing total resistance at the terminations of multiple branches in a 1D or 3D arterial tree is to use Moore's Law [199], recognising that the distal resistance at any one branch is likely to be related to the radius of that branch (in the healthy state). To support the testing of this hypothesis in this cohort the outlet radius (r_{out}) for each vessel was extracted from the 3D volume mesh.

It was reported in recent studies [200, 201] that, for severe stenosis, the myocardial resistance at baseline tends to be lower because of an adaptation of the body to maintain the same myocardial blood flow. In this case the vasodilatory ability of the myocardial resistance is partially impaired or limited. This hypothesis was also tested in the current cohort by plotting the myocardial resistances at baseline and stable hyperaemia against the FFR reported in the Cathlab (FFR_{CL}) and the stable hyperaemia FFR (FFR_{HY}) and against the Z_2, as indicators of

the stenosis severity. Moreover, patients' characteristics were also considered in order to identify possible influence of gender, age, BMI, smoking status, myocardial infarction event.

For this type of classification, 81 lesions were taken in account.

Statistical analysis (un-paired T-test and One–way ANOVA) was performed within GraphPad Prism (GraphPad Software, La Jolla California USA).

6.3.2 Classification on the relationship between adenosine concentration and myocardial resistance

The analyses discussed in the previous section are concerned with the identification of key features of the adenosine response, but do not examine the dynamic nature of the response.

The measurements in the study cohort support the analysis of this dynamic, using the local model of the coronary branch to produce time series results for the myocardial resistance (R_{myo}) and the adenosine concentration (C_{myo}).

In this paragraph the focus is the influence of the myocardial parameters on the adenosine response observed effectively in the myocardium itself. From the previous modelling results (Chapter 3 and Chapter 5) it is evident that the systemic circulation is the major driver of the maximal concentration and time response in the myocardium. So hypothesising the same aortic concentration profile, the aim was to understand how the stenosis and the myocardial properties impact on the myocardial response. For this it was necessary to isolate the systemic and the global influence on the signal of the myocardial resistance and adenosine concentration obtained from the local tuning model.

FFR at stable hyperaemia (FFR_{HY}), myocardial resistance at baseline ($R_{myo,BL}$) and hyperaemia ($R_{myo,HY}$) were analysed to seek associations with:

- values of the maximal adenosine concentrations in the aorta ($C_{AO,max}$) and in the myocardium ($C_{myo,max}$);

- the difference between $C_{AO,max}$ and $C_{myo,max}$ as absolute and percentage values;
- the difference between the respective time to reach the plateau for the maximal concentrations.

The delay of the myocardium response is caused by the intrinsic delay in the aortic concentration and it might be also caused by the delay in the myocardial reaction to vasodilation associated with a certain value of myocardial concentration.

6.4 RESULTS AND DISCUSSION

6.4.1 Classification based on the myocardial resistance trends

The available data from the previous study using CFD analysis to define the patient specific stenosis characteristics supports the analysis of 81 lesions in total to classify patients based on the myocardial resistance as absolute value and percentage in change.

6.4.1.1 Patients demographic and lesions' characteristics

In total 81 lesions (62 patients) were considered for this analysis and the demographic description is shown in table 6.1.

5 lesions were located in the diagonal (DX), 47 in the left anterior descendent (LAD), 2 in the left main stem (LMS), 15 in the coronary artery (RCA) and 12 in the left circumflex (LCX).

Table 6.1: Demographic data and comorbidities of the sub-cohort (62 patients) used for the classification of adenosine response based on the myocardial resistance change.
Peripheral Vascular Disease (PVD), Chronic Obstructive Pulmonary Disease (COPD), myocardial infarction (MI).

Patient demographic		**Num% - mean (SD)**
Male		70%
Age (years)		61.8 (SD 9.4)
BMI		28.7 (SD 3.9)
Hypertension		51.7 %
PVD		1.6 %
Previous MI		38.7 %
Type II diabetes		22.6 %
Hyperlipidaemia		59.7 %
COPD		0 %
Smoking status:	*Never*	25.8%
	Ex-smoker	46.7 %
	Current	12.9 %

The average P_d/P_a measured in the Cathlab during baseline is 0.84 (SD 0.15) and the average FFR is 0.72 (SD 0.15).

The lesions were selected with the criteria of a value of P_d/P_a reported in the Cathlab below 0.95. The CFD process developed by Morris [92] based on the quadratic equation between pressure gradient and flow (Eq.6.1) provides reliable characteristics, and therefore distal resistances, for severe stenosis, although it is not reliable for mild stenosis, due to the movement of wires or imperfect calibration during the angiogram. The threshold of a baseline P_d/P_a of 0.95 was arbitrarily chosen. An additional criterion for the selection of the lesions, was the pressure gradient measured at baseline above 4 mmHg. In some cases, the pressure gradient across the stenosis resulted very small (below 1 mmHg or even negative).

Figure 6.4 shows the distribution of the coefficients Z_1 and Z_2, which have respectively an average value of $1.53*10^9$ (SD $2.58*10^9$) Pa s m^{-3} and $1.64*10^{15}$ (SD $2.94*10^{15}$) Pa^2 s^2 m^{-6}. As a preliminary indicator, and to give context, it is noted that the linear and nonlinear coefficients based on Poiseuille and Bernoulli drops for a 'typical' coronary are of the order of 10^8 Pa s m^{-3} and of the order of 10^{14} Pa^2 s^2 m^{-6} respectively for a 75% reduction area between the inlet and the minimum radius.

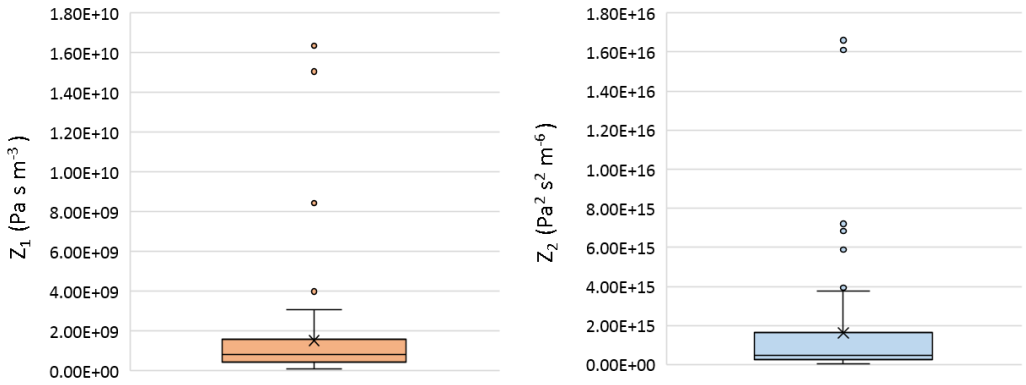

Figure 6.4: Distribution of coefficients Z_1 and Z_2.

Figure 6.5 shows the relationship between the coefficients and the FFRs both measured in Cathlab (FFR_{CL}) and the stable FFR defined with the algorithm in Chapter 4 (FFR_{HY}). An increase of both Z_1 and Z_2 was observed as the degree of stenosis is increased, indicating higher pressure drops across the lesion, with a R^2 coefficient of 0.21 with regards of the FFR_{CL} and

slightly higher with regards of the FFR_{ST} (0.27). While the Z_1 and Z_2 coefficients are directly related with the lesion severity, the FFR is also determined by the myocardial resistance and this might generate the low correlation between them.

Figure 6.6 shows the relationship between the myocardial resistance at baseline and stable hyperaemia and the outlet radius of the vessel considered. As expected, for smaller vessel the resistance results are higher in both baseline and hyperaemia.

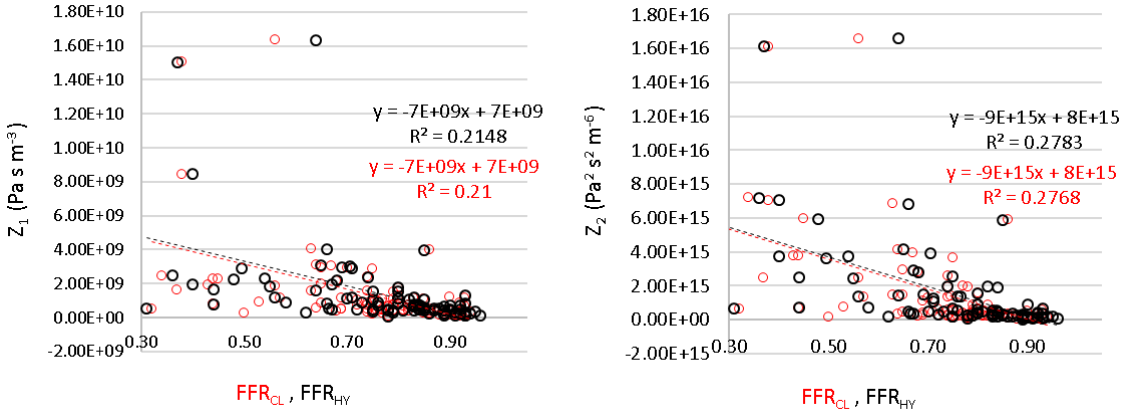

Figure 6.5: Correlation between the FFR and the stenosis coefficients. FFR_{CL} (in red), FFR_{HY} (in black) and the coefficients Z_1 (left) and Z_2 (right).

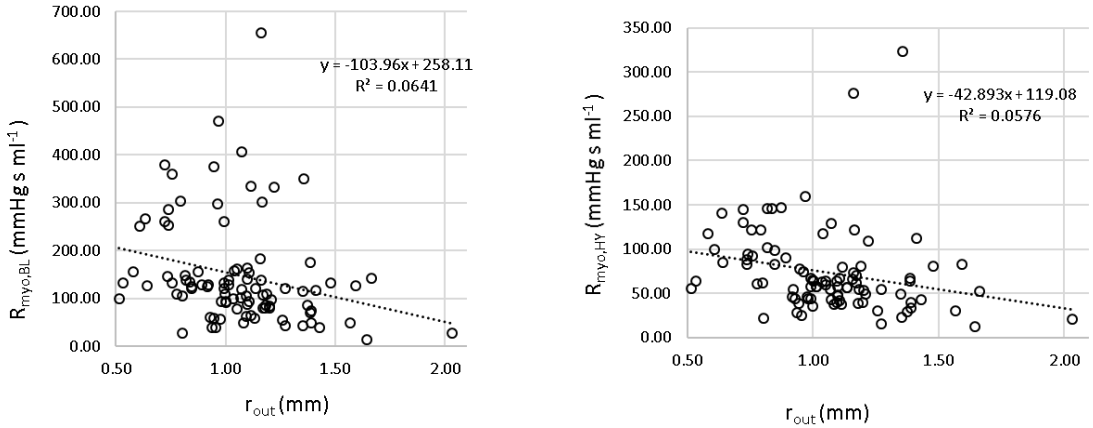

Figure 6.6: Relationship between the outlet radius, r_{out}, of the vessel and the myocardial resistance at baseline, $R_{myo,BL}$, and stable hyperaemia, $R_{myo,HY}$.

6.4.1.2 Average hyperaemic response: myocardial resistance and blood flow

The average myocardial resistances at baseline, peak and stable hyperaemia were respectively 136.35 (SD 86.5) mmHg s/ml, 63.4 (SD 31.1) mmHg s/ml and 72.1 (SD 44.9) mmHg s/ml.

The average blood flows at baseline, peak and stable hyperaemia were respectively 1.10 (SD 0.69) ml/s, 1.76 (SD 0.92) ml/s and 1.63 (SD 0.90) ml/s.

Overall the expected behaviour for both resistance and blood flow was observed, although the high standard deviations indicated high variability of these values (Figure 6.7). Nevertheless, the average value of baseline myocardial resistance for the analysed cases results were higher than what expected on average data of pressure and flow in the coronaries (Chapter 2 Paragraph *2.1.1.3 Coronaries modelling).* It needs to be considered that resistances and flow results in this paragraphs are related with termination of individual branches, while in Chapter 2 the whole myocardium compartment was considered.

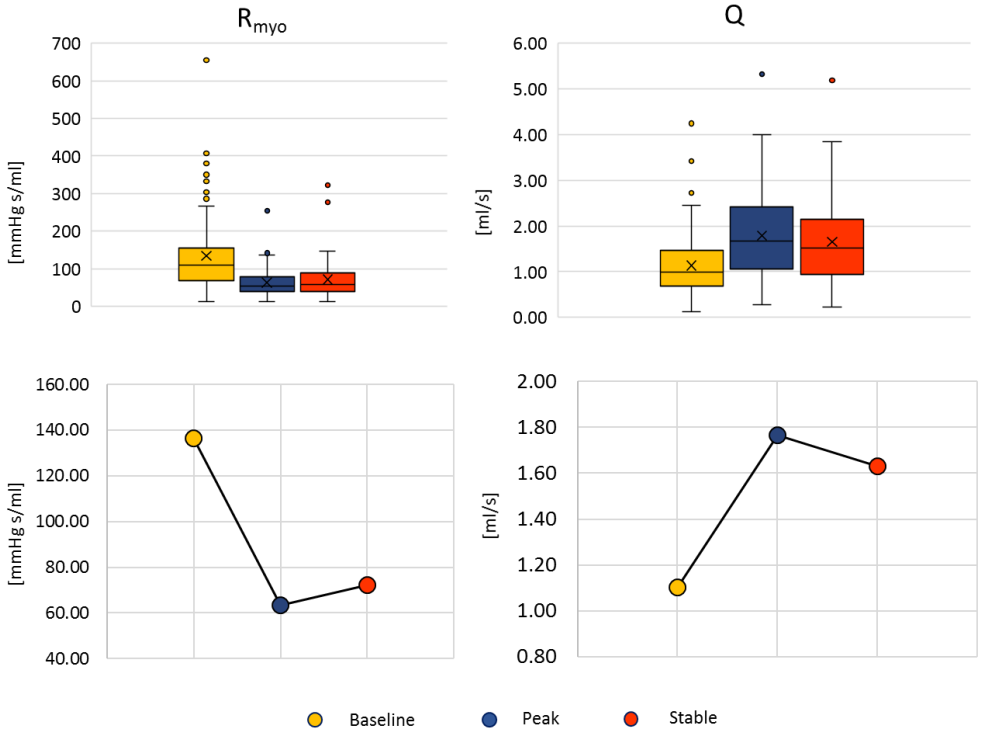

Figure 6.7: Average and distribution of R_{myo} (left) and Q (right) obtained with coefficients from CFD. The values are averaged for each phase of the adenosine response: baseline, peak and stable.

6.4.1.3 Classification based on myocardial resistances during baseline and stable hyperaemia: absolute values and change

In this section results of R_{myo} during baseline ($R_{myo,BL}$), hyperaemia ($R_{myo,HY}$), the absolute change (ΔR_{myo}) and the % of change ($\%\Delta R_{myo}$) between baseline and hyperaemia are reported. In particular, the hyperaemic resistance results, reported already by Morris [92], are shown separated from the others, which this project is focused on.

First of all, the objective was to identify correlation between $R_{myo,BL}$, ΔR_{myo} and $\%\Delta R_{myo}$.

Figure 6.8 shows the $R_{myo,BL}$ against ΔR_{myo} and $\%\Delta R_{myo}$. In the first relationship the linear coefficient is 0.66 and the correlation coefficient is 0.83, indicating a high correlation between the two variables. This is what is physiologically expected in the myocardium. The second relationship shows that for low resistances a small change in percentage during hyperaemia is associated, while for the higher resistances the percentage of change is close to 0.61, consistent with the first relationship.

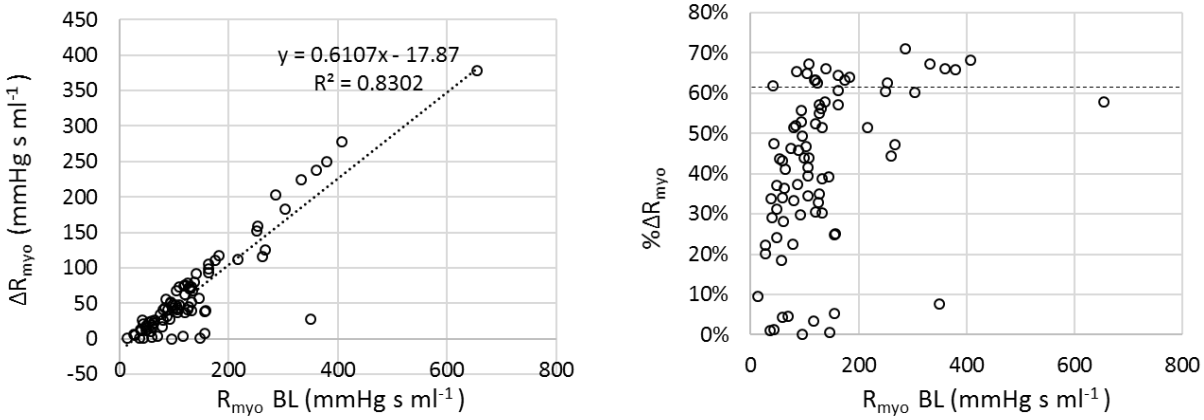

Figure 6.8: Correlation between the myocardial resistance at baseline (R_{myo} BL) and (left) the absolute change of myocardial resistance (Δ_{Rmyo}) and (right) the percentage change of myocardial resistance (% Δ_{Rmyo}).

This study supports the idea that the hyperaemic resistance might reasonably be estimated from the baseline resistance if the latter is known, especially when it is in the upper range. Measurement at baseline only is possible with an adjustment of the current clinical protocol, but this is already invasive and, although the extrapolation to hyperaemia would negate the

requirement for adenosine infusion and this might be preferable for patient comfort, the potential errors in the extrapolation, in combination with the fact that relatively few FFR measurements are actually made, strongly limits the value of this process.

A weak correlation is expected between the myocardial resistance and the lesion severity, represented by the P_d/P_a. This is because the ratio between proximal and distal pressure has implicitly taken in account the myocardial resistance, from which the distal pressure is dependent. However, in case of severe stenosis it is supported the idea of physiological compensation of the myocardium to reduce the overall resistance of the coronary circulation and maintain an adequate coronary blood flow [200, 201].

Figure 6.9 shows the relationship between P_d/P_a at baseline and the $R_{myo,BL}$, between the FFR_{HY} and $R_{myo,HY}$ and between FFR_{HY} and ΔR_{myo} and $\%\Delta R_{myo}$. Data suggest that for higher P_d/P_a at baseline, the myocardial resistance tends to be higher for mild stenoses, although the correlation coefficient is very small (Figure 6.9 – top right and bottom left). Observing the relationships between FFR_{HY} and $R_{myo,HY}$ and then ΔR_{myo} no particular trend that allows to identify how the myocardial resistance influence the FFR was identified (Figure 6.9 – bottom left and right). Regarding the relationship between FFR_{HY} and $\%\Delta R_{myo}$, a higher vasodilation in mild stenosis compared to the more severe ones is observed, because naturally, starting from a higher value of resistance it is possible to observe a high vasodilation (Figure 6.9 – bottom right).

The main challenge remains the ability to predict the baseline myocardial resistance. To make this prediction it is necessary to understand why patients have different values of myocardial resistance at baseline, including identification of the data that is available for the patient (demographics, comorbidities) that most strongly influence this parameter.

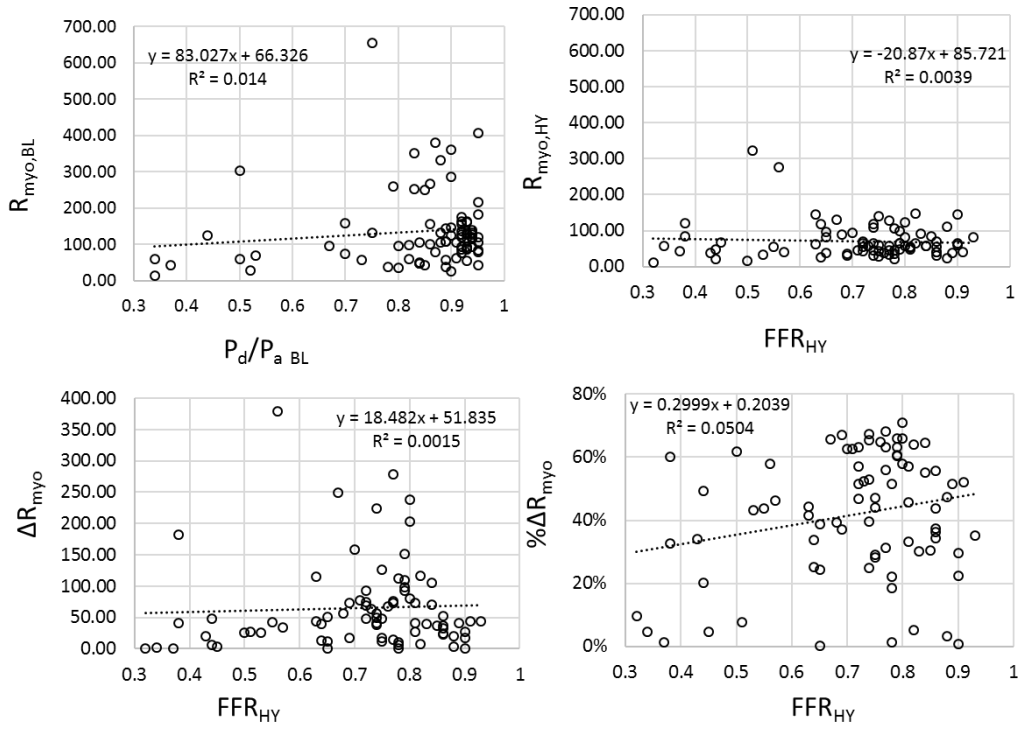

Figure 6.9: Relationship between P_d/P_a and R_{myo}.
Top left P_d/P_a at baseline and $R_{myo,BL}$ on the right; Top right) FFR_{HY} and $R_{myo,HY}$; Bottom left) FFR_{HY} and ΔR_{myo}; FFR_{HY} and $\%\Delta R_{myo}$

Lesions were divided into 4 groups: 1st group with 54 lesions in LAD, DX, 2nd groups with 16 lesions for the RCA, 3rd group with 9 lesions for the LCX and 4th group with 2 lesions in the LMS. Values of $R_{myo,HY}$, $R_{myo,BL}$, ΔR_{myo} and $\%\ \Delta R_{myo}$ are summarised in table 6.2 and shown in figure 6.10 in terms of mean and standard mean error.

At stable hyperaemia the average values of R_{myo} were 63.8 (SD 41.8) mmHg s/ ml, 91.9 (SD 72.8) mmHg s/ ml, 85.6 (SD 44.2) mmHg s/ ml and 34.8 (SD 7.13) mmHg s/ ml respectively for each group.

The average values of R_{myoBL} are 124.4 (SD 103.2) mmHg s/ ml, 157.6 (SD 99.0) mmHg s/ ml, 154.6 (SD 107.4) mmHg s/ ml and 79.9 (SD 8.3) mmHg s/ ml respectively for the 1st, 2nd, 3rd and 4th group.

The average ΔR_{myo} from baseline to stable hyperaemia are 60.5 (SD 71.3) mmHg s/ ml, 65.6 (SD 62.1) mmHg s/ ml, 69.0 (SD 79.4) mmHg s/ ml and 45.1 (SD 15.5) mmHg s/ ml respectively for each group.

The average % ΔR_{myo} from baseline to stable hyperaemia are -42.6% (SD 19.3%), -39.6% (SD 21.8%), -35.9% (SD 26.2%) and -56.4% (SD 14.3%) respectively for each group. This is consistent with results reported in the literature [115].

As can be observed the standard deviations are high compared to the average values and this does not support the identification of a pattern of distinction between the myocardial resistances in each cardiac area supplied by the different vessels.

Table 6.2: Average and standard deviation results for $R_{myo,HY}$, R_{myoBL}, ΔR_{myo} and $\%\Delta R_{myo}$ for each group of vessel.

	R_{BL} mmHg s/ ml	R_{HY} mmHg s/ ml	ΔR_{myo} mmHg s/ ml	% ΔR_{myo}
1st group *LAD, DX*	124.4 (SD 103.2)	63.8 (SD 41.8)	60.5 (SD 71.3)	-42.6 % (SD 19.3 %)
2nd group *RCA*	157.6 (SD 99.0)	91.9 (SD 72.8)	65.6 (SD 62.1)	-39.6 % (SD 21.8 %)
3rd group *LCX*	154.6 (SD 107.4)	85.6 (SD 44.2)	69.0 (SD 79.4)	-35.9 % (SD 26.2 %)
4th group *LMS*	79.9 (SD 8.3)	34.8 (SD 7.13)	45.1 (SD 15.5)	-56.4 % (SD 14.3 %)

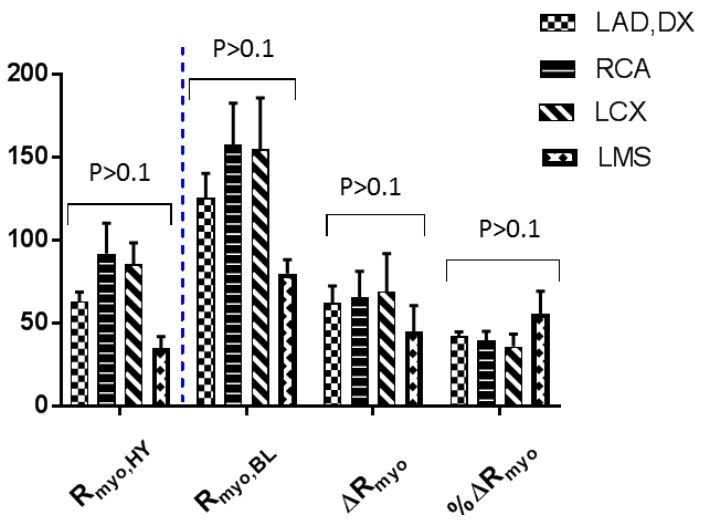

Figure 6.10: Histograms representing the distribution of $R_{myo,HY}$, R_{myoBL}, ΔR_{myo} and $\%\Delta R_{myo}$ for each group of vessels.
$R_{myo,BL}$, $R_{myo,HY}$ and ΔR are in mmHg s/ml, $\%\Delta R_{myo}$ is in percentage. Results are reported with means and SEM.

In figure 6.10 it can be observed that LMS has a smaller distal resistance both at baseline and hyperaemia, if compared to the other group of vessels. This is expected because LMS is a larger vessel and its downstream resistance is represented by the parallel of LAD, DX and LCX.

RCA and LCX show higher distal resistances compared to the LAD and DX group. The ΔR_{myo} follows the same trend, while the $\%\Delta R_{myo}$ shows a higher percentage for the LMS compared to the other groups.

In the following figures, histograms are used to represent the patients' profile and compare them, to seek to identify correlation with patient pathologies/conditions. The patients' profiles in terms of age, gender, BMI, smoking status, other comorbidities and myocardial infarction location are summarised into a number of graphs to identify any possible influence of any of these characteristics on the value of R_{myoBL}, $R_{myo,HY}$, ΔR_{myo} and $\%\Delta R_{myo}$. Each case is reported in one column and they are arranged in ascending order of the reported parameter. Figure 6.11 shows the profiles considering $R_{myo,BL}$; figure 6.12 shows the profiles considering $R_{myo,HY}$; figure 6.13 shows the profiles considering ΔR_{myo}; figure 6.14 shows the profiles considering $\%\Delta R_{myo}$. On visual inspection of the histograms, none of the represented comorbidities appears to correlate with the value of the myocardial resistance and/or its change during adenosine vasodilation, with the exception of the COPD. In figure 6.11 it can be seen that patients with COPD have a small $R_{myo,BL}$. Some conditions, such as hyperlipidaemia and hypertension, are common in this cohort, but no correlation with myocardial resistance is observed. Some of the pathologies, such as COPD, PDV and asthma, are uncommon in this cohort and so no firm conclusion can be drawn.

Focusing on the relevant variables that are expected to determine the myocardial condition, such as age, BMI, smoking status and previous myocardial infarction event and location, an attempt was made to identify any possible correlation with $R_{myo,BL}$, $R_{myo,HY}$, ΔR_{myo} and $\%\Delta R_{myo}$ (Figure 6.15). Statistic between the different groups was calculated with non-parametric T-test

and One-way ANOVA considering a Gaussian distribution. Data are presented with mean and standard error of the mean (SEM).

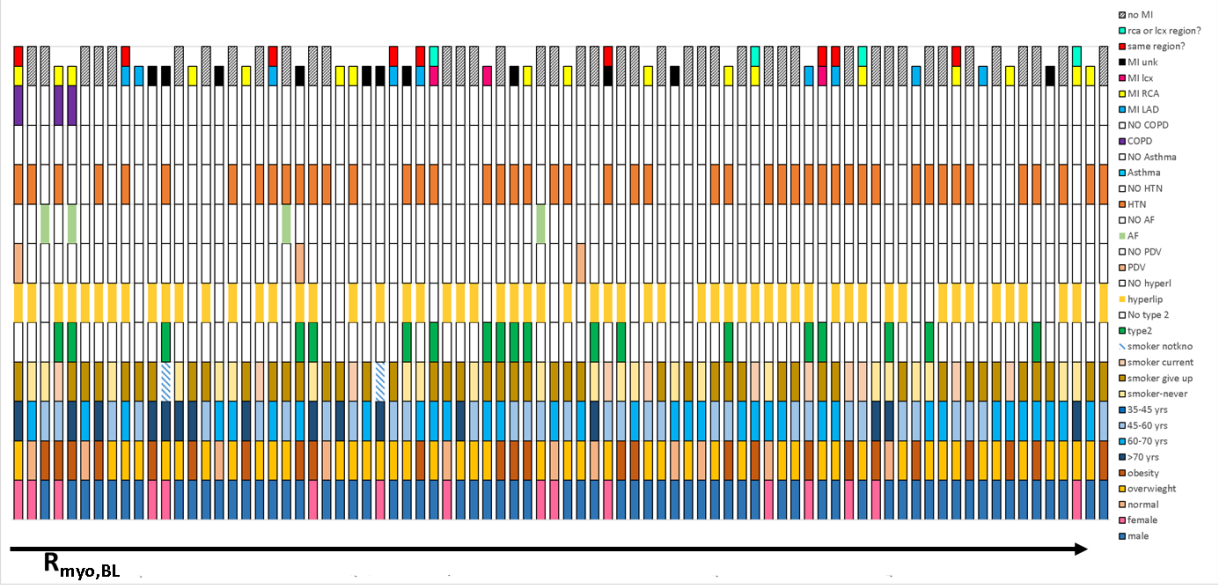

Figure 6.11: Patients' profiles arranged in ascending order of $R_{myo,BL}$.
Each column represents a single lesion. Each raw represents a specific characteristic of the patient, starting from the bottom: gender (male-female), BMI (normal-overweight-obese), age (35 to 45, 45 to 60, 60 to 70, over 70), smoking status (never-given up-current), comorbidities (type II diabetes, hyperlipidaemia, peripheral vascular disease, atrial fibrillation, hypertension, asthma, COPD, myocardial infarction and location.

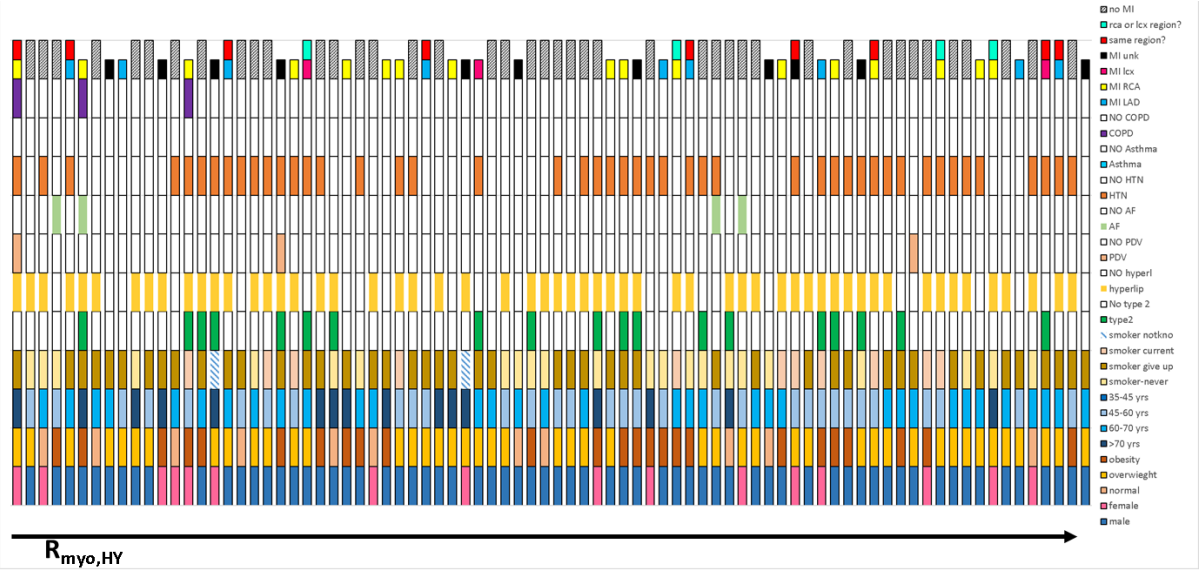

Figure 6.12: Patients' profiles arranged in ascending order of $R_{myo,HY}$.
Each column represents a single lesion. Each raw represents a specific characteristic of the patient, starting from the bottom: gender (male-female), BMI (normal-overweight-obese), age (35 to 45, 45 to 60, 60 to 70, over 70), smoking status (never-given up-current), comorbidities (type II diabetes, hyperlipidaemia, peripheral vascular disease, atrial fibrillation, hypertension, asthma, COPD, myocardial infarction and location.

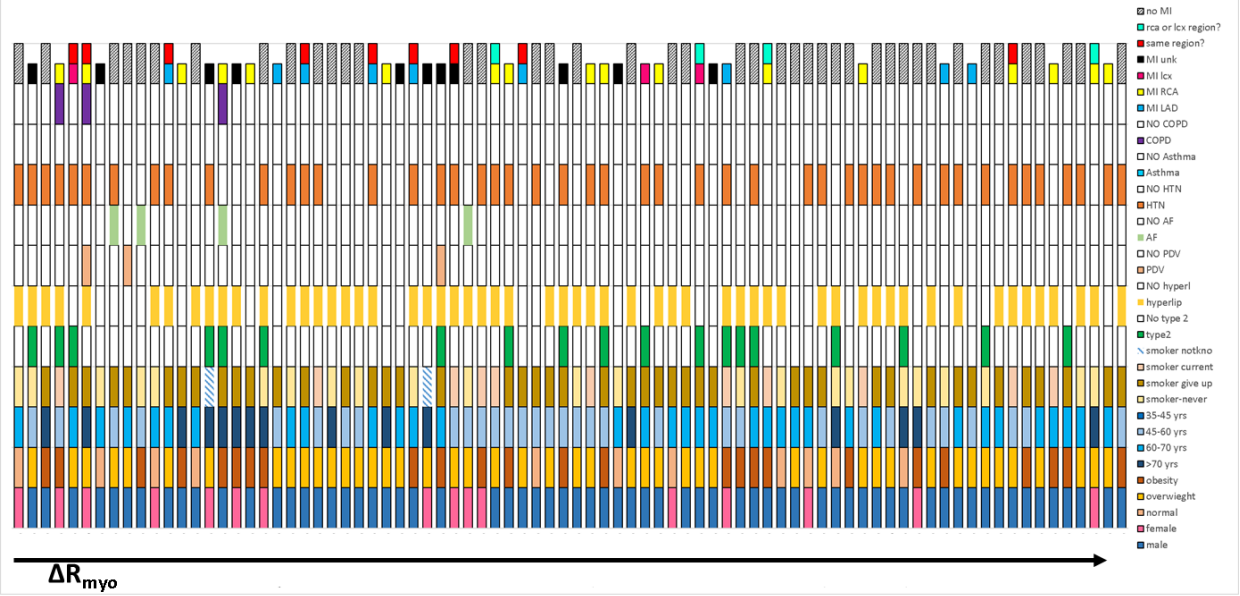

Figure 6.13: Patients' profiles arranged in ascending order of change of R_{myo}.
Each column represents a single lesion. Each raw represents a specific characteristic of the patient, starting from the bottom: gender (male-female), BMI (normal-overweight-obese), age (35 to 45, 45 to 60, 60 to 70, over 70), smoking status (never-given up-current), comorbidities (type II diabetes, hyperlipidaemia, peripheral vascular disease, atrial fibrillation, hypertension, asthma, COPD, myocardial infarction and location.

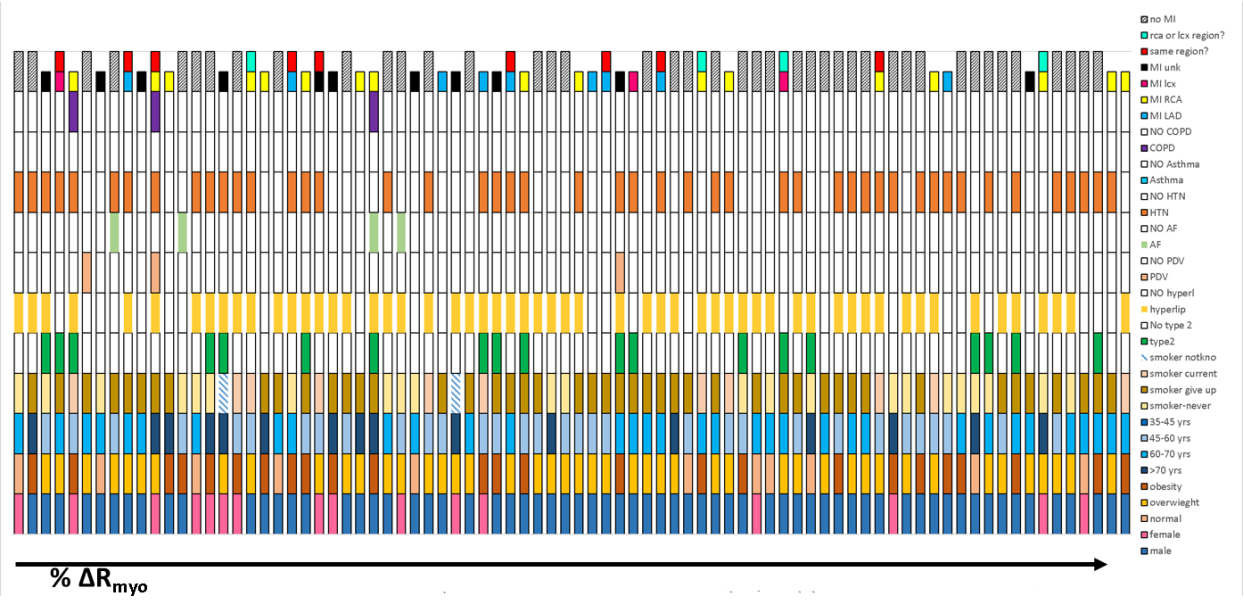

Figure 6.14: Patients' profiles with crescent order of $\%\Delta R_{myo}$.
Each column represents a single lesion. Each raw represents a specific characteristic of the patient, starting from the bottom: gender (male-female), BMI (normal-overweight-obese), age (35 to 45, 45 to 60, 60 to 70, over 70), smoking status (never-given up-current), comorbidities (type II diabetes, hyperlipidaemia, peripheral vascular disease, atrial fibrillation, hypertension, asthma, COPD, myocardial infarction and location.

Figure 6.15-A represents the distribution of the $R_{myo,BL}$, $R_{myo,HY}$, ΔR_{myo} and $\% \Delta R_{myo}$ in smokers (current and ex-smokers) and non-smokers, (57 vs 23 samples). A slight difference between the two groups of patients can be observed, although it is not statistically significant: smokers tend to have a stiffer myocardial microcirculation at baseline, although during hyperaemia the difference is less pronounced.

Figure 6.15-B represents the distribution of the $R_{myo,BL}$, $R_{myo,HY}$, ΔR_{myo} and $\% \Delta R_{myo}$ according to the BMI: 11 normal BMI (BMI<25), 46 overweight (25<BMI<30), 25 obese (BMI>30). At baseline obese and overweight patients show a similar value of myocardial resistance, higher than patients with normal BMI. A similar trend is also observed for the hyperaemic resistance and a similar absolute change in resistance, although the percentage change results similar for all the groups. P - values were above 0.05, conferring non significance to the results.

Figure 15-C shows the comparison between 3 groups of patients classified by age. Patients of 60-70 years of age (34 samples) show the highest value of resistance for both baseline and hyperaemic, followed by the 45-60 years old patients (32 samples) and then by the patients over 70 years old (16 samples). Again, P - values were above 0.05, therefore there is lack of significance. An increase of myocardium stiffness is expected in old patients, but our data is contradictory.

Finally, the aim was to investigate the influence of any previous event of myocardial infarction (MI) and its location, if known, in relation with the coronary vessel with the studied lesion. Considering then the MI event and its location in the three cardiac regions (anterior, posterior and inferior), any influence on the myocardial resistance was attempt to be identified. The groups are: patients who did not have MI (42 samples) and patients who did have a previous MI. Among the latter, then there is a group where the MI occurred in the region of the heart supplied by the vessel with the lesion (9 samples), a group where the region of the heart supplied by the vessel with lesion is different from that one where the MI occurred (17

samples) and finally a group the it is not known if the MI region and the region supplied by stenotic vessel are the same (14 samples) , because it is not reported where the MI occurred or because the stenotic vessel is an RCA or LCX and these vessel can supply both posterior and inferior based on the specific anatomy of the coronary circulation in each patient, for which there are no data.

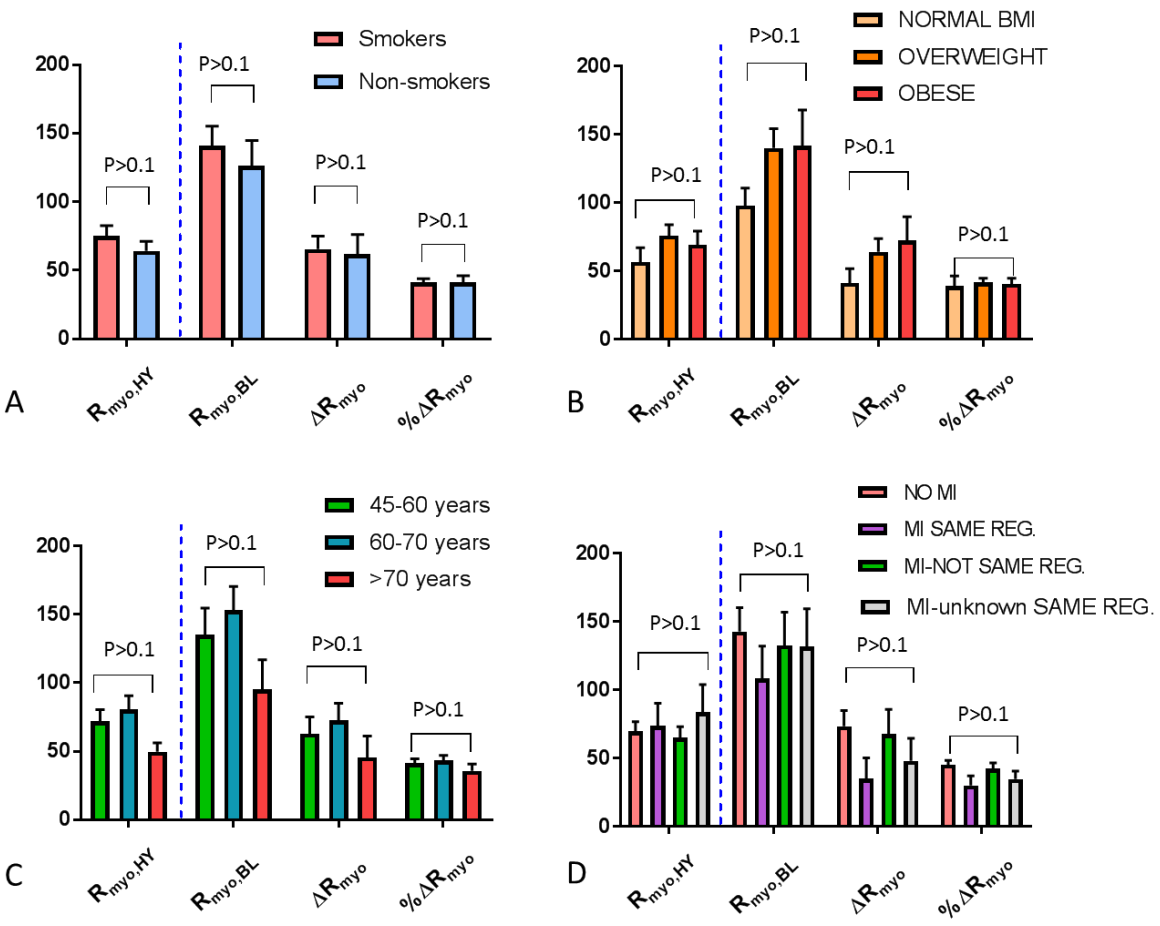

Figure 6.15: Histograms representing $R_{myo,BL}$, $R_{myo,HY}$, ΔR_{myo} and $\%\Delta R_{myo}$ for the relevant variables for the myocardial condition.
$R_{myo,BL}$, $R_{myo,HY}$ and ΔR_{myo} are in mmHg s/ml, is in percentage. Results are presented with means and SEM.A) Smoking condition: Smokers vs Non-smokers. B) BMI: Normal vs Overweight vs Obese. C) Age: 45-60 years of age vs 60-70 years of age vs >70 years of age. D) Previous MI: no MI vs MI in the region supplied by the coronary artery with the lesion vs MI in a different region supplied by the coronary artery with the lesion vs MI and region unknown relative to the supplied lesion region.

Figure 15-D shows the comparison between the $R_{myo,BL}$, $R_{myo,HY}$, ΔR_{myo} and % ΔR_{myo} in each group. It is observed that patients with MI in the same region of the stenotic vessel show the lower value of $R_{myo,BL}$, ΔR_{myo} and % ΔR_{myo}. There is not a clear distinction between the values

of the parameters in patients with no MI and patients with MI overall. Once again P-values were above 0.05.

In none of these graphs it is possible to identify any cluster of data related with the specific characteristic presented: smoking status, age, BMI and previous MI, suggesting that a larger cohort of patients might be necessary to produce statistical significance.

6.4.2 Classification of adenosine response based on myocardial adenosine concentration

6.4.2.1 Patients demographic and lesions' characteristics

In the previous sections the analysis was focused on the interpretation of the measured responses, independently of any underpinning model of the system (except that the coronary flows and stenosis characterisations were computed from a CFD model). In this the focus is switched to the investigation of whether there is any correlation of the response with computed, model-based, adenosine concentration. A total number of 43 lesions in 27 patients were considered for this study. Patients were selected based on the availability of the clinical demographic and image data described in chapter 5, based on which a personalised global cardiovascular model was constructed, and from which the aortic concentration of adenosine was calculated. The demographic description of the patients is reported in Table 6.3.

The lesions were located in different coronary arteries: 18 in the LAD, 13 in the RCA, 7 in the LCX, 3 in the LMS and 2 in the DX.

The average FFR for these 43 lesion was 0.76 (SD 0.14) considering the FFR reported in the Cathlab (FFR_{CL}) and 0.79 (SD 0.12) considering the FFR_{HY}, obtained with the algorithm described in Chapter 4 ($FFR_{ST,0.04Hz}$). The average values of Z_1 and Z_2 were respectively $1.6 \cdot 10^9$ (SD $2.6 \cdot 10^9$) $Pa \cdot s \cdot m^{-3}$ and $1.7 \cdot 10^{15}$ (SD $2.9 \cdot 10^{15}$) $Pa^2 \cdot s^2 \cdot m^{-6}$ (Figure 6.16). Figure 6.17 shows

their distribution associated with the lesion's severity (FFR_{CL}, FFR_{HY}) and, in particular, Z_1 and Z_2 increased as the FFR decreased, consistent with expectation.

Table 6.3: Demographic data and comorbidities of the sub-cohort (27 patients) used for the local tuning optimisation.
Peripheral Vascular Disease (PVD), Chronic Obstructive Pulmonary Disease (COPD), previous myocardial infarction (MI).

Patient demographic		**Num% - mean (SD)**
Male		81%
Age (years)		66.3 (SD 11.7)
BMI		27.5 (SD 4.9)
Hypertension		66.7 %
PVD		11.1 %
Previous MI		59.3 %
Type II diabetes		7.4 %
Hyperlipidaemia		70.4 %
COPD		7.41 %
Smoking status:	*Never*	29.6%
	Ex-smoker	70.4 %
	Current	11.1 %

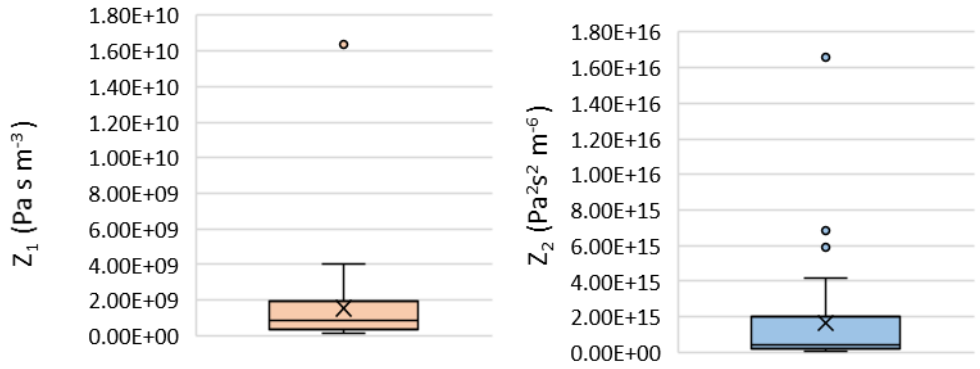

Figure 6.16: Distribution of the coefficient Z_1 ($Pa \cdot s \cdot m^{-3}$) (left) and Z_2 ($Pa^2 \cdot s^2 \cdot m^{-6}$) (right) characteristic of the 51 lesions.

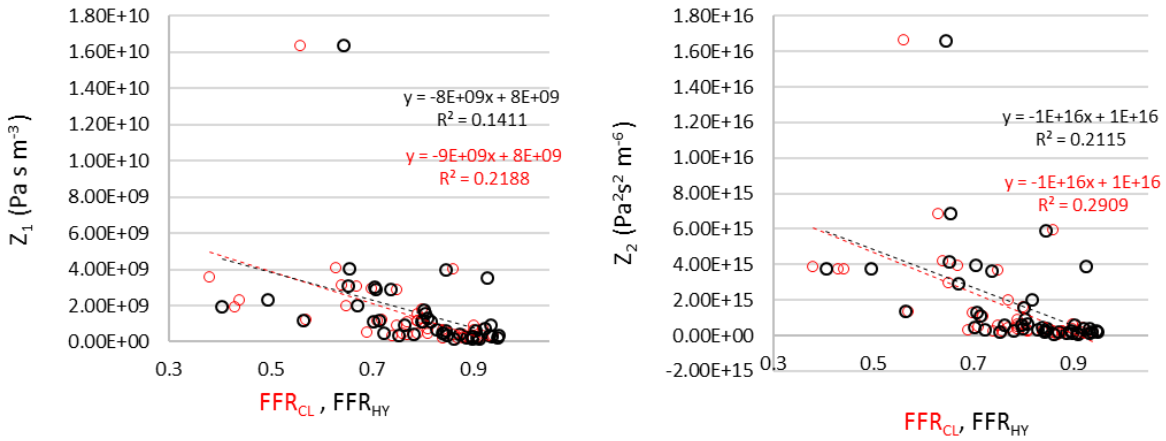

Figure 6.17: Z_1 and Z_2 relationship with FFR (FFR_{CL} and FFR_{HY}).
43 stenoses' quadratic and linear coefficients (Z_1 and Z_2) are reported in relation to the relative severity represented by the FFR (FFR_{CL} and FFR_{HY}).

6.4.2.2 Optimisation results

The parameters of the branching tree structures for each patient were computed using the optimisation process described in paragraph *6.2.2.2*. The average fitness value was equal to 0.32. The simulation time for each optimisation is between 1 and 2 s.

6.4.2.2.1 Patient-specific α, β and γ and errors between targets and model results

The myocardial coefficients α, β and γ were calculated using the stable hyperaemia resistance, $R_{myo,HY}$. In some cases the residuals remained relatively high with the parameters constrained to lie within physically plausible ranges. The average and standard deviation of the 3 coefficients are: for α 0.78 (SD 0.02), for β 47.1 (SD 11.1) and for γ 1.68 (SD 0.23). Results are shown in Figure 6.18. The average number of vessel in the capillary generation (the last one) was $6.76 \cdot 10^7$.

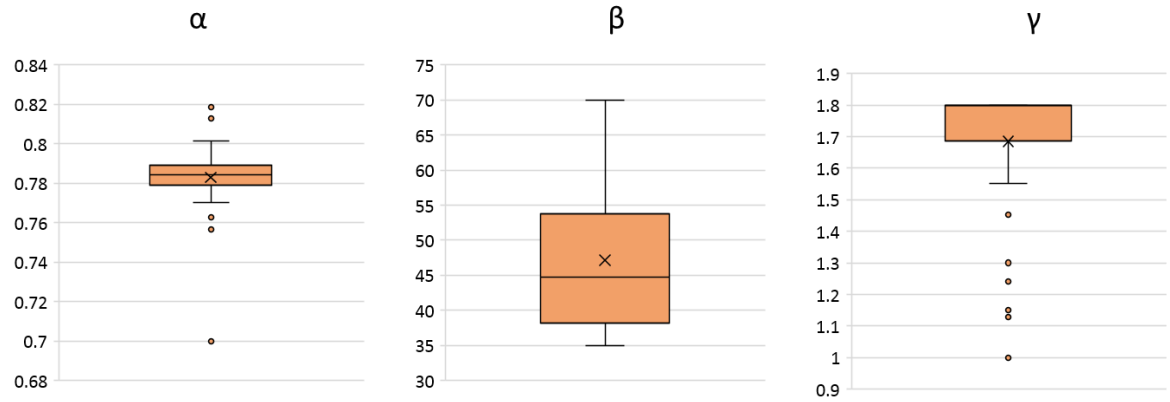

Figure 6.18: Distribution of α, β and γ results obtained with the optimisation.

Figure 6.19 shows the comparison the target $R_{myo,BL}$ (Panel A), V_B (Panel B) and $R_{myo,HY}$ (Panel C) against the optimised results in terms of simple linear relationship, Bland-Altman and % error distribution. The correlation is high for $R_{myo,BL}$ and $R_{myo,HY}$ with values above 0.8, while for V_B the correlation is lower.

For $R_{myo,BL}$ and $R_{myo,HY}$ a better correlation for the smaller values of resistances was observed, while for higher values the error was higher. This suggest that the model does not represent all

range of myocardial resistances, but could represent the myocardium resistance within 10 and 200 mmHg s/ml.

Considering the results of the optimisation, in our cases there are some cases where the resistances presented high values and in order to represent these values, obtained with the Z_1 and Z_2 coefficients at baseline and hyperaemia, the selected approach was to assume a linear relationship between the resistances and the blood volume of myocardium using the coefficient $C_{BL\text{-}HY}$ as explained in Eq.6.12 and 6.13.

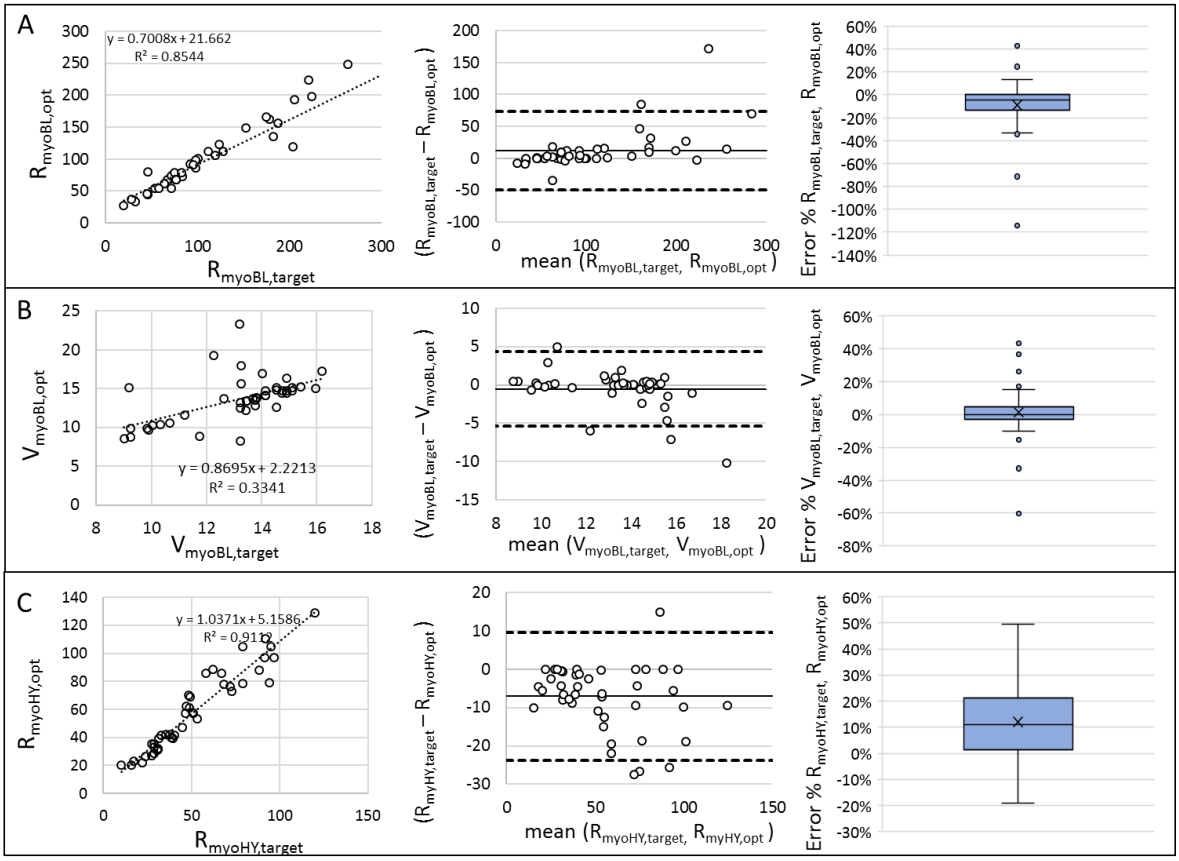

Figure 6.19: Comparison between targets and model results.
Panel A) $R_{myo,B}$. Panel B) V_B. Panel C) $R_{myo,HY}$. Units of resistance are mmHg s/ml, units of volume are ml.

6.4.2.2.2 Patient-specific baseline and hyperaemic myocardial blood volume

The average V_{BL} estimated with Eq.6.8 and Eq.6.9 based on BSA, left ventricular mass and density of blood in the cardiac tissue, was equal to 13.03 ml (SD 1.99), while the model produces a value of 13.6 ml (SD 3.0).

The average V_{HY} was equal to 16.2 ml (SD 4.6) using as reference the generic model with coefficient $C_{BL\text{-}HY}$ equal to 1.66 and an average of 17.07 ml (SD 4.16) calculating $C_{BL\text{-}HY}$ with the results of the optimisation considering the relationship at Eq.6.13.

6.4.2.3 Adenosine concentration and time plateau values in the myocardium

The personalised branching tree model enabled the estimation of the volume change of the myocardium in the hyperaemic state. Figure 6.20 illustrates the computed concentration profiles for two cases, comparing the profile including the computed volume change with that in which the volume is assumed constant at its baseline value. The figure indicates that the concentration profile is slightly affected by the inclusion of this term. And in both cases the myocardium concentration is higher than what was obtained with the generic model simulations in Chapter 3 (~$1 \cdot 10^{-4}$ mg/ml).

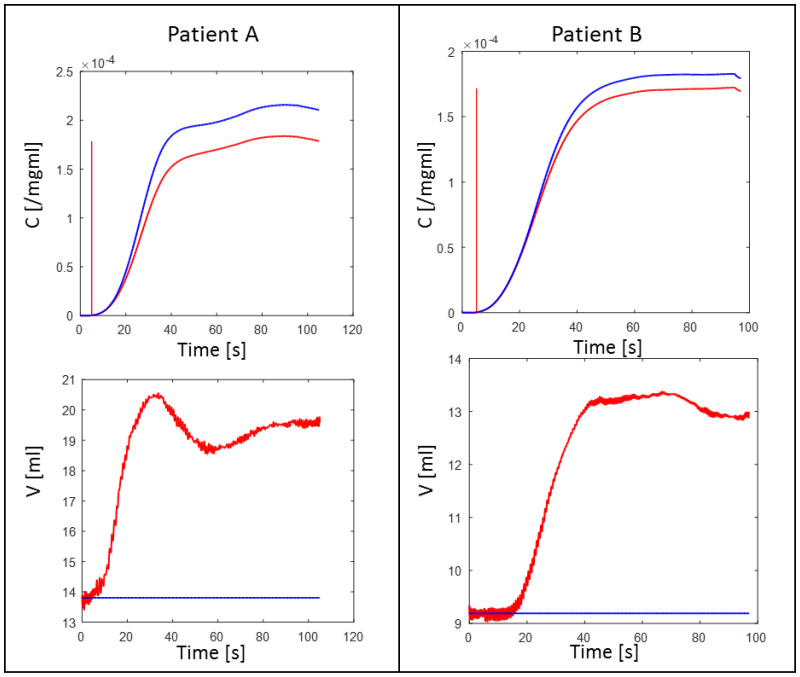

Figure 6.20: Two examples of results of blood volume, V, and adenosine concentration, C, in patient-specific myocardium without (blue) and with (red) vasodilation phenomena.

The average plateau value for the concentration was $1.51 \cdot 10^{-4}$ mg/ml (SD $5.81 \cdot 10^{-5}$mg/ml), while the average time necessary to reach the plateau following commencement of the adenosine infusion was 60.64 s (SD 10.61 s). Both the plateau value and the time to reach it

showed a high SD compared to the value of the means, indicating the high inter-patient variability of the adenosine concentration. The reason of the variability of the maximum adenosine concentration in the myocardium and of the time to reach plateau is principally caused by the aortic concentration of adenosine as discussed in Chapter 3. The average time to reach maximal hyperaemia in the myocardium, from when the maximum in aortic concentration occurs (average of 47 s for the personalised model in Chapter 5), was about 13 seconds. The different values of maximal concentration and time necessary to reach the maximum in the myocardium are highly influenced by the aortic profile of concentration, but also the myocardium resistance and the severity of stenosis influences the myocardial concentration profile.

Figure 6.21 shows the relationships between the lesion severity, expressed by the FFR_{HY}, and the plateau adenosine concentrations in the aorta and in the myocardium (A), the difference in time between the aortic maximal concentration and the myocardial maximal concentration (B), the difference between the aortic and myocardial maximum concentration as absolute value (C) and percentage (D) respectively.

On average it is observed that, independently of the lesion severity, the myocardium concentration reached about half of the concentration in the aorta and that for mild stenoses there was an increase of the absolute difference of the concentrations, less pronounced in the results reported as percentage. In addition, the difference in time to reach plateau in the aorta and in the myocardium appears to be higher for less severe stenoses.

In all the cases the correlation was very weak, indicating that the lesion severity does not influence the distribution of the adenosine concentration and therefore the vasodilation response.

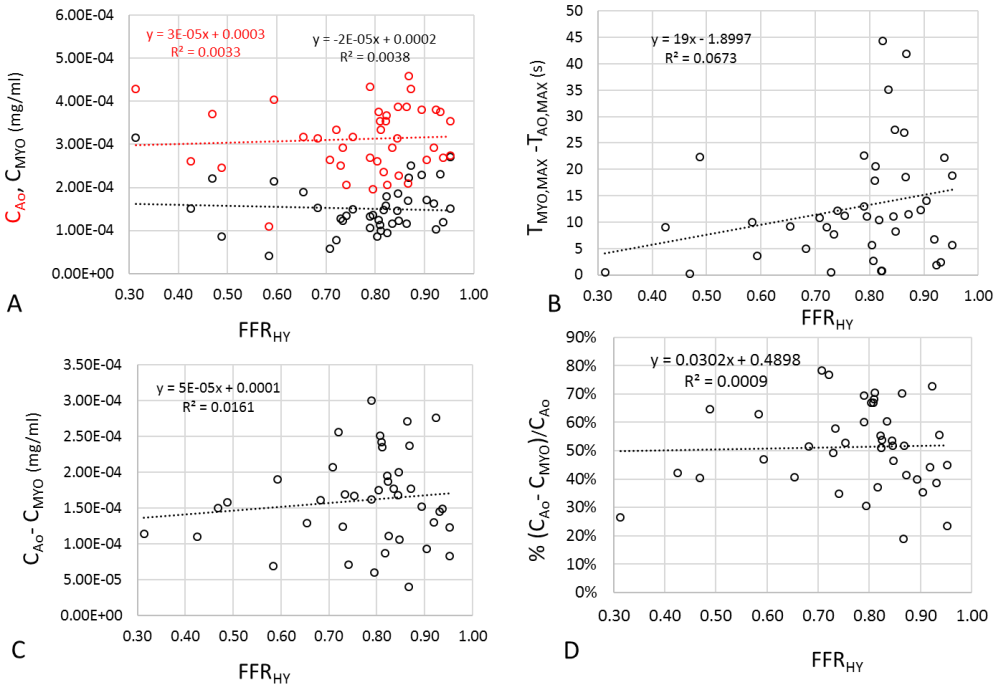

Figure 6.21: Relationships between lesion severity (FFR$_{HY}$) and the plateau concentration and time values in the aorta and in the myocardium.
A) FFR$_{HY}$ vs maximal aortic concentration, C$_{AO}$ (in red), and maximal myocardial concentration, C$_{myo}$ (in black). B) FFR$_{HY}$ vs the difference between the time to reach concentration plateau in the aortic concentration and the one in the myocardial concentration. C) FFR$_{HY}$ vs the difference between maximal aortic concentration, C$_{AO}$ and maximal myocardial concentration, C$_{myo}$. D) FFR$_{HY}$ vs the difference between maximal aortic concentration, C$_{AO}$ and maximal myocardial concentration, C$_{myo}$, expressed in %.

The influence of the myocardial distal resistance at baseline and hyperaemia in the maximal myocardium concentration was then investigated, as shown in Figure 6.22.

With regards of the R_{myoBL} (Figure 6.22 - left) it is observed that for higher myocardial resistances the maximal myocardial concentration is lower (Figure 6.22-A) and takes a longer time (Figure 6.22-B), due to the reduced myocardial blood flow. When the C_{myo} is compared with the maximal aortic concentration, C_{AO}, both as absolute (Figure 6.22-C) and the percentage (Figure 6.22-D) differences, for high myocardial resistances the maximal myocardial concentration increases. This highlights the high influence of the aortic concentration defined by the systemic characteristics of the individual.

Same considerations can be done for the results in figure 6.22 - right with regards to the $R_{myo,HY}$ (Figure 6.22-E,F,G,H) .

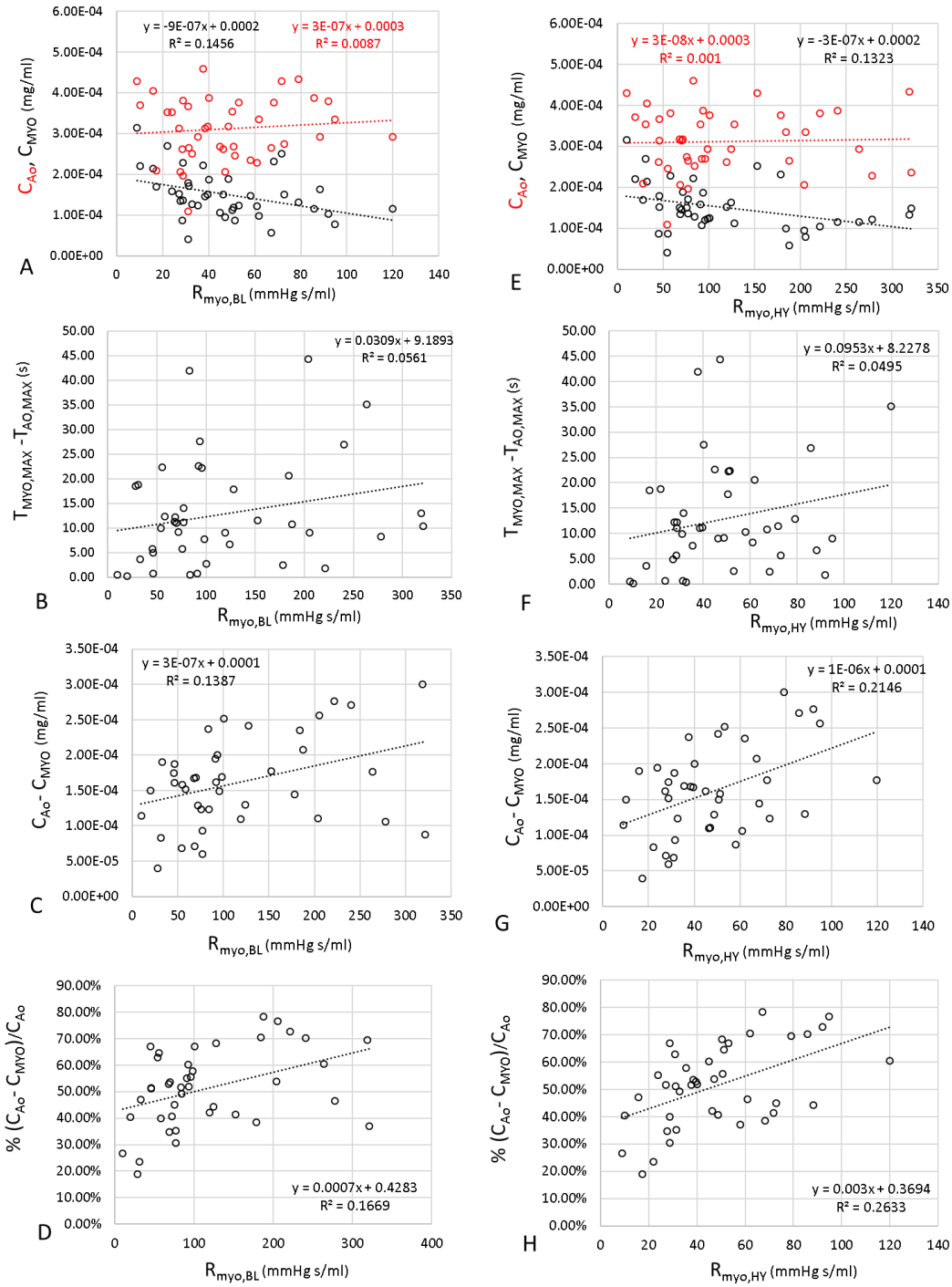

Figure 6.22: Relationships between R_{myo} and the plateau concentration and time values in the aorta and in the myocardium.

Panels on the left show results for the $R_{myo,BL}$ and panel on the left for the $R_{myo,HY}$. Panels A, E) R_{myo} vs maximal aortic concentration, C_{AO} (in red), and maximal myocardial concentration, C_{myo} (in black). Panels B, F) R_{myo} vs the difference between the time to reach concentration plateau in the aortic concentration and the one in the myocardial concentration. Panels C, G) R_{myo} vs the difference between maximal aortic concentration, C_{AO} and maximal myocardial concentration, C_{myo}. Panels D, H) R_{myo} vs the difference between maximal aortic concentration, C_{AO} and maximal myocardial concentration, C_{myo}, expressed in %.

A comparison between the time delays between the time to reach plateau concentration in the aorta in the myocardium obtained with the model and the time to reach peak response in the myocardial resistance obtained from the data (and the CFD model) allowed to investigate if the model provided reliable results in terms of the time delays. Table 6.4 reports the mean, SD and range of each of these time. As expected, the T_{myo} was higher than T_{ao} on average about 13 seconds, indicating that the delay given by the system highly influences the response in the myocardium. Comparing these results with the time to reach minimum resistance (equivalent to the peak response), the results were as expected, with about 53 s to reach peak and about 60 s to reach maximum concentration.

Table 6.4: Comparison of time delay to reach plateau concentration obtained with the model and the time delay to peak response in the R_{myo}. T_{ao} and T_{myo} are the time to reach respectively aortic and myocardial maximal concentration in the aorta, ΔT is the difference between them, T_{peak} is the time necessary to the R_{myo} to reach its minimum value. Results are reported in mean, SD and range. Units are in seconds.

	Mean	SD	Range
T_{ao}	47.64	5.67	43.13 - 65.5
T_{myo}	60.67	10.58	46.47 - 90.41
ΔT	12.81	10.82	0.19 - 44.35
T_{peak}	53.25	17.20	24.83 – 92.83

The range of the peak response time includes also lower values suggesting that there is a saturation concentration and, therefore, the myocardium reached its maximal vasodilation.

No conclusions can be drawn with regards to the concentration values in terms of the saturation values and the minimum value to trigger the vasodilation, because there is no measured data available in this specific study and the literature does not provide information.

In addition, with regards to the myocardial time response the delay in the actual vasodilation for a certain adenosine concentration should be taken in account and our data do not allow this type of analysis where it is necessary to separate and analyse the different phenomena.

6.4.3 Limitations

The main limitations encountered in this part of the project related to the coronary patient-specific personalisation were essentially associated with the limited amount of patient specific data in relationship with the number of parameters of the model.

The lack of patient specific data on the myocardial blood volume has led the development of a tree-structured model and the use of some generic patient data and the literature data to make a prediction of it, but the main problem lies on the validation on patient data.

The tree-structure model is very simple in order to run an optimisation with few targets. More complex models, which try to investigate the different mechanisms of vasodilation, are published in the literature.

The problem of the validation process is applicable for the myocardial blood volume, as well as the concentration of adenosine in the coronary during invasive angiography. Measurements ensure a validation process of the model against them. Having more patient data, it would be potentially possible to improve the optimisation process and consider to optimize also the range of reactive vessel to adenosine for each patient.

Moreover, they could be used in the whole cardiovascular model as a target and therefore get better optimisation results for the whole system.

To understand the effect of the patients' characteristic a study with a high number of patients should be planned considering a comparison between groups of patients with a specific pathology with other groups without it. It is also worth to mention and remember though that it is common to have a number of comorbidities in patient with CAD which might have a different level of severity or a different diagnostic time. Therefore, the combination of these can be very different in each patient.

6.5 CONCLUSIONS

In conclusion, the available patients' data can be used to build a patient specific model of the coronary branch, with the help of CFD simulation and 3D reconstruction of the artery.

It is challenging the definition of patient-specific boundaries conditions in terms of the myocardial resistance.

This chapter attempted to identify any correlation between the patient physiological condition and its response to adenosine from the myocardial point of view.

In a first analysis, the FFRs and the stenosis and myocardial microvasculature properties defined with the segmentation and the CFD model described in the PhD thesis of Dr. Morris [92] were investigated.

The relationship between the FFRs and the stenosis coefficient Z_1 and Z_2 showed a trend as expected, indicating that severe stenoses have higher values for the two coefficients. The relationship between the outlet radius of the considered vessel and the distal resistance at baseline and stable hyperaemia indicated that for smaller vessels the resistance resulted higher in both baseline and hyperaemia.

The average behaviours of the myocardial resistance and the blood flow showed an expected trend. Myocardial resistance during hyperaemia appeared to be 61% of the myocardial resistance at baseline, although if the baseline resistance was already low during baseline the vasodilation was not so effective.

Classification of myocardial resistance at baseline and hyperaemia and the absolute and relative change according to the region of the myocardium did not show any difference and, therefore, the location cannot be used as parameter to predict the values of myocardial resistance.

Unfortunately, no particular relationship between the myocardial adenosine response and the patient profile, considering gender, age, BMI, smoking status and myocardial infarction event, could be identified.

Other pathologies, such as hypertension and hyperlipidaemia were present in the majority of patients, making almost impossible to identify a distinction between the two categories.

On the other hand, other pathologies, such as asthma, PVD, COPD, diabetes II, were too rare and again this makes difficult to define any particular difference between patients with and without pathologies.

Another additional complexity is related with the lack of information of the severity and the duration of the pathologies. In the majority of the cases there were more than one in the same patient, and it was difficult to separate their single influence on the adenosine response. These features are challenging from the point of view of the modelling implementation.

The challenge to predict the value of the myocardial resistance based on the patient profile is still open.

A second analysis then was performed on the adenosine response in terms of time and adenosine concentration plateau. A tree model structure was personalised for the specific-patient myocardium with a number of assumptions to define the change in myocardial volume during hyperaemia and calculate the myocardial adenosine concentration profile. This type of model in the end showed that it is a better representation of the phenomena, although it is difficult to validate against measurements. Results suggest that the myocardial response is strongly influenced by the aortic concentration profile and by the myocardial microvasculature resistance with regards to the plateau concentration and time.

CHAPTER 7

CONCLUSIONS AND FUTURE WORK

There is increasing interest in personalised medicine; developing the best treatments and interventions for each individual based on their own unique characteristics, including co-morbidities and life-style. The work described in this PhD thesis is in line with this new healthcare philosophy, where patient-specific data are integrated into computational tools to represent the patient's physiology and the impact of disease and potential treatments.

The specific focus of this thesis is to provide an estimate of myocardial resistance and its hyperaemic response to adenosine based on the individual characteristics of the patient. The myocardial resistance is crucial for an accurate computation of vFFR.

Through all the chapters limitations and conclusions have been presented and this final chapter aims to summarise them.

7.1 THESIS LIMITATIONS

1. The major limitation of the model is related to the incomplete representation of the real physiology in the cardiovascular system limiting therefore the possibility of an accurate prediction and personalisation of the model itself. This has been furthermore increased by the de-coupling approach between systemic and coronary circulations in order to simplify the personalisation process in relation with the available clinical data. No model can represent the full complexity of the human system, but in this work the emphasis has been

2. on the development of a minimal systems model in order to maximise the stability of the personalisation process.
3. The lumped-parameter models represent a significant simplification of reality and are intrinsically incapable of capturing some of the real physiology of the cardiovascular system, compared to other type of more sophisticated modelling such as 1D or 3D models, where more features can be represented with more realistic results, at the cost of increasing the level of details and inputs necessary to personalise them.
4. In the model developed in this thesis all reported elements of the adenosine response are not represented: only the vasodilation effect was taken into account with the relative barocontrol response, ignoring other mechanisms involved.
5. Simplifying hypotheses have been assumed in the different processes:
   - the distribution of blood volume, taken from the literature data;
   - a Poiseuille's resistance for the coronary tree-structure model, ignoring effects of wave propagation and compliance of the vasculature;
   - instantaneous distribution of the species within each compartment;
   - a null physiological concentration of adenosine;
   - the myocardial volume variation during adenosine response, considered to be linear and not varying according to the stiffness of myocardium and its consequently reduced compliance;
   - the arbitrary adenosine concentration threshold to trigger the vasodilation effect and its immediate effects without delays associated with the control mechanism.
6. Some input and output model results were impossible to validate against measurements. This is valid for:
   - blood volume distribution in all compartments;
   - the adenosine concentration profile in the different compartments during the infusion;

- adenosine concentration threshold to trigger vasodilation and to saturation;
- the physiological delay associated with the control mechanisms;
- myocardial blood volume and its variation during hyperaemia.

7. The personalisation of the systemic cardiovascular system suffered from inconsistent clinical data due to non-simultaneous measurements and different techniques. A strategy consisting of several approximations was considered to bring consistency within the clinical data for each patient.
8. The personalisation of the local coronary circulation found its main limitation in the limited amount of patient specific data compared with the number of the model parameters and a simple representation with tree-structure model has been considered to evaluate the variation of the myocardial volume during adenosine response.
9. Overall simulations were expensive in computational time and this is not compatible with clinical timescale, reducing therefore the applicability of these methods.

7.2 THESIS CONCLUSIONS

The conclusions of this PhD project, already reported at end of each of the previous chapters, are now summarised in this final paragraph.

1. A 0-D cardiovascular model including the major compartments (systemic, pulmonary and coronary circulations and a 4-chambered heart) and regulatory mechanisms (short-term regulatory pathways related to barocontrol) was developed based on data obtained from the published literature and it can represent the distribution of blood pressure, flow and volume in all the compartments.
2. Based on a number of assumptions, the developed model is able to represent the adenosine response as a function of the concentration of the drug in the target vessels for vasodilation.

The results for a generic, non-patient-specific model, were consistent with the average response in terms of variation of aortic pressure and heart rate reported in the literature. The results obtained from the generic model also justified simplification of the parameter personalisation, decoupling the systemic and coronary models to study them separately.

3. The systemic cardiovascular model was personalised at baseline using clinical data available for each patient (heart rate, cardiac output, ejection fraction and the invasive aortic pressure cycle-averaged signal) and results showed good reproduction of clinical data. The main outcome from this part of the project was the demonstration and quantification of the significant influence of the systemic cardiovascular system on the adenosine concentration profile in the aorta in terms of its maximum value and the time taken to reach this peak. Results suggest that the aortic concentration of adenosine is dependent on cardiac output, as would be expected intuitively. Values obtained for the maximum concentration are of the order of those described in the literature.
4. The invasive pressure data recorded during FFR assessment and the P_d/P_a traces were analysed to describe typical phenotypes of adenosine response and to identify association and correlations with patient profile (gender, age, BMI smoking status and comorbidities). Here no definite conclusions could be drawn as the results indicate that any links were weak.
5. An algorithm to post-process the raw pressure data and identify the minimum P_d/P_a and the P_d/P_a during stable hyperaemia was developed. This is a step towards standardisation of the process of FFR assessment which might be applied in clinical practice to improve the current high level of subjectivity when operators assess stenoses severity. Different schools of thought exist to arrive at the decision to treat or not treat; one suggests that the minimum P_d/P_a should be used, whilst the other suggests that the stable P_d/P_a is more appropriate for this purpose and the potential clinical impact of this type of choice was investigated. The algorithm does not solve the problem of identifying the correct FFR in terms of the minimum

or the stable P_d/P_a, but underlines that the lack of standardisation needs to be resolved. From the analysis of the P_d/P_a, it also emerged that, for some patients, it is not possible to identify a stable period. This supports the selection of the minimum P_d/P_a as the FFR.

6. The invasive pressure data and patient-specific aortic concentrations obtained from the global model were employed in the coronary tuning, together with characterisations of the stenoses from CFD analysis carried out by Dr. Morris. The coronary model also included the effect of vasodilation, assuming an increase of myocardial volume proportional to its resistance variation. Average results of myocardial resistance and blood flow at baseline, peak and hyperaemia results in physiological ranges and, moreover, showed the expected trends. The results for myocardial resistance at baseline were linearly correlated with the hyperaemic resistance with a 60% coefficient. This is also consistent with the literature.
7. Investigation of the correlation between the myocardial resistance at baseline, the myocardial resistance at hyperaemia, its change between the two phases as an absolute and percentage value and the characteristics of the patient has been carried out, but this did not produce strong correlations which could allow a prediction of the myocardial resistance in any states.
8. It is interesting to note that coronary modelling can provide an estimation of coronary flow. This is perhaps clinically more relevant than FFR. FFR represents a ratio of the coronary reserve, while flow gives an indication of whether the myocardium is adequately perfused which is independent of the stenosis severity.
9. The coronary model was able to produce the myocardial adenosine concentration profile for each lesion considered. As defined in the global model, the delay in the myocardial response to adenosine is mainly determined by the systemic cardiovascular system. The results showed that the delay between the maximum concentration in the aorta and the maximum

concentration in the myocardium was less dependent on the lesion severity but rather, was dependent in the myocardial resistance at both baseline and hyperaemia.

7.3 FUTURE WORK

Using *in silico* models to inform personalised medicine shows great promise to advance the future of healthcare. This thesis considers an example of this approach describing the development, and use, of a patient-specific cardiovascular model to describe the adenosine response. The limitations and assumptions made throughout the development of the project need to be addressed if further progress is to be made.

A number of challenges were encountered in the process of optimisation. The first was related to the number of parameters in the model and the uncertainty of these in relation to the data available. Simplistically, it could be argued that the more complex the model the better it might be expected to represent a system but, equally, as the number of parameters increases tuning becomes more challenging or, indeed, impossible if the number of variables which can be measured clinically are limited. In addition, an uncertainty analysis using physiological ranges of the model parameters is necessary to increase the confidence in the model.

Another issue was related to inconsistencies in the clinical data collected using different techniques and at different time points, and a strategy was needed to create a set of consistent input data for the optimisation process of the global system. The optimisation process also suffered from the lack of a more comprehensive set of parameters during hyperaemia. For example, continuous measurement of cardiac output or stroke volume could be used to optimise the model under both baseline and hyperaemic conditions. Unfortunately, there is currently no simple non-invasive clinical method to collect such data which could be used in the Cathlab.

Improvement of the code and additional computational power are also required to make the simulations quicker and being acceptable for clinical timescale, exploiting for example a machine learning approach.

A larger size of the cohort would also help perhaps in finding associations between the myocardial hyperaemic response in terms of the myocardial resistance and patient characteristics, providing a more homogenous distribution of comorbidities. Pathologies such as hypertension or hyperlipidaemia were very common in our cohort whilst others, such as asthma, peripheral vascular disease, COPD and diabetes II, were relatively rare and therefore, in both extremes, it is difficult to determine the effect of pathology on the adenosine response.

Another challenge that needs to be addressed is concerning the relationship between $R_{myo}(t)$ and $C_{myo}(t)$ to identify patient-specific values of adenosine concentrations which initialise the vasodilatory myocardial response or saturate the vasodilation process.

For these, it is necessary to have confidence in the coronary model and measurement of coronary blood flow and myocardial and aortic concentrations of adenosine should be performed during the adenosine infusion to validate the model.

The relationship between R_{myo} and C_{myo} could add information on the patient-specific response allowing these to be classified based on the minimum adenosine concentration that stimulates vasodilation. An important effect that needs to be considered is the delay in myocardial response when control mechanisms are involved.

Another important aspect to take into account in the decision-making process for coronary lesion treatment is to consider the life-style of the specific patient in order to personalise the model and study the effect of the coronary stenosis under the average workload of the specific individual.

In the context of FFR measurement and personalisation of the assessment of CAD whilst maintaining objectivity, “FFR for Life” (FFR4L) involves activity monitoring during the

patient's daily routine. This together with information about frailty, comorbidities, cardiac function and aerobic capacity in patients with CAD contextualises the specific stenosis.

Non-invasive data for pressure, heart rate and number of steps can be monitored with ambulatory devices and an agenda of the daily activities should be reported.

Monitoring activity should be performed for a number of consecutive days before and after the procedure. These data can provide information about the heart workload during daily routine.

This information, together with the invasive pressure collected during angiogram, could be used to personalise the systemic and the coronary model and gain an understanding of the impact of a specific coronary lesion under different physiological conditions.

APPENDIX

The steady-state pressure gradient across the stenosis is determined by a quadratic equation which includes Poiseuille's equation for the viscous losses ($Z_1 \cdot Q$), and by Bernoulli's equation for the inertial losses ($Z_2 \cdot (Q)^2$) as reported in Eq.A1.1.

$$\Delta P = Z_1 \cdot Q + Z_2 \cdot (Q)^2 \qquad \text{(Eq.A.1)}$$

Segmentation and 3D reconstruction from angiographic images were obtained for each vessel with Philips software (Philips Healthcare, Best, NL). ANSYS ICEM and ANSYS CFX (ANSYS, Inc. PA, USA) and subsequently used in order to respectively build the volumetric meshes and run the Computational Fluid Dynamic (CFD) simulations. As boundaries conditions, flows of 1 ml/s (Q_1) and 3 ml/s (Q_3) were set to obtain the respective pressure gradients (ΔP_1, ΔP_3) across the lesion. The two lesion-specific parameters Z_1 and Z_2 were then calculated solving the system of equation in Eq.A1.2:

$$\begin{cases} \Delta P_1 = Z_1 \cdot Q_1 + Z_2 \cdot (Q_1)^2 \\ \Delta P_3 = Z_1 \cdot Q_3 + Z_2 \cdot (Q_3)^2 \end{cases} \qquad \text{(Eq.A.2)}$$

where Q_1 and Q_3 are known, and ΔP_1, ΔP_3 are the solutions of the CFD.

The workflow of this project is briefly represented in the diagram in figure A1.1.

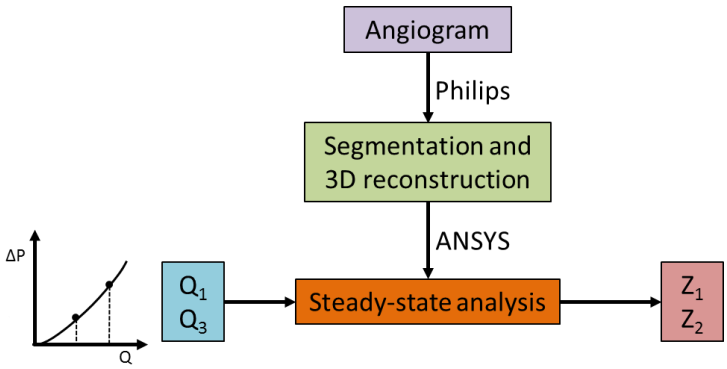

Figure A.1: Workflow to define the stenosis characteristics Z_1 and Z_2 starting from the angiogram. Coronary arteries were segmented from the angiographic images and 3D reconstructed with Philips tools. CFD simulation in ANSYS were run for each volume mesh setting as boundaries two values of flow to solve the quadratic relationship between pressure gradient and flow.

REFERENCES

[http://www.nhs.uk/]

[http://www.napavalley.edu/people/briddell/Documents/BIO%20218/22_LectureOutline.pdf]

1. Seeley R.R.T.D. Stephens P. Tate Editor^Editors. 1996, Inc.
2. Thibodeau G.A. K.T. Patton. 4th ed. 1999, St. Louis: Mosby. xxxiii, 1083 p.
3. Feigl E.O., Physiological Reviews, 1983. **63**(1): p. 1-205.
4. Levick J., London, UK, 2003.
5. Kim J.E. B.K. Koo, Korean Circulation Journal, 2012. **42**(7): p. 441-446.
6. Shah N.R.R. Al-Lamee J. Davies, IJC Heart and Vasculature, 2014. **5**: p. 20-25.
7. Schrijver M., Archives of Physiology and Biochemistry, 2003. **111**(2): p. 77-158.
8. Taylor C.A.T.A. Fonte J.K. Min, Journal of the American College of Cardiology, 2013. **61**(22): p. 2233-2241.
9. De Bruyne B. J. Sarma, Heart, 2008. **94**(7): p. 949-959.
10. Pijls N.H. B. De Bruyne. 2000: Springer.
11. Dattilo P.B.A. PrasadE. Honeycutt et al., Journal of the American College of Cardiology, 2012. **60**(22): p. 2337-2339.
12. Echavarria-Pinto M.R. PetracoT.P. van de Hoef et al., EuroIntervention, 2016. **11**(9): p. 1013-1019.
13. Morris P.D.D. RyanA.C. Morton et al., JACC Cardiovasc Interv, 2013. **6**(2): p. 149-57.
14. Marchais S.J.A.P. GuerinB. Pannier et al., Drugs, 1993. **46**(2): p. 82-87.
15. Thibodeau G. K. Patton Editor^Editors. 1993, Inc.
16. Habib A.N. LachmanK.N. Christensen et al., Europace, 2009. **11**(suppl 5): p. v15-v21.
17. Noheria A.C.V. DesimoneN. Lachman et al., Journal of Cardiovascular Electrophysiology, 2013. **24**(1): p. 1-6.
18. Elad D. S. Einav, Standard handbook of biomedical engineering and design. McGraw-Hill, New York, 2003: p. 3.1-4.1.
19. Katz L. H. Feinberg, Circulation Research, 1958. **6**(5): p. 656-669.
20. Duncker D.J. R.J. Bache, Physiological Reviews, 2008. **88**(3): p. 1009-1086.
21. Duncker D.J.R.J. Bache D. Merkus, Journal of Molecular and Cellular Cardiology, 2012. **52**(4): p. 802-813.
22. Hoffman J. J. Spaan, Physiological Reviews, 1990. **70**(2): p. 331-390.
23. Quarteroni A., SIAM News, 2001. **34**(5): p. 1-3.
24. Fung Y. Editor^Editors. 1984, Springer-Verlag, New York, Inc.
25. Mantero S.R. Pietrabissa R. Fumero, Journal of Biomedical Engineering, 1992. **14**(2): p. 109-116.
26. Allen D.G. J.C. Kentish, Journal of Molecular and Cellular Cardiology, 1985. **17**(9): p. 821-840.
27. Sarnoff S.J. E. Berglund, Circulation, 1954. **9**(5): p. 706-718.
28. Mirzaee M.R.O. GhasemalizadehB. Firoozabadi et al., Wcecs 2008: World Congress on Engineering and Computer Science, 2008: p. 27-33.
29. I. K., J. Biomedical Science and Engineering, 2013. **6**: p. 92-99
30. Shi Y.P. Lawford R. Hose, Biomed Eng Online, 2011. **10**: p. 33.
31. Van De Vosse F.N. N. Stergiopulos Editor^Editors. 2011. p. 467-499.
32. Toy S.M.J. Melbin A. Noordergraaf, Biomedical Engineering, IEEE Transactions on, 1985. **BME-32**(2): p. 174-176.
33. Westerhof N.G. Elzinga P. Sipkema, Journal of applied physiology, 1971. **31**(5): p. 776-781.

34. Westerhof N.J.-W. Lankhaar B.E. Westerhof, Medical & biological engineering & computing, 2009. **47**(2): p. 131-141.
35. Wang J.-J.A.B. O'BrienN.G. Shrive et al. 2002.
36. Burattini R. G. Gnudi, Medical and Biological Engineering and Computing, 1982. **20**(2): p. 134-144.
37. Stergiopulos N.B.E. WesterhofJ.J. Meister et al. in *Engineering in Medicine and Biology Society, 1996. Bridging Disciplines for Biomedicine. Proceedings of the 18th Annual International Conference of the IEEE*. 1996.
38. Guyton A.C.T.G. Coleman H.J. Granger, Annual Review of Physiology, 1972. **34**: p. 13-46.
39. Suga H.K. Sagawa A.A. Shoukas, Circulation Research, 1973. **32**(3): p. 314-322.
40. Korakianitis T. Y. Shi, Medical Engineering and Physics, 2006. **28**(7): p. 613-628.
41. Liang F.Y. H. Liu, Jsme International Journal Series C-Mechanical Systems Machine Elements and Manufacturing, 2005. **48**(4): p. 484-493.
42. Sun Y.M. BesharaR.J. Lucariello et al. Vol. 272. 1997. H1499-H1515.
43. Hann C.E.J.G. ChaseT. Desaive et al., Computer Methods and Programs in Biomedicine, 2010. **99**(1): p. 75-87.
44. Sughimoto K.F.Y. LiangY. Takahara et al., Journal of Thoracic and Cardiovascular Surgery, 2013. **145**(5): p. 1367-1372.
45. Magosso E. M. Ursino, Am J Physiol Heart Circ Physiol, 2001. **281**(5): p. H2036-52.
46. Ursino M., Am J Physiol, 1998. **275**(5 Pt 2): p. H1733-47.
47. Ursino M.M. Antonucci E. Belardinelli, American Journal of Physiology - Heart and Circulatory Physiology, 1994. **267**(6 36-6): p. H2531-H2546.
48. Ursino M.A. Fiorenzi E. Belardinelli, Computers in Biology and Medicine, 1996. **26**(4): p. 297-312.
49. Ursino M. C.A. Lodi, Am J Physiol, 1998. **274**(5 Pt 2): p. H1715-28.
50. Ursino M. E. Magosso, Am J Physiol Heart Circ Physiol, 2003. **284**(4): p. H1479-93.
51. Ursino M. E. Magosso, American Journal of Physiology-Heart and Circulatory Physiology, 2000. **279**(1): p. H149-H165.
52. Ursino M. E. Magosso, American Journal of Physiology-Heart and Circulatory Physiology, 2000. **279**(1): p. H166-H175.
53. Cheng L.A. AlbaneseM. Ursino et al., American Journal of Physiology - Heart and Circulatory Physiology, 2016. **310**(7): p. H922-H937.
54. Fresiello L.B. MeynsA. Di Molfetta et al., Frontiers in Physiology, 2016. **7**: p. 189.
55. Fresiello L.G. FerrariA. Di Molfetta et al., Journal of Biomedical Informatics, 2015. **57**(Supplement C): p. 100-112.
56. Fresiello L.A.W. KhirA.D. Molfetta et al., Artificial Organs, 2013. **37**(3): p. 237-247.
57. Fresiello L.A. KhirA. Molfetta et al. Vol. 36. 2013. 749-57.
58. Cheng L.O. IvanovaH.-H. Fan et al., Respiratory Physiology & Neurobiology, 2010. **174**(1): p. 4-28.
59. Hester R.L.A.J. BrownL. Husband et al., Frontiers in Physiology, 2011. **2**: p. 12.
60. Blanco P.J.P.R. TrenhagoL.G. Fernandes et al., International Journal for Numerical Methods in Biomedical Engineering, 2012. **28**(4): p. 412-433.
61. Neidlin M.S.J. SonntagT. Schmitz-Rode et al., Medical Engineering & Physics, 2016. **38**(4): p. 380-390.
62. Li X. J. Bai, Medical and Biological Engineering and Computing, 2001. **39**(4): p. 480-487.
63. Williams N.D.Ø. Wind-WillassenA.A. Wright et al., Mathematical Medicine and Biology: A Journal of the IMA, 2014. **31**(4): p. 365-392.

64. Heldt T.E.B. ShimR.D. Kamm et al., Journal of Applied Physiology, 2002. **92**(3): p. 1239-1254.
65. Lu K.J.W. ClarkF.H. Ghorbel et al., American Journal of Physiology - Heart and Circulatory Physiology, 2001. **281**(6): p. H2661-H2679.
66. Geven M.C.F.V.N. BohtéW.H. Aarnoudse et al., Physiological Measurement, 2004. **25**(4): p. 891-904.
67. Itu L.P. SharmaV. Mihalef et al. in *Biomedical Imaging (ISBI), 2012 9th IEEE International Symposium on*. 2012.
68. Maasrani M.I. AbouliatimG.V. Ruggieri et al. in *19th International Conference on Electrical Machines, ICEM 2010*. 2010.
69. Pietrabissa R.S. ManteroT. Marotta et al., Medical Engineering and Physics, 1996. **18**(6): p. 477-484.
70. Maasrani M.I. AbouliatimM. Harmouche et al., Journal of Biomedical Science and Engineering, 2011. **4**(01): p. 34.
71. Maasrani M.I. AbouliatimV. Ruggieri et al. in *Electrical Machines (ICEM), 2010 XIX International Conference on*. 2010. IEEE.
72. Maasrani M.A. DrochonI. Abouliatim et al., Computer Methods in Biomechanics and Biomedical Engineering, 2010. **13**: p. 93-94.
73. Maasrani M.J.-P. VerhoyeH. Corbineau et al., Annals of biomedical engineering, 2008. **36**(7): p. 1163-1174.
74. Kim H.J.I.E. Vignon-ClementelJ.S. Coogan et al., Annals of Biomedical Engineering, 2010. **38**(10): p. 3195-3209.
75. Cornelissen A.J.M.J. DankelmanE. VanBavel et al., American Journal of Physiology - Heart and Circulatory Physiology, 2000. **278**(5 47-5): p. H1490-H1499.
76. Maasrani M.J.P. VerhoyeH. Corbineau et al., Computer Methods in Biomechanics and Biomedical Engineering, 2008. **11**: p. 151-152.
77. Vignon-Clementel I.E.C.A. FigueroaK.E. Jansen et al., Computer Methods in Biomechanics and Biomedical Engineering, 2010. **13**(5): p. 625-640.
78. Kim H.J.C.A. FigueroaI.E. Vignon-Clementel et al., Proceeding of the Asme Summer Bioengineering Conference - 2007, 2007: p. 317-318.
79. Manor D.U. DinnarS. Sideman et al. in *[1989] Proceedings. Computers in Cardiology*. 1989.
80. Cornelissen A.J.M.J. DankelmanE. VanBavel et al., American Journal of Physiology-Heart and Circulatory Physiology, 2002. **282**(6): p. H2224-H2237.
81. Cornelissen A.J.M.J. DankelmanE. VanBavel et al., American Journal of Physiology-Heart and Circulatory Physiology, 2000. **278**(5): p. H1490-H1499.
82. Lloyd-Jones D.R.J. AdamsT.M. Brown et al., Circulation, 2010. **121**(7): p. e46-e215.
83. Garrone P.G. Biondi-ZoccaiI. Salvetti et al., Journal of Interventional Cardiology, 2009. **22**(6): p. 527-536.
84. Nallamothu B.K.J.A. SpertusA.J. Lansky et al., The Assessing Angiography (A2) Project, 2013. **127**(17): p. 1793-1800.
85. Morris e.a., Cardiovascular interventions, 2013. **6**(2).
86. Pijls N.J. Van SonR. Kirkeeide et al., Circulation, 1993. **87**(4): p. 1354-1367.
87. Siebes M.S.A. ChamuleauM. Meuwissen et al., Am J Physiol Heart Circ Physiol, 2002. **283**(4): p. H1462-70.
88. Wellnhofer E.J. OsmanU. Kertzscher et al., Atherosclerosis, 2011. **216**(2): p. 277-282.
89. Wellnhofer E.L. GoubergritsU. Kertzscher et al., BioMedical Engineering OnLine, 2006. **5**(1): p. 39.
90. Li Y.J.L. Gutiérrez-ChicoN.R. Holm et al., Journal of the American College of Cardiology, 2015. **66**(2): p. 125-135.

91. Naghipoor J. T. Rabczuk, Computers in Biology and Medicine, 2017. **90**(Supplement C): p. 15-22.
92. Morris P.D. Editor^Editors. 2016, University of Sheffield.
93. van de Hoef T.P.M. MeuwissenJ. Escaned et al., Nature Reviews Cardiology, 2013. **10**: p. 439.
94. Bech G.J.W.B. De BruyneN.H.J. Pijls et al., A Randomized Trial, 2001. **103**(24): p. 2928-2934.
95. Fearon W.F.A.C. YeungD.P. Lee et al., American Heart Journal, 2003. **145**(5): p. 882-887.
96. Morris P.D.D.A. Silva SotoJ.F.A. Feher et al., Jacc. Basic to Translational Science, 2017. **2**(4): p. 434-446.
97. CLAUSEN J.P. J. TRAP-JENSEN, Circulation, 1970. **42**(4): p. 611-624.
98. Westerhof N.G. Elzinga P. Sipkema, J Appl Physiol, 1971. **31**(5): p. 776-781.
99. Nadler S.B.J.U. Hidalgo T. Bloch, Surgery, 1962. **51**(2): p. 224-232.
100. Parkin W.G., Crit Care Resusc, 1999. **1**(3): p. 311-21.
101. Guyton A.C., The American Journal of the Medical Sciences, 1965. **219**(1): p. 122.
102. Guyton A.C.A.W. Lindsey B.N. Kaufmann, American Journal of Physiology, 1955. **180**(3): p. 463-468.
103. Guyton A.C.D. Polizo G.G. Armstrong, American Journal of Physiology, 1954. **179**(2): p. 261-267.
104. Guyton A.C.T.Q. RichardsonB.H. Douglas et al., Circulation Research, 1962. **11**(3): p. 431-&.
105. Lentner C. 1990: Ciba-Geigy.
106. Maceira A.S. PrasadM. Khan et al., Journal of Cardiovascular Magnetic Resonance, 2006. **8**(3): p. 417-426.
107. Scharhag J.G. SchneiderA. Urhausen et al., Journal of the American College of Cardiology, 2002. **40**(10): p. 1856-1863.
108. Kawel N.E.B. TurkbeyJ.J. Carr et al., Circulation. Cardiovascular imaging, 2012. **5**(4): p. 500-508.
109. Hyde E.R.A.N. CooksonJ. Lee et al., Annals of Biomedical Engineering, 2014. **42**(4): p. 797-811.
110. Arthurs G. M. Sudhakar, Continuing Education in Anaesthesia, Critical Care & Pain, 2005. **5**(6): p. 207-210.
111. Pittman R.N. in *Colloquium Series on Integrated Systems Physiology: From Molecule to Function*. 2011. Morgan & Claypool Life Sciences.
112. Dash R.K. J.B. Bassingthwaighte, Annals of biomedical engineering, 2010. **38**(4): p. 1683-1701.
113. Petersson J. R.W. Glenny, European Respiratory Journal, 2014. **44**(4): p. 1023-1041.
114. Ursino M.M. Antonucci E. Belardinelli, Am J Physiol, 1994. **267**(6 Pt 2): p. H2531-46.
115. Layland J.D. CarrickM. Lee et al., Jacc-Cardiovascular Interventions, 2014. **7**(6): p. 581-591.
116. Pelleg A. R.S. Porter, Pharmacotherapy, 1990. **10**(3): p. 157-174.
117. Fuller R.W.D.L. MaxwellT.B.G. Conradson et al., British Journal of Clinical Pharmacology, 1987. **24**(3): p. 309-317.
118. Gupta J.P.a., 2013.
119. Duncker D.J.R. Stubenitsky P.D. Verdouw, American Journal of Physiology-Heart and Circulatory Physiology, 1998. **275**(5): p. H1663-H1672.
120. Tarkin J.M.S. NijjerS. Sen et al., Circulation-Cardiovascular Interventions, 2013. **6**(6): p. 654-661.

121. Tune J.D.M.W. GormanK.N. Richmond et al., Faseb Journal, 1999. **13**(5): p. A1083-A1083.
122. Tune J.D.K.N. RichmondM.W. Gorman et al., American Journal of Physiology-Heart and Circulatory Physiology, 2000. **278**(1): p. H74-H84.
123. Yada T.K.N. RichmondR. van Bibber et al. Vol. 276. 1999. H1425-H1433.
124. Saltelli A.K. Chan E.M. Scott. Vol. 1. 2000: Wiley New York.
125. Kappel F. J. Batzel, 2006 28th Annual International Conference of the IEEE Engineering in Medicine and Biology Society, Vols 1-15, 2006: p. 6314-6317.
126. Wilson R.F.K. WycheB.V. Christensen et al., Circulation, 1990. **82**(5): p. 1595-1606.
127. De Bruyne B.N.H.J. PijlsE. Barbato et al., Circulation, 2003. **107**(14): p. 1877-1883.
128. Arumugham P.V.M. FigueredoP.B. Patel et al., Eurointervention, 2013. **8**(10): p. 1166-1171.
129. Echavarria-Pinto M.N. GonzaloB. Ibanez et al., Circulation-Cardiovascular Interventions, 2014. **7**(1): p. 35-42.
130. Jeremias A.R.J. WhitbournS.D. Filardo et al., American Heart Journal, 2000. **140**(4): p. 651-657.
131. Khashaba A.A. Mortada A. Omran, Clinical Medicine Insights: Cardiology, 2014. **8**(4062-CMC-Intracoronary-Versus-Intravenous-Adenosine-Induced-Maximal-Coronary-Hyp.pdf): p. 17-21.
132. Rossen J.D.J.E. QuillenJ.A.G. Lopez et al., Journal of the American College of Cardiology, 1991. **18**(2): p. 485-491.
133. Seo M.K.B.K. KooJ.H. Kim et al., Circulation-Cardiovascular Interventions, 2012. **5**(3): p. 401-405.
134. Biaggioni I.T.J. KillianR. Mosquedagarcia et al., Circulation, 1991. **83**(5): p. 1668-1675.
135. Biaggioni I.B. OlafssonR.M. Robertson et al., Circulation Research, 1987. **61**(6): p. 779-786.
136. Biaggioni I.O.J. OnrotD. Kincaid et al., Clinical Research, 1985. **33**(2): p. A280-A280.
137. Ogilby J.D.A.S. IskandrianW.J. Untereker et al., Circulation, 1992. **86**(3): p. 887-895.
138. Hori M. M. Kitakaze, Hypertension, 1991. **18**(5): p. 565-574.
139. van de Hoef T.P.F. NolteM.C. Rolandi et al., Journal of Molecular and Cellular Cardiology, 2012. **52**(4): p. 786-793.
140. Chilian W.M. S.M. Layne, Circulation Research, 1990. **66**(5): p. 1227-1238.
141. Marcus M.L.W.M. ChilianH. Kanatsuka et al., Circulation, 1990. **82**(1): p. 1-7.
142. Kanatsuka H.K.G. LampingC.L. Eastham et al., Circulation Research, 1989. **65**(5): p. 1296-1305.
143. Jones C.J.H.L. KuoM.J. Davis et al., Circulation, 1995. **91**(6): p. 1807-1813.
144. Johnson N.P.D.T. JohnsonR.L. Kirkeeide et al., Jacc-Cardiovascular Interventions, 2015. **8**(8): p. 1018-1027.
145. J.P. G., 2017.
146. Toth G.G.N.P. JohnsonA. Jeremias et al., Journal of the American College of Cardiology, 2016. **68**(7): p. 742-753.
147. Sen S.J. EscanedI.S. Malik et al., Journal of the American College of Cardiology, 2012. **59**(15): p. 1392-1402.
148. Götberg M.E.H. ChristiansenI.J. Gudmundsdottir et al., New England Journal of Medicine, 2017. **376**(19): p. 1813-1823.
149. Davies J.E.S. SenH.-M. Dehbi et al., New England Journal of Medicine, 2017. **376**(19): p. 1824-1834.
150. Matsuo H. Y. Kawase, Cardiovascular Intervention and Therapeutics, 2016. **31**(3): p. 183-195.

151. Schiavazzi D.E.A. BarettaG. Pennati et al., International Journal for Numerical Methods in Biomedical Engineering, 2017. **33**(3): p. e02799-n/a.
152. Edwards L.K.P. MorrisA. Siddiqui et al., Archives of Disease in Childhood. Fetal and Neonatal Edition, 2007. **92**(3): p. F210-F214.
153. Fagih A.A., Saudi Medical Journal, 2016. **37**(5): p. 592-592.
154. Cain P.A.R. AhlE. Hedstrom et al., BMC Med Imaging, 2009. **9**: p. 2.
155. Cohen-Solal A.B. CaviezelD. Himbert et al., J Hypertens, 1994. **12**(5): p. 591-600.
156. Laskey W.K.H.G. ParkerV.A. Ferrari et al., J Appl Physiol (1985), 1990. **69**(1): p. 112-9.
157. Lewis J.F.L.C. KuoJ.G. Nelson et al., Circulation, 1984. **70**(3): p. 425-31.
158. McDonough J.R. R.A. Danielson, J Appl Physiol, 1974. **37**(4): p. 579-83.
159. Rerych S.K.P.M. ScholzG.E. Newman et al., Ann Surg, 1978. **187**(5): p. 449-64.
160. Broome M.E. MaksutiA. Bjallmark et al., Biomedical Engineering Online, 2013. **12**.
161. Gul R. Editor^Editors. 2016, Freie Universität Berlin.
162. Hernández-Ramırez A.A. Fraguela-Collar R. Lemuz-López, Advances in Pattern Recognition: p. 53.
163. Olansen J.B.J.W. ClarkD. Khoury et al., Computers and Biomedical Research, 2000. **33**(4): p. 260-295.
164. Lungu A. Editor^Editors. 2015, University of Sheffield.
165. Cope D.K.F. GrimbertJ.M. Downey et al., Crit Care Med, 1992. **20**(7): p. 1043-56.
166. Zhong L.D.N. GhistaE.Y. Ng et al., Proc Inst Mech Eng H, 2006. **220**(5): p. 647-55.
167. Biaggioni I.J. OnrotA.S. Hollister et al., Life Sciences, 1986. **39**(23): p. 2229-2236.
168. Shryock J.C. L. Belardinelli, The American Journal of Cardiology, 1997. **79**(12, Supplement 1): p. 2-10.
169. Yada T.O. HiramatsuH. Tachibana et al., American Journal of Physiology-Heart and Circulatory Physiology, 1999. **277**(5): p. H1931-H1939.
170. Camici P.G. O.E. Rimoldi, Journal of Nuclear Medicine, 2009. **50**(7): p. 1076-1087.
171. Dawson D. S. Firoozan, International Journal of Cardiology, 2000. **73**(2): p. 105-113.
172. Ganz W.K. TamuraH.S. Marcus et al., Circulation, 1971. **44**(2): p. 181-195.
173. Greve A.M.L.-Y. HsuS. Vasu et al., Journal of Cardiovascular Magnetic Resonance, 2014. **16**(Suppl 1): p. P21-P21.
174. McCommis K.S.H. ZhangT.A. Goldstein et al., Jacc-Cardiovascular Imaging, 2009. **2**(11): p. 1313-1320.
175. Miyata-Fukuoka Y.H. KawaiO. Iseki et al., Journal of Echocardiography, 2016. **14**(4): p. 163-170.
176. Motwani M.A. KidambiA. Uddin et al., Journal of Cardiovascular Magnetic Resonance, 2015. **17**.
177. Schindler T.H.A. QuercioliI. Valenta et al., Seminars in Nuclear Medicine, 2014. **44**(4): p. 274-293.
178. Waller A.H.R. BlanksteinR.Y. Kwong et al., Current Cardiology Reports, 2014. **16**(5): p. 483.
179. Zarinabad N.A. Chiribiri M. Breeuwer, Current Cardiovascular Imaging Reports, 2013. **7**(1): p. 9246.
180. Crystal G.J.H.F. Downey F.A. Bashour, Am J Physiol, 1981. **241**(2): p. H194-201.
181. Judd R.M.J.R. Resar F.C.P. Yin, American Journal of Physiology, 1993. **265**(4): p. H1038-H1047.
182. Le D.E.A.R. JayaweeraK. Wei et al., Heart, 2004. **90**(10): p. 1199-1205.
183. Morgenstern C.U. HöljesG. Arnold et al., Pflügers Archiv, 1973. **340**(2): p. 101-111.
184. Munford R.S.G.K. Mcmullan W.D. Love, Circulation research, 1965. **17**(2): p. 155-159.

185. Chatterjee N.O. BaneB.S. Spottiswoode et al., Journal of Cardiovascular Magnetic Resonance, 2015. **17**(1): p. W11.
186. Cullen J.H.M.A. HorsfieldC.R. Reek et al., J Am Coll Cardiol, 1999. **33**(5): p. 1386-94.
187. Indermuhle A.R. VogelP. Meier et al., American Journal of Physiology-Heart and Circulatory Physiology, 2011. **300**(6): p. H2327-H2327.
188. Klassen G.A.J.B. AgarwalP.H. Tanser et al., Circulation research, 1970. **27**(2): p. 185-195.
189. Bruinsma P.T. ArtsJ. Dankelman et al., Basic Research in Cardiology, 1988. **83**(5): p. 510-524.
190. Spaan J. Vol. 124. 2012: Springer Science & Business Media.
191. Goyal A.J. LeeP. Lamata et al., Ieee Transactions on Medical Imaging, 2013. **32**(1): p. 56-72.
192. Hein T.W.L. Belardinelli L. Kuo, Journal of Pharmacology and Experimental Therapeutics, 1999. **291**(2): p. 655-664.
193. Hein T.W. L. Kuo, Circulation Research, 1999. **85**(7): p. 634-642.
194. Feliciano L. R.J. Henning, Clinical Cardiology, 1999. **22**(12): p. 775-786.
195. Dodge J.T.B.G. BrownE.L. Bolson et al., Circulation, 1992. **86**(1): p. 232-246.
196. Iberall A.S., Mathematical Biosciences, 1967. **1**(3): p. 375-395.
197. Olufsen M.S.C.S. PeskinW.Y. Kim et al., Annals of Biomedical Engineering, 2000. **28**(11): p. 1281-1299.
198. Zhou Y.F.G.S. Kassab S. Molloi, Physics in Medicine and Biology, 1999. **44**(12): p. 2929-2945.
199. Moore J.E.J.N. GuggenheimA. Delfino et al., J Biomech Eng, 1994. **116**.
200. Bache R.J., A Functional Assessment of Coronary Health, 1998. **98**(13): p. 1257-1260.
201. Gould K.L.K. Lipscomb C. Calvert, Circulation, 1975. **51**(6): p. 1085-1094.